Polymorph Control of Pharmaceuticals within a Continuous Oscillatory Baffled Crystalliser

A thesis presented for the degree of
Doctor of Philosophy
in the Faculty of Science
of the University of Strathclyde

by

Naomi Elizabeth Barbara Briggs

Strathclyde Institute of Pharmacy and Biomedical Sciences
March, 2015

Declaration of Author's Rights

This thesis is the result of the author's original research. It has been composed by the author and has not been previously submitted for examination which has led to the award of a degree.

Signed:

Date:

Acknowledgements

Abstract

Continuous processing is a widely used application that provides a number of benefits to manufacturing including improved process control and high quality products. The continuous oscillatory baffled crystalliser (COBC) is a type of continuous platform that enables crystallisation and growth of pharmaceutical systems, moving crystallising solutions and suspensions through a series of baffled tubes. Application of oscillatory flow results in the formation of eddy currents enabling an efficient mixing and near-plug net flow experience of the bulk solution. The enhanced turbulence provides the possibility of linear scale up and uniformity in bulk solution environment (distributions of shear rates and temperature gradients are reduced) alongside the decoupling of mixing and net flow resulting in long residence times. Considering this, COBC systems offer promise to the enable effective operation and scaling of pharmaceutical crystallisation to industrial-sized processes.

Residence time distributions (RTD) in a DN15 COBC have been studied for the first time as a function of flow and oscillatory conditions, illustrating operation with a near-plug profile. A novel moving fluid (MF) batch oscillatory baffled crystalliser has been developed as an improved model of the hydrodynamic conditions in a DN15 COBC and thus eliminates many of the assumptions made during the tradition approach for moving to continuous oscillatory flow. This batch system was combined with imaging technology to investigate nucleation and fouling. Experiments illustrated variations in nucleation kinetics for L-glutamic acid polymorphs when comparted to the tradition batch platforms, thus highlighting the importance to use representative systems for crystallisation scale-up.

Polymorph control during continuous oscillatory crystallisation was investigated using two pharmaceutically relevant systems: L-Glutamic Acid and Carbamazepine. Due to excessive fouling in the COBC during spontaneous nucleation, continuous processes were designed and operated to decouple the two step crystallisation process. Through the use of seeding,

fouling could be eliminated, and a focus on the control over particle growth could be made. In addition, a basic methodology from batch to continuous oscillatory baffled crystallisation is presented to achieve polymorphic control.

This work has advanced the practical and scientific understanding towards a methodology for successful oscillatory flow operation in addition to the possibilities of a control approach, through implementation of process analytical technologies, thus facilitating the rapid development and understanding of COBC processes in future studies.

Awesome Quote

Contents

List of Figures

List of Tables

List of Abbreviations

1,3-bis(m-nitrophenyl)urea	MNPU
5-Methyl-2-[(2-nitrophenyl)amino]-3-thiophenecarbonitrile	ROY
Active Pharmaceutical Ingredient	API
Attenuated Total Reflectance Fourier Transform Infrared	ATR-FTIR
Baffle Spacing	BS
Carbamazepine	CBZ
Centre for Innovative Manufacturing in Continuous Manufacturing and Crystallisation	CMAC
Classic Nucleation Theory	CNT
Computation Fluid Dynamics	CFD
Continuous Oscillatory Baffled Crystalliser	COBC
Continuous Oscillatory Baffled Reactor	COBR
Continuous Stirred Tank Crystalliser	CSTC
Critical Quality Attributes	CQA
Design of Experiments	DoE
Differential Scanning Calorimetry	DSC
Dynamic light scattering	DLS
European Medicines Agency	EMA
Focused Beam Reflectance Measurement	FBRM
Food and Drug Administration	FDA
Generally regarded as safe	GRAS
Heater/chiller	HC
Infrared	IR
Isonicotinamide	INA
L-Glutamic Acid	LGA
Metastable Zone Width	MSZW
Mixed Suspension Mixed Product Removal	MSMPR
Moving Baffle	MB
Moving Fluid	MF

Nuclear Magnetic Resonance	NMR
Oscillatory Baffled Crystalliser	OBC
Particle Imaging Velocimetry	PIV
Particle Size Distribution	PSD
Plug Flow Reactor	PFR
Primary Nucleation	1^yN
Process Analytical Technology	PAT
Quality by Design	QbD
Quality by Testing	QbT
Residence Time	RT
Residence Time Distribution	RTD
Scanning electron microscopy	SEM
Secondary Nucleation	2^yN
Segmented Flow Tubular Reactor	SFTR
Simultaneous Thermal Analysis	STA
Solution Mediated Polymorphic Transformation	SMPT
Stirred Tank Crystalliser	STC
Stirred Tank Reactor	STR
Thermogravimetric Analysis	TGA
Ultra violet	UV
Volume Equivalent Spherical Diameter	VESD
With respect to	wrt
X-Ray Powder Diffraction	XRPD

Nomenclature

μ	Chemical potential (Eqn. 1.1 &1.2)
	Fluid viscosity (kgm^{-1}s^{-1})
#	with respect to the beta polymorph of L- Glutamic Acid
*	with respect to the alpha polymorph of L- Glutamic Acid
$\emptyset_\rho$	Crystal density (kgm^{-3})
ΔG_{crit}	Critical energy change
$\epsilon_{\mathbf{OBC}}$	Power density of an OBC
$\epsilon_{\mathbf{STC}}$	Power density of an STC
A_B	Area of a baffle (m)
A_{COBC}	Surface area of a baffled COBC.
A_c	Area
A_v	Surface area of a vessel
B_N	total number of baffles in the system
BS_r	Baffle spacing ratio
B_T	Baffle thickness
C^*	Equilibrium solution concentration (figure 1.10)
C_D	Coefficient of discharge of the baffles
C_d	Drag coefficient
C_i	crystal solution interface concentration (figure 1.10)
D_m	Distance (m)
D_s	Diameter of stirrer (m)
E_G	Activation energy
G_V	Volume excess free energy
G_s	Surface excess free energy
G_v	Free energy change of the transformation per unit volume
N_b	Number of baffles per unit length of OBC (m^{-1})
N_s	Stirring speed (rpm)
P_o	Impeller power number
T_i	Initial temperature (°C)

T_{nuc}	Nucleation temperature
T_{sol}	Solubility temperature
T_x	Temp at distance x
V_L	Volume of liquid in STC (m^3)
V_m	Velocity (m/min)
V_t	Terminal velocity (ms^{-1})
a^*	Activity of a saturated solution
a^*	Activity of a saturated solution
$k_{b\ het}$	Homogeneous nucleation rate constant
k_b	Nucleation rate constant
k_{bcf}	Burton, Cabrera and Frank growth rate parameter
k_g	Growth rate constant
r_c	Critical radius
t_g	Time taken to reach a detectable size
t_{ind}	Induction time
t_n	Time to form a critical nucleus
t_r	Relaxation time
t_x	Time to reach distance x (min)
μ_0	Standard potential
μ_2	Second moment
μ_3	Third moment
μ_L	Chemical potential of a solution
μ_S	Chemical potential of a solid
χ_o	Centre-to-peak amplitude (m)
$\emptyset$	Crystal diameter (m)
C2(t)'	Model response
D	Vessel dispersion number
D_o	Orifice hole diameter (m)
f	Frequency (Hz)
G_0	Free energy of a saturated solution

G_1	Free energy of a kinetically stable polymorph
G_2	Free energy of a thermodynamically stable polymorph
TR	Transfer function
T_t	Transition temperature
α	Baffle free ratio
A	A constant
C	Solution concentration
	Dimensionless concentration (Eqn. 2.8)
CR	Cooling rate (°C min^{-1})
D	Column diameter (m)
D	Baffle diameter (m)
E	Axial dispersion coefficient (m^2 s^{-1})
FR	Flow rate
G	Free energy (Eqn. 1.8 & 1.9, figure 1.21)
	Growth rate
J	Nucleation rate
L	Length
M	Mass of tracer (kg)
Pe	Peclet number
R	Gas constant (8.314 J mol^{-1} K^{-1})
RT	Residence time (min).
Re_n	Net flow Reynolds number
Re_o	Oscillatory Reynold number
S	Supersaturation ratio
St	Strouhal number
T	Temperature
V	Volume (cm^3)
Z	Dimensionless length
a	Activity
b	Nucleation order

g	Order of growth
g	Gravitational acceleration (9.81 ms^{-2})
k	Boltzmann constant (1.3805 x 10^{-23} JK^{-1})
p	Growth constant
	Upstream concentration (Eqn. 2. 12)
r	Radius
t	time
t	Time
u	Superficial mean velocity (m s^{-1})
x	Distance
α	Baffle free area
γ	Interfacial tension
δ	Diffusion layer thickness (figure 1.10)
θ	Dimensionless time
ν	Molecular volume (table 1)
ρ	Density (kg m $^{-3}$)
σ	Relative supersaturation
	Variance (Eqn. 2.5, 2.7)
τ	Mean residence time
υ	Fluid velocity (m^{3}s^{-1})
ψ	Velocity ratio

Chapter 1. General Introduction

1.1   Background

Therapeutic treatments are most commonly distributed to patients as solid dosage forms containing an active pharmaceutical ingredient (API). Solid APIs fall into 2 categories: crystalline and amorphous. Crystalline materials have long range order with regular repeating units within the solid state structure, whereas amorphous substances only have short range order. Crystalline materials are grouped into polymorphs, co-crystals, solvates and salts depending on how the components arrange themselves in the crystal lattice (Figure 1.1).
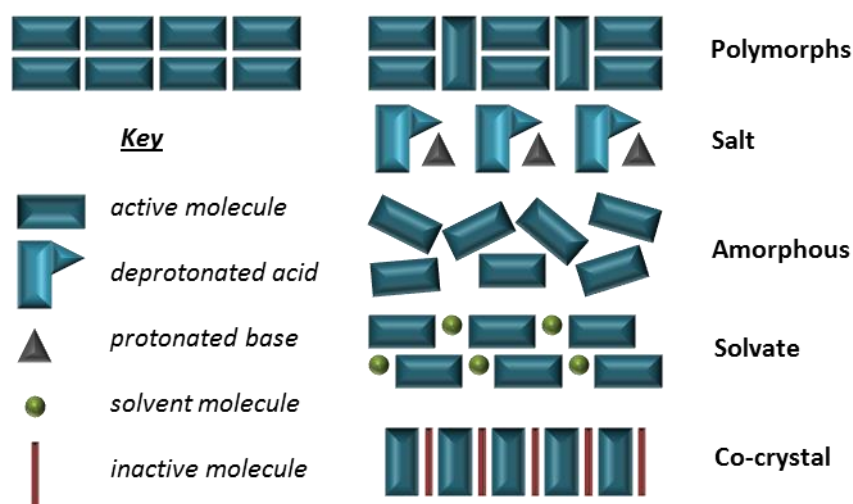
Figure 1.1: Solid form arrangements. Adapted from Reference 1.

Higher solubilities and faster dissolution rates are typically observed with amorphous materials, but they are intrinsically more difficult to characterise and less physically and chemically stable therefore not always ideal for APIs due to their short shelf life after production.[2] Crystalline materials make up the majority of pharmaceutical products administered to patients[3] owing to longer stability properties amongst others. However, how these materials crystallise and the resulting solid state structure will influence the

physiochemical properties and hence dictate the likelihood of that pharmaceutical to be placed on the market for therapeutic use.

It is common during drug development to find chemical entities with the desired biological effect but not possessing the appropriate physical properties for patient consumption, for example poor solubility. In these scenarios, tailoring the drug solid state structure is a desired approach to improve the physical performance while retaining the integrity for therapeutic effect. Common methods used to investigate solid forms for improving drug properties include co-crystallisation[4,5] and salt screening.[6]

When crystal engineers began developing novel co-crystals for improved performance of pharmaceutical materials, the solid form classification system became increasingly complex and there were challenges around naming and definition of these solid forms. Given the high regulatory nature of the pharmaceutical industry, the Food and Drug Administration (FDA) issued concerns over the correct classification and since then these entities have been grouped under multi-component systems; details on the classification system of solid APIs can be found in Figure 1.2.
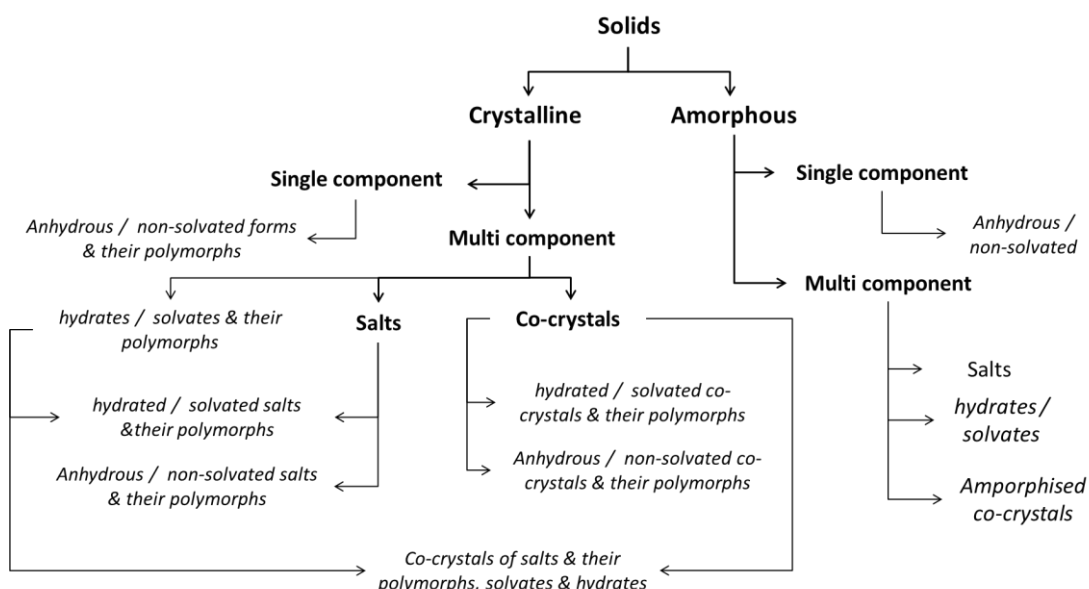
Figure 1.2: Solid state classification system. Adapted from Reference 7.

As the solid state structure will define pharmaceutical performance, control and characterisation of these materials is an integral part of the drug development and production process. Physical characterisation of the solid state can be carried out using a spectrum of techniques,[8,9] these include infrared (IR) spectroscopy, Raman spectroscopy, solid-state nuclear magnetic resonance (NMR) spectroscopy, x-ray powder diffraction (XRPD), and differential scanning calorimetry (DSC).

During the early stage of a drug development process within industry, polymorph screening is routinely carried out to assess the possibility of new forms appearing. A change in polymorphic form can occur during elevated temperature and pressure changes the material may experience moving through the drug manufacturing process. To evaluate solid phase consistency throughout processing, characterisation techniques are frequently performed on the bulk material after every new stage in the production line.

Ritonavir, trade name Norvir®, is a renowned example of polymorphism challenges in the pharmaceutical industry. The drug was manufactured and dispatched to market shelves without the knowledge of a second more stable polymorph, and during storage, the API converted to a more stable phase. This thermodynamically stable form was less soluble, resulting in a lower bioavailability, and the drug became unfit for patient consumption. The product was recalled from market two years after its release in 1998 proving a costly situation for the company, leaving patients deferred to another product until the API could be redeveloped.[10] There have been several reports of market recall events due to polymorphism issues, since Ritonavir, including a recall of 60 million tablets of the blood pressure medication Avalide® and 1.5 million tablets of the blood thinner Coumadin (warfarin sodium 2-propanol solvate), both in 2010.[11]

1.2   Continuous manufacturing of pharmaceuticals

Continuous manufacturing is not a new concept and has been applied over several industries for decades, including food, chemicals, plastics, polymers, oil and gas. However, the pharmaceutical industry has almost solely relied upon batch methods for primary processing, specifically crystallisation.[12] Over previous decades drivers to reduce production costs were not a priority due to the high value end products, but over recent years the need to improve current processing technology and product quality has become increasingly important. As a consequence, the continuous manufacturing of pharmaceuticals has received much interest throughout industry and academia.[13-18] The Novartis-MIT Centre for Continuous Manufacturing, supported by $65 million from Novartis, and recent birth of the Centre for Innovative Manufacturing in Continuous Manufacturing and Crystallisation (CMAC) UK, supported by over £80 million, highlights some of the current investments made in this area.

Pharmaceutical manufacturing can be broken down into many stages, including primary and secondary processes (Figure 1.3). Primary stages involve production of the API, this is generally a chemical synthesis commonly followed by a crystallisation/re-crystallisation stage. Following this, physical manipulation of the API is typically carried out, for example a size reduction process, before the material is sent downstream for secondary manufacturing. The secondary processing involves formulation of the API with excipient, this includes procedures such as powder blending, extrusion, granulation, tableting and further processing such as coating or encapsulation, before the resulting dosage form is packed and transported for storage and distribution.
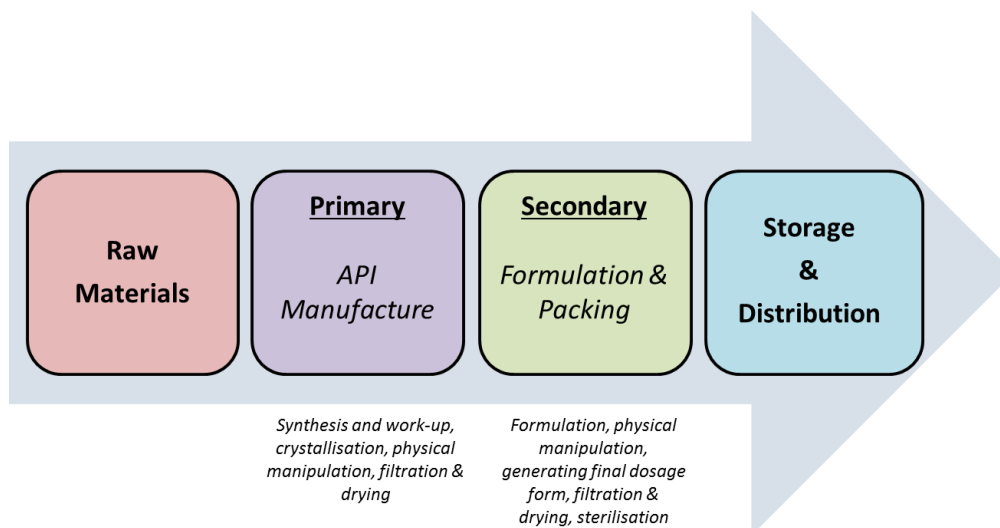
Figure 1.3: Overview of current pharmaceutical manufacturing supply chain. Schematic illustrating the unit operations between raw materials and the distribution of a final drug product.

The critical stage between primary and secondary manufacturing of APIs is the crystallisation step. How this stage is designed and controlled will result in specific physical properties of the API including polymorphic form, morphology, and particle size distribution (PSD). Despite progress in this area over the last several decades,[19] crystallisation is still poorly understood and leads to an array of manufacturing problems.[20] Many downstream secondary processes run into issues due to lack of consistency and batch to batch variations of the solid APIs. This high variability and lack of process control and understanding,[19] results in the production of poor quality drugs.

There are several advantages in the implementation of end to end continuous manufacturing when compared to the currently adopted approaches,[21-23] these include drivers such, as safer more efficient processes, as typically continuous systems have smaller volumes when compared to batch processes, thus smaller amounts of materials and solvents are taking part in the process at any given time. Reactants are also continuously added and withdrawn from the system therefore large volumes of potentially volatile and/or toxic materials are not in the same space for

prolonged periods of time. Superior heat transfer, when compared to an equivalent sized batch system, leads to greener chemistries as desired temperatures can be reached readily without excessive heat input or extraction, this leads to novel reaction conditions, and can reduce solvent use. Improved scalability has also been illustrated due to advanced mixing regimes within continuous operations. Accumulating these advantages reduces the time taken for novel products to move from research and development to industrial manufacturing plants and hence reduce time to market, thus resulting in further economic and environmental benefit in addition to providing better product consistency and improved efficiency.[24]

There are also several challenges surrounding the adoption of new processing methodologies. Capital investment is needed for new technologies given that existing facilities and supply chains are focused around batch technologies. Continuous processes are often more complex requiring greater control and effort in the early development stages to determine the key process parameters that must be controlled. Efforts are therefore required to overcome gaps in understanding and fundamental knowledge of the rate processes and transformations, then apply these to continuous process development. Ensuring the workforce has the required skills to develop and operate continuous operations has also been identified as a challenge: workers traditionally have a batch processing experience and mind-set. Another hurdle to be overcome is the adoption of continuous process submissions by the regulators including the FDA and European Medicines Agency (EMA) given the pharmaceutical industry is highly regulated and therefore traditionally risk averse and conservative in adopting new manufacturing technologies. Quality and consistency monitoring is a further consideration[25] whereby existing methods may change to more flexible methods to accommodate continuous processing, for example using in-line PAT for monitoring of critical quality attributes (CQAs).

New motivations in the pharmaceutical sector include drives such as those for personalised medicines requiring the need of flexible and small scale

manufacturing technologies. The application of continuous processing provides an opportunity to deliver some of these targets through scale down and scale-out of continuous platforms such as continuous micro reactors. Scale down offers the possibility to produce small amounts of specific materials when required, hence no excess production and storage of high value APIs, alongside offering an opportunity for mobile manufacturing systems allowing the distribution and production of pharmaceuticals at the point of use, hence improving access to specific medicines in remote places. One of the more feasible approaches for companies is to start and adapt, or investigate, continuous processing in the early stage of new drug development schemes prior to commencing manufacture.

It is also worth noting that continuous manufacturing may not be applicable or best suited to all processes. The current challenge also lies in modelling and experimentally validating the kinetic and physical parameters of processes within continuous systems to make informed decisions as to when continuous methods or technologies are more suited for the desired production process. Developing research in this area and elevating the number of examples and studies will help to establish design strategies and workflows for best choice of processing equipment and methods. This will help to accelerate the adoption of continuous manufacturing as a suitable route to improved products over the adequate batch processes that are currently relied upon. These workflows will provide guides, directing educated decisions, to keep specific unit operations within the manufacturing chain as batch or to convert them to continuous.

1.3   Basic considerations for crystallisation

Crystallisation is a separation and purification process and can be broadly defined as a phase change in a liquid which produces a crystalline material. Crystals are highly regular repeating structures and during formation they drive out solid impurities present in solution. There are several different methods by which crystallisation can be induced including evaporation, cooling, melt and anti-solvent. Often methods are combined to improve crystallisation control.[26-28] Solution crystallisation is widely used in the pharmaceutical industry although other methods are available. There are two main stages of crystallisation; nucleation and crystal growth, both are dependent on supersaturation as the primary driving force.

1.3.1 Supersaturation and control

When a solution is saturated, it is in equilibrium with the solid solute, the chemical potential (μ) of the solution phase (μ_L) and the solid crystalline phase (μ_S) are equal so the difference in chemical potential, at equilibrium, is zero. This can be described by:

$$\Delta\mu = \mu_L - \mu_S = 0$$

Eqn. 1.1

For a given composition and conditions (constant temperature and pressure) when $\Delta\mu$ is positive, the solution is undersaturated and dissolution is the thermodynamically favoured process. Under conditions where $\Delta\mu$ is negative, the solution will be supersaturated and nucleation and crystal growth can take place to return the system to equilibrium.[29]

The chemical potential is defined by the standard potential (μ_0) and the activity (a), this allows the driving force for crystallisation to be expressed in terms of the supersaturation:

$$\mu = \mu_0 + RT \ln a \qquad \text{Eqn. 1.2}$$

where R = gas constant (8.314 J mol^{-1} K^{-1}), T = temperature, a = activity of a saturated solution. This can be expressed as:

$$\frac{\Delta\mu}{RT} = \ln\left(\frac{a}{a^*}\right) = \ln S \qquad \text{Eqn. 1.3}$$

where S is:

$$S = exp^{\left(\frac{\Delta\mu}{RT}\right)} \qquad \text{Eqn. 1.4}$$

The two most common ways to express supersaturation are the supersaturation ratio (S) defined by:

$$S = \frac{C}{C^*} \qquad \text{Eqn. 1.5}$$

where C = solution concentration and C^* = equilibrium solution concentration (at a constant temperature and pressure) and the relative supersaturation (σ) given by:

$$\sigma = \frac{C - C^*}{C^*} \qquad \text{Eqn. 1.6}$$

There are numerous methods to control supersaturation within a solution,[30,31] the two most common ways in chemical processing are cooling (via temperature) and anti-solvent. These methods are commonly preferred due to the ability of providing greater control over supersaturation compared with evaporative crystallisation. Specific systems will nucleate at varying levels of supersaturation and this physical process is very sensitive to a wide range of

process conditions including cooling rate, agitation, temperature and impurities.[29]

In a cooling crystallisation the temperature difference from the point of solubility, T_{sol}, to spontaneous nucleation, T_{nuc}, (point of supersolubility) is known as the metastable zone width (MSZW), ΔT, and can be defined by:

$$\Delta T = T_{sol} - T_{nuc}$$
Eqn. 1.7

MSZW measurements can be used to study the effects of changing various parameters on the nucleation kinetics of the crystallisation process, hence providing information for crystallisation control. MSZWs can be measured in various ways including imaging, turbidity and focused beam reflectance measurement (FBRM).[32,33] Figure 1.4 shows a typical phase diagram illustrating a cooling crystallisation, highlighting the typical trajectory for a spontaneous nucleation and subsequent growth of particles. Starting from a region of undersaturation (where the temperature is greater than the solubility temperature) and with applied cooling, the system moves through the solubility into a labile region where the solution is supersaturated. Once supersaturation reaches a critical level (the supersolubility or metastable boundary) nucleation occurs before the resulting nuclei and subsequent crystals follow a trajectory of crystal growth. The difference in temperature between the point of solubility and the point of nucleation is known as the MSZW.
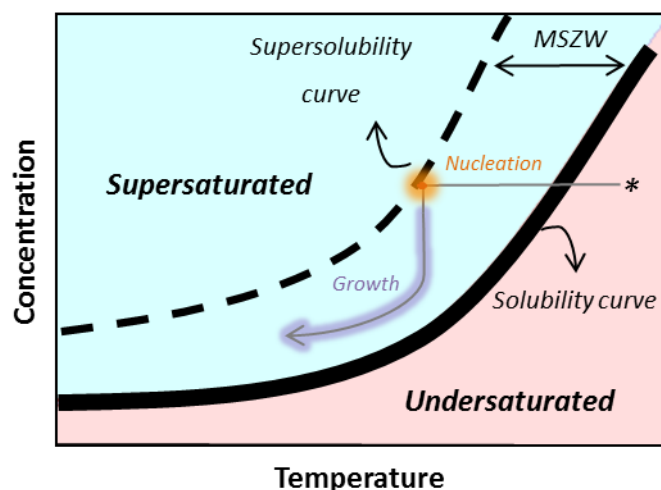
Figure 1.4: Diagram illustrating a typical solution cooling crystallisation process. Following the path (—) from * (a *T* > solubility i.e. a point of undersaturation), with applied cooling, the system moves through supersaturated regions to a point of nucleation(●), before following a trajectory of crystal growth(—). Adapted from Reference [29].

The MSZW defines the boundary between the labile solution and where spontaneous nucleation can occur. Metastable solutions are supersaturated but primary nucleation may not occur, however growth of crystals and/or seed particles will occur in this region. The MSZW is dependent on the nucleation kinetics and can be influenced by several parameters[34,35] including; temperature profile, rate of generating supersaturation, solution history, presence of impurities, fluid dynamics, agitation and volume.

General rules have been outlined in the literature in terms of the impact of equipment design and process operation can affect the MSZW during cooling and anti-solvent crystallisations. An example of these general trends include increasing agitation (leading to intense mixing and/or higher sheer) and slower cooling rates resulting in the MSZW narrowing.[36-39] A recent investigation on MSZW performance illustrates a volume dependency, with larger volume systems providing a narrower MSZW owing to the stochastic nature of nucleation.[40] However, overall nucleation theory has developed little in the last 50 years, partly due to the challenges in measuring rapid

processes at the molecular scale.[41-43] As a consequence there are no first principles kinetic expressions to describe nucleation.

1.3.2 Nucleation mechanisms

Nucleation occurs in a supersaturated solution where components start to combine together forming stable, critical nuclei, which act as sites for crystal growth. Primary and secondary nucleation are the two reported mechanisms by which stable nuclei are produced (Figure 1.5). Primary nucleation refers to all cases of nucleation (homogeneous and heterogeneous) taking place in systems where no crystalline matter is present i.e. describing the first nucleation event from a supersaturated solution. Secondary nucleation refers to the nucleation that is induced as a result of crystals present in solution (seeding and attrition).
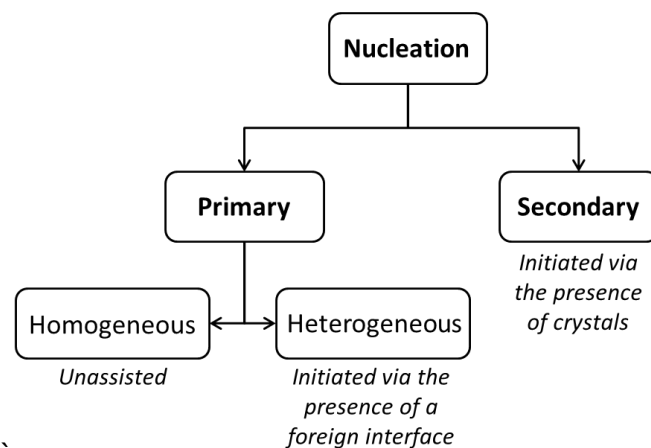
Figure 1.5: Diagram illustrating the various types of nucleation. Adapted from Reference [44].

Primary nucleation takes place though one of two main pathways; homogeneous nucleation or heterogeneous nucleation. During homogeneous nucleation the fusion of components in a 'clean' solution (one which contains

no foreign particulates) takes place randomly, spontaneously and unaided, whereas in heterogeneous nucleation the presence of foreign particles act as sites for nucleation. Heterogeneous nucleation is most common as many systems will likely contain species such as bubbles or impurities. These foreign entities reduce the free energy required for nucleation and hence nuclei appear more readily, and at lower supersaturations, than would be the case for homogeneous nucleation.

Nuclei in a saturated solution continuously form and re-dissolve. In a supersaturated solution the molecular movement is much more restricted, there are more solute molecules/clusters present, and the formation of nuclei is more favourable. Stable nuclei form due to coagulation of many unstable nuclei to form clusters; however these clusters require growing above a certain critical size before they can survive in solution. Assuming these clusters are spherical droplets with a radius r, the excess free energy (ΔG) for their formation can be calculated by the sum of the enthalpy required for creating a new surface and the enthalpy of condensation of the resulting sphere,[29] described by:

$$\Delta G = \Delta G_s + \Delta G_V = 4\pi r^2 \gamma + \frac{4\pi}{3} r^3 \Delta G_v \qquad \text{Eqn. 1.8}$$

The surface excess free energy (ΔG_s) is given by the surface area and the interfacial tension (γ), and the volume excess free energy (ΔG_V) is given by the volume of the droplet and the enthalpy of condensation per unit volume, where ΔG_v is the free energy change of the transformation per unit volume. Figure 1.6 shows a plot of ΔG_s, ΔG_v and ΔG as a function of r.
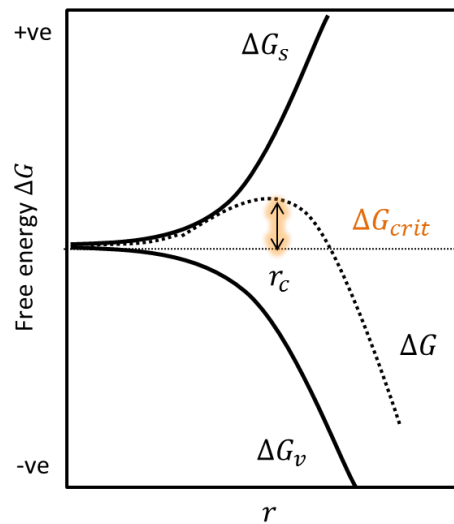
Figure 1.6: Energy diagram illustrating requirements of a critical nucleus. At sizes below r_c the process is energetically unfavourable, the free energy of the system increases during the addition of a new entity and nuclei will dissolve. When r_c is exceeded, the free energy of the system starts to decrease and the addition of more units will result in a further decrease in energy therefore a favourable state for progression and stabilisation of the nuclei. Adapted from Reference [29].

It can be seen a critical size (r_c) must be met before a system becomes energetically favourable for growth. The maximum value, ΔG_{crit}, corresponds critical size for the formation of a spherical cluster. Where the change in free energy with respect to size equals zero r_c can be expressed as:

$$r_c = \frac{-2\gamma}{\Delta G_v}$$ Eqn. 1.9

The energy needed for the formation of a critical nucleus can then be calculated, using equations 1.8 and 1.9, using the following expression:

$$\Delta G_{crit} = \frac{16\pi\gamma^3}{3(\Delta G_v)^2} = \frac{4\pi\gamma r_c^2}{3}$$ Eqn. 1.10

The rate at which these nuclei are formed, i.e. number of nuclei formed, per unit volume, per time, is known as the nucleation rate, J. It is dependent on

supersaturation and a number of other factors including temperature. Modelling and prediction of nucleation is a highly complex process. Table 1.1 summaries some of the empirical relationships commonly used in the literature to describe nucleation kinetics.

Table 1.1: Commonly used nucleation expressions. Adapted from 45.

Nucleation	Expression	Comments	Ref.
Primary	$J = k_b S^b$		46
Homogeneous	$J = A\,exp\left[\dfrac{-16\pi\gamma^3 v^2}{3k^3 T^3 (\ln S)^2}\right]$		29
Heterogeneous	$J = k_{b\,het}\,exp\left[\dfrac{-16\pi\gamma^3 v^2 f(\psi)}{3k^3 T^3 (\ln(\sigma+1))^2}\right]$	$f(\psi)$ corrects for nucleation on foreign surfaces	47
Secondary	$J = k_b S^b \mu_2$		48
	$J = k_b S^b \mu_3$		49
	$J = k_b\,exp - \dfrac{\Delta E_G}{T}\sigma_s^b \mu_3^k$	k_b temperature dependent	50
	$J = k_b \sigma_s^b \mu_3 (L_{min})^j$	L_{min} minimum size for crystals to take part in collisions causing secondary nucleation	51,52
	$J = k_b S^b N^1 \mu_2^j$ $J = k_b S^b N^1 \mu_3^j$	Includes crystal agitation and crystal-crystal effects	53

Classic nucleation theory assumes that nucleation takes places instantaneously once a certain level of supersaturation is reached. This is not necessarily the case, nucleation can occur sometime after a given system has reached a supersaturation value at isothermal conditions. This is known as the induction time, t_{ind}, and can be describe as follows:[29]

$$t_{ind} = t_r + t_n + t_g$$ Eqn. 1.11

where t_r = time for system to reach an isothermal state, t_n = time for critical nucleus formation, t_g = time for nucleus to reach a detectable size. Measurement of these individual stages (t_r, t_n and t_g) is extremely difficult experimentally due to limitations in detecting small nuclei, therefore induction times are normally measured from the time at which the desired supersaturation is reached to the point where nuclei in solution are first detected. In reality this is an over estimation of induction time as nucleation will have occurred sometime before the present of particles can be identified.

Classic nucleation theory (CNT) suggests that nucleation occurs via a step wise process, by which a single nucleus is added to a unstable cluster at any one time (as the simultaneous collision of the required number of nuclei is an unlikely event).[29] Once the unstable cluster reaches the critical size it becomes stable and can grow into a large crystal. Recent work suggests that nucleation occurs via a 2 step model.[54] Here solute molecules aggregate to form fractional clusters, in the first stages of nucleation, later rearranging into a stable structure (Figure 1.7).
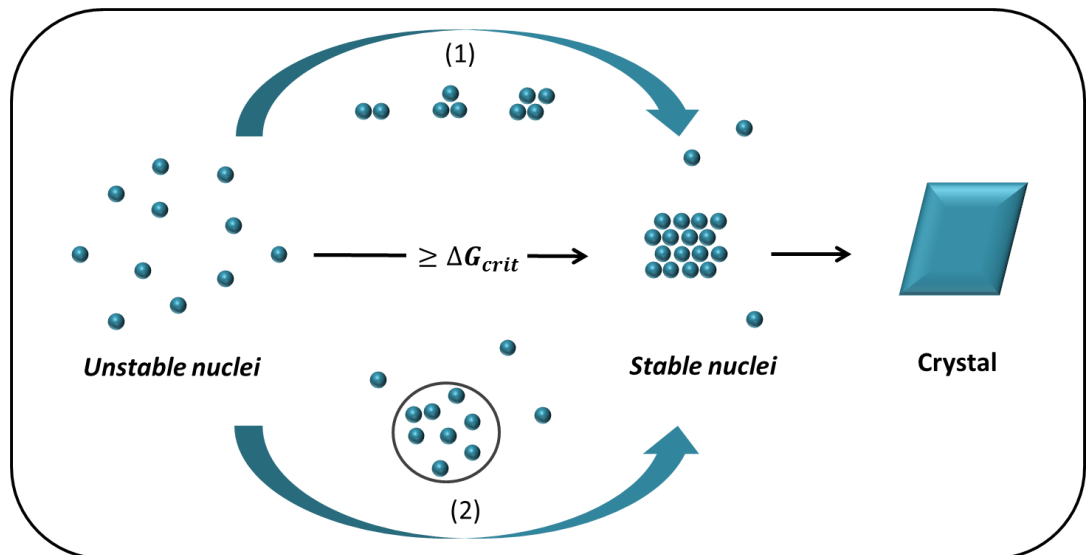
Figure 1.7: Diagram illustrating the two main nucleation theories. Classic (1) suggests a stepwise addition of molecules to an unstable regular lattice cluster before reaching a critical size whilst 2-step (2) nucleation proposes molecular aggregates from and once a critical size is reached molecules rearrange into a regular lattice. Adapted from Reference 54.

Secondary nucleation occurs when there are parent crystals present in a solution. These parent crystals induce the formation of new nuclei, through several methods, typically contact nucleation. Crystals can impact with the vessel walls, the impeller, or each other and break depositing smaller crystals and/or nuclei into the bulk solution (collision breeding or microattrition). Fluid shear forces may also be sufficient to produce secondary nuclei from a crystal surface[48] (surface breeding). Proposed mechanisms are shown in Figure 1.8. Secondary nucleation occurs at lower supersaturations than primary nucleation therefore having its own characteristic metastable zone width (Figure 1.9). Secondary nucleation is generally an unfavourable process during crystallisation as it can lead to broad distributions in crystal sizes. However, in some cases secondary nucleation can be desired when the production of new nuclei in solution, having the same characteristic of the parent crystals, is targeted, for example seeding processes.
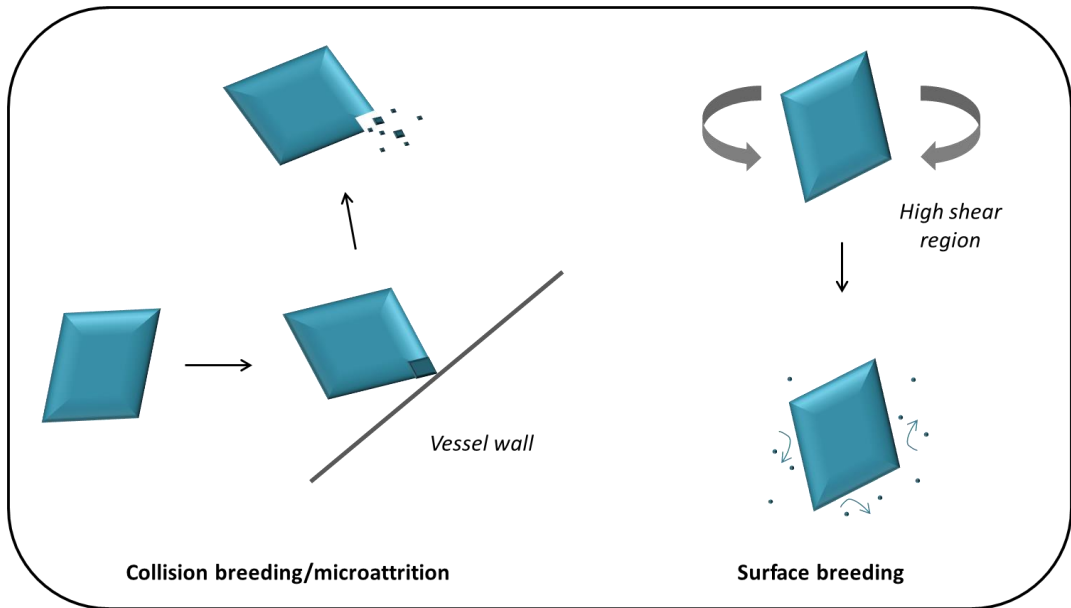
Figure 1.8: Schematic illustrating the mechanisms of secondary nucleation. Crystal impact with vessel wall (left) depositing smaller crystals and/or nuclei into the bulk solution. Fluid shear forces (right) produce secondary nuclei from a crystal surface.
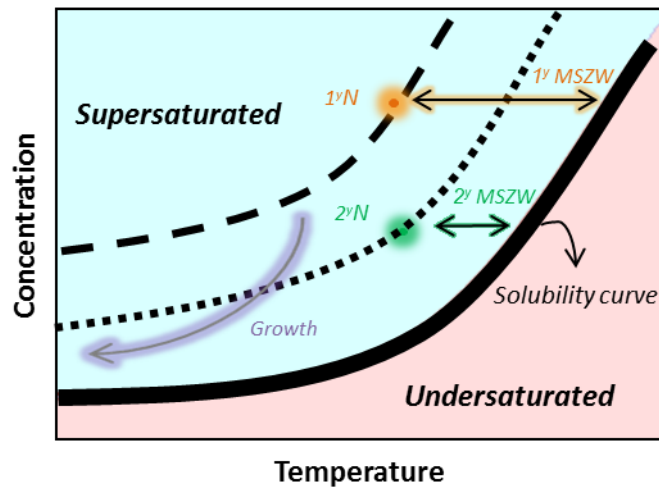
Figure 1.9: Phase diagram for a cooling crystallisation. The MSZW for primary nucleation (1^yN) highlighted in orange, the MSZW for secondary nucleation (2^yN) highlighted in green, and the trajectory and area within the phase diagram where crystal growth will occur is highlighted in purple. Adapted from Reference 55.

19

Secondary nucleation is the most common mode of nucleation in industrial crystallisation processes.[56] To ensure that product characteristics are similar e.g. the same polymorph is obtained, often a small amount of product is purposely left in the vessel as seed material prior to the next batch. Even when seeding or secondary nucleation is not the target for the process, it can often take place due to small crevices in reactor walls trapping previous product. Secondary nucleation can be advantageous to allow the system to progress and nucleate with the same polymorph, but it can also lead to processing issues such as fines, leading to large PSDs, if supersaturation levels are not controlled, thus resulting in complications in downstream processing.

Nucleation is the kinetically controlled first step to a crystallisation process and remains one of the most challenging steps in a crystallisation process to understand characterise and control. Predictions and understanding of this phenomenon are based on empirical formulas, and generally control is achieved by varying experimental operating conditions until the desired target response is achieved. Due to the complex nature in prediction and control of nucleation, industrial applications of crystallisation are often designed around avoiding spontaneous primary nucleation and rely upon seeding strategies to control product outcome.

1.3.3 Crystal growth and control

Crystal growth is the latter stage of crystallisation following nucleation, where the nuclei grow into larger, stable, faceted crystalline particles. As long as the system remains in a supersaturated state, crystals present will continue to grow, the rate of this is dependent on an array of factors including impurities, supersaturation, temperature, agglomeration and agitation.

There are many different models and theories around the mechanism of crystal growth. In general there are 2 stages of growth, firstly solute molecules diffuse from the bulk solution and adsorb onto the crystal surface,

before progressing to the second stage which involves the molecules integrating themselves into the crystal lattice; both stages taking place under different concentrations (Figure 1.10). The concentration (C_i) between the diffusion and adsorption layers, is not easy to measure experimentally so an overall driving force of C-C* is often used.[29]
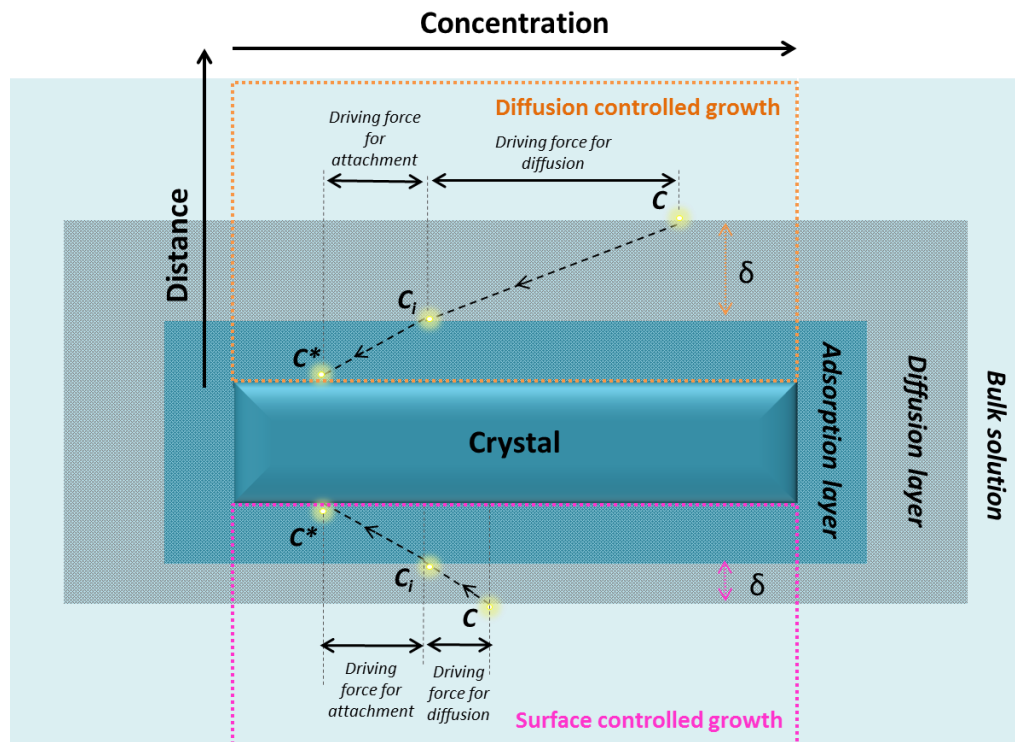
Figure 1.10: Schematic of the crystal-solution interface of a growing crystal. Molecules from the bulk solution move through the diffusion layer to reach the adsorption layer. Once here they will mitigate over the crystal face before linking to the crystal lattice at a position where the attractive forces are the greatest. C, Ci and C* denote the bulk, crystal-solution interface and equilibrium solubility respectfully and δ is the diffusion layer thickness.

If the growth rate is limited by the transfer of molecules through the diffusion layer, it is said to be diffusion or mass transfer limited, whereas when growth is primarily limited by resistance of attachment at the growth surface, this is known as surface integration controlled growth. When diffusion limited growth

occurs, this effects the thickness of the diffusion layer, therefore special attention to mixing and fluid flow around the crystals needs to be made.

The simplest expression describing crystal growth is the rate of increase of length, expressed as follows:

$$G = \frac{dL}{dt}$$

Eqn. 1.12

However, crystal growth equations can also incorporate overall driving force and temperature effects. For example:

$$G = A \exp\left(\frac{-E_G}{RT}\right)\Delta C^g$$

Eqn. 1.13

where G = growth, L = length, A = a constant, E_G = activation energy, g = order of overall crystal growth. Many other growth models and expressions are used, a summary of the common models utilised can be found in Table 1.2.

Table 1.2: Commonly used growth expressions. Adapted from 45.

Mechanism	Expression	Comments	Ref
Size independent growth	$G = k_g S^g$		57,58
Size dependent growth	$G = k_g S^g (1 + \gamma L)^p$ $G = k_g S^g (1 + \gamma L)$		59
Power law growth	$G = k_g S^g L^p$		60
(BCF) Growth model	$G = \frac{k_g}{k_{bcf}} S^2 \tan h \left[\frac{k_{bcf}}{\sigma_s}\right]$	Effects of surface defects included	61
Arrhenius growth expression	$G = k_g exp\left[-\frac{\Delta E_G}{RT}\right]\sigma_s^g$	Temperature dependent k_g. Semi-empirical relationship	56

A recent investigation[62] on the effect of supersaturation on the growth rate of indomethacin, showed significant deviation from model predicted growth rate coefficients at supersaturations below 6 (Figure 1.11). Results indicate, when $S > 6$, growth of indomethacin was diffusion controlled and the model could accurately predict growth rate coefficients. Below this threshold, significant deviation from the model was observed and the growth process was thought to be surface controlled. In this particular study, the crystal surface was also investigated; results indicated that seed crystals possessing lower energy surfaces had a reduced growth rate. This highlights the need to understand when growth processes are diffusion or surface dominated. This knowledge will inform model choice for prediction, together with understanding the impact of surface properties on crystal growth.
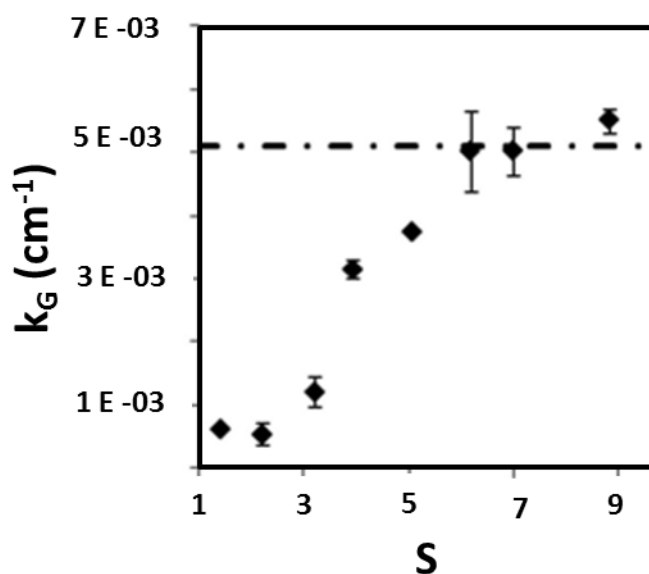
Figure 1.11: Indomethacin growth rate plotted as a function of supersaturation. The dashed line overlaid on the graph represents the predicted growth rate coefficient. [62]

Seeding is a common method used to control the growth of crystals as it decouples nucleation from growth process and allows operation at low supersaturations away from the metastable limit. Seeding strategies include using model based approaches[63] and methods based on supersaturation control.[64] Typical techniques for the production of seeds include milling, high shear mixing, blending, grinding, and sieving. These processes can significantly impact the properties and quality of the seed material, for example milling can expose hydrophobic surfaces[65] introduce disorder and amorphous material,[66] induce phase transformations[67] and create surface roughness, which in turn will have an impact on the growth process and resulting product.

An accurate understanding of how crystal growth processes proceed is an important aspect to crystallisation process development and prediction. The possession of reliable models facilitates the design of processes for target end crystal sizes required for downstream processing and/or target therapeutic effect. Poor control and understanding can lead to a variety of problems for API manufacture and formulation.

1.4 Desired objectives from crystallisation processes

To maximise the end product and manufacturing efficiency there are a variety of objectives desired from the crystallisation, Figure 1.12 illustrates target outcomes from crystallisation process development in order of importance.[68] The most critical attribute of a commercial drug product is chemical purity as this dictates patient safety on administration. Following this the next frequently required properties are physical phase purity, i.e. the desired solid form, and specifications on crystal size and shape (depending on impact to bioavailability and chemical stability). As previously discussed the bioavailability can be dictated by the solid state arrangements and the PSD.[69] If variations in physical form or PSD significantly impacts on the therapeutic performance of the drug substance, there is a regulatory requirement to manufacture the product within a certain specification to ensure consumer safety and drug efficiency.[70]
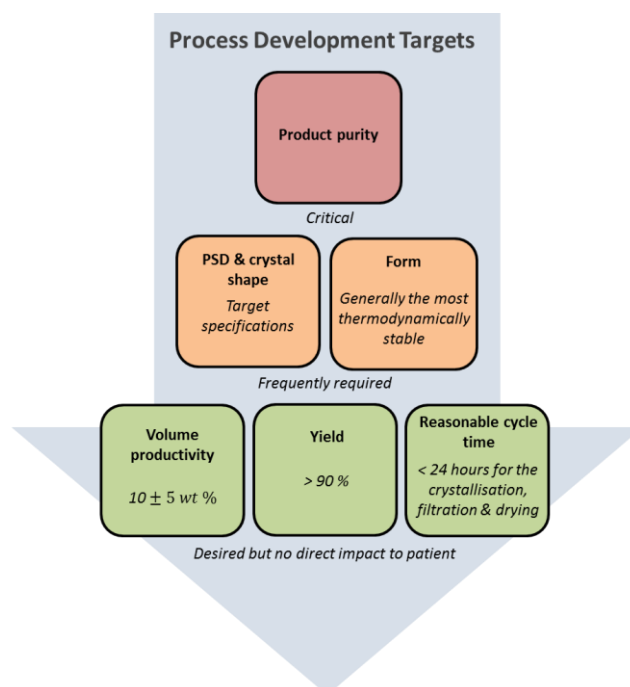
Figure 1.12: Target outcomes of pharmaceutical crystallisation process development. Outcomes are listed in order of priority, from critical properties to those desired for operation efficiency.

Once product attributes that dictate therapeutic requirements are met from a process, optimisation of other parameters, including product yield and cycle time, becomes a focus in order to maximise efficiency and productivity. Whilst these desired targets have no direct impact on the patent, drivers for economically viable processes in a highly cost aware and environmentally friendly world become of significant importance for realistic and deployable manufacturing processes.[68] Table 1.3 shows the product attributes resulting from the crystallisation process and the secondary effect on the API and production performance.

Table 1.3: Measurable particle attributes. Attributes can affect therapeutic performance and processing ability, and may be analysed by a variety of techniques. Adapted from Reference 19.

Attribute	Secondary effect	Methods of analysis
Particle size	Dissolution rate/profile, bulk powder flow, compactibility, filterability,	FBRM, Dynamic light scattering (DLS), microscopy, laser diffraction
PSD	Dissolution rate/profile, filterability, bulk powder flow, compactibility, processing consistency,	FBRM, DLS, laser diffraction , microscopy
Morphology	Filterability, mechanical strength, bulk powder flow, compactibility, processing consistency,	Microscopy
Polymorph	Physical properties, melting point, solubility, bioavailability	XRPD, DSC, spectroscopy
Surface	Bulk powder flow, agglomerate/aggregation formation, growth rate	Microscopy, contact angle

There are many routes by which crystalline material can be tailored to result in more favourable characteristics, for example needles and flakes are the most difficult to handle from a processing point of view, they are difficult to filter, dry and formulate. In addition, crystal morphology can be manipulated through choice of solvent,[71] tailor made additives,[72] and surfactants,[73] as illustrated in Figure 1.13. Six different morphologies of calcium carbonate are shown, each of which were obtain through crystallisation in different solvents.

Figure 1.13: Electron microscopy images of CaCO$_3$ crystals. Images illustrate six different morphologies of CaCO$_3$ (a-f) obtained through crystallisation in different solvents.[74]

A complication when engineering crystal systems, using solvent choice as an example, is that changing solvent leads to a change in solubility of the material. This change in solubility can have drastic effects on crystal properties and yield. Unfortunately this interdependency holds true for several of the targeted process outcomes. This makes process development a challenging task, and more often than not one of compromise.

1.4.1 Particle size distribution

For drug absorption within the body there are several steps which take place when taking solid oral immediate release drug products. This includes release of the API, dissolution, and absorption across cell membranes to the circulation system. The rate at which the drug reaches the circulatory system is determined by the slowest step. For drugs with poor aqueous solubility the dissolution rate is often the rate determining step, therefore the rate determining step on drug bioavailability.[75] For dissolution rate limited drug products, particle size and PSD play an important role on this dissolution process.[76] From a bioavailability perspective, smaller particles are the preferred choice whereas from a manufacturing perspective these are difficult to handle and larger crystals are preferred.

In general APIs are more readily absorbed by the body with reduced particle size, as the surface area is increased thus increasing the dissolution behaviour. Depending on the targeted route of administration different particle sizes of API are desired, for example, with bronchodilator drugs which are inhaled, such as salbutamol, the particle size must be small enough to travel deep into the lung but also large enough to be retained in the body. Pharmaceuticals commonly require processing of the bulk crystallisation material to obtain the features desired of a final dosage form, this often involves the adjustment of the drugs particle size due to the lack of particle size control during the crystallisation process. Where the crystallisation process fails to deliver the desired particle size, size reduction techniques are deployed routinely,[77] Figure 1.14 highlights some of the common routes taken to manipulate particle size.
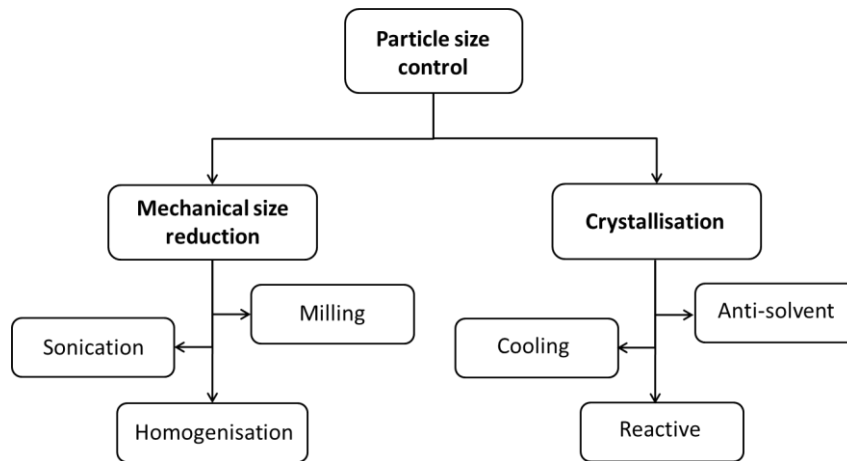
Figure 1.14: Routes to controlling particle size. Flow diagram illustrating various routes taken to tailor particle size.

Downstream secondary manufacturing processes can be significantly hindered by poor control of the PSD during the crystallisation process, for example, uncontrolled secondary nucleation during crystallisation can result in the production of fines, a population of smaller particles co-existing with the larger bulk population of particles. These fines can lead to broad and bimodal PSDs which can significantly increase the filtration time and lead to blockages during slurry extraction. This can not only influence the product quality but also has severe implications to the process economics. Figure 1.15 and Figure 1.16 show examples of images and particle size data for good and poor control over size during crystallisation where the target output is a uniform size of 50 and 300 μm respectively.
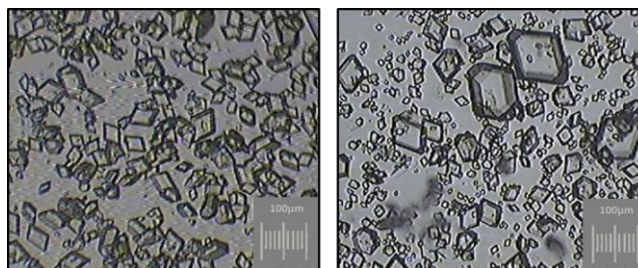
Figure 1.15: Microscope images of a crystals. The images show crystals with reasonably uniform PSD (left) and a poor PSD (right).
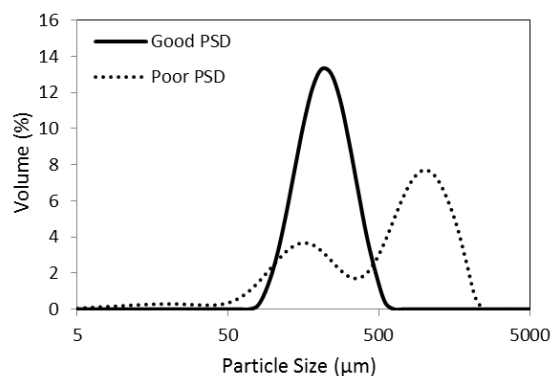
Figure 1.16: Examples of measured particle size distributions.

Fines tend to arise from either secondary nucleation or attrition. Secondary nucleation can occur when crystals already present in a saturated solution have a catalysing effect on the nucleation process; here nucleation is induced again but at supersaturations lower than spontaneous nucleation. Controlled crystal growth will reduce the likelihood of spontaneous secondary nucleation.[78,79] Different approaches have been taken to try and eliminate fines, many of which are based upon improved crystallisation control. Temperature cycling is one such strategy in which fines can be removed during cooling crystallisation.[79] Here heating and cooling cycles are utilised which encourage the dissolution of fine material and the growth of larger particles, a schematic representation of the phase diagram during this procedure is shown in Figure 1.17. After a primary nucleation event and subsequent growth phase has occurred, the system can be programmed to heat, thus dissolving any populations of smaller crystals, before another cooling phase is initiated. Repetition of these cycles can be triggered from PAT responses if a population of small particles appear due to the supersaturation reaching the metastable zone for secondary nucleation. These cycles can be set to continue until the population of crystals have reached the desired size. A recent example of the improved particle size properties of a cardiovascular API using this technique, when compared to a standard linear cooling profile, is shown in Figure 1.18. Here optical and SEM

images show larger crystals, with minimal fine material, when a temperature cycling methodology is applied.
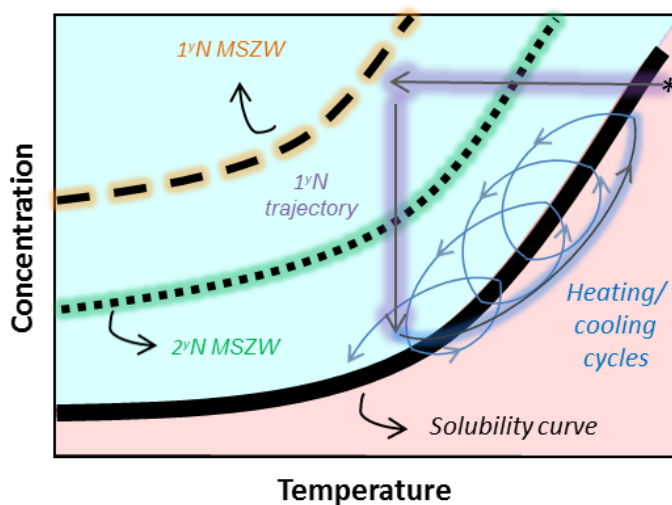
Figure 1.17: Cooling crystallisation phase diagram. Schematic illustrating the temperature trajectory (blue line) followed during a temperature cycling crystallisation approach for particle size control.
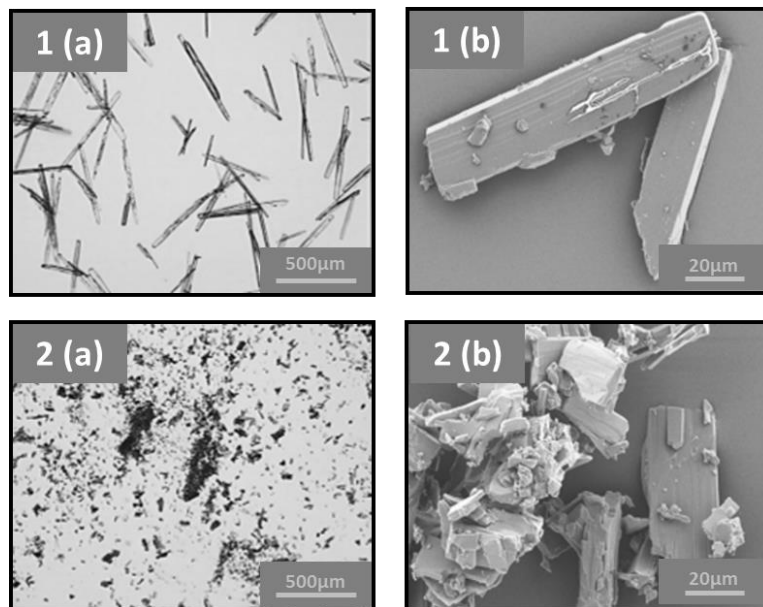
Figure 1.18: Effect of temperature profiles on crystal product. Optical (a) and SEM (b) images of crystal products obtained from temperature cycling, 1, and linear cooling, 2.[80]

Fines can also appear as a result of the breakage of crystals during crystallisation is known as attrition. This occurs due to collisional or fluid mechanical breakup, resulting from crystal-crystal, crystal-agitator and crystal wall collisions. The possibility of breakage depends on the mechanical strength of the crystal and the applied breaking forces, for this reason attrition can be somewhat more difficult to control.[79,81,82] Trouble regions for attrition within crystallisers are located in the areas of highest shear, typically around the impeller.

Aggregation and agglomeration are further processes that can occur during crystallisation and affect both the crystal growth and the resulting crystal size distributions. Aggregates being defined as clusters of loosely bound crystals easily disintegrated, whereas agglomerates are clusters where the crystals have become tightly interlocked with each other and only disintegrate under excessive force. These are generally unwanted processes during crystallisation due to their impact on growth rates and complications with processing and sizing, although in some cases its can be advantageous to manipulate this process to product particles with improved attributes. One such example of favourable agglomeration during crystallisation is that of spherical crystallisation. Here control over the agglomeration process results in spherical crystalline material with improved physical and mechanical properties such as flowability, compatibility and bioavailability.[83]

1.4.2 Particle size measurement

There are several common methods of measuring and characterising particle size distributions in solid materials. A list of the most common techniques used within industry can be found in Table 1.4. However, many techniques derive PSD from indirect measurements. Although, particles are complex three-dimensional shapes, they are commonly described by a single number, or a distribution of single numbers. For example, laser diffraction analysis systems report particle size as a volume equivalent spherical diameter

(VESD). As such, laser diffraction is particularly suited to spheres or similar, i.e. particles with a block like morphology. Indeed, laser diffraction fails to accurately describe particles with a large aspect ratio (Figure 1.19). Similarly FBRM methods are not particularly well suited to accurately describe large aspect ratio particles. Chord lengths are measured as the laser beam interacts with particle surface and reflected light is propagated back to the detector. When measuring particles, the most common chord length will be represented in the distribution. For needles this will be the shortest length, however for shorter aspect ratio particles this will be much closer to the diameter (Figure 1.20).
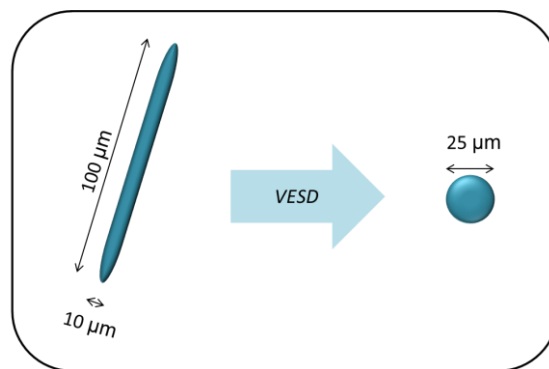
Figure 1.19: Volume equivalent spherical diameter. Schematic illustrating the VESD approximation of a large aspect ratio particle.
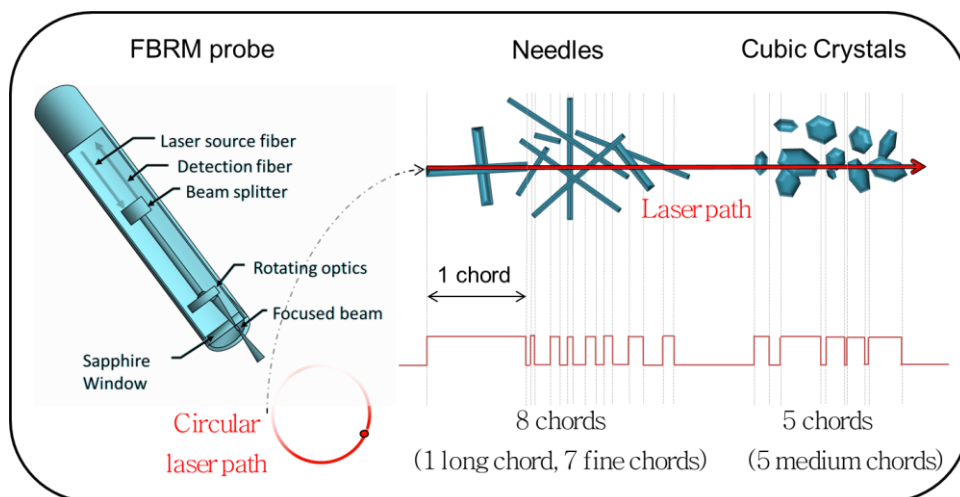
Figure 1.20: FBRM and chord lengths. Schematic illustrating chord length measurements made using FRBM.

Table 1.4: Particle size measurement techniques. Various measurement techniques exist for determining particle size, table summarises the common technologies.

Technique	Optimal shape	Description	Size range (µm)
Laser diffraction	●■	Measures light scattering. Interpretation results in a volume equivalent spherical diameter (VESD) PSD. Wet or dry dispersions.	0.1 – 5000
Light scattering	●■	Illumination through laser beam, visualisation of scattered light from particles (not an image). Wet dispersions.	0.001 – 2
Chord length (FBRM)	●■	Measures backscattered light from a focal point, results in a chord length distribution of sizes. Wet dispersions.	1 – 5000
Electrozone sensing	●■ ▬ ▬	Coulter counter principle. Provides number, concentration and volume of particles. Requires suspension in an electrical conducting solution.	0.4-1600
Imaging Microscope	●■ ▬ ▬	Visual images. Wet or dry. 2D information.	0.001 - 10000

● = Spherical, ■ = block-like, ▭ = needle-like, ▬ = plate-like

Sample preparation before sizing can be another challenge in obtaining accurate information on particle size. For example using techniques which require dry materials leads to manipulation of samples generated form slurries. During filtration and drying to obtain these dry samples particle attributes can change, for example particles maybe break or agglomerate. A similar scenario could also be observed during wet suspension techniques where agglomerates may already be present in the slurry samples and the

agitations provided during sizing methods may break up these particles. In both cases this can result in misleading information about the true state of particles during the process. From this point of view imaging is a key element in visualising and characterising the true state drug substance particles,[84] and coupling of this with other particle sizing techniques is a powerful tool for the characterisation of particle size.

Control over particle size remains a challenge within the chemical industries due to the difficulties in control and prediction of growth and other crystal processes such as attrition and agglomeration. The need for robust particle sizing techniques which are fit for purpose for the resulting product and for representative sizing information is also a challenge. The use of inline sizing techniques and with advancements in imaging for particle size provides improving characterisation alongside the coupling of technologies to further confirm and enhance information. Methodologies using feedback control strategies provide real time control and tailoring of particle size during the process allowing the generation of improved PSD and a means to control the process to result in the desired size.

1.4.3 Polymorphism and phase transformation

Polymorphism is the ability of a material to exist in more than one crystalline form, species are chemically identical but constituents arrange themselves differently within the crystal lattice. The most renowned example of polymorphism is probably carbon in the various forms including diamond and graphite, 5-Methyl-2-[(2-nitrophenyl)amino]-3-thiophenecarbonitrile (ROY) is another famous example owning to its highly polymorphic nature, having 10 known forms[85], six of these are shown in Figure 1.21.

Figure 1.21: Polymorphic forms of ROY.[86] Image showing 6 of the 9 different polymorphs of ROY.

Polymorphism is a wide spread phenomena that is observed in over half of all drug substances, and it has been suggested that the possibility of polymorphism should never be excluded regardless of how well studied, the American chemist Walter McCrone famously stated: "the number of forms of a given molecule is proportional to the time, money and experiments spent on that compound".[87] Advances in crystal structure prediction for polymorphism offer increasing opportunities to predict the number of multiple forms from molecular structure alone.[88.89] However these methods are extremely computationally intensive and are not yet able to cope with the typical complexity of many organic molecules and so knowledge of all relevant experimental forms in terms of process design and control is obtained through an experimental approach utilising extensive screening programmes.

The solid state defines physiochemical properties and different polymorphs exhibit different properties such as morphology, solubility, melting point, stability, dissolution rate, and hygroscopicity. This leads to different bulk performance properties such as tableting behaviour and flowability, therefore affecting the overall product manufacturing and therapeutic performance. Considering this, the characterisation of polymorphic properties and understanding the control of phase purity is a highly important during process development.

The most thermodynamically stable polymorph under ambient conditions is generally the most desirable form for commercial products owing to

thermodynamic stability and the associated elimination of the risk of phase transitions to more stable forms during manufacture or storage. In some cases, when the stable form may not meet the therapeutic requirements, it can be advantageous to produce and manufacture the metastable form (due to the higher dissolution rates which may be needed for rapid absorption and therapeutic concentrations within the body).[90] It is a common occurrence during crystallisation for a metastable form to appear first, this can be explained by Ostwald's rule of stages which states that within an unstable system the first transition state results from the smallest loss of free energy, the system need not necessarily transform to the most stable state first,[44] an explanation of this is shown in Figure 1.22.
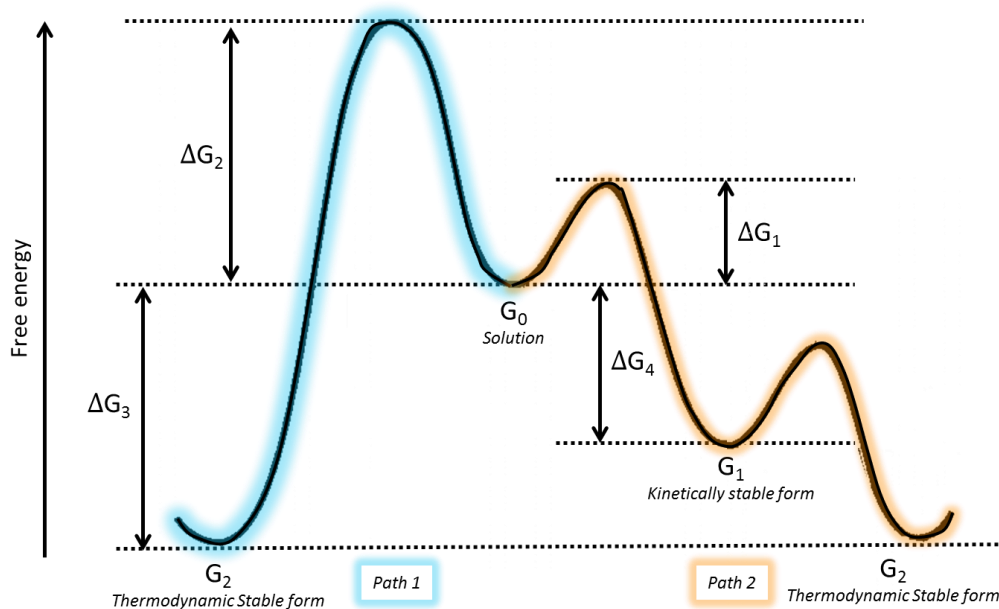
Figure 1.22: Energy diagram illustrating free energy changes during the formation of stable and metastable polymorphic forms from solution. When a solution is in a supersaturated state G_0, the activation energy required to convert to the kinetic form ΔG_1, is less than the energy needed for the solution to proceed directly to the stable form ΔG_2, hence often crystallisation processes follow path 2 by which the change in energy is smaller, rather than progressing via path 1. Overall the change in free energy from an unstable solution to the stable phase ΔG_3, is greater than the change to the metastable phase ΔG_4, i.e. G_2 has less free energy than G_1 therefore G_2 being the most stable form.

The most stable form will have the lowest Gibbs free energy, and hence lowest solubility in solution. In some cases there is a transition point where the stability of the thermodynamically stable and unstable forms can change. This scenario leads to a classification of the system i.e. systems are described as either monotropic or enantiotropic. For monotropic polymorphic systems, the solubilities do not cross over the temperature range, whereas for enantiotropic systems the solubility's will have a point of intersection, Figure 1.23. When dealing with an enantiotropic system the temperature at which the curves intersect is known as the transition temperature (T_t), here the relative stabilities of the forms in solution change. Pharmaceutical systems showing an enantiotropic relationship include glycine, D-mannitol, roxithromycin, carbamazepine and candesartan cilexetil.
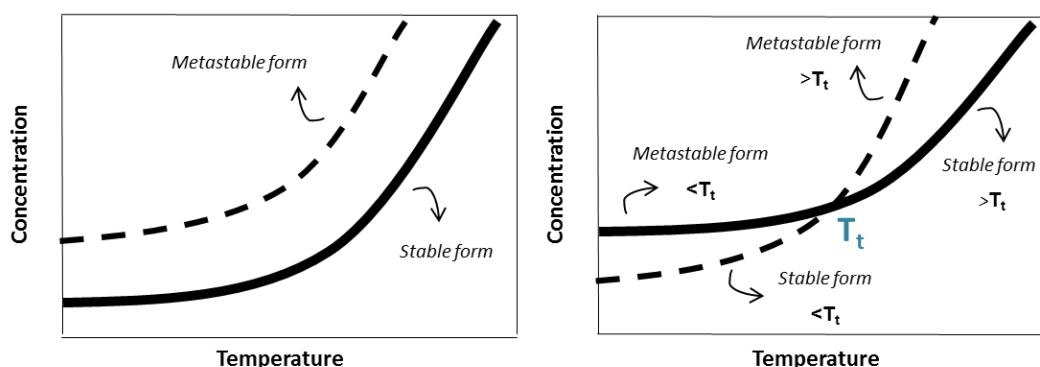
Figure 1.23: Solubility profiles of monotropic and enantiotropic polymorphic systems. The temperature dependant solubility of 2 polymorphs do not cross over the temperature range when the polymorphs are monotropically related (left), however when the polymorphs show enantiotropism (right), the temperature dependant solubility curves of both forms with intersect at a transition temperature and the relative stabilities in solution will change.

When working with metastable polymorphs in solution there is a possibility that a solution mediated polymorphic transformation (SMPT) can take place because the metastable form is always supersaturated with respect to the stable form. It is generally thought that the stable form nucleates on the

surface of the metastable phase and following a mass transfer controlled dissolution, the stable from grows as the metastable phase dissolves. An example of this during crystallisation of sulphathiazole is shown in Figure 1.24, were the SEM images allow clear observation of the stable phase growing on the metastable surface. The evolution and disappearance of each phase during the SMPT can be quantified using on-line spectroscopy such as Raman, an example of this is shown in Figure 1.25 during the SMPT of piracetam from form II to form III. Experimental conditions can be altered to retard or accelerate this process depending on the kinetics driving the transformation.
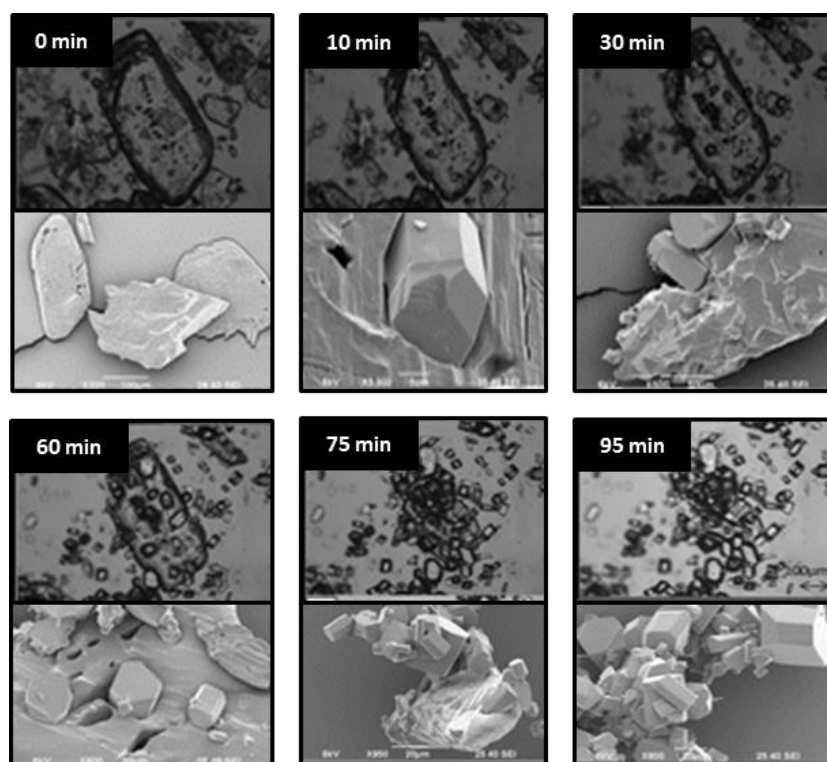
Figure 1.24: Optical microscope and SEM images of sulphathiazole crystals. Images illustrate the solution mediated polymorphic transformation of sulphathiazole.[91]
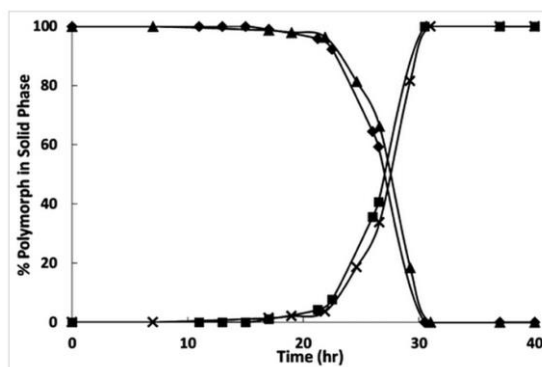
Figure 1.25: Solution mediated polymorphic transformation of piracetam. Raman spectroscopy data illustrating the solution mediated transformation of form II to form III piracetam.[92]

The ability of manipulating experimental conditions to selectively choose polymorphic outcome has drawn much attention[93-100] alongside that of polymorph prediction. Due to the current limitations in polymorph prediction, understanding and lack of real time process control, polymorphism is still one of the major challenges in pharmaceutical community.

1.4.4 Crystallisation process control

To be able to control a process, it must firstly be understood. A process can be described as well understood when firstly all critical sources of variability are identified, explained and managed by the process and secondly product quality a can be accurately and reliability predicted over the design space established for the materials used, process parameters, manufacturing, environmental and other conditions.[19]

The aim to develop a robust crystallisation process that reproducibly delivers the desired particle attributes is based on knowledge of variables such as the kinetics of nucleation, growth, attrition, agglomeration, and supersaturation, and these are directly linked to the input operation and system variables alongside choice of platform as can be seen in Figure 1.26. The area of crystallisation process control, in general, has advanced considerably in

recent years with advanced models describing kinetics and population balance models available from the literature as well as in commercial packages such as *gCrystal*. This has also been significantly improved due to the application of process analytical technology (PAT). PAT offers real-time on-line and in-line information on crystallisation variables to be monitored The utilisation of probes such as ultra violet (UV), Raman and IR can provide useful information such as levels of supersaturation, polymorph formation and/or transformation during the crystallisation process.[80,101-104]

Traditionally a quality-by testing (QbT) approach is used during process design and development, where product quality is determined by off-line testing at the end of the process. This method is undesirable as industrial scale batches, typically in the range of 10000 L vessels, produce tons of product and where specifications are not met the failed batches lead to environmentally irresponsible processing and substantial profit losses through wastage of materials, energy and labour etc. The Quality-by-Design (QbD) approach PAT offers provides the opportunity for process conditions to be adapted during operation, providing an environment to produce the desired outcome, before process completion.[103,105-107]
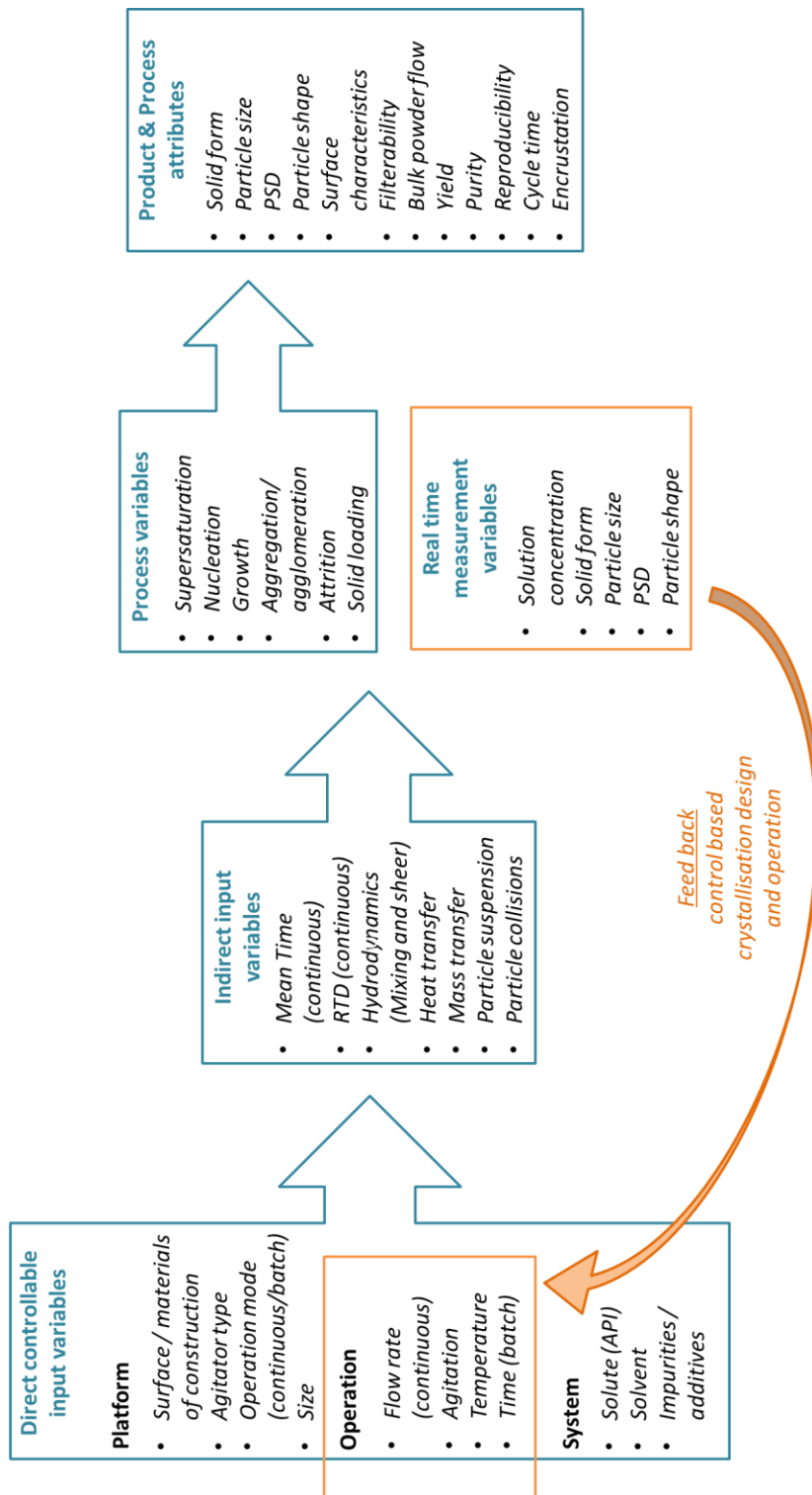
Figure 1.26: Relationship between process variable and product attributes. Flow diagram illustrating the dependency between input variables and process variables required for controlling product attributes.

1.5 Crystallisation technology and performance

The general definition of a crystalliser is a piece of apparatus that can create an environment suitable for the formation and growth of crystalline material. There are generally two modes of operation for crystallisation, batch and continuous. The most commonly used mode of operation for crystallisation is batch using stirred tank reactors (STRs), also known as stirred tank crystallisers (STCs). The most commonly utilised continuous crystallisation platforms are the mixed suspension mixed product removal (MSMPR) which is essentially a STC with a net flow entering and exiting the vessel, and the continuous stirred tank crystalliser (CSTC) which is a cascade of STCs in series. Alternative continuous platforms exist including continuous tubular designs such as the continuous oscillatory baffled reactors (COBRs) and segmented flow reactors (SFRs) which are often referred to as plug flow reactors (PFRs), however these platforms are not heavily in operation throughout the pharmaceutical industries. Continuous crystallisers are generally categorised into two groups, back mixed and plug flow. CSTCs are typically known to be back-mixed systems whereas tubular systems are often plug flow. A summary of the common platform designs, mixing and flow performance can be found in Figure 1.27.

Other types of crystalliser are also available including draft tube (DT) crystallisers, and static mixers. DT systems are commonly used for industrial crystallisation processes. Here crystallisations are typically carried out from the melt where a slow moving propeller circulates the magma of growing crystals within the vessel. The design allows larger grown crystals to essentially sediment in the vessel before being extracted and fines are recirculated where they are removed via different methods including heating or mixing with dilute feed. Despite being well characterised these systems are not always optimal for pharmaceuticals due to the nature of the design and operation, crystals may settle when they have grown typically resulting in larger crystal populations (500-1200μm), therefore not suitable where smaller size ranges are desired.

Basic crystalliser designs

Batch
STR

Continuous
MSMPR when n =1
CSTC when n > 1

Continuous
Tubular
(PFR's)

Examples of tubular platforms

Segmented flow reactor

Oscillatory baffled reactor

Immiscible fluid /
inert gas

Reactant mixture

Fluid oscillation

Stationary orificed baffles

Typical mixing performance

(a) *(b)* *(c)*

CFD flow patterns within a 200 L STR

CFD flow patterns within a DN30 baffled PFR

Typical RTD responses of continuous platforms

Concentration — Time

Dirac δ input

Concentration — Time

Typical CSTR response (backmixed)

Concentration — Time

Typical PFR response

Concentration — Time

True Plug flow response

Figure 1.27: Basic crystallisation platforms, mixing and flow performance.

System design and operation can have a huge impact on the hydrodynamic environments and resulting product attributes (previously described in section 1.4.4) and the adoption of continuous crystallisation platforms has drawn increasing interest in pharmaceutical industry. Process benefits may include more efficient heat transfer resulting from higher surface area to volume ratio, advanced mixing regimes providing a means to achieve plug flow, and improved scale-up capabilities hence reducing process development time from lab to manufacturing scale when compared to the equivalent batch operation.

There are several important features that a crystalliser should offer depending on the crystallisation process to be implemented. For example, with a cooling crystallisation the crystalliser should be able to provide efficient heat transfer during the cooling procedure. Poor heat transfer leads to temperature gradients resulting in supersaturation gradients within the bulk solution, thus potentially impacting product quality. For example supersaturation gradients can have a huge impact on the nucleation process influencing the formation of the undesired polymorphic form or causing variations in growth rates.

Mixing is the dominate factor effecting other process within systems (described in Figure 1.28) and its uniformity (in terms of uniform mass transfer and fluid hydrodynamics) is another major impact factor on a crystallisation process. Mixing should be sufficient to suspend any crystalline material that is formed and ideally the applied agitation should provide a homogeneous environment to allow for uniform growth of the crystalline material in addition to preventing regions of local high or low supersaturation. Large scale batch STCs can result in a non-uniform mixing environment (i.e. the extremely varied flow conditions, local velocities, shear rates and energy dissipations rates). An example of this is found in Figure 1.27 (a) and (b)[108] where the CFD flow patterns show highest velocity vectors and turbulent dissipation rates respectively around the impeller tip within a 200 L STC.
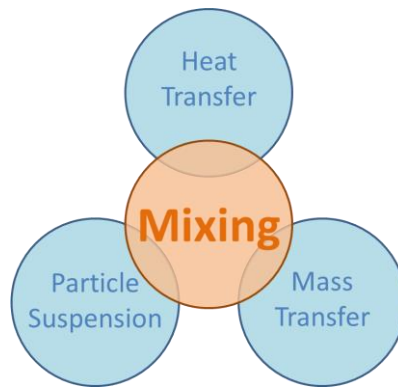
Figure 1.28: Dominant processes affected by mixing.

Tubular crystallisers can provide an improvement on environment uniformity in which the shear rates at any given position within the system are much closer to that of the average shear within the vessel. An example of such a comparison in shear rate uniformity is illustrated by Ristic *et al.*[109] Here the temporal shear rate distributions were compared for an impeller driven vessel versus oscillatory flow mixing. It was shown that at a given time within an STC, up to 90 % of particles remained within the low shear region (0 - 40 s^{-1}) the other 10 % residing in areas close to the impeller surface, baffle tips and shaft surface and experiencing shear from 40 - 10,000 s^{-1}. In comparison to oscillatory flow, the percentage of particles in low shear regions was dropped to below 10 %, Figure 1.27 (c). The volume average shear rate in oscillatory flow was also shown to be of nearly 1 order of magnitude higher than the STC arrangement, the STC operated at 800 rpm having a volume averaged shear rate of 20 s^{-1}, where the OBC operated at 10 Hz and 5 mm having a value of 179 s^{-1}.

These tubular designs are also attractive platforms due to their ability to operate at steady state and in near plug flow regimes. Plug flow is often the desired type of flow for continuous operation as it provides uniform mixing environments, ensures all fluid elements experience exactly the same conditions and that they spend the same amount of time within the reactor. Plug flow is only one of three characteristic types found in continuous systems; these are described in Figure 1.29.
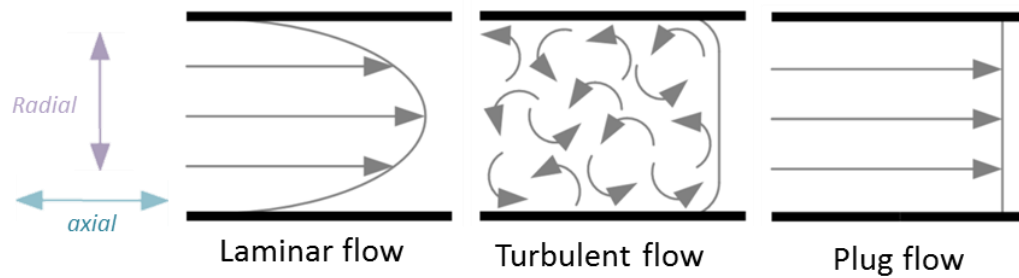
Figure 1.29: Types of Flow.

With laminar flows the velocity in the centre of the tube is equal to the flow of the incoming fluid, whereas the velocity of the fluid at the reactor walls is moving slower due to drag forces. This gives a parabolic velocity profile; hence there is a velocity gradient along the radial direction of the reactor, and fluid elements have different residence times. With turbulent flows the parabolic velocity profile becomes flattened, the velocity gradient becomes less, and there is less deviation between the residence times of the fluid elements. This consequently improves the homogeneity within the solution and components will have a more consistent experience throughout their time in the vessel. For plug flow to be achieved, three main criteria must be satisfied; the velocity profile in the direction of flow is flat i.e. velocity gradient is equal to zero; there is complete mixing in the radial direction; there is no mixing in the axial direction. Once plug flow is achieved all elements spend exactly the same time in the system and have a uniform process experience. Therefore this is an attractive environment to generate and grow crystals as in theory, given the same inputs, this environment would produce a population of identical crystals.

In reality true plug flow can never be achieved in any vessel but it has been shown, through residence time distribution (RTD) experiments, that "near plug flow" (or more correctly highly turbulent flow) dominates in tubular systems like the COBR[110-112] and SFRs.[113] RTD experiments involve the injection of a detectable tracer and monitoring of the exit concentration time response. The experimental curves can then be used to calculate deviation

from true plug flow. The characteristic tracer responses from continuous flow system are illustrated in Figure 1.27.

Computational fluid dynamics (CFD) alongside particle imaging velocimetry (PIV) are other commonly used methods to study flow within systems. CFD simulates and predicts the fluid performance in vessels whereas PIV is used experimentally to measure particle movement within a flowing system. Recent CFD reviews include the investigation of polyolefin in fluidised bed reactors,[114] modelling for drying processes,[115] and the investigation of heat transfer within impinging jet systems.[116] There are also several recent PIV reviews which cover a scope of activities including utilisation for complex and turbulent flows,[117] analysing bubble dynamics in microchannels,[118] and advancements and coupling of this method with other optical techniques to deal with highly concentrated particle suspensions.[119]

A summary of continuous crystallisation platforms and the systems investigated in the literature is given in Table 1.5. There are a variety of other platforms that can be used to create crystalline materials each with their own characteristic performance. Spray drying has been illustrated to create crystalline nanopharmaceuticals[120] the nature of the technique allows the formation of tiny droplets to be formed which are rapidly dried producing small crystals. Impinging jet and electrospray crystallisation are further examples of crystallisation techniques by which small crystallites are typically produced. Technologies such as these can then be coupled with other platforms to provide suitable environments for growth and hence control the final product size. For example seeds of L-asparagine monohydrate were generated using an impinging jet and fed into an STC for growth to the desired size.[121]

Table 1.5: Reported investigations using continuous crystallisation. Summary of literature showing various materials investigated using continuous crystallisation technologies

MSMPR		Cascade		Tubular	
System	Ref	System	Ref	System	Ref
Melamine phosphate	122	Aliskiren hemifumarate	123	Lipoic acid – nicotinamide	124
Paracetamol	125	Cyclosporine	126	API	35
Magnesium ammonium phosphate	127	Pharmaceutical intermediate	128	Ketoconazole, flufenamic acid, L-Glutamic Acid	129
Sodium bicarbonate	130			Calcium carbonate	131
Deferasirox	132			Benzoic acid	133
Adipic acid	134			Acetylsalicylic acid	135,136
Benzoic acid	133				
Cyclosporine	137				
Ascorbic acid	138				
Lactose	139				
Sugar	140				
Calcium carbonate	141				
L-Glutamic acid	142,143				
Potassium sulfate	144				

1.5.1 Process Scale-up

The scale up procedure from lab crystallisers to industrial scale is notoriously challenging. In general the more complex a process, the more challenges occur during scale up, and the ease of this is determined by the mixing in the system. The main concern when utilising batch STCs is that mixing cannot be linearly scaled due the complexity of agitation and heat transfer in these vessels. Most research in crystallisation process development is carried in small scale laboratory equipment (typically ≤ 0.001 m^3 vessels). At this scale mass and heat transfer is reasonable, the mixing is uniform, and the process is kinetically controlled.

Once processes are scaled up (to for example a 10 m^3 STC) the mixing is non-uniform and the process is mass or heat transfer limited. Specific heat transfer area decreases with scale due to the surface area to volume ratio decreasing as the vessel size increases (Figure 1.30). This means that cooling rates obtainable in large industrial scale STCs are significantly lower than those achievable in a lab scale. The poor heat transfer capabilities of STCs have been highlighted through the means of CFD where temperature gradients can be clearly seen moving from the impeller to the vessel walls.[145,146] This configuration and corresponding heat transfer performance also leads to temperature gradients and non-uniform process conditions impacting target product uniformity.
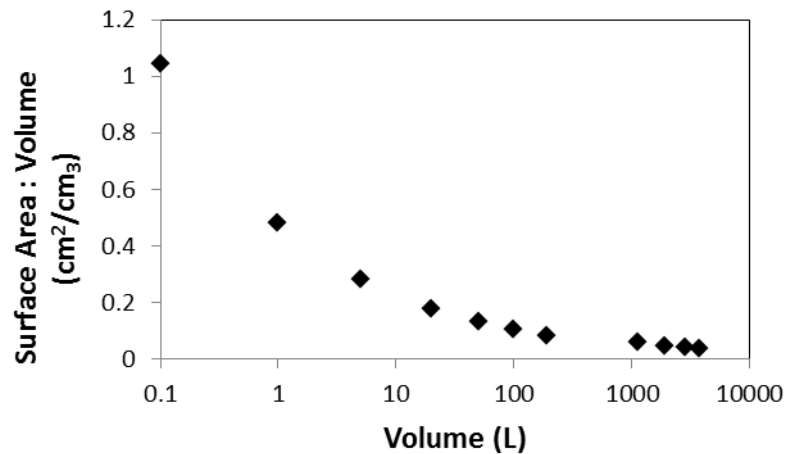
Figure 1.30: Relationship between surface area-to-volume ratio with increasing scale. Adapted from 147.

There are a number of rules, given parameters or tools that are used to scale up processes including; power density, Reynolds number, mixing time, volume-averaged shear rate, computational simulations, mass transfer coefficient, impeller tip speed, and averaged droplets size. The relationship between a number of these parameters, at a constant power density, is shown in Figure 1.31. Here the challenge with scale up can be observed. Using this diagram and focusing in the scalability of solid suspension as an example, it is shown that scaling up to a vessel 1000 times the volume results in the need of about 500 times more energy input to ensure similarity. Comparing this energy input to that of the relationship to shear, it can be observed that 100 times more energy is needed to ensure similarity, hence 5 times more energy has been added than needed, i.e. the shear would be significantly higher. High sheer regions can significantly impact on crystallisation processes, for example sheer regions around the impeller tips are known to act as areas for crystal breakages and hence increased likelihood of unwanted attrition process and associated problems with PSD control.
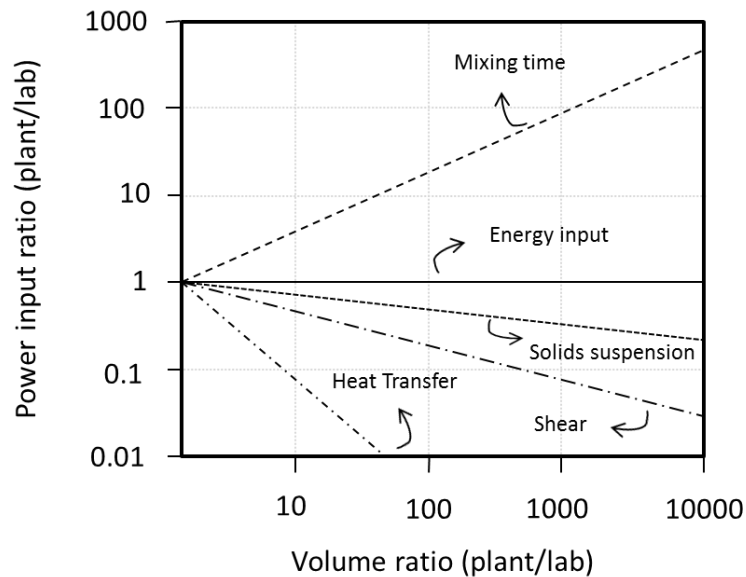
Figure 1.31: Scale-up relationships. Adapted from Reference 19.

Scale-up is dependent on obtaining sufficient understanding of the processing system (solute and solvent) and equipment used. Once understanding of process kinetics and platform performance is achieved the system can be taken through the scale-up procedure to manufacturing scale. However due to the interdependency in platform characteristics, process development stages are often required to successfully scale the process to full sized production.

The need for robust workflows, scalable platforms, system understanding and reliable scale-up procedures will facilitate the accelerated transition from lab scale systems (up to a few litres) to pilot and plant scale systems with minimal time and resources, ensuring time to market is minimised. It is worth noting that scale-up may not always be the desired route for manufacture, there may be cases where scale down is desirable. For example, the production of personalised medicines can require small quantities of drugs, on demand at remove places thus small scale platforms will be required. A further alternative to scale-up of processing is scale-out, where a multiple systems are operated in parallel rather than increasing one platforms geometry. This can be advantageous when scale-up is proving particularly

challenging. Operating on the same scale to which the CQAs are optimised for a process but in parallel, can provide a methodology to produce the desired quantities of material.

1.6   Motivation for research

Considering the basic principles outlined for crystallisation, the challenges around control and design of optimal processes in addition to the drivers for continuous processing in the pharmaceutical community, this research is focused on the development and control of continuous crystallisation using pharmaceutically relevant systems. The first experimental chapter, Chapter 4, focuses on understanding and characterisation of the DN15 COBC platform in terms of its mixing performance via RTD experiments. Here the axial dispersion model is used and comparisons of the experimentally measured responses are compared to previous reports. Chapter 5 involves a crystallisation study on L-glutamic acid, here the standard approach for oscillatory mixing scale-up was used via batch crystallisations to scope ideal conditions for continuous application before COBC experiments were completed. Due to some unexpected results obtained in Chapter 5, Chapter 6 is focused around designing and developing an improved batch system to provide increased similarity with the continuous platform and thus more accurate information on COBC behaviour. The final experimental chapter, Chapter 7, is focused on the application of a workflow towards continuous oscillatory baffled crystallisation. Here a seeded crystallisation investigation was completed with the polymorphic API carbamazepine.

Chapter 2. Aims & Objectives

2.1 Aims

The overall aim of the research described in this thesis is the investigation of continuous oscillatory baffled flow and its application to continuous crystallisation of pharmaceutically relevant compounds. The overarching goal is to establish polymorph control during continuous crystallisation. To achieve both understanding of the selected system, in terms of solvents and compounds, an understanding of the platform is essential. Four research areas are presented, outlining considerations needed during the transition from small scale crystallisations to pilot scale continuous oscillatory baffled crystallisation.

2.2 Objectives

Identification of the operating domain in terms of oscillatory conditions within a 25 m DN15 continuous oscillatory baffled crystalliser (COBC) and successive characterisation of the resulting flow performance under this operating space is a key deliverable of the research presented in this thesis. This includes the development and validation of a method for measuring and thus characterising the residence time distribution behaviours, in addition to the selection of a suitable plug flow model to allow comparisons with reported studies in other plug flow platforms.

Due to plethora of literature around crystallisations with L-glutamic acid, the commercial availability and associated low toxicity, this compound was selected for preliminary investigative studies within oscillatory flow. This work includes a focus on developing process understanding by identifying conditions required for polymorph selection in a small scale batch and following a reported basic workflow from batch towards continuous crystallisation. Other targeted objectives include illustrating and understanding control over the product polymorphic form for the first time during continuous oscillatory baffled crystallisations, whilst identifying any practical challenges associated with system operation.

As this research progressed, the need for an improved method towards continuous oscillatory crystallisation became evident. This resulted in target objectives of designing and developing an improved model system for assessment of continuous crystallisation behaviour and developing a method to monitor fouling on a vessel surface. A further target, after the improved system was operational, was to design and implement a work flow for continuously seeded continuous crystallisations for polymorph control of the highly polymorphic API Carbamazepine.

Chapter 3. Materials & Methods

3.1 Materials

L-glutamic acid (LGA) was purchased from *Sigma Aldrich* (β form, ≥98.5%, CAS 56-86-0 FCC), and Carbamazepine (CBZ) was purchased from *Molekula* (Form III, CAS 298-46-4). Deionised water was sourced on-site from a *Thermo Scientific Barnstead RO* water purification unit. Ethanol was purchased from *Fisher Scientific* (99.8+% (GLC), CAS 64-17-5). All other reagents and solvents were purchased from *Sigma* or *Fisher Scientific*.

3.2 Methods

Crystalline materials were characterised (solid phase, particle size, and morphology) using both in-line and off-line techniques. These included x-ray powder diffraction (XRPD), Raman spectroscopy, Infrared spectroscopy, Focused Beam Reflectance Measurement (FBRM), Laser Diffraction, and Microscopy. Concentration of solutes molecules were monitored using inline ultra violet (UV) transflectance and attenuated total reflectance fourier transform infra-red (ATR FTIR) techniques. For LGA and CBZ samples, solid slurries where removed, immediately filtered (*Millipore* 0.45 µm papers), and washed before drying in an over at 40 °C until constant mass.

3.2.1 X-Ray Powder Diffraction

XRPD is a widely adopted technique for identification of polymorph materials.[148,149] Polymorphic forms of the same compound are chemically identical however the molecules arrange themselves within the lattice differently. This results in different polymorphs exhibiting distinct diffraction patterns thus XRPD is a powerful tool to distinguish between mixed phase and polymorphic pure samples. The sensitivity of this technique can have a 0.5 wt% lower boundary of detection[150] and it has been reported that there is no other technique superior to x-ray diffraction for accuracy over phase quantification.[148] However, power diffraction will only provide information on

the crystalline solid state therefor is not suitable technique for solution phase identification for example.

Solid materials were characterised off-line via XRPD. XRPD fingerprinting was performed on ~50 mg of dried sample placed in a 28 well plate, supported by kapton film (7.5 µm thickness). Data was collected on a *Bruker AXS* D8 Advance transmission diffractometer that was equipped with θ/θ geometry, primary monochromatic radiation (Cu Kα1λ= 1.54056Å), a Braun 1D position sensitive detector (PSD) and an automated multi-position x-y sample stage. Data was collected from 4-35° 2θ with a 0.015° 2θ step size and 1 s step^{-1} count time.

For improved angular resolution and signal to noise ratio, phase purity was assessed using rotating capillary geometry collections. Samples were lightly ground using a mortar and pestle and loaded into a borosilicate capillary (0.7 mm diameter) before XRPD analysis. Data was collected using a *Bruker-AXS D8 Advance* powder diffractometer equipped with a primary monochromator (Cu K$_{\alpha 1}$ radiation), transmission capillary geometry and a *Bruker Lynxeye* position-sensitive detector. XRPD powder patterns were compared with known standards using *Bruker-AXE* software *Eva 2* or a Pawley-type fit made to the data with the known unit cell parameters using *Dash 3.3.2*.

3.2.2 Spectroscopy

Spectroscopy is an important technique used for both qualitative and quantitative identification of chemical entities and a number of modes of analysis available including off-line bench top spectrometers and fibre coupled probes.[151] There are several advantages associated with using probes on-line of a process rather than relying on off-line techniques,[152] these include collection of real-time information providing opportunities for process conditions to be adapted during operation and eliminating the need for manual sampling which can introduce artefacts to the sample. However challenges also exist including probes introducing local changes in the

hydrodynamic environment, ensuring probe position is optimised to provide representative sampling of the process stream and the introduction of dead zones where solids can accumulate around the probe shaft. Alternatives to in-line probes include non-invasive methods where the equipment does not make any contact with the process stream.

Various types of probes for on-line analysis are available including ATR, transflectance and reflectance. Details of which can be found elsewhere,[153] however generally ATR type probes are advantageous to use when measuring solution concentration within slurries, due to the small path lengths, whereas transfectance type systems are most accurate when determining concentrations without the presence of particles. In the work presented here, in-line determination of solute concentrations were performed using transflectance and ATR (Figure 3.1) probes and solid phase was determined on-line using a non-invasive probe. Off-line analysis of materials was carried out using bench top spectrometers.
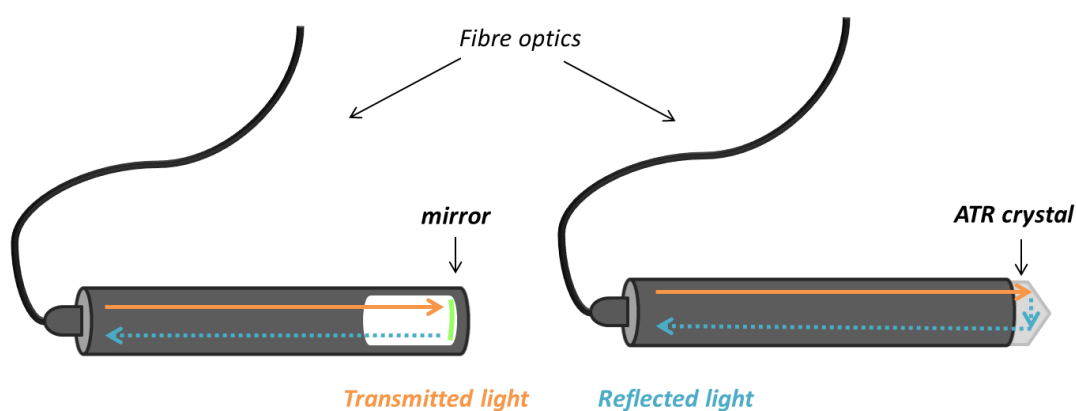
Figure 3.1: Spectroscopy probes. Both transflectance (left) and ATR (right) probes are coupled to the spectrometer via fibre optic cable(s).

3.2.2.1   Raman Spectroscopy

Raman spectra were collected on a *DXR* Raman microscope (*Thermo scientific*), equipped with Olympus viewing optics. Samples were excited with

a diode-pumped solid-state laser operating at 532 nm equipped with a DXR 532nm filter. Laser illumination was focussed onto the sample (1 µm diameter) using a 20x magnification objective lens. Approximately 50mg of sample was placed on a microscope slide for analysis, and spectra of 5 separate crystals were recorded. Data were collected over a frequency range of 500-4000 wavenumbers (cm^{-1}). Spectra were analysed using *OMINIC* software.

Raman spectra were collected online using a *Kaiser RXN1* spectrometer equipped with a PhAT probe head, a 785 nm external cavity diode laser operating up to 400 mW, and a charge coupled device (CCD) detector. The non-invasive PhAT probe attachment had a 25 cm working distance and a variable spot size of 1, 3 or 6 mm. Data were acquired using *iC Raman* software. Prior to spectra collection, the instrumentation was validated using cyclohexane. During data acquisition, laser light was directed at the non-jacketed bends of the COBC system and the probe was housed in a black box to limit shield the probe from stray light.

3.2.2.2   Infra-Red Spectroscopy

Attenuated total reflection Fourier transform infra-red (ATR-FTIR) spectra were collected offline using a Thermoscientific, *Nicolet iS10* FTIR, spectrometer equipped with a smart iTR sampling accessory. Spectra were collected over 16 scans and a frequency range of 550-4000 wavenumbers (cm^{-1}) with 4 cm^{-1} resolution. Approximately 10 mg of sample was loaded onto the spectrometer for analysis. Spectra were analysed using *OMNIC* software.

In-situ FTIR measurements were collected using a *Mettle Toledo ReactIR* 15 ATR-FTIR probe, connected via a flexible AgX fiber conduit to a ReactIR spectrometer. Mid-IR spectra (650 - 4000 cm^{-1}) were acquired over 16 scans with 4 cm^{-1} resolution. Spectral analysis was performed using *iC IR* software. Background measurements (air) and a reference solvent spectrum (ethanol) were acquired prior to sample collections.

3.2.2.3 Ultraviolet visible optical transmission spectroscopy

Ultraviolet-visible (UV-vis) optical transmission spectroscopy was performed inline using a UV transflectance probe (5 mm path length) connected to a *Carl Zeiss MCS* 501 UV spectrometer equipped with a CLD500 deuterium lamp (220 – 620 nm). Data were acquired at 5 second intervals (190 – 320 nm) using *Aspect Plus* software version 1.76.

3.2.3 Imaging

3.2.3.1 Microscopy

Optical images were acquired using a *Motic* B1 series microscope equipped with 4x, 10x, 40x and 100x magnification objective lenses. Images were visualised using *Motic* Images 2.0 software.

3.2.3.2 Particle Vision Measurement

In situ images of slurry were acquired using Particle Vision Measurement (PVM) probes (*Mettler Toldeo* V819 series). Images were acquired every 1 minute.

3.2.4 Particle Sizing

3.2.4.1 Focused Beam Reflectance Measurement

Focused beam reflectance measurement (FBRM) data were acquired using a *Lasentec* FBRM *S400* or *G400* probe attached to a control computer. FBRM data was analysed using either *Lasentec* data review or *iC FBRM* software.

For off-line FBRM, solid samples were prepared as a slurry (dried solids were re-suspended in a saturated solution). Slurries were stirred at 400 rpm in a beaker using the FBRM standard set-up apparatus. Unless otherwise stated, data were collected for 10 minutes with an acquisition time of 30 seconds.

Cord length distributions (CLD) were exported to excel as either un-weighted or square weighted number distributions for further analysis.

3.2.4.2   Laser Diffraction

Laser diffraction measurements were carried out using a *Mastersizer* 2000, or 3000 system (*Malvern* Instruments). Powder samples were dispersed in a saturated solution using a *Hydro2000SM* or *HydroMV* dispersion unit. Solid sample was added to the dispersion until the laser obscuration (internal parameter of the instrument used to avoid multiple scattering effect) reached 6 %. Five measurements were averaged for each sample and the following parameters calculated: the volume distribution over 100 logarithmically spaced size bins from 0.01-10,000 µm; d(0.5), the particle diameter corresponding to 50 % of volume distributions; d(0.1), the particle diameter corresponding to 10 % of volume distributions; d (0.9), the particle diameter corresponding to 90 % of volume distributions; d (4,3), the volume weight mean; and d (3,2), the surface weighted mean.

3.2.5 Thermal Analysis

Sample mass loss and melting points were measured using simultaneous thermal analysis (STA), comprising Differential Scanning calorimetry (DSC) and thermogravimetric analysis (TGA). A *Netzsch STA 449 C* thermocouple, equipped with *Netzsch CC* 200 liquid nitrogen supply system and Netzsch CC200 C control unit was used. Approximately 10 mg of solid sample was scanned at 10 °C min^{-1}

Chapter 4. Characterisation of a Continuous Oscillatory Baffled Crystalliser

4.1 Introduction

Crystallisation systems possess unique operating characteristics, such as density, viscosity and solid loading, each can influence crystallisation performance.[154] Additionally, when operating under oscillatory flow, specific oscillatory frequencies and amplitudes must be achieved to ensure particle suspension sufficient to avoid sedimentation and blockage, and these characteristics are often interdependent (Figure 1.26). For example, the suspension of higher solid loading systems requires greater oscillation intensities.[155] Other interdependent factors are shown in Figure 4.1. These include the mean residence time (τ), which is influenced by net flow rate, and impacts the resulting particle size distribution (PSD), which in turn is dependent on supersaturation, growth rates, and crystal number. As such, oscillatory conditions differ between different solid and solvent systems, all must be considered when designing a continuous crystallisation process.
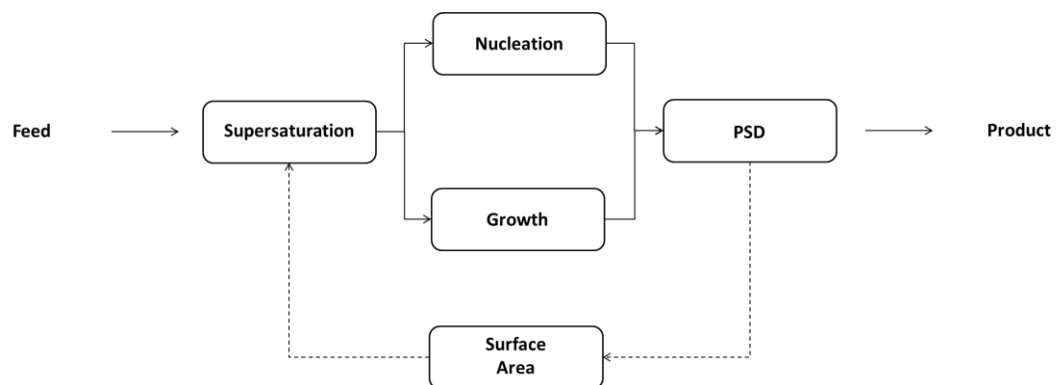
Figure 4.1: Interacting processes during continuous crystallisation.[29]

In general, continuous platforms must deliver a suitable environment for the generation, suspension and movement of particles, whilst maintaining a level of supersaturation sufficient to allow particle growth. To achieve the required operating conditions in a DN15 continuous oscillatory baffled crystalliser (COBC) various oscillatory conditions, residence times and net flow rates will

be employed depending on the specific compound of interest, solvent system and crystallisation method. To provide information on the flow performance and operating space that will be used for crystallisations, a range of operating conditions must therefore be characterised.

4.1.1 The Continuous Oscillatory Baffled Crystalliser

The basic construction of the COBC is a series of periodically spaced orificed baffles, across which a fluid oscillation is applied. The COBC system is made up of a series baffled glass tubes (straights) and bends connected to an oscillation source. A main feed is pumped into the system providing a net flow and, where temperature control is required, heater/chillers (HCs) circulate coolant through the shell of the glass straights. A basic schematic and the geometry of the COBC straights are illustrated in Figure 4.2 and Figure 4.3, respectively.

1.	Feed Tank	5.	Bellows
2.	Peristaltic pump	6.	Peek Collar
3.	Control Box	7.	Thermocouple
4.	Linear motor	8.	Heater/Chiller
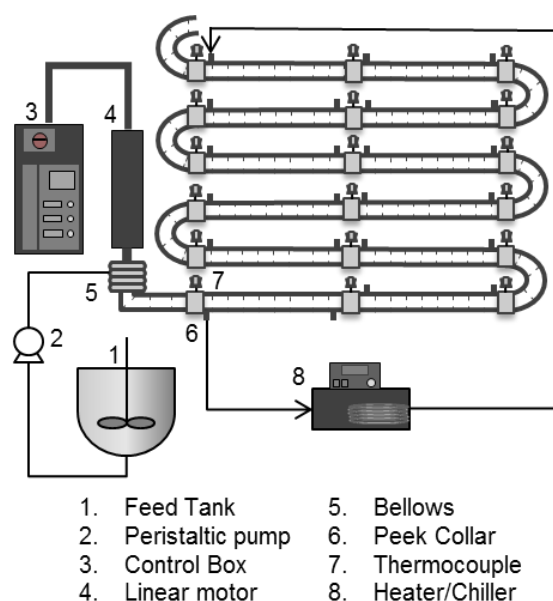
Figure 4.2: DN15 COBC setup. Simplified schematic illustrating the set-up of the DN15 COBC.
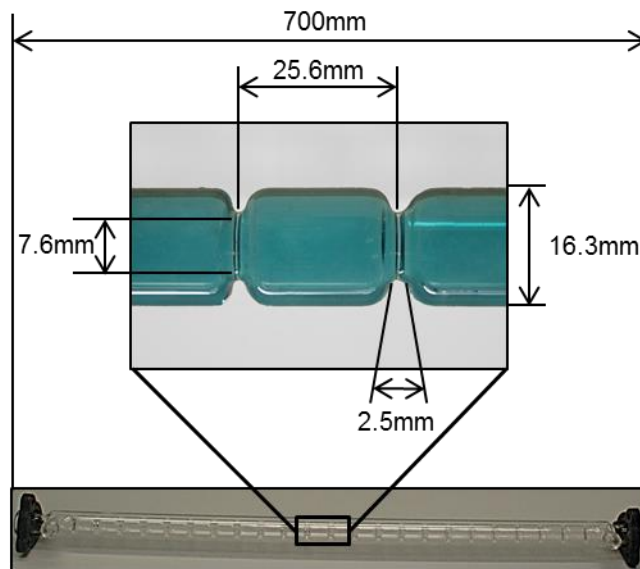
Figure 4.3: COBC Geometry. Photograph of a single DN15 COBC glass straight. Inset shows a magnified image of a single interbaffle zone, with dimensions indicated.

During oscillatory motion (forward and backstroke) of flow through the baffles, strong radial mixing is achieved. Eddies are formed downstream of the baffle on the forward stroke, whilst these eddies are dissipated on the back stroke as new eddies are created upstream of the baffle (Figure 4.4). This repetitive creation and cessation of eddies results in a chaotic flow that provides efficient mixing within each interbaffle zone.
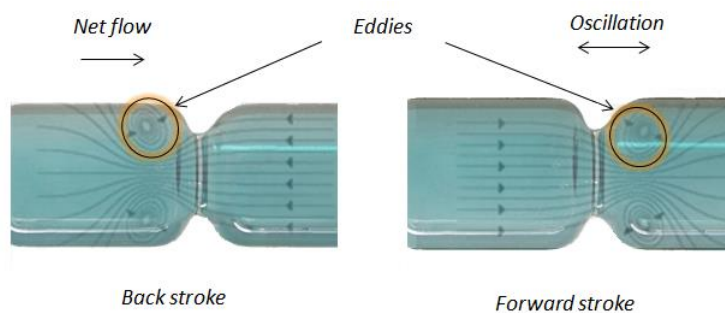
Figure 4.4: Flow interaction within baffled tubes. Photograph of baffles with flow patterns superimposed. Eddies are generated due to oscillatory flow.

Continuous oscillatory flow may be described by three dimensionless numbers: Re_o, the oscillatory Reynolds number; St, the Strouhal number; and Re_n, the net flow Reynolds number.[156] These are governed by the following equations:

$$Re_o = \frac{2\pi f \chi_o \rho D}{\mu}$$
Eqn. 4.1

$$St = \frac{D}{4\pi\chi_o}$$
Eqn. 4.2

$$Re_n = \frac{\rho u D}{\mu}$$
Eqn. 4.3

where D = column diameter (m), χ_o= centre-to-peak amplitude (m), f = frequency (Hz), ρ = density (kgm^{-3}), μ = fluid viscosity (kgm^{-1}s^{-1}), and u = mean velocity (ms^{-1}). Re_o describes the intensity of oscillatory mixing applied within the tube, where $2\pi f \chi_o$ is the maximum oscillatory velocity (ms^{-1}). St is the ratio of the column diameter to the oscillation amplitude, and is a measure of the eddy propagation inside each interbaffle zone. St is inversely proportional to χ_o. Re_n, the classic dimensionless number describing flows in pipes, is the ratio of inertial to viscous force within a flow.

Dominant oscillatory flow is required to maximise the effect of the eddy shedding cycle. Thus, flow should be fully reversing and for this to hold true Re_o should be ≥ Re_n. A velocity ratio, ψ, was proposed to relate the oscillatory velocity to the net flow velocity and is described by:[157]

$$\psi = \frac{Re_o}{Re_n}$$
Eqn. 4.4

In addition to the aforementioned equations (4.1 – 4.4) describing oscillatory flow, Peclet numbers (Pe) are often used to describe the deviation from ideal

flow behaviour in tubular systems, the higher the value the more plug flow like the system is. The axial dispersion coefficient (E) is another term that can be used for flow identification, the relationship between these two numbers can be expressed as follows:[158]

$$Pe = \frac{uL}{E} = \frac{L^2}{Pe\tau}$$

Eqn. 4.5

Pe numbers of approximately 1 suggest a back mixed flow behaviour (CSTR like), whereas Pe greater than 50 suggest a near plug flow environment.[159] A characterisation system proposed by Ni,[160] details corresponding values indicating levels of deviation from plug flow, details can be found in Table 4.1.

Table 4.1: Table illustrating a flow characterisation system. Values expressed in terms of Pectlet number and axial dispersion coefficient.

Flow Characterisation	$\dfrac{E}{uL}$	Pe
Plug flow	0	∞
Small amount of dispersion	0.002	500
Intermediate amount of dispersion	0.025	40
Large amount of dispersion	0.2	5
Mixed flow	∞	<1

A major advantage of OBC technology is that mixing is achieved through the oscillatory cycle and is decoupled from the overall net flow.[161] This permits advanced mixing regimes and extended residence times under relatively low net flow conditions. For example, a 25 m DN15 COBC operating under oscillatory conditions of 1 Hz, with a 30 mm amplitude and a flow rate of 50 gmin^{-1} has a residence time of approximately 90 minutes, where Re_o = 1500 and Re_n = 65. To achieve comparable mixing intensity (same Reynolds number) in an non-baffled and non-oscillated tubular system of the same dimensions, the net flow rate would need to be increased from 50 gmin^{-1} to 1200 gmin^{-1}, which would result in an approximate residence time of only 4 minutes (i.e. 5% of oscillatory baffle flow). The ability to extend the mean residence time, under plug flow conditions, at a similar mixing intensity, is advantageous to slow processes such as crystallisation, where there is a need for longer residence times. Such longer residence times are required for the induction of nucleation and the subsequent growth of crystals and a uniform mixing environment facilitates uniform crystal growth. For these reasons, the oscillatory baffled system is an attractive platform for continuous crystallisation processes.

4.1.2 Residence time distribution

RTD analysis is a standard method that is typically used to understand and analyse flow. Characterising of RTDs in different continuous operations is the first step in the design, optimisation and scale up of many manufacturing processes in the chemical industry. However, a correlation of RTD and end product is performed infrequently.[162] Furthermore, the RTD of a 25 m DN15 COBC has not been reported, and by providing such information, the present study seeks to improve our understanding of the mixing and flow performance of this specific COBC platform.

Plug flow is the desired type of flow during continuous operations and can be defined as the orderly flow of fluid elements, where no single element

overtakes another in the direction of flow (Section 1.5). As a result, all elements spend the same time in the reactor and there is perfect mixing along the radial direction. As true plug flow is difficult, if not impossible, to achieve, species moving through a tubular reactor may take different routes and take different times to pass through. Such non-ideal flow can be assessed by calculating E, the exit age distribution function or the RTD function (Section 4.2.1). Once the flow performance is characterised, it can be used to assess the impact of flow on crystallisation and product attributes.[163] Taking particle size distribution as an example, it is expected that a broader RTD will result in a broader product PSD. However, studies one the effect of experimental RTDs on crystal product PSD are limited, although applications for other solid unit operations, including power blending, extrusion, rotary drums and fluidised beds, are more commonly been reported.[163]

In general, RTD experiments are performed by injecting a tracer that can be detected as it elutes the system. This provides a means to obtain concentration of a species, at specific distance, as a function of time. Flow behaviour, as characterised by tracer experiments, are most often analysed using the dispersion and the tanks in series models.[164] The difference between these two models is that the dispersion model assumes the reactor is a continuous path and the deviation from plug flow is based around the dispersion of an ideal point source, whilst the tanks-in-series model divides the reactor into compartments with discrete stages and the deviation from plug flow is related to the number of discrete stages in the platform. Whilst the tanks-in-series model is emerging as a useful tool for modelling flow in meso-scale OBR systems,[158,165] the dispersion model remains the most common model for oscillatory flow systems.[166-168]

The diffusion model, first proposed in the early 1950s and based on the principles of molecular diffusion, was first used to describe axial dispersion in oscillatory flow by Mackley and Ni in 1991.[169,170] When a tracer is monitored at a single point in the system, the axial dispersion from the injection point, to

the monitoring point, is modelled with the assumption that the tracer injection impulse was "perfect" i.e. the impulse can be described by the direct delta function (no axial dispersion); this is known as the perfect pulse method. This method was proposed in the early 1950s.[170] In practice, it is impossible to inject an ideal bolus of tracer. To remove the need to assume a perfect pulse, the tracer concentration may be measured at two or more positions downstream from the injection point, the imperfect pulse technique (Figure 4.5). From these RTD curves the axial dispersion coefficient can be calculated.[171]
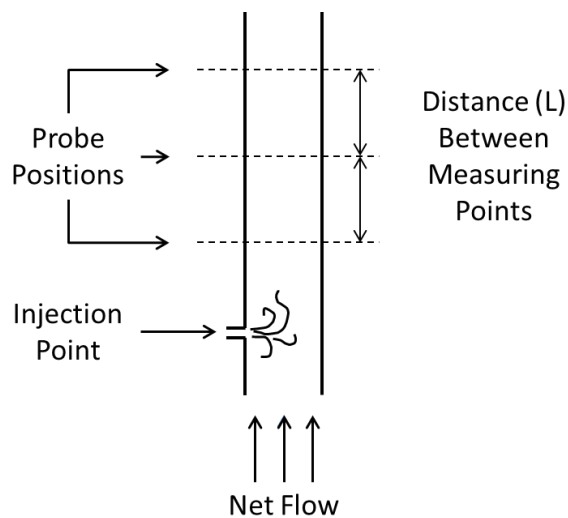
Figure 4.5: Imperfect pulse technique.[170] Simplified diagram illustrating the injection of a tracer into a tubular vessel. Probes are positioned downstream of the injection point.

RTDs have been analysed for numerous oscillatory flow set-ups and a range of baffle geometries (summarised in Table 4.2). These studies highlight the superiority of oscillatory flow mixing, compared to non-oscillatory flow, in tubular geometries with or without baffles. Additionally, operating conditions achieving near plug flow and minimum axial dispersion are described.

Table 4.2: Previous RTD studies of oscillatory baffled mixing technologies.

Tube ID (mm)	System length (m)	BS_r	Baffle ID (mm)	α	Re_n	Re_o	St	Results	Ref.
23	0.67	1.5	13	0.44	110	100 - 3300	0.3 - 9	D/uL: 0.025 - 0.128	172
51	2.5	1.5	32	0.61	40, 106	160 - 2500	0.8, 2	1/Pe: 0.8 - 2	173
25	1.08	1.5	16	0.34	128	40-3600	0.35-4	D/uL: 0.030-0.10	169
25	6.3	1.5	16	0.34	106 - 3400	100 - 750	0.4 – 3	D/uL: 0.003 - 0.012	174
25	1	1.5	16	0.34	42, 424, 128	150-1600	0.35-4	Dispersion not calculated	161,175
								RTD review	176
23.5	2.9	1.5	12		95, 127, 190, 252	0 -2500	0.4-3.8	tanks-in-series model	157
40	25	1.8	32	0.21	160-250	2000-8000	0.4-0.8	D/uL: 0.8 – 1.6	110
50	0.5	1.5	11	0.78	-	500-6000	1.0	Axial dispersion (batch)	177
4.4		3.0	1.6	0.87		0-1600		Axial dispersion	159
5	9	3	1.6	0.87	10 - 58	100-1000	0.08-0.4	D/uL minimum when $Re_o = 100 - 300$	158

A common conclusion of RTD studies is the recommendation of certain reactor geometry, one such parameter is the relative baffle free area, α, defined as:

$$\alpha = \frac{D_o}{D}$$

Eqn 4.5

where D_o is the orifice hole diameter and D is the baffle diameter (m). Another, the baffle spacing ratio (BS_r) is describe by:

$$BS_r = \frac{BS}{D}$$

Eqn 4.6

where BS is the distance between baffles. Baffle thickness should also be consistent. In this regard, optimal values of relative baffle free area between 0.2 - 0.22, baffle spacing ratio between 1.5 and 1.8, and a baffle thicknesses of 2 - 3mm have been reported.[178] Additionally, ideal operating velocity ratios of between 2 – 10 and Re_o ≥100 have been suggested.[157]

Despite a growing interest in the use of COBCs, particularly for the continuous crystallisation of active pharmaceutical ingredients, a complete understanding of crystallisation processes with COBCs is lacking. Studies performed to date have utilised COBCs with a range of geometries, as a result, it is particularly difficult to make appropriate comparisons. Variations in platform geometry can influence scalability of oscillatory baffled systems.[179] As baffle materials and geometries are not always consistent between oscillatory baffled devices, the work described in this chapter evaluates the axial dispersion of a single orificed baffled crystalliser (*Nitech Solutions Limited* DN15 COBC) for a range of operating conditions.

4.2 Experimental

To characterise the DN15 COBC, the RTDs were calculated from concentration profiles of sodium benzoate (tracer), injected into the COBC. The absorption wavelength peak maximum of sodium benzoate (λ_{max}), as measured using a UV transflectance probe (5 mm path length) was determined as 226 nm. The absorbance of sodium benzoate was calibrated against known concentrations (Figure 4.6, $R^2 = 0.9988$).
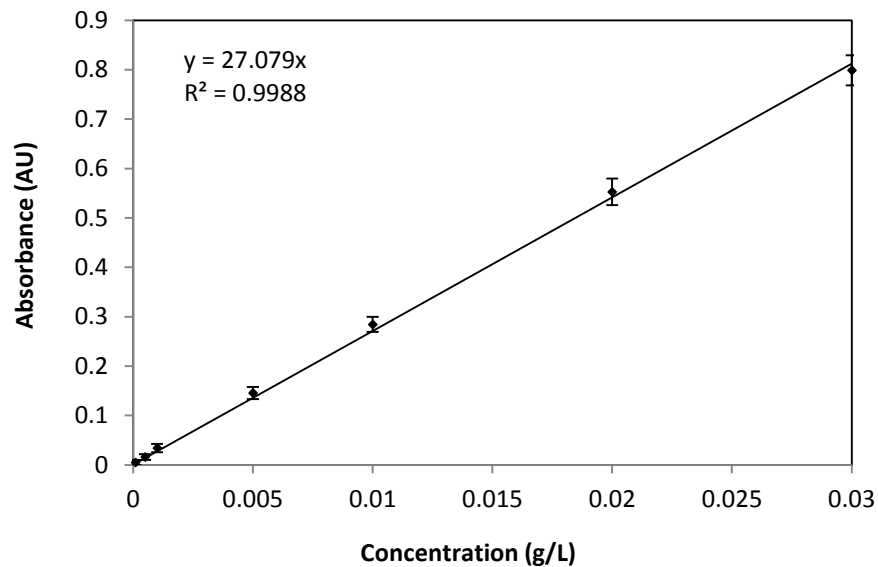
Figure 4.6: Calibration of sodium benzoate. Plot illustrating the linear increase in sodium benzoate absorbance, as a function of concentration. Data acquired using a UV transflectance probe.

The Beer-Lambert law, used to calculate absorbance, assumes that absorbing molecules do not interact with each other, and each molecule has an equal probability of absorbing a photon. At high concentrations individual particles of analyte no longer behave independently of each other, hence to ensure no loss of linearity following the Beer Lambert law, the optimal concentration of tracer to be injected was determined. A series of 3 ml tracer concentrations were injected, and their concentration profiles measured over 5 straights in the presence of flow conditions producing the sharpest RTD curve (oscillation frequency, 3 Hz; oscillation amplitude, 30 mm; flow rate,

200 gmin^{-1}). From these experiments, 5 gL^{-1} was determined to be the optimal concentration. The tracer was rapidly injected into a flange-fitting injection port (Figure 4.7) using a syringe. The syringe was connected to the injection port via marprene tubing. The tracer was injected over a period of approximately 0.5 s, to achieve a consistent, near instantaneous dosing, in comparison to the time-scale of the experiment (100 – 8000 s). The tracer absorbance was measured at 3.8 (position 1) and 15.9 m (position 2) along the length of the COBC using a UV probe inserted into a COBC collar using a PTFE compression fitting (Figure 4.8). Ideally, the tracer absorbance would be measured at multiple positions simultaneously. However, due to access of a single UV probe, multiple experiments were carried out in order to measure absorbance, and subsequently calculate the concentration-time response at various distances downstream of the tracer injection port.
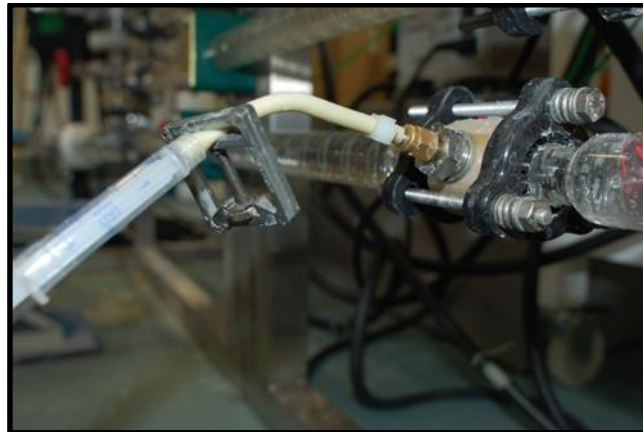
Figure 4.7: COBC tracer injection port. Photograph of the COBC setup showing the injection port. A syringe is connected to the port via marprene tubing.
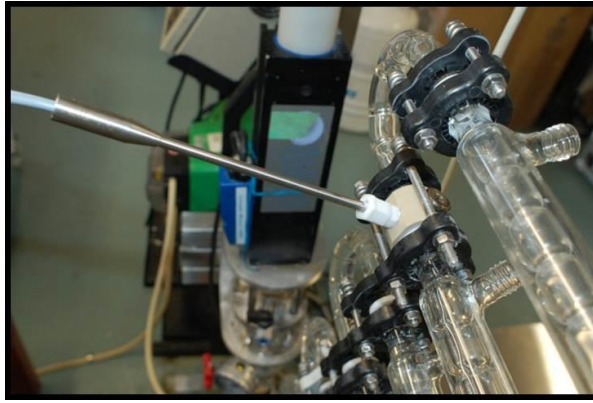
Figure 4.8: UV transflectance probe setup. Photograph of the UV transflectance probe fixed inline on the DN15 COBC via a connecting PEEK collar.

Utilising UV transflectance for the in-line investigation of RTD behaviour in a oscillatory baffled system has not previously been reported. To date the most commonly used method for detecting tracer concentrations is the measurement of fluid conductivity, although other methods such as laser absorption and imaging are beginning to receive attention.[177,180] To investigate the effects of various operating parameters (Re_o and Re_n) on axial dispersion, and identify optimal regions for operation, a design of experiments (DoE) approach was implemented. DoE provides a base to increase process understanding, using the least amount of experiments possible, for the identification of important factors which affect a process.[181] Experiments are designed to identify how input variables impact the output variables allowing the rapid development and optimisation of new and existing processes, details of application can be found elsewhere.[182] For COBC investigations, the variable input settings are Re_o and Re_n, thus a high and low frequency and amplitude were selected in addition to a high and low net flow rate (Table 4.3). The output variable is the RTD profile and this was quantified using the calculated axial dispersion coefficient and Peclet numbers.

Table 4.3: DoE design space for RTD experiments.

Frequency (Hz)		Amplitude (mm)		Flow rate (g/min)	
High	Low	High	Low	High	Low
3	1	30	10	200	50

Further the data were exported, stored and processed using an electronic lab notebook (ELN) type approach enabling the use of automation to input raw data files, carry out calculations and modelling thus simplifying the characterisation of the reactor. The benefit of this includes the reduction in time and lower likelihood of experimental error during transfer an input of data.

4.2.1 Modelling axial dispersion

As described in Section 4.1.2, there are two commonly used methods of calculating axial dispersion within a reactor. The following sections describe how these models were used to investigate the RTD in the DN15 COBC.

4.2.1.1 Perfect pulse

The perfect pulse model of tracer injection, used for calculating the axial dispersion through flow systems, assumes that there is no dispersion of the tracer with time, as shown in Figure 4.9.
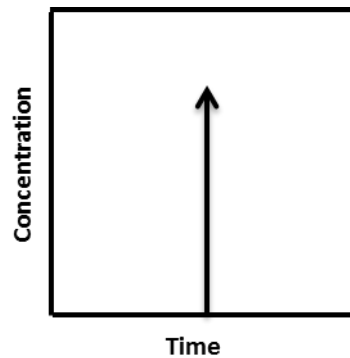
Figure 4.9: Dirac δ input.

The axial dispersion E, was obtained by solving the following equation:[164]

$$\sigma_\theta^2 = \frac{\sigma^2}{\tau^2} = 2 \left(\frac{E}{uL}\right) - 2 \left(\frac{E}{uL}\right)^2 (1 - e^{-\frac{uL}{E}}) \qquad \text{Eqn. 4.7}$$

where σ^2 is variance i.e. a measure of the spread of the RTD curve. The mean residence time, τ, was calculated from the experimental concentration and time data using :

$$\tau = \frac{\sum t_i C_i \Delta t_i}{\sum C_i \, \Delta t_i} = \frac{\sum t_i C_i}{\sum C_i} \qquad \text{Eqn. 4.8}$$

where t_i is the experimental time with a given concentration, C_i. The variance, is calculated using:

$$\sigma^2 = \frac{\sum t_i^2 C_i \, \Delta t_i}{\sum C_i \, \Delta t_i} - \left[\frac{\sum t_i C_i \, \Delta t_i}{\sum C_i \, \Delta t_i}\right]^2 = \frac{\sum t_i^2 C_i}{\sum C_i} - \left[\frac{\sum t_i C_i}{\sum C_i}\right]^2 \qquad \text{Eqn. 4.9}$$

Given experimentally a perfect pulse of tracer cannot be achieved, the imperfect pulse method is applied to provide more realistic description of the experimental tracer profile.

4.2.1.2   Imperfect pulse

The imperfect pulse method for determining axial dispersion accounts for the finite dispersion of tracer concentration over the duration of the injection. The basic differential equation representing the dispersion model, used previously to describe dispersion in oscillatory flow mixing (Table 4.2), is represented by:

$$\frac{\partial C}{\partial \theta} = \left(\frac{E}{uL}\right)\frac{\partial^2}{\partial Z^2} - \frac{\partial C}{\partial Z} \qquad \text{Eqn. 4.10}$$

where C is the nomalised concentration; θ is dimensionless time, $\theta = ut/L$; Z is dimensionless length, $Z = x/L$; u (ms^{-1}) is the mean axial velocity; L (m) is the length of reactor used; E (m^{2}s^{-1}) is the axial dispersion coefficient; and t is time, measured from the tracer injection. This differential equation permits the prediction of pulse profile, from the calculated axial dispersion coefficient, downstream from the original measurement. This equation permits the prediction of a pulse profile, from the calculated axial dispersion coefficient, downstream from the original measurement.

The imperfect pulse model was fitted to experimental data, and completed using procedures described in detail elsewhere.[158] Concentrations were normalised using the following equation:

$$C(t) = \frac{c(t)}{\int_0^\infty c(t)dt} = \frac{C_{pulse}}{\frac{M}{v}} = \frac{C_i}{\sum C_i \Delta t_i} \qquad \text{Eqn. 4.11}$$

The mass of tracer flowing through the system was calculated from the area under the RTD curve (summation of $C_i \Delta t_i$), where M is the mass of tracer (kg) and v is fluid velocity m³s⁻¹. This material balance allows confirmation of tracer recovery once the experiment is complete.

A transfer function, $TR(t)$, was applied to convert the upstream response (to the downstream response, described by:

$$TR(t) = \sqrt{\frac{Pe\tau}{4\pi t^3}} \, exp \left\{ \frac{-Pe}{\frac{4t}{\tau}} \left(1 - \frac{t}{\tau} \right)^2 \right\} \qquad \text{Eqn. 4.12}$$

Using the Pe number, the axial dispersion coefficient was calculated following equations 4.5. The model response $C_2(t)'$ at position 2 was calculated by convolving the measured input response $C_1(t)'$ and the model transfer function $TR(t)$:

$$C_2(t)' = \int_0^t TR(t-p)C_1(p)\mathrm{d}p. \qquad \text{Eqn. 4.13}$$

where p is the time response downstream and t is the time response from the upstream response. The model calculated response $C_2(t)'$ was then compared to the experimental $C_2(t)$ using the target function defined as:

$$\Delta C = \sum_{i=1}^N \{C_2(t_i) - C_2(t_i)'\}^2 \qquad \text{Eqn. 4.14}$$

The *Pe* number was varied to find the value resulting in minimal difference between the calculated and predicted responses, this value was taken as the *Pe* number of the system. A representative result obtained using this fitting procedure is shown in Figure 4.10. Using the Pe number obtained from the minimal difference between predicted and observed values, an overlay of the raw data with the predicted response can be plotted (Figure 4.10, right panel).
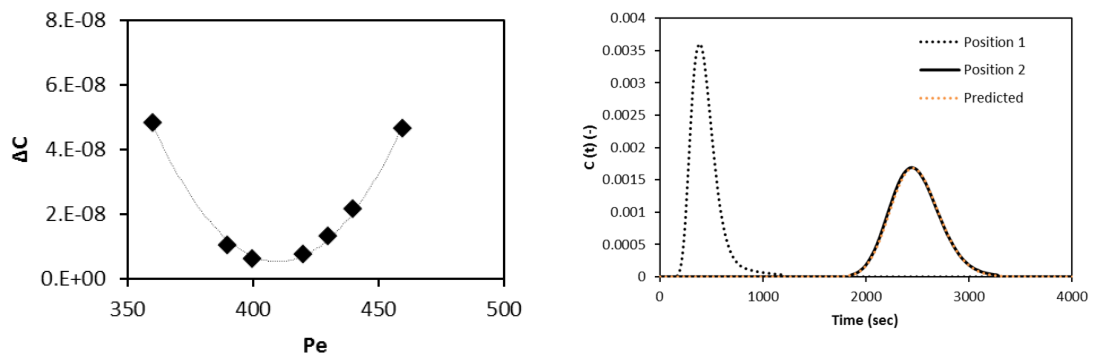
Figure 4.10: Application of Peclet number. Difference plot (left) used to determine the Peclet number, and representative concentration data (right, dotted and solid black; 100 g/min, 30 mm amplitude, 1 Hz), with the model response overlaid (orange).

4.3   Results & discussion.

Following the DoE design space described in Table 4.3, experiments where completed in duplicate. However, observations made during the progression of the project suggested discrepancies in achieved fluid oscillation amplitudes when compared to input settings from the control box. A retrospective calibration was carried by positioning an unbaffled DN15 glass straight vertically at the outlet of the COBC (Figure 4.11), partially filling this straight with water and then monitoring the displacement at various control box setting (without net flow).
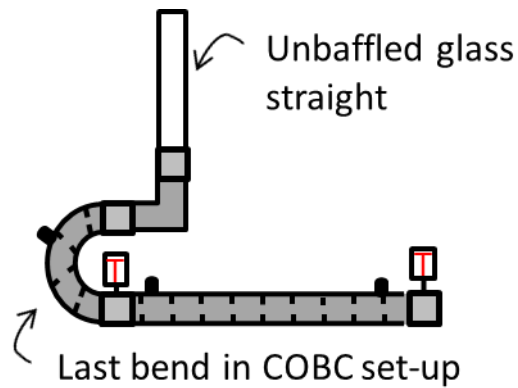
Figure 4.11: Set-up for oscillation calibration.

This retrospective calibration series showed that the intensity of oscillation deviated substantially from input conditions (Table 4.4), thus targeted oscillatory conditions were not met throughout these experiments and modelling of the design space, for prediction of RTD behaviour over the range of possible working conditions in the COBC, could not be completed.

Table 4.4: DoE conditions. Table showing DOE target conditions and experimental amplitudes, using the same input setting on control box for the oscillation. The difference between conditions was due to incorrect calibration of the control box and oscillation damping along the length of the COBC.

DoE	Target conditions			Achieved
Expt. No	Frequency (Hz)	Amplitude (mm)	No. of COBC straights used	Amplitude (mm)
1	1	10	5	66
2	3	10	5	18
3	1	30	5	141
4	3	30	5	33
5	1	10	19	36
6	3	10	19	9
7	1	30	19	65
8	3	30	19	14
9	1	10	5	66
10	3	10	5	18
11	1	30	5	141
12	3	30	5	33
13	1	10	19	36
14	3	10	19	9
15	1	30	19	65
16	3	30	19	14
17	2	20	11	25
18	2	20	11	25
19	2	20	11	25

Notably, oscillation amplitude characteristics were dependent on the length of the COBC set-up despite constant input settings, dampening of oscillations was observed to increase with length (Figure 4.12). There was also found to be interdependence on the amplitude, observations showing a significant reduction in amplitude with respect to an increase in frequency (Figure 4.13). This oscillation damping along the system was thought to be due to the oscillatory wave losing energy as it dissipates through the system. Energy will be lost overcoming friction at the vessel walls and during fluid contact with the baffles for example. The interdependence of amplitude with increased frequency is thought to be a limitation of the linear motor used in the set-up i.e. the maximum velocity specification does not account for the payload of the equipment. For example, the bellows and fluid filled COBC add resistance therefore work against the linear motor. This results in the higher velocity oscillations (higher frequencies) exceeding the capabilities of the motor and therefore it cannot maintain the amplitude.
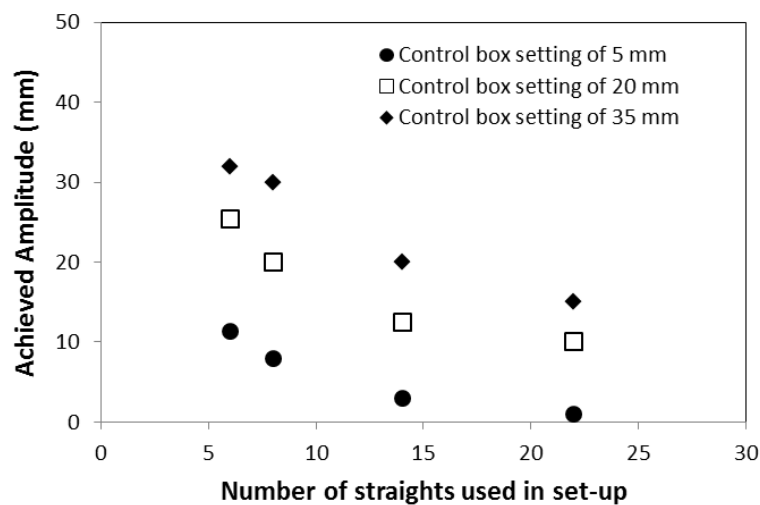
Figure 4.12: Calibration of DN15 COBC amplitude against distance. Graph illustrating a decrease in amplitude as the number of straights in the COBC system is increased (fixed frequency of 3 Hz).
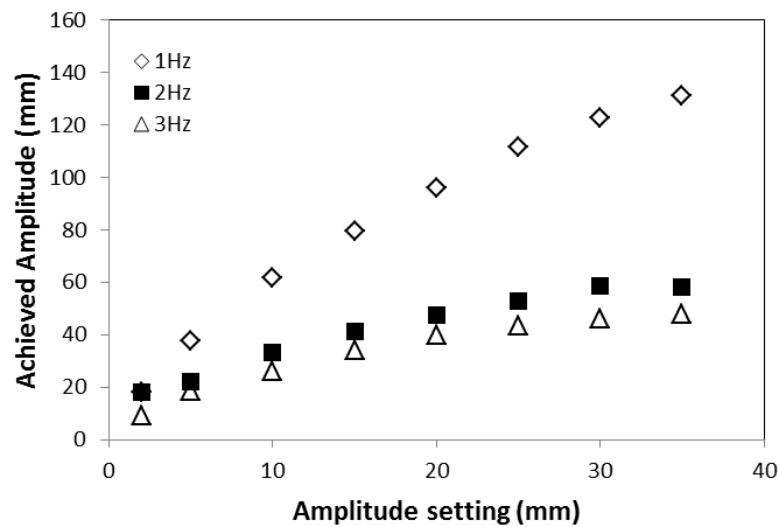
Figure 4.13: Calibration of DN15 COBC amplitude. Graph illustrating the interdependence of amplitude and frequency, as measured in a fixed set-up of 12 COBC straights.

The oscillation amplitudes were calculated in retrospect using this calibration and results shown in this chapter are presented with the assumption that no oscillation damping occurs. Experimental conditions and results obtained using imperfect pulse modelling calculations are given in Table 4.5. Corresponding RTD responses and imperfect pulse models are shown in Figure 4.14. It should be noted that the predicted responses are in good agreement with experimental data. For each experiment, the corresponding vessel dispersion number and axial dispersion coefficient were calculated. This information is included in Appendix 1 alongside calculated flow and mixing conditions.

Table 4.5: Experimental conditions and resulting Pe number for the imperfect pulse modelling

Expt. ID	Amp.	Freq.	FR	position	Pe	Fig label
NB_07_005_A		1	50	1	**150**	A
NB_07_008_A	38	1	50	2		
NB_07_005_E		1	50	1	**550**	**B**
NB_07_009_A	38	1	50	2		
NB_07_004_D		1	200	1	**650**	**C**
NB_07_008_E	38	1	200	2		
NB_07_004_H		1	200	1	**1100**	**D**
NB_07_008_D	38	1	200	2		
NB_07_005_C		1	50	1	**110**	**E**
NB_07_007_E	66	1	50	2		
NB_07_005_I		1	50	1	**250**	F
NB_07_009_C	66	1	50	2		
NB_07_004_B		1	200	1	**210**	**G**
NB_07_007_G	66	1	200	2		
NB_07_004_F		1	200	1	**290**	**H**
NB_07_008_I	66	1	200	2		
NB_07_005_B		3	50	1	**5500**	**I**
NB_07_007_F	9	3	50	2		
NB_07_005_F		3	50	1	**4000**	**J**
NB_07_009_B	9	3	50	2		
NB_07_004_C		3	200	1	**1800**	**K**
NB_07_008_G	30	3	200	2		
NB_07_004_G		3	200	1	**1600**	L
NB_07_008_H	30	3	200	2		
NB_07_005_D		3	50	1	**350**	M
NB_07_008_B	14	3	50	2		
NB_07_005_H		3	50	1	**650**	N
NB_07_009_E	14	3	50	2		

Table 4.3 continued…

Expt. ID	Amp	Frq	FR	position	*Pe*	Fig label
NB_07_004_A		3	200	1	**7000**	**O**
NB_07_008_C	14	3	200	2		
NB_07_004_E		3	200	1	**2700**	**P**
NB_07_008_F	14	3	200	2		
NB_08_89A		1	50	1	**140**	**Q**
NB_08_95B	30	1	50	2		
NB_08_89B		1	50	1	**150**	**R**
NB_08_95_C	30	1	50	2		
NB_08_89E		1	100	1	**550**	**S**
NB_08_93C	30	1	100	2		
NB_08_89F		1	100	1	**410**	**T**
NB_08_97A	30	1	100	2		
NB_08_87A		1	200	1	**500**	**U**
NB_08_93D	30	1	200	2		
NB_08_87C		1	200	1	**500**	V
NB_08_93F	30	1	200	2		
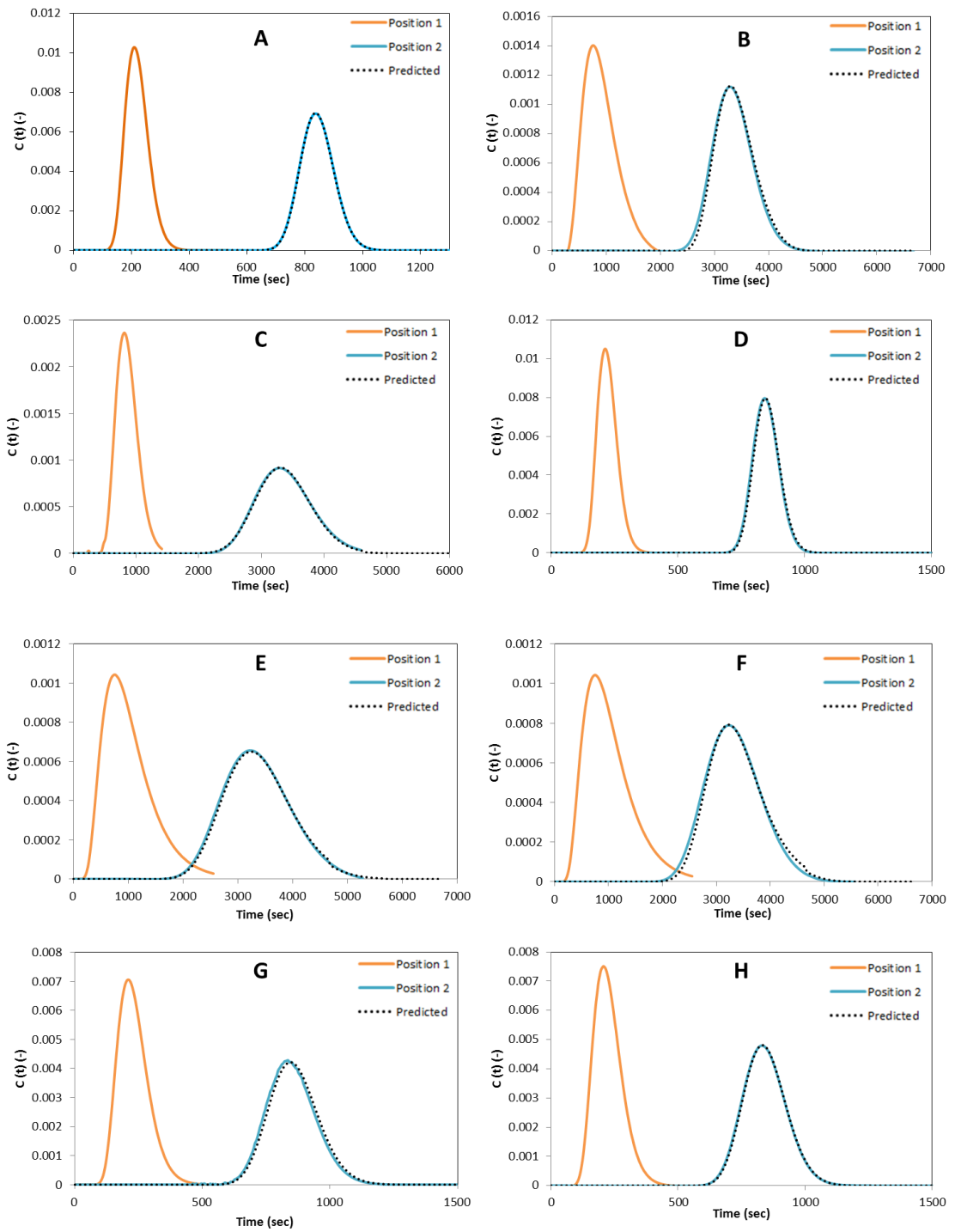
Figure 4.14: Experimental and imperfect pulse model responses. Raw data (orange and blue) with the model response overlaid (dotted black).
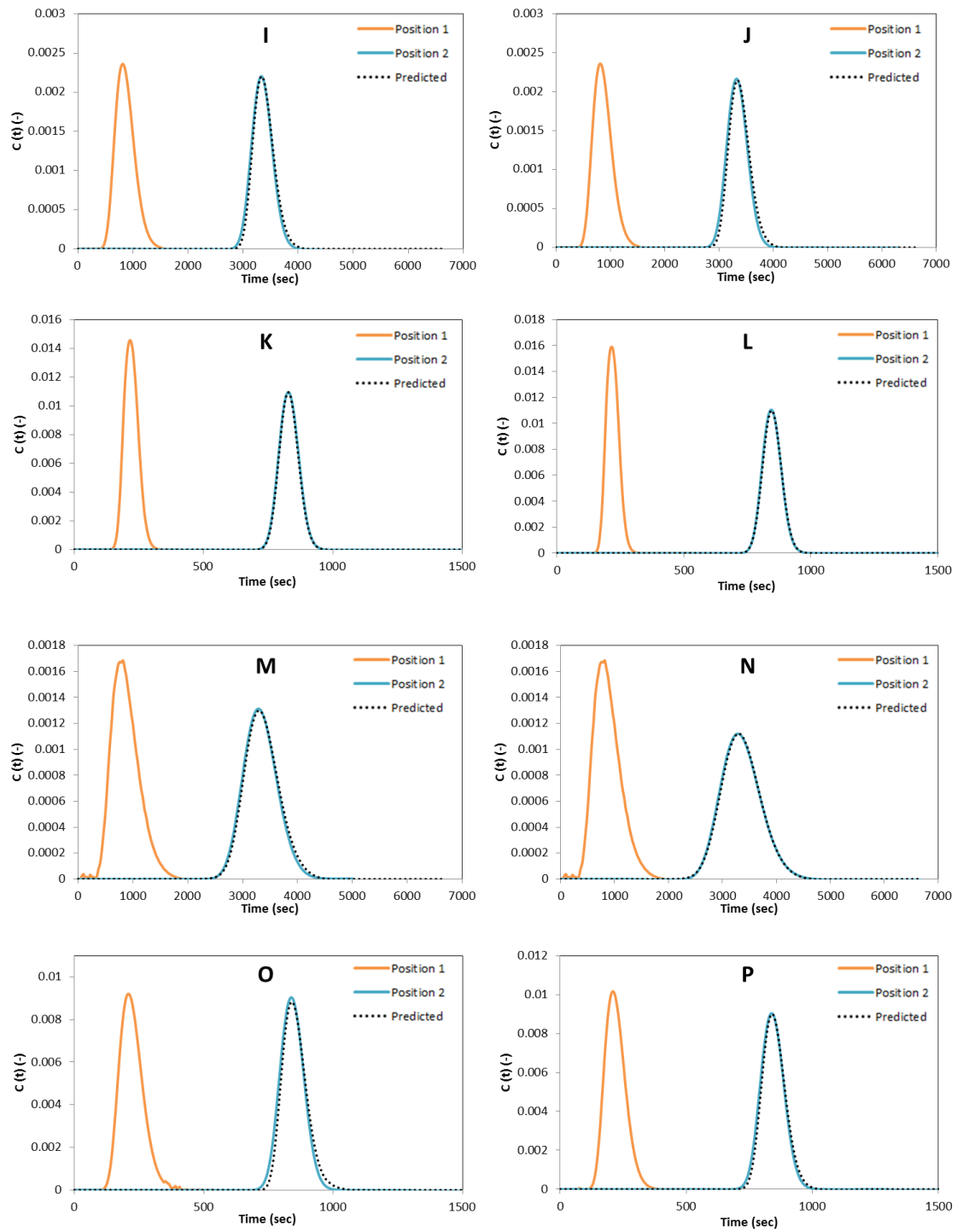
Figure 4.13 continued…
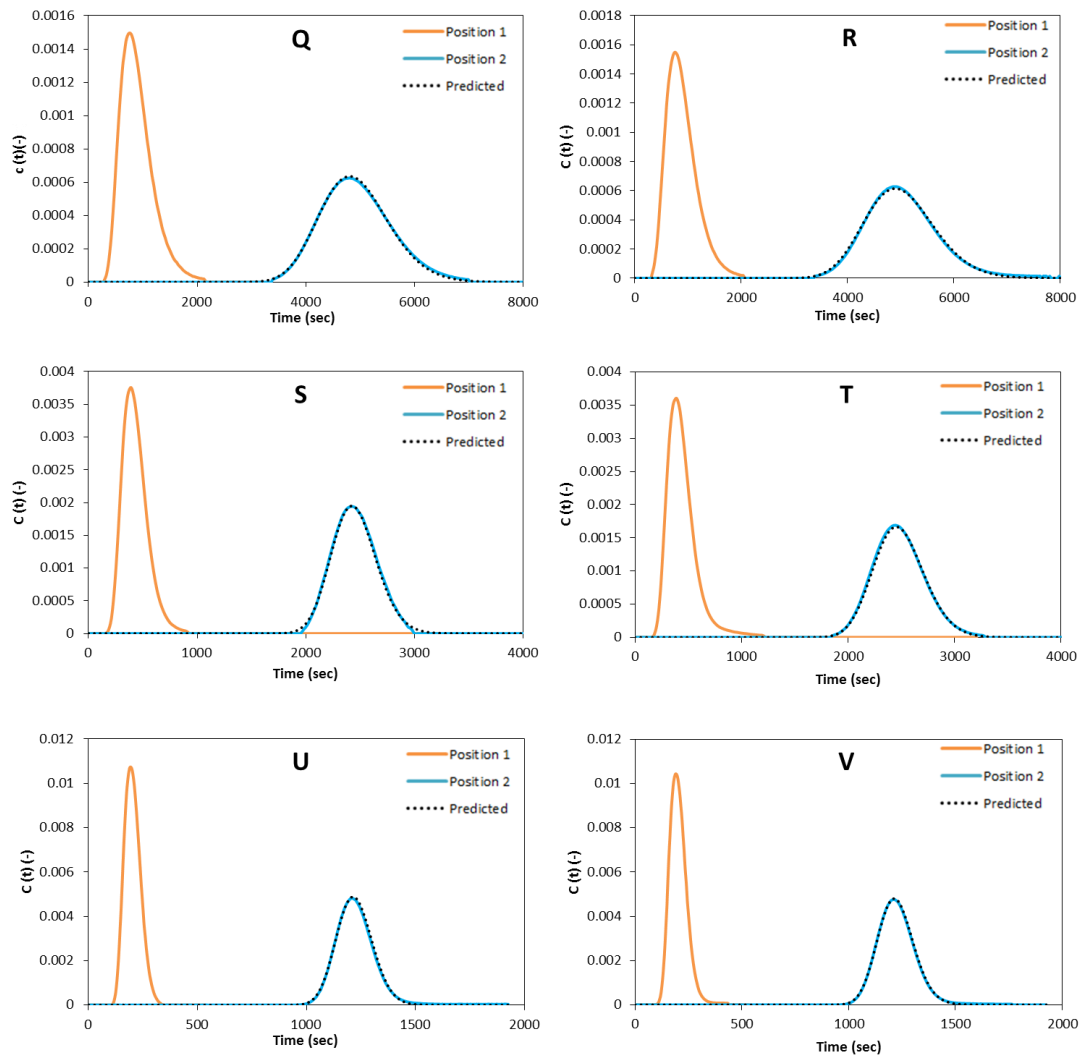
Figure 4.13 continued…

For all experimental conditions investigated E is shown to be below 0.02 which suggests there is only a moderate deviation form plug flow[164] under the operating conditions investigated with the DN15 COBC. The experimental conditions used in the study alongside the Peclet number and axial dispersion coefficient can be found in Appendix 1. An experimental consistency validation was also performed by comparing the amount of tracer calculated from experimental results and the known injected amount (0.0115 g) alongside the calculated mean calculated and measures residence time are also found in Appendix 1.

The results highlight the same general trends that are observed in the previous reports,[157,172,179,183] where increasing Re_o and φ results in an increase in E, (Figure 4.15 and Figure 4.16) and increasing St results in a decrease in the E (Figure 4.17). This is as to be expected as increasing Re_o provides an increase in oscillation intensity and more turbulence in the system, hence increased dispersion. Increasing Re_o whilst keeping Re_n constant (thus increasing φ) delivers increased turbulence to the flow therefore increases dispersion. It would be expected that the Investigation of Re_o <1000 and $\boldsymbol{\varphi}$ < 4 should result in a graph showing a minimum dispersion.

As St is inversely proportional to the amplitude, the higher the amplitude the greater the axial mixing, therefore the greater the dispersion. Here, investigations of St > 0.26 should result in a graph showing a minimum dispersion. Figure 4.18 shows the dimensionless E curves from all experiments. This graph has then been overlaid with a graph adapted from Levenspiel, [160,164] (Figure 4.19). In this figure the axial dispersion values are characterised into 5 stages, ranging from mixed to plug flow. According to this characterisation system small and intermediate deviations from plug flow are achievable.
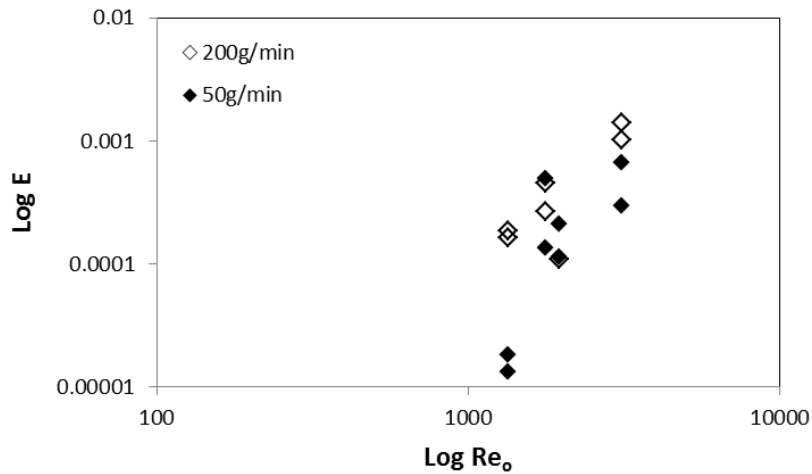
Figure 4.15: Dependence of axial dispersion on oscillatory Reynold's number. Graph illustrating an increase in the calculated axial dispersion coefficient as Re_o is increased. Increased Re_o results from an increase in dispersion caused by the increased oscillation frequency.
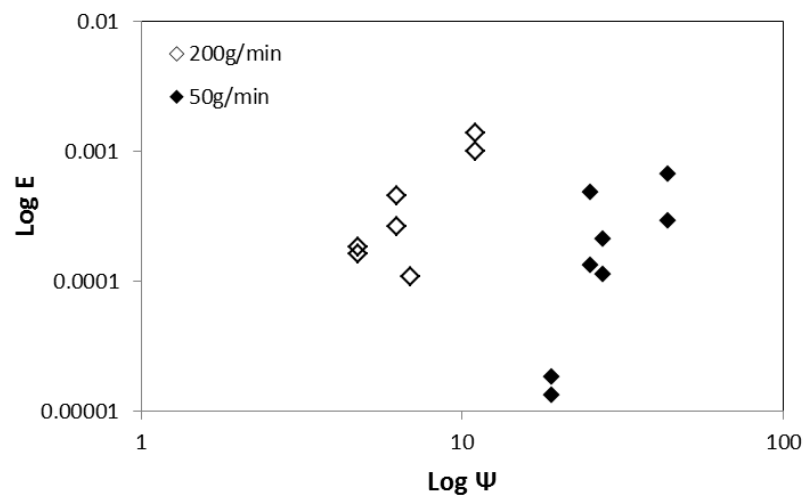
Figure 4.16: Dependence of axial dispersion on velocity ratio. Graph illustrating that an increase in the velocity ratio results in increased axial dispersion. Increasing Re_o, whilst keeping Re_n constant, results in increased turbulence and increased dispersion.
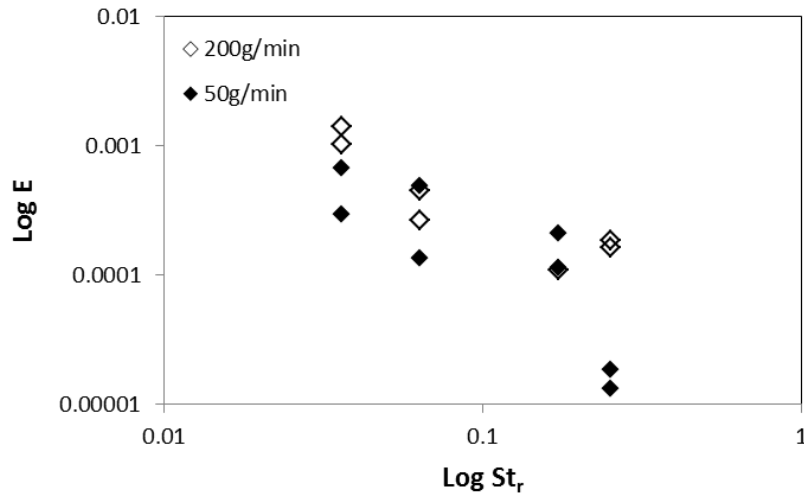
Figure 4.17: Dependence of axial dispersion on Strouhal number. Graph illustrating a decrease in the calculated axial dispersion coefficient as the St number increases. St is inversely proportional to the amplitude. Larger amplitudes result in greater axial mixing and greater dispersion.
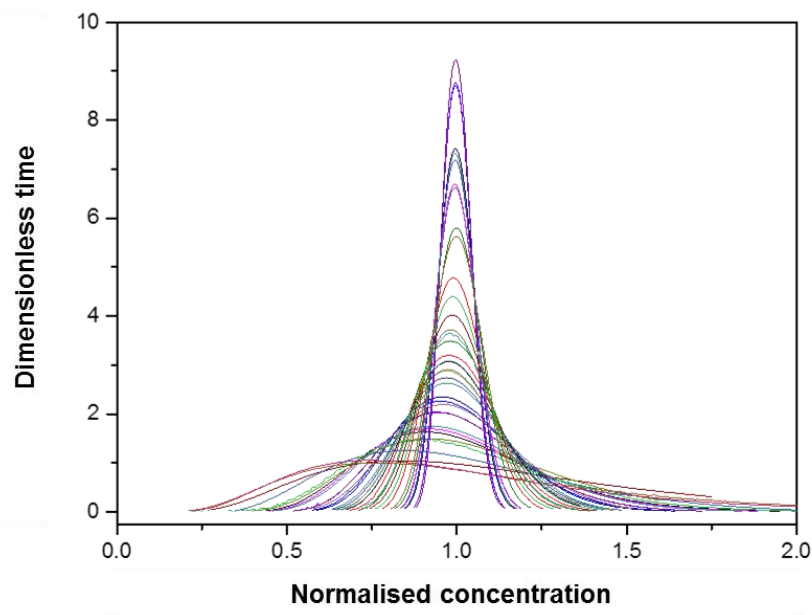
Figure 4.18: Dimensionless E curves. Experimental dimensionless E curves, calculated using the perfect pulse model, for Re_n and Re_o in the ranges of 65 – 260 and 1500 – 3300 respectfully.
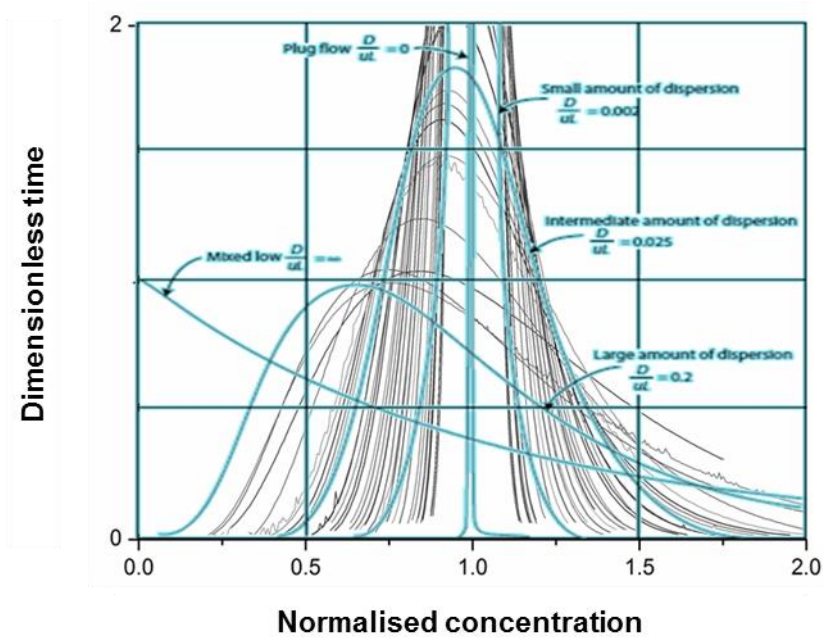
Figure 4.19: Comparison of experimental and theoretical dimensionless E curves. Overlay of experimental dimensionless E curves (black), calculated using the perfect pulse model, with a published characterisation system (blue). [160,164]

4.4 Summary

The overall aim of this work was to determine mixing characteristics in a DN15 COBC under accessible oscillatory and flow conditions. Under the conditions investigated in this study, the DN15 achieves low axial dispersion and operates with near plug flow. However, increasing Re_o and decreasing St, results in an increase in axial dispersion and a deviation from plug flow. Due to the low magnitude of this deviation, there is a wide operating window in which reasonable plug flow can be achieved and, as such, the platform has good potential to support controlled crystallisation processes.

This study presents the first application of UV absorbance measurements to assess RTD in a PFR. Concentration profiles obtained by UV absorbance were validated with known concentrations injected into and recovered from the COBC system. The relationship between oscillatory flow conditions and the axial dispersion were defined for the DN15 COBC, allowing operating conditions to be tailored to achieve near plug flow or to meet the needs of specific processes. This study also provides the first demonstration of the significant oscillation damping that occurs over extended lengths of a COBC system. Oscillation dampening has potentially significant implications for flow control, particularly for larger volume/length reactors. This highlights the need to develop better engineering solutions for the oscillation control, (see Appendix 3).

Whilst oscillation damping did not impact on the measurement of accurate RTD curves, it did prevent a systematic study of oscillatory conditions due to the need for retrospective calibration of the applied oscillatory conditions (Table 4.4). This raises interesting opportunities for crystallisation in terms of the impact of variable oscillatory mixing. For example, damping of oscillations could be advantageous in situations where more intense mixing is required, at the start of the process, to induce nucleation readily.[184] Oscillation damping may also have application in the control of shear sensitive systems, as a reduction in shear, due to reduced mixing intensity, along the length of

the system could minimise the formation of fines.[185] Conversely, oscillation dampening could also be problematic as more intense mixing may be needed to suspend the crystals as they grow to larger sizes.[155] In such a situation this damping effect would be unfavourable. A greater understanding of the change in mixing intensity along the tubular reactor is required to permit accurate control over critical process parameters.

Chapter 5. Crystallisation of LGA in Oscillatory Baffled Flow

5.1 Introduction

Despite being studied for hundreds of years, crystal formation and growth is a collective of phenomena of which knowledge is remarkably limited. The inability to fully characterise many crystallisation systems stems from difficulties obtaining reliable data for detecting the formation and subsequent growth of crystal nuclei. Confounding this process, many organic compounds exhibit polymorphism (they may exist in more than one crystal form, Section 1.4.3). As a consequence of physiochemical properties, e.g. bioavailability and solubility, being dependent on crystal forms,[1] the regulation of polymorph formation, growth and transformation is a fundamental requirement for crystallisation control.

In an effort to insure uniform mixing and flow environments during crystallisation, residence time distribution (RTD) performance of a DN15 continuous oscillatory baffled crystalliser (COBC) was characterised (Chapter 4). COBC systems enable crystallisation and growth of pharmaceutical systems, moving crystallising solutions and suspensions through a series of baffled tubes. The application of oscillatory flow, whilst new material is continuously introduced into the reactor, results in the formation of eddy currents within the baffles, enabling an efficient mixing, and near-plug net flow experience of the bulk solution. The enhanced turbulence (in radial direction of the vessel) provide the possibility of linear scale up and uniformity in bulk solution environment (distributions of shear rates and temperature gradients are reduced) alongside the decoupling of mixing and net flow resulting in long residence times. Considering this, COBC systems offer promise to the enable effective operation and scaling of pharmaceutical crystallisation processes to industrial-sized processes.

5.1.1 L-Glutamic acid

L-Glutamic acid (LGA, **Figure** 5.1) is a naturally occurring non-essential amino acid that is present in many food products, and is classified as a pharmaceutically relevant material.[186] LGA is frequently used as a flavour enhancer and is also incorporated into drugs used to treat a number of medical conditions such as hypoglycaemia, epilepsy, and Parkinson's disease[187]. It is also an important neurotransmitter[188] that is important for learning and memory[189].
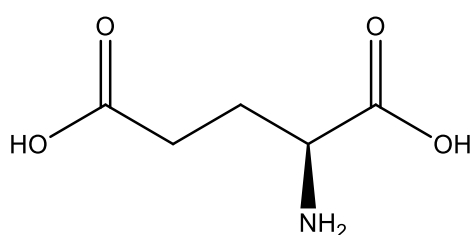
Figure 5.1: Molecular structure of L-glutamic acid. Figure showing the molecular structure of LGA, systematic name (S)-2-aminopentanedioic acid.

As it appears on the Generally Regarded as Safe (GRAS) list approved by the FDA, and the crystallisation properties have been well studied,[143,190-195] LGA is a good candidate for the development of a COBC crystallisation process. A continuous crystallisation process utilising seeding and a CSTR platform for the production of the metastable alpha form was successfully patented in 1968.[196] In 2010 a continuous anti-solvent crystallisation was reported producing exclusively the stable β polymorph.[129] More recently an MSMPR set-up was used to study the aqueous continuous cooling crystallisation of LGA.[142] Of direct relevance, LGA has been successfully crystallised in a batch oscillatory baffled column.[37,38,197] However, continuous crystallisation of LGA has not been studied under the distinct process conditions provided using the COBC technology and specifically the DN15 COBC (Chapter 4).

LGA has only two known polymorphs:[198,199] the metastable alpha and stable beta. Therefore, LGA is an ideal system to investigate polymorphic outcome of the crystallisation process in a COBC. Polymorphism is due to inherent differences in the crystal packing arrangements of the molecules (Figure 5.2) as such, each form has its own characteristic XRPD pattern (Figure 5.3). LGA crystal polymorphs also have distinct characteristic morphologies, the alpha form exhibits prismatic crystal morphology, whilst the beta form appears as a plate or as a needle-like shape (Figure 5.4).
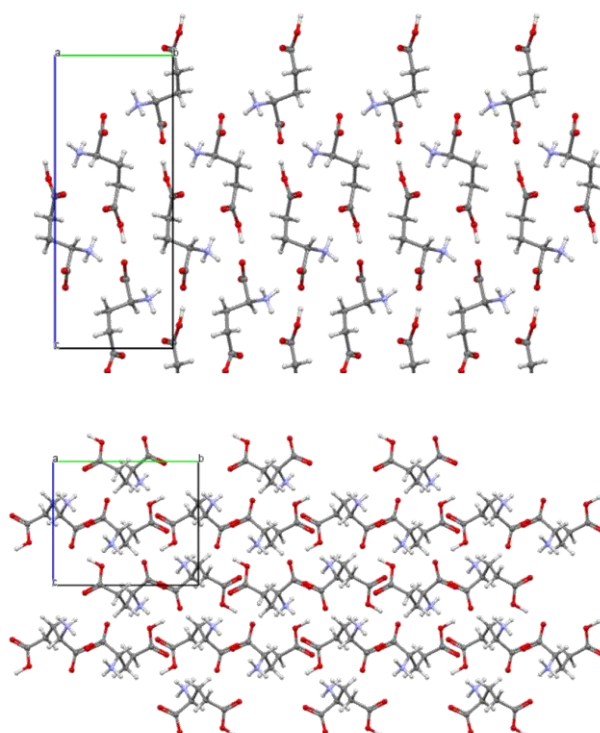
Figure 5.2: LGA packing arrangements. Two forms of LGA are known to exist: beta (top) and alpha (bottom), CCDC references LGLUAC and LGLUAC02 respectively.[198,199]
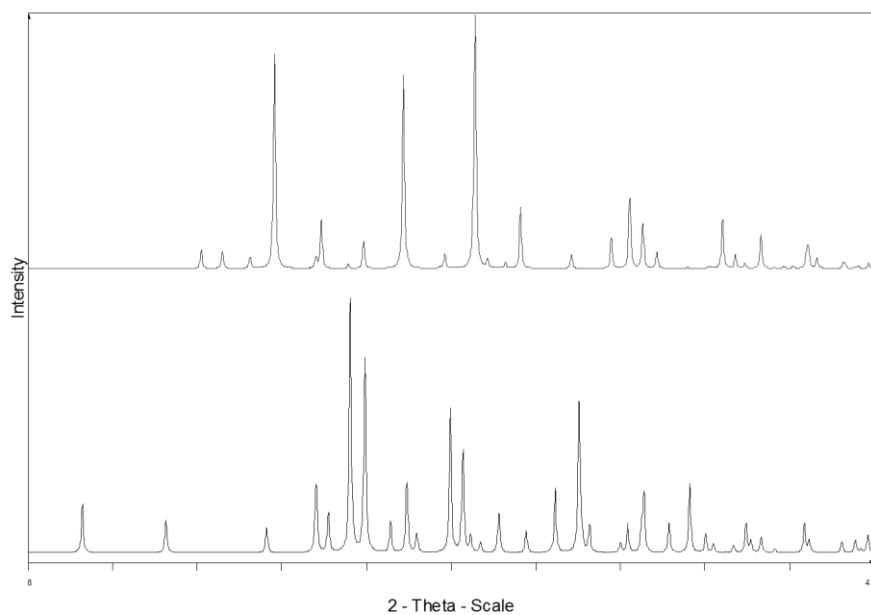
Figure 5.3: Overlay of XRPD patterns of LGA. The two polymorphs of LGA exhibit distinct XRPD spectra. The alpha form (top) and the beta (bottom), obtained from experimental crystallisations.
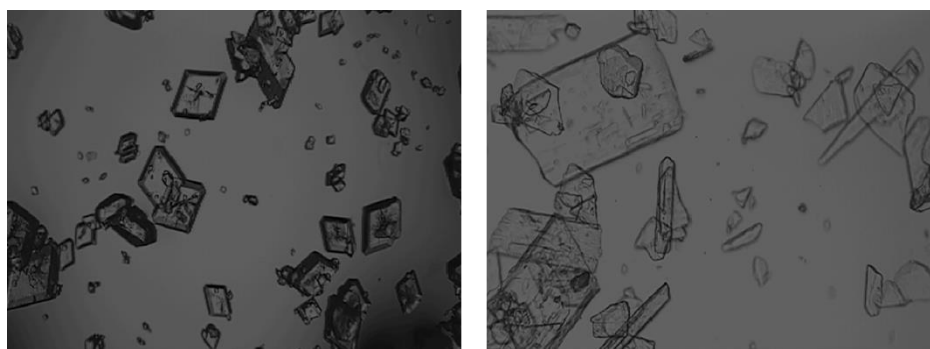
Figure 5.4: LGA polymorphic habits. The polymorphic forms of LGA exhibit different crystal morphologies. The alpha form (left) appears as prismatic crystals, whilst the beta form (right) appears as plate- or needle-shaped crystals. Images are of experimentally grown LGA crystals.

Polymorph selection of LGA has been achieved using a variety of techniques. These include cooling crystallisation, in both batch STC and OBC,[37,38,190,197] and reactive crystallisation using supersaturation control.[30,200] ATR-FTIR spectroscopy to monitor solution concentration has also permitted the control of LGA supersaturation in seeded batch cooling crystallisations[195] and reactive crystallisations.[201] Raman spectroscopy has been used to monitor reactive and cooling crystallisation,[194,202] whilst population balance modelling has also been used to model PSDs resulting from LGA crystallisations.[203-206] The wealth of thermodynamic and kinetic information provides the knowledge required to inform the development of a continuous crystallisation process. Reassuringly, the control of LGA polymorphism is consistent across most studies; Table 5.1 shows the proposed LGA crystallisation design space. Typically, the stable form may be selected by crystallising at high temperatures, high concentrations and by cooling over long time periods. Whilst employing faster cooling rates, with lower final temperatures and lower concentrations, favours the production of the alpha polymorph of LGA.

Table 5.1: LGA crystallisation design space. Summary of the crystallisation control of LGA .[37,38,190,191,194,197,207]

Polymorph		Transformation Rate
Concentration		Increases with increased agitation.
High (>45 g/L)	Low (<30 g/L)	Decreases with scale.
β	α	**MSZW**
Temperature		Increases with increased cooling
High (>45 °C)	Low (<20 °C)	rate.
β	α	Decreases with increased agitation.

The first stage in the design of a cooling crystallisation process is the determination of the temperature dependant solubility of the compound of interest in the selected solvent. Figure 5.5 shows the solubility of both alpha and beta forms of LGA in water across the temperature range of 10 – 80 °C, obtained by gravimetric analysis.[193] The solubility curves illustrate the monotropic relationship of LGA polymorphs, the metastable alpha showing the higher solubility over all temperatures. This solubility difference can cause LGA to undergo a solution mediated polymorphic transformation (SMPT) to the more thermodynamically favourable, lower solubility, beta form. Attempts to control and manipulate the transformation kinetics resulting in this SMPT have included the variation of a number of process conditions (cooling rate, agitation, *T*, hold time).[191,194,202,203,208] Increasing temperature may increase the rate of SMPT, and elevated agitation may also favour the isolation of the alpha form of LGA. The effect of additives on the crystal morphologies, growth rates, and transformation times have also been investigated.[192,207,209]
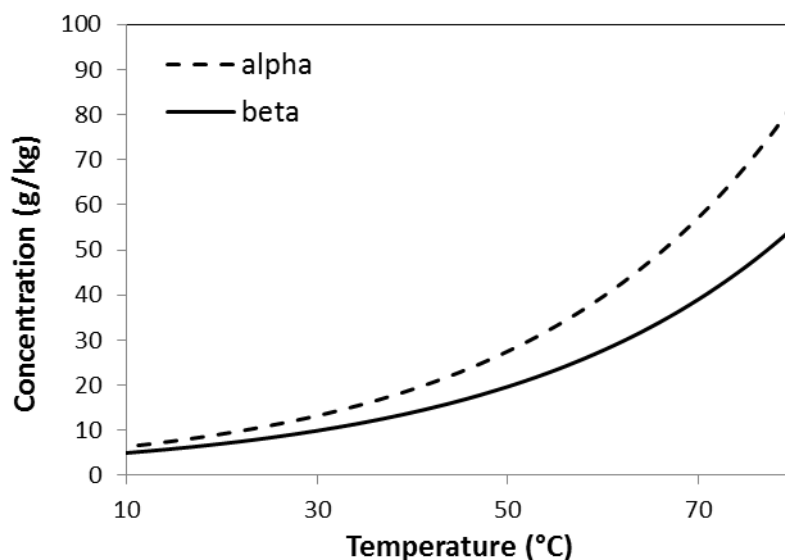
Figure 5.5: Solubility of alpha and beta LGA in water. Data obtained through gravimetric analysis.[193]

5.1.2 Crystallisation in an oscillatory baffled crystalliser

Over the last decade, oscillatory baffled platforms (Chapter 4) have received increasing interest due to their potential promise as a technology for efficient crystallisation control. Crystallisation related literature of oscillatory baffled platforms is summarised in Table 5.2. In terms of the translation of batch crystallisation processes to a continuous oscillatory baffled crystallisation, there have been limited studies.[35,124,210]. Ni *et al.*,[35] describe the development of a continuous crystallisation process of an API molecule and report a practical approach to the development of a 25 m DN25 COBC system. Cooling rates and agitation in a batch OBC were used to define the operating conditions to achieve the desired morphology and particle size. The continuous crystallisation[35] delivered a significant reduction in process time reducing from 10 hours, in an industrial scale STC, to 12 minutes in the COBC. This is clearly a significant benefit in terms of potential reduced production costs, however the report does not provide a detailed description of the final conditions and only a limited discussion of the underpinning reasons for this result is presented.

.

Table 5.2: Current literature on oscillatory baffled crystallisations.

Batch/Conti.	Method	System	Conclusions	Ref.
Batch	Cooling	Paracetamol	Production of higher quality crystals in terms of PSD, surface and microstrain	211-213
Batch	Cooling & Seeding	L-glutamic acid	Higher nucleation rates promotes narrow MSZW, polymorph control	37,38,197
Continuous	Cooling	Aspirin	Successful production and operation of COBC system for 7 days	210
Batch & Continuous	Cooling	API (AstraZeneca)	Successful scale up to continuous. Batch system allowed production of desire morphology and improved PSD than previous method. Continuous production allowed the crystallisation process to be cut down from nearly 10hours to just over 10 minutes.	35
Batch	Cooling, antisolvent	Paracetamol	Non-invasive imaging used as a method for detection of nucleation, MSZW, growth rates, PSD and mean crystal sizes.	214-216
Batch	Cooling, seeding	Sodium Chlorate	Moving baffles design promotes unexpected nucleation of the opposite enantiomer of the seed crystal used.	217-219
Batch & Continuous	Cooling	L-glutamic acid, Mannitol	Non-invasive Raman used to monitor the crystallisation process. Polymorph control with a change in oscillatory conditions	220
Batch & Continuous	Cooling, antisolvent	Lipoic Acid: Nicotinamide co-crystal	Successful scale up from small scale to production scale. Spherical crystallisation via a possible emulsion crystallisation.	124
Batch	Cooling	Adipic Acid	Population balance modelling approach is more accurate for predicting nucleation kinetics	221

A study involving vanisal sodium and aspirin focused on establishing a cleaning strategy for the COBC.[210] Here a 12 m DN15 system was operated with 2 heater/chillers for temperature control and experiments were ran for 7 days producing both materials at high purity without fouling. This study only reports the final continuous operating conditions with no detail on the process development methodology.

An investigation using non-invasive Raman spectroscopy details monitoring of nucleation and resulting polymorphic form during batch (moving baffle) and continuous oscillatory baffled crystallisation of LGA and D-mannitol.[220] This work details the impact of various oscillatory conditions on particle properties and compares oscillatory mixing to STC platforms. Here limited operation with COBC technology is highlighted due to challenges of blockages and encrustation. Both the metastable and stable polymorphic forms of D-mannitol where observed during continuous operation, however the production of only the metastable form of LGA was reported with no production of the stable beta polymorph.

The most recent study on a COBC system was a co-crystallisation[124] scaled up in a similar manner to the Ni API study.[35] Crystallisation conditions (cooling profile and oscillatory parameters) were first assessed in a batch system then applied to continuous crystallisation in the COBC. The 25 m DN15 COBC was operated for up to four crystalliser residence times producing pure co-crystalline solid in the form of spherical agglomerates. No fouling was reported during the continuous crystallisation. Although both of these studies reported final continuous operating conditions,[35,124] the details provided with regards to process development are inadequate to inform upon the development of a generic workflow towards crystallisation utilising a COBC platform.

Although approaches for translating liquid phase processes from batch to continuous oscillatory baffled flow systems have been reported in the literature,[179,222-224] these do not specifically address the additional considerations required when dealing with complex multi-step, multiphase

processes such as crystallisation. Moreover control of polymorphic form in a COBC has not been addressed. Therefore, this chapter therefore seeks to develop continuous cooling crystallisation processes with selectivity over both of the well characterised alpha and beta polymorphic forms of LGA in a COBC.

5.2 Experimental

5.2.1 Batch crystallisations of LGA in STC and OBC

Batch crystallisations were carried out in a 500ml OBC system (Figure 5.6). A baffle string was oscillated through the solution via a linear motor attached to a control box. STC experiments were performed using a 500 ml vessel, and agitation was applied by a 2 blade impeller attached to an overhead stirrer (Figure 5.7).
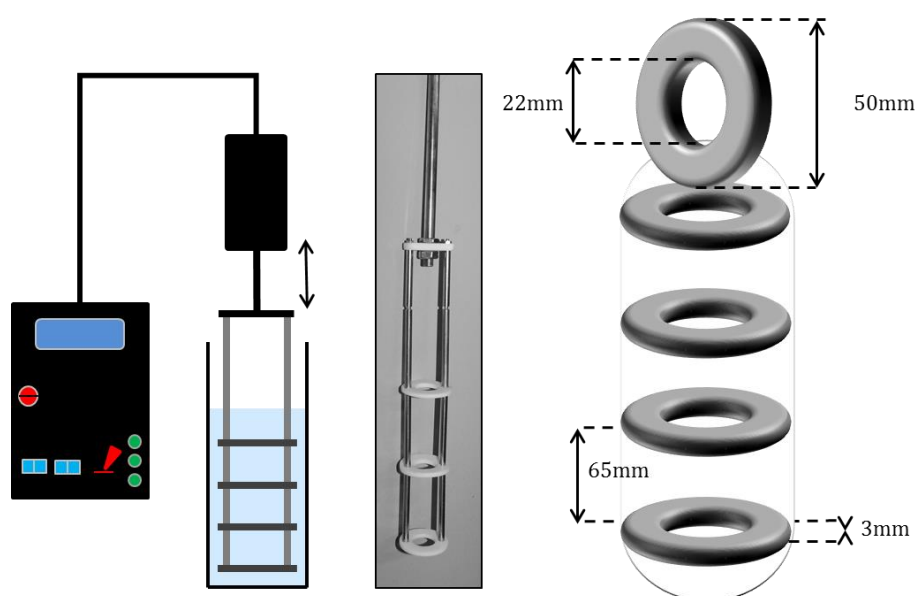
Figure 5.6: Batch OBC set-up and dimensions. Schematic showing the batch OBC system with control box and linear actuator (left), photograph of a baffle string (centre) and baffle shape including dimensions (right).

Batch vessels were jacketed and temperature was controlled by a heater/chiller (HC) that circulated water coolant around the jacket. HCs were programmed to cool at 1°C min^{-1} or, where crash cooling was required for rapid heat extraction, a second HC was pre-set to the desired end temperature and the jacket connections were rapidly changed over. When FBRM was used for nucleation detection, the nucleation temperature was determined at the point where the number of counts increased about 500.
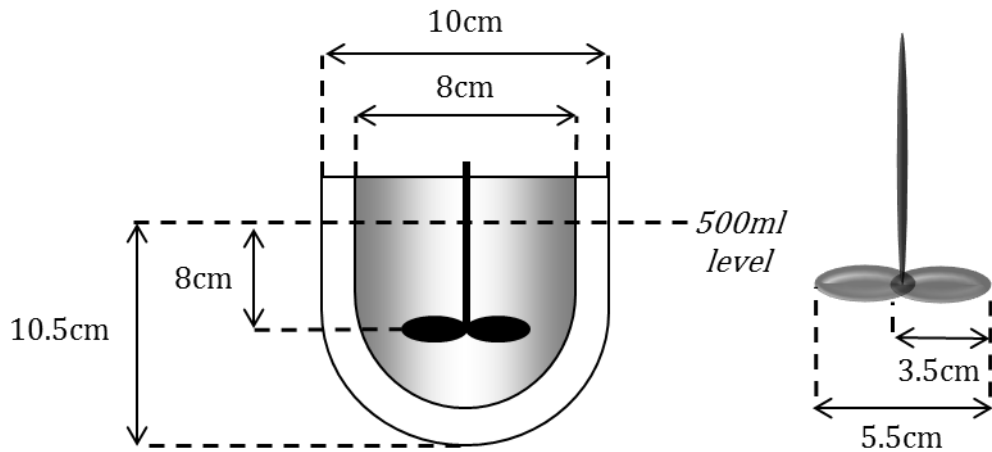
Figure 5.7: Batch STC set-up and dimensions. Schematic showing STC set-up used for crystallisations, dimensions of vessel (left) and impeller (right) are shown.

Due to the difference in flow regimes between STCs and OBCs, the two systems cannot be accurately compared using process parameters such as stirring speed. Instead, the power dissipated by the system, defined by the power density (ϵ), W m^{-3}, was calculated. The power density is the amount of power applied to a system per unit volume, and the calculation of ϵ provides a basis for comparative work in different reactors.[217] The power density for an STC (ϵ_{STC}) was calculated from:[225]

$$\epsilon_{STC} = \frac{P_o \rho N_s^3 D_s^5}{V_L}$$

Eqn. 5.1

where P_o = power number of the impeller used, ρ = density (kg m $^{-3}$), N_s = stirring speed (rpm), D_s = diameter of stirrer (m), V_L = volume of liquid in STC (m^3). There are two common models used to estimate power density within an OBC; the quasi-steady flow model and the eddy acoustic model. The eddy acoustic model incorporates the effects of flow interaction with the baffles whilst the quasi-steady flow model assumes the pressure drops in oscillatory flow and in non-oscillatory flow are equal at constant velocity, details of both models can be found elsewhere.[226] As quasi-steady flow has been validated

for amplitude and frequencies directly relevant to operating conditions used in this current work (Chapter 5), it was selected for use. The power density of an OBC (ϵ_{OBC}) was calculated by:[226]

$$\epsilon_{OBC} = \frac{2\rho N_b}{3\pi C_D^2}\left(\frac{1-\alpha^2}{\alpha^2}\right)\chi_o^3\,(2\pi f)^3 \qquad \text{Eqn. 5.2}$$

where N_b = number of baffles per unit length of OBC (m^{-1}), C_D = the coefficient of discharge of the baffles (normally 0.7),[197] χ_o= oscillation amplitude, centre-to-peak (m), f = oscillation frequency (Hz).

LGA was crystallised in an OBC, operated at 20 mm (peak-to-trough) and 2 Hz, or an STC, operated at 300 rpm. The power dissipated by the OBC and the STC were 546 Wm^{-3} and 459 Wm^{-3} respectively. These values are within the working ranges of previously reported oscillatory baffled crystallisation studies.[37,212,217] The power number for the impeller used was calculated to be 2.8 according to the rules described by Nienow.[227] Six crystallisation experiments (3 concentrations of LGA and 2 cooling profiles) where performed using each of the systems, covering the DoE design space shown in Table 5.1. To ensure complete dissolution of starting material, solutions where held at 10 °C above the solubility temperature for 30 minutes prior to commencement of experiments. Experimental parameters are described in Table 5.3.

Table 5.3: Experimental conditions for batch LGA studies

Conc. (g/Kg)	Sol. T (°C)[#]	Start T (°C)	End T(°C)	CR (°C/min)	Hold time (min)
20	48	58	20	1	0
35	66	76	20	1	0
45	73	83	20	1	0
20	48	58	20	CC	30
35	66	76	20	CC	30
45	73	83	20	CC	30

Sol. = solubility, # =with respect to beta LGA, CR = cooling rate, CC = crash cooled (as described in 5.2.1).

5.2.2 Unseeded continuous crystallisations of LGA

Unseeded continuous crystallisations were performed in a COBC system comprising of 22 straights and 11 bends. The system was mounted vertically, as shown in Figure 5.8. Water coolant was circulated through the jackets in a counter current by six HCs. The temperature zones controlled by each of the HCs are shown in colour. Fluid oscillation was provided by a fluid filled bellow unit controlled by custom electronics (housed in a control box). Before tube lines were changed over to supply the feedstock, both the COBC and the bellow unit were flushed with solvent using peristaltic pumps. During crystallisation, slurries were collected at the outlet. The temperatures, at the boundary between each HC controlled temperature zone, were recorded manually from thermocouples inserted into the COBC through PEEK collars.
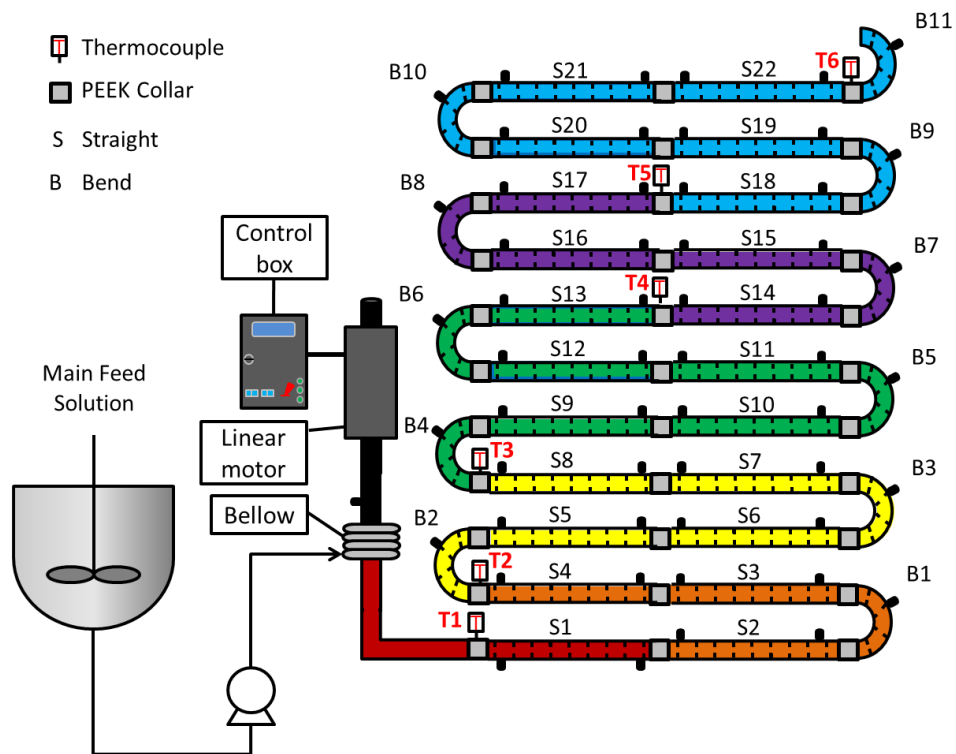
Figure 5.8: COBC set-up for unseeded crystallisations. Photograph (top) and schematic (bottom) of the COBC crystallisation system. Thermocouples are labelled in red and the 6 temperature zones are indicated by colours (zone 1 S1, zone 2 S2 – S4, zone 3 S5 – S8, zone 4 S9 – S13, zone 5 S14-S17 and zone 6 S18 – S22).

To prevent heat loss and possible premature crystallisation of the feed stock during entrance to the COBC, the temperature of S1 was matched to that of the main feed solution. This was done by attaching the same HC to the jackets of both S1 and the main feed vessel. The solution was cooled across subsequent COBC sections (S2-4; S5-8 etc.). The temperature profile over the entire COBC was set to achieve a linear cooling rate using the following calculations. First, flow rates (FR) were calculated from the reactor volume (V) and the required residence time (RT) described by:

$$FR = {V}/{RT}$$
<div align="right">Eqn 5.3</div>

Fluid velocities (V_m) were then calculated from flow rates using:

$$V_m = {RT}/{A_c}$$
<div align="right">Eqn 5.4</div>

where A_c is the area of a COBC straight. The time for a fluid element to reach to reach a certain distance (t_x) was then calculated from:

$$t_x = {D_m}/{V_m}$$
<div align="right">Eqn 5.5</div>

where D_m is distance. The temperature at a certain distance (T_x) could then be calculated from knowledge of the initial starting temperature (T_i) and the cooling rate, described by:

$$T_x = T_i - (CR)t_x$$
<div align="right">Eqn 5.6</div>

Table 5.4 and Figure 5.9 show an example of calculating the desired cooling profile and the experimental data gathered during the run. During the continuous unseeded crystallisation experiments various cooling rates were applied and experimental conditions can be found in Appendix 2.

Table 5.4: Example of a cooling profile used for an unseeded COBC experiment. The table shows calculated linear cooling profile and measured temperature data.

Section	No. of Straights	Distance (m)	T Calculated (°C)	Time (min)	T Recorded (°C)
1	0	0	70.0	0.0	71.9
	1	0.7	50.0	2.3	
2	2	1.66	47.0	5.8	
	3	2.36	46.2	8.2	
	4	3.32	45.2	11.5	45.5
3	5	4.02	44.5	14.0	
	6	4.98	43.5	17.3	
	7	5.68	42.8	19.7	
	8	6.64	41.8	23.1	41.7
4	9	7.34	41.0	25.5	
	10	8.3	40.0	28.8	
	11	9	39.3	31.3	
	12	9.96	38.3	34.6	
	13	10.66	37.6	37.0	37.6
5	14	11.62	36.6	40.3	
	15	12.32	35.9	42.8	
	16	13.28	34.9	46.1	
	17	13.98	34.1	48.5	34.2
6	18	14.94	33.1	51.9	
	19	15.64	32.4	54.3	
	20	16.6	31.4	57.6	
	21	17.3	30.7	60.1	
	22	18.26	29.7	63.4	29.5
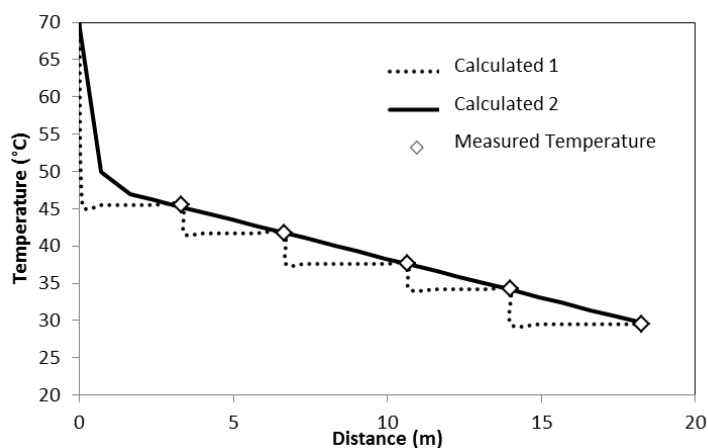
Figure 5.9: Example of a linear cooling profile for cooling crystallisation in a COBC. Plot showing calculated and measured temperature values. Calculated 1 corresponds to the theoretical step change assuming the fluid moving into the temperature zones reach the chiller set point temperature instantaneously, Calculated 2 corresponds to the theoretical linear cooling profile described by equations 5.3 – 5.6.

5.2.3 Seeded continuous crystallisation of LGA in a COBC

Seeded crystallisations of LGA were performed in a COBC mounted horizontally, as shown in Figure 5.10. The growth solution and the seed suspension were supplied by two independently heated STCs, with peristaltic pumps used to provide flow. The main feed growth solution was prepared at 2 concentrations, and the seed suspension prepared at 2 seed loadings. The total length and volume of the system were 25 m and 5.1 L, respectively. However, as the seeding port was located between straights 2 and 3, only 30 straights and 8 bends were used for growth. This resulted in a reduced system volume of 4.6 L). The second straight (S2) was used to cool the solution to a supersaturation of approximately 1. The temperature of straight S2 and the seed suspension were controlled by the same HC. To maximise control over the temperature profile, 24 thermocouples were used to record the cooling profile of thirteen temperature zones. Operating conditions can be found in Table 5.5.
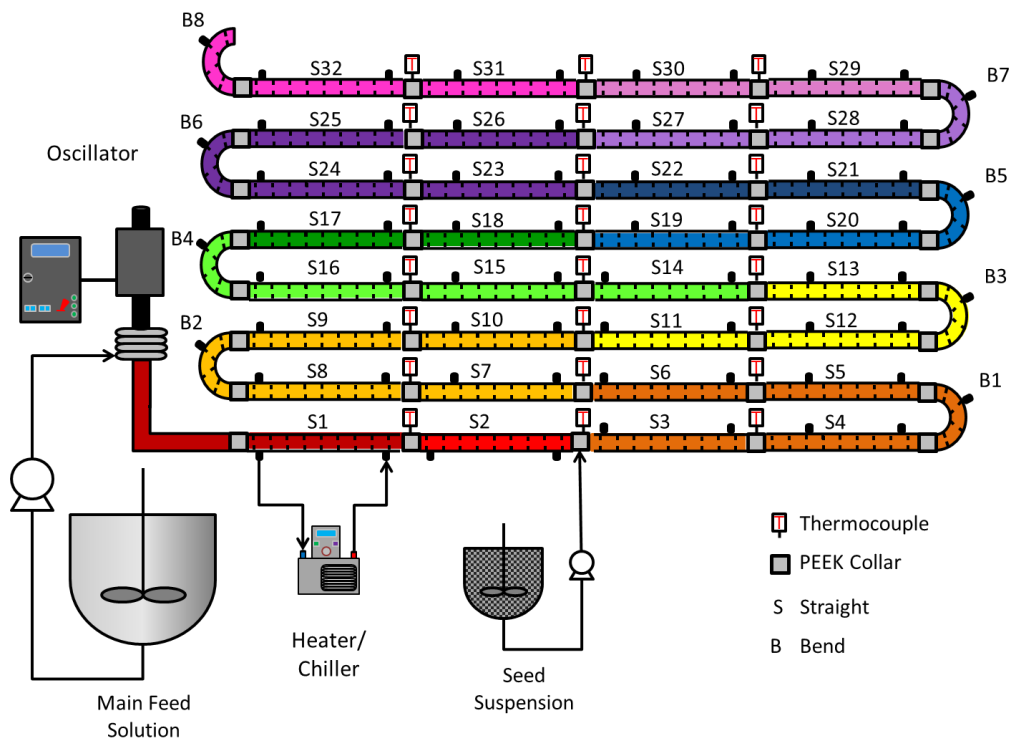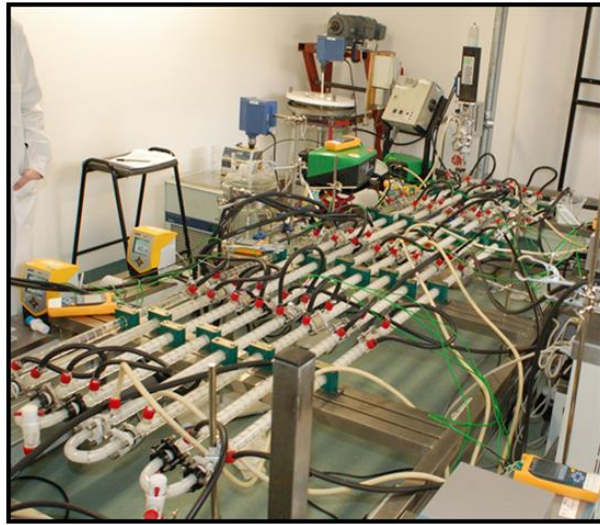
Figure 5.10: COBC set-up for seeded crystallisations. Photograph (top) schematic (bottom) of the seeded COBC crystallisation platform. Thermocouple positions are shown, and the 13 temperature zones are indicated by colours (zone 1 S1, zone 2 S2, zone 3 S3–S6, zone 4 S7–S10, zone 5 S11-S13, zone 6 S14–S16, zone 7 S17–S18, zone 8 S19–S20, zone 9 S21–S22, zone 10 S23–S26, zone 11 S27–S28, zone 12 S29–S30 and zone 13 S31–S32)

Table 5.5: COBC seeded crystallisation operating parameters

Freq	Amp	Main flow (g/min)	Seed flow (g/min)	Re_n	Re_o	Ψ	St
1	30	30	20	70	1400	20	0.008

5.3 Results & discussion

5.3.1 Batch crystallisation

Batch experiments were carried out to obtain process conditions required for the continuous crystallisation. To enable comparison of performance between batch crystallisation platforms, a similar power density was used for both batch STC and OBC studies. Polymorph control was achieved under the conditions used in the batch OBC. However, full polymorph control was not possible under a comparable power input in the STC set-up, and control over both polymorphs of LGA was not achieved (Table 5.6). Kinetic data can be found in Table 5.7 and it can be observed that when a controlled cooling rate (1 °C/min) is applied to the systems, under comparable power densities, the MSZW (ΔT) of the OBC is narrower than the STC. It can also be noted that for the lowest concentration studied (20 g/kg), the STC failed to nucleate during both applied cooling profiles, whereas under the same time frame the OBC nucleated in both cases. It can therefore be concluded that the OBC appears to promote nucleation more readily when compared to STC system, which is in agreement with other studies.[37,220] It is postulated that the effective mixing environment and heat transfer capabilities of the OBC enable uniform control over crystallisation conditions. Here, selectivity between the two solid forms of LGA was achieved. Representative crystals, obtained from the OBC and STC systems are shown in Figure 5.11.

Table 5.6: Polymorphic forms of LGA obtained from batch crystallisations.

Concentration (g/kg)	CC		1°C/min		Cooling Rate Platform
	OBC	STC	OBC	STC	
20	α		β		
30	α	α and β	β	αandβ	
40	α	α and β	β	β	

Table 5.7: Kinetic information obtained from batch crystallisation studies.

Applied Cooling	Concentration (g/kg)	OBC			STC		
		Nuc. (°C)	S	ΔT (°C)	Nuc. (°C)	S	ΔT (°C)
CC	20	20	2.2*	22			
	30	20	3.3*	33	20	3.3*	33
	40	20	4.3*	40	20	4.3*	40
1°C/min	20	33.4	1.8#	9.6			
	30	36.1	2.5#	24.9	31.6	2.8#	29.4
	40	48.8	2.1#	11.8	37.9	3.1#	32.1

*Nuc. = nucleation temperature, * = wrt alpha, # = wrt beta.*
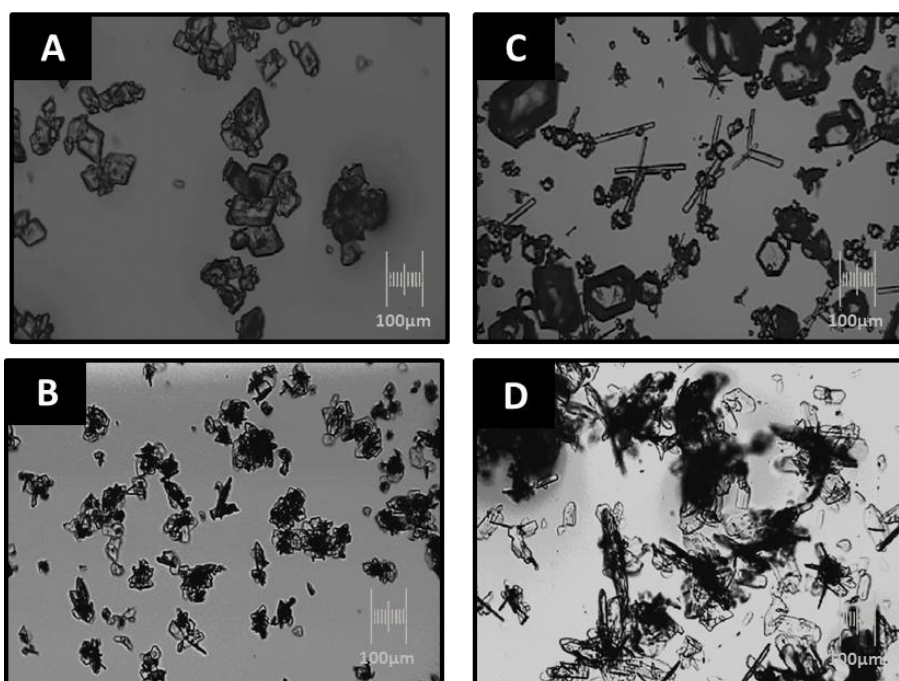
Figure 5.11: Microscopy images of product. Optical microscope images of crystals produced collected from batch crystallisation, α (A) and β (B) LGA from an OBC, mixed α and β (C) and β LGA product (D) from a STC.

5.3.2 Unseeded continuous crystallisation of LGA

When crash cooling was implemented over a series of concentrations, the alpha form of LGA could be isolated routinely in the batch OBC. Exclusive production of the alpha form of LGA was also achieved under similar conditions (power density, and cooling profiles) implemented in the COBC under continuous operation. Unexpectedly, fouling of the surface of the glass baffle tubes was observed during these COBC experiments: crystals began to grow on the inside of the glass walls, coating the entire surface (Figure 5.12). This encrustation led to blockages and shutdown of the process. This build-up of solids will also interfere with heat transfer and overall mass balance of the process. There are many terms in the literature to describe the phenomenon of unwanted solid deposition on reactor walls or other surfaces exposed to the process (e.g. PAT probes), these include scaling, encrustation, fouling or bearding. Encrustation is discussed in more detail in Chapter 6.
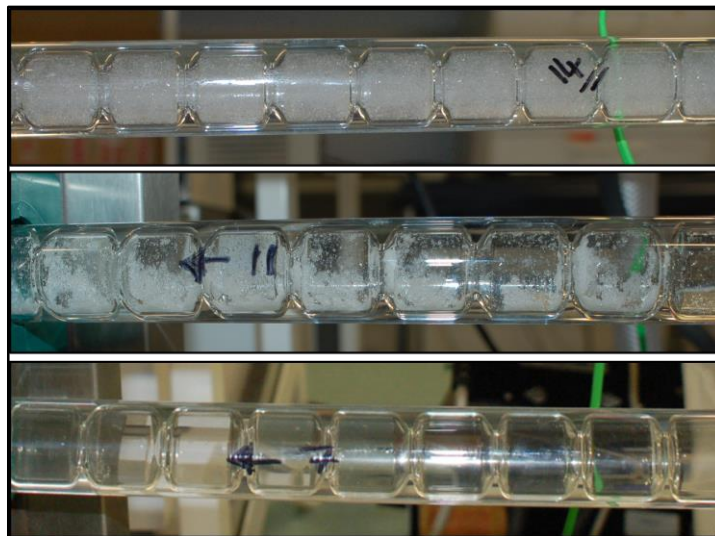
Figure 5.12: Encrustation during unseeded crystallisation in COBC. Straight 7 shows a clear solution prior to nucleation, straight 11 shows severe encrustation and straight 14 showing a straight that contains encrusted walls with a dense suspension of crystalline material flowing through.

Encrustation limited the investigation of nucleation of LGA in the COBC. Encrustation is a severe problem in continuous crystallisation processes, particularly when operated for extended periods, as it can disrupt heat transfer, supersaturation, back pressure, oscillatory conditions and size control. This loss of control led to restriction and blockages of the baffles (Figure 5.13), complete blockages of the tubes, and in some cases deformation of the bellow driving the oscillation (Figure 5.14). Encrustation occurs due to the high supersaturation within the system during cooling and results in uncontrolled nucleation.[228] Problems associated with fouling and encrustation highlight the need to ensure adequate control of supersaturation throughout the crystallisation process, and to ensure sufficient growth surface is available to minimise nucleation, growth and/or attachment of crystals at the vessel surface in preference to a growing crystal surface in the bulk.
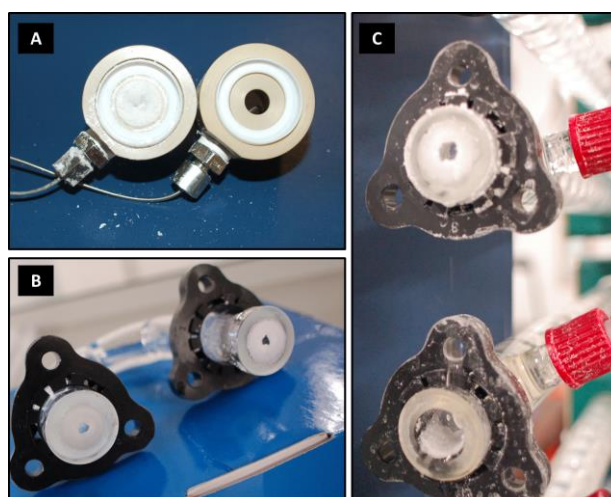
Figure 5.13: Blockages during unseeded crystallisations in the COBC. Photographs showing PEEK collars (A) with a complete blockage (left) in comparison to a clean collar (right), partial blockage and restriction of a COBC bend (B) and the partial blockage of a COBC straight (C).
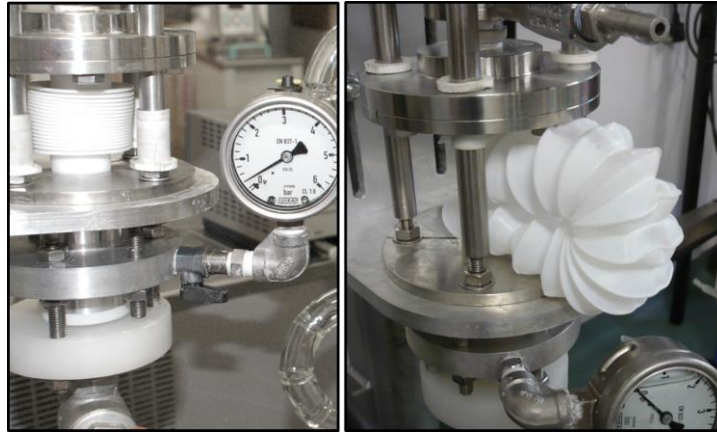
Figure 5.14: DN25 bellow unit. Photographs showing the bellow unit pre blockage (left), and post blockage (right).

One of the most interesting observations during unseeded experiments was the noticeable back propagation of nucleation under near plug flow (i.e. under limited back mixing conditions) after the onset of primary nucleation at a given point in the reactor, Figure 5.15. Assuming the diffusion of nuclei are governed by Ficks first law of diffusion,[75] in an unmixed system, the time taken, t, for a nuclei to diffuse a distance x, can be described by:

$$t = \frac{x^2}{2D}$$
<div align="right">Eqn 5.7</div>

where D is the diffusion coefficient of the nuclei. Thus, a molecular nucleus that was formed in straight 14, 11.4 m from the bellow, would take at least 37 minutes to diffuse back towards the bellow. During unseeded LGA COBC experiments (section 5.2.2) observed times for movement of the nucleation front over 10 - 18 m were ca. 20 minutes. The diffusion excludes the flow in opposite direction and because larger clusters of molecules would be expected to diffuse more slowly, clearly one or more other mechanisms must be responsible for the observed behaviour (i.e. rapid progression of nucleation front against the net flow during near plug flow operation).
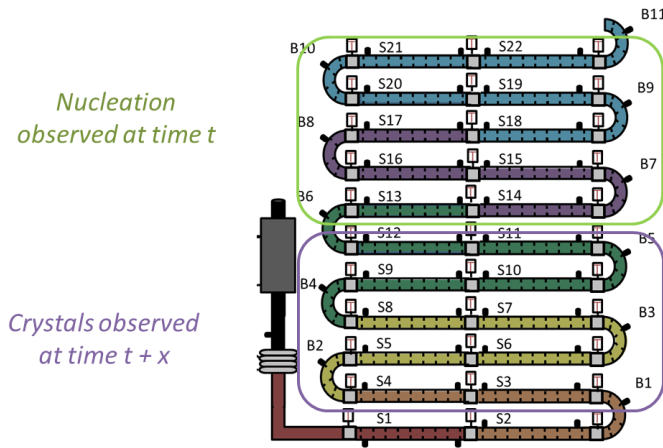
Figure 5.15: Observed movement of nucleation position during unseeded crystallisations. The first sign of nucleation appearing at time, t, at a given position along the rig, and sometime later, at a time t + x, crystals are observed at a position upstream of the original observed nucleation point.

The apparent propagation of nucleation was observed in all of the unseeded crystallisation experiments carried out. Typically crystals would be present in all upstream straights after a single residence time prior to the first observation of nucleation. From the RTD experiments (Chapter 4) it can be shown that the COBC was operated at near plug flow conditions and so back mixing within the system should be limited and not the dominant process.[164]

The proposed mechanism (Figure 5.16) suggests, due to the oscillations within the system, crystals move against the direction of net flow during the back stroke (i.e. upstream towards the inlet) with a distance depending on the applied amplitude. These crystals then act as parent crystals triggering secondary nucleation. This cycle of self-seeding may lead to the successive birth of new crystals on each oscillatory back stroke, moving the effective secondary nucleation front upstream of the original nucleation point. In this scenario, it is to be expected that secondary nucleation will continue to occur until the supersaturation is sufficiently low and secondary nucleation is no longer favoured. This effect is therefore unique to oscillatory PFRs and would not be observed in non-oscillatory PFR systems. Further work is merited to

understand how this effect may be controlled as part of an effective seeding strategy, potentially as an alternative to continuous seeding.
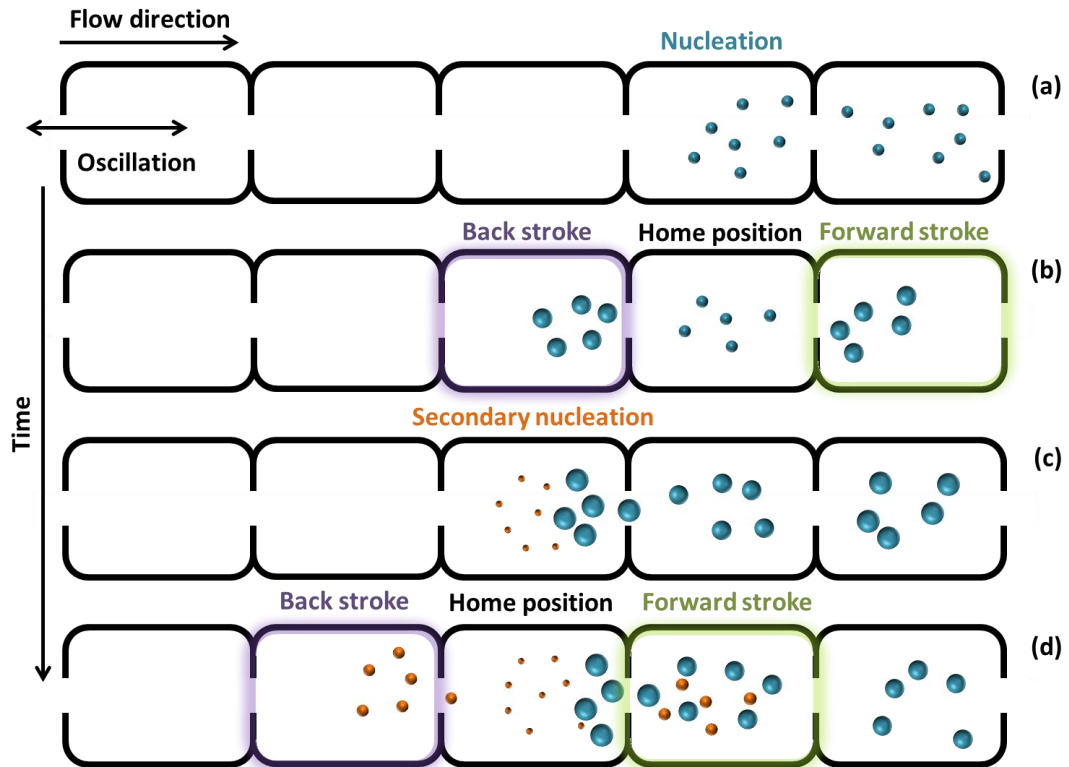
Figure 5.16: Secondary nucleation propagation mechanism hypothesis in a COBC. When a primary nucleation event occurs under continuous oscillatory flow (a), nuclei will be forced into the two adjacent baffle cells on both the back and forward stroke of the oscillation (b). This can promote secondary nucleation (c) and effectively creating a self-seeding mechanism for the system that nucleates cells upstream of the nucleation event, even under plug flow conditions.

Recently, Myerson *et al.*,[229] described contact secondary nucleation as a method of creating seeds within tubular flow systems. Here a single parent crystal was glued in the centre of a tubular device with a net flow of supersaturated solution. When the crystal was rotated with applied stress (optimised to avoid microabrasion or breakage), secondary nucleation could be generated in the exit fluid stream. This method was applied for both

glycine and acetaminophen, and the resulting sizes of both materials were in the order of 10 µm. It is reasonable to suggest that the same principle of inducing secondary nucleation, from parent crystals in contact with fresh supersaturated solution in flow, could be applied to the COBC during oscillatory motion. Crystal contact with baffles, walls and/or other crystals in the slurry during oscillation could be enough to remove the adsorbed solute layer from these parent crystals resulting in secondary nuclei.[230]

Control of secondary contact nucleation has been demonstrated, using closed-loop feedback control, to remove fines during batch acetaminophen crystallisation in an STR.[79] In this study, automated feedback from FBRM was used to control temperature cycling of the bulk solution after primary nucleation took place. Heating cycles were triggered when the number of small counts from the FBRM increased above a certain threshold i.e. the temperature cycles were related to the occurrence of a secondary nucleation event. After dissolution of these fines, cooling was enabled and heating cycles were initiated on the FBRM detection of the next secondary nucleation event.[79] This work illustrates the importance of defining the MSZW for secondary nucleation and benefits of working within it to achieve size control.

In over 30 continuous unseeded crystallisation experiments, the COBC exclusively produced the metastable alpha phase. In a small number of these unseeded COBC studies trace amounts of the beta form where observed. This is in sharp contrast to the batch OBC experiments (section 5.3.1). However, the COBC always fouled during studies where supersaturation was increased into the labile region of the phase diagram, i.e. to promote primary nucleation of LGA crystals. It is clear that the nucleation conditions were different in the COBC than from other reported systems (Table 5.1) most likely a consequence of the different mixing and/or shear conditions. Owing to their high specific surface area, COBCs offer excellent heat transfer properties. However at high supersaturations, the high specific surface area provides a large competing surface for nucleation and/or deposition of particles. Investigation of this phenomenon is required at smaller scale prior

to testing in the full continuous rig (the approach developed is described in Chapter 6). For the remainder of this work, the methodology taken was to eliminate the need for primary nucleation and minimise supersaturation within the COBC through the use of seeding.

5.3.3 Seeded Crystallisation of LGA in a COBC

Seeding permits the operation of crystallisation processes at lower supersaturations.[44] Seeding should reduce the probability of encrustation within the COBC system as the need to drive the system to high supersaturation to induce primary nucleation is eliminated. This is a common strategy used to control crystallisation and in particular polymorphic form and particle size.[231] The introduction of seed crystals removes the reliance on the stochastic nucleation step and allows predetermined seeds (of desired form, morphology, number and size) to be introduced to a marginally saturated mother liquor. However the generation of seeds can be a challenging task: production can involve milling, slurry handling, resuspension and introduction of seeds whilst avoiding agglomeration.[232]

To produce seed crystals, ball milling was performed on the raw material for 1 hour, resulting in a mean seed size of ca. 50 μm. Other work[233] utilising a turbulent jet reverse anti-solvent process, produced beta LGA seeds with a mean size of about 10 μm. Figure 5.17 shows the particle size of seeds produced from the continuous anti-solvent process in comparison to those from ball milling. Due to the smaller size and narrower size distribution, the seeds produced using the continuous process were used. Figure 5.18 shows microscopy images of the seeds used throughout these experiments. The effect of high and low seed loadings, and feed solution concentrations, on the bulk supersaturation and growth of seed particles were assesed by completing a series of four experiments, details are found in Table 5.8.
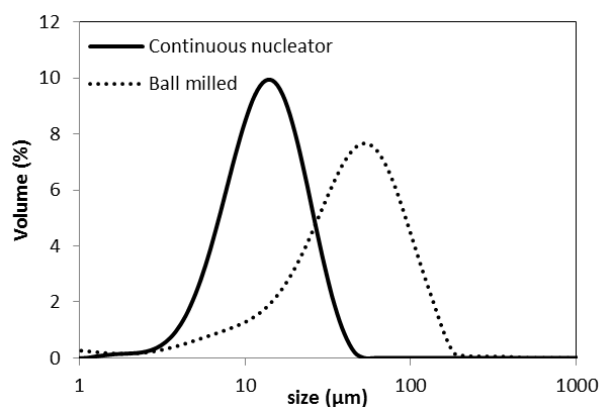
Figure 5.17: PSDs of LGA seeds Plot showing the PSD of LGA seed crystals produced from ball milling (dotted) and continuous anti-solvent process (solid).
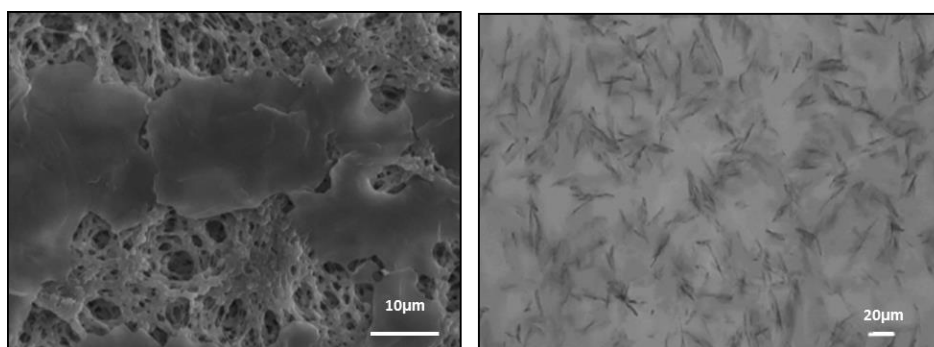
Figure 5.18: Seed Crystals used for the crystallisation of LGA in a COBC. SEM (left), optical microscope (right) images of representative sample of LGA seed crystals. The seed obtained from the continuous anti-solvent process display a flake like morphology.

Table 5.8: Experimental concentrations used for seeded COBC experiments.

Seed mass loading	Feed Solution	
	High 40g/kg	Low 18g/kg
High 0.4 (g/kg)	Expt. 1	Expt. 2
Low 0.1 (g/kg)	Expt. 3	Expt. 4

Utilising the mean particle size and the assumption of a monodisperse distribution of spherical seeds, the mass of a single seed crystal (M_p) can be calculated by:

$$M_p = \rho \Big/ \frac{4\pi}{3} r_p^3$$

where ρ = density in kg/cm^3, r_p = radius of seed crystal (cm). Thus, the mass of one LGA seed crystal is 7.6 x 10^{-7} g. This results in a seed number loading of 5.2 x 10^5 and 1.3 x 10^5 for the high and low seed mass loadings respectfully. Cooling profiles were designed to remain approximately constant over 4 experiments to allow for investigation over the crystallisation design space and to assess supersaturation and growth. The cooling profiles were approximated from linear growth rates at different concentrations and seed loadings. Owing to the nature of the heat transfer efficiency in the COBC, the actual temperature profiles used in the experiments were a series of temperature step changes approximating a smooth parabolic profile (Figure 5.19).
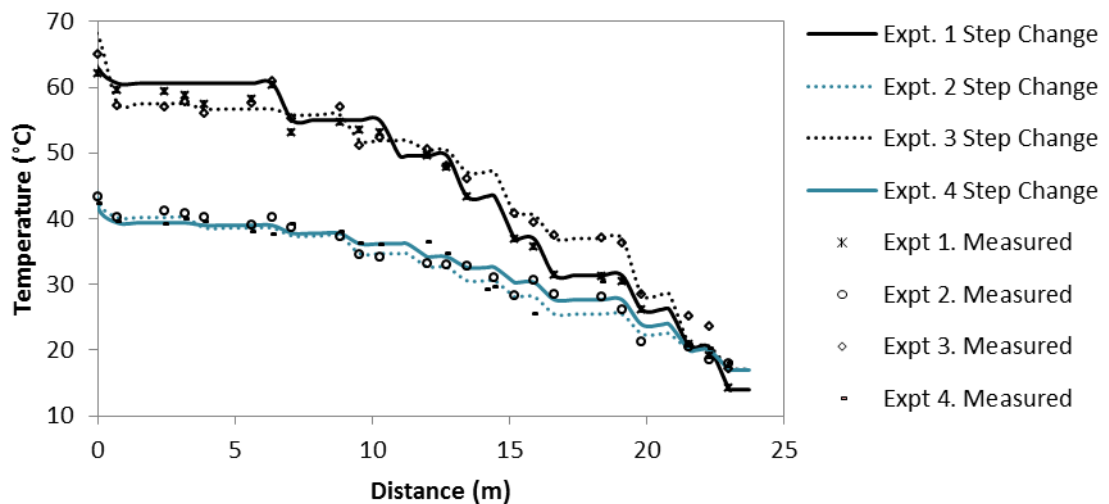
Figure 5.19: Cooling profiles for seeded LGA COBC experiments. Plot showing measured and calculated step change cooling profiles for seeded COBC experiments.

Figure 5.20 shows the resulting final product PSDs for each of the experiments. Experiments 1, 2, 3 and 4 resulted in mean particle sizes of 320, 240, 90 and 70 µm respectively. Inspection of the product confirms that PSDs result from agglomerated crystals, Figure 5.21 shows a picture which is representative of the beta crystals obtained from all of the seeded COBC runs. The linear growth assumptions did not consider agglomeration and therefore it was not possible to model the growth of LGA accurately. However successful modelling of PSDs of LGA within other crystallisation platforms in the absence of agglomeration have been reported.[142] Other reports include modelling of process phenomena including agglomeration population balance models.[234]
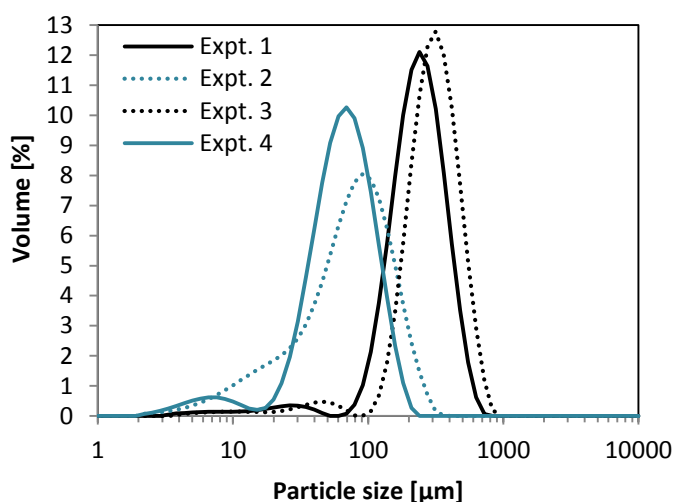
Figure 5.20: PSDs from seeded LGA crystallisations in the COBC. Plot showing the PSDs from experiments 1, 2, 3 and 4 (Table 5.8). The mean particle sizes were 240, 90, 320 and 70 µm respectfully.
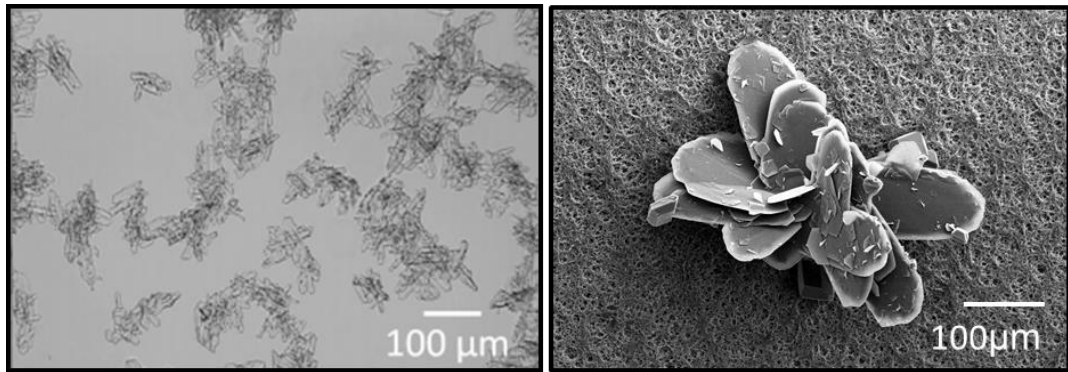
Figure 5.21: Images of crystal product from seeded crystallisations. Optical (left) and SEM (right) images of agglomerated product crystals (expt. 2, Table 5.8) obtained from a seeded COBC cooling crystallisation process.

Fouling was only observed in experiment 3 which was anticipated to produce the highest supersaturation during the crystallisation due to the low seed loading. This was confirmed from sample measurements (Figure 5.22). Supersaturation data plotted on the phase diagram, alongside the reported MSZW (Figure 5.23), illustrates operating beyond regions where spontaneous nucleation is favoured. When a high feed solution concentration with a low seed loading is used (expt.3), the supersaturation increases exponentially. The resulting end supersaturation was nearly double that for experiments 1, 2 and 4 (Figure 5.23). Based on these results it can be recommended that the supersaturation within the DN15 COBC be maintained within 1.6 (at 60 °C) increasing to 3.0 (at 20 °C) i.e. within the MSZW. Designing the cooling profile to maintain this range of supersaturations will best enable control over growth whilst avoiding primary nucleation of the metastable phase and fouling on the walls of the vessel.
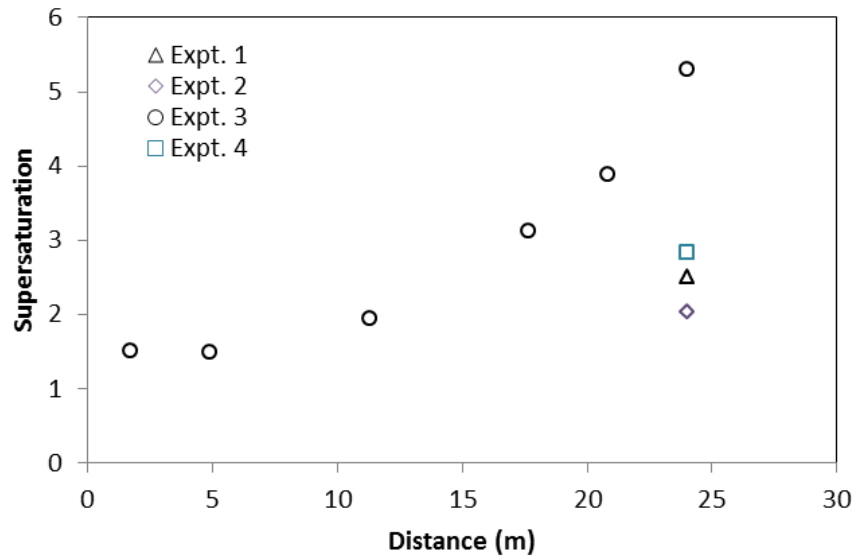
Figure 5.22: Supersaturation profile along the COBC. Plot of supersaturation level along the COBC for experiment 3. Final supersaturation values from experiments 1, 2 and 4 are included for reference.
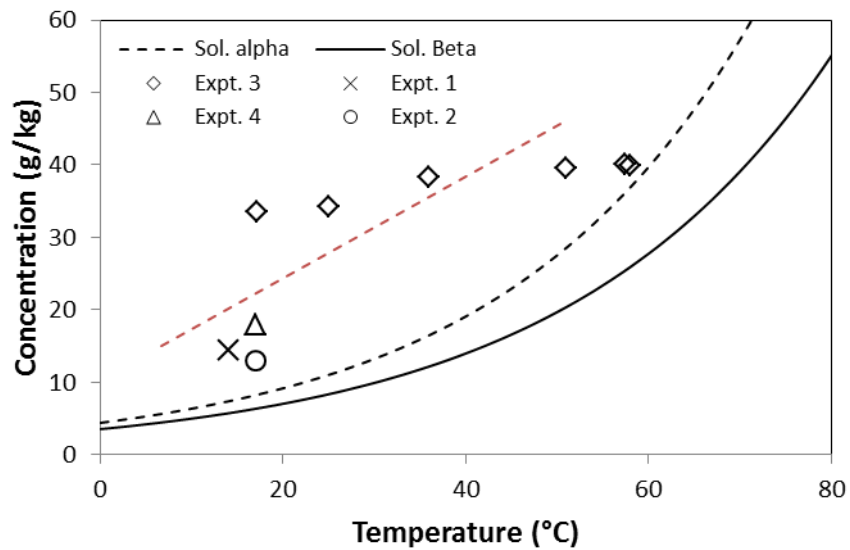
Figure 5.23: Phase diagram of alpha and beta LGA. Plot of the solubility phase diagram of LGA[193] with the supersaturation levels obtained from seeding experiments 1 – 4 (Table 5.8), the red line indicating the MSZW.[37]

To measure supersaturation values along the COBC, custom sampling bends (Figure 5.24) were designed and positioned at bends 1, 2, 4, 6 and 7 for experiment 3 (Figure 5.10). Slurry samples were extracted and rapidly filtered. Subsequently, solutions were evaporated and supersaturations were calculated after weighing the resulting crystal product using a mass balance.
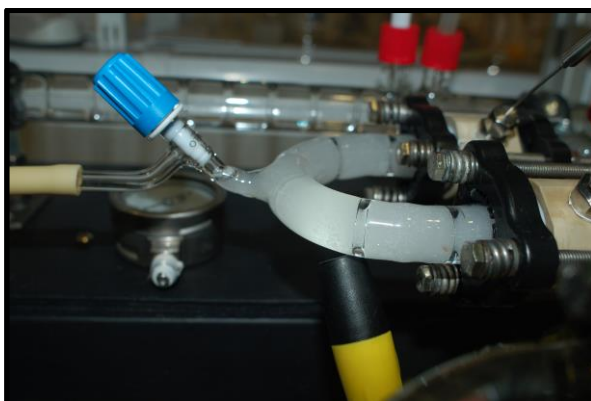
Figure 5.24: COBC slurry sampling bend. Photograph of a standard COBC bend adapted with glass arm and a minimised dead volume stop clock adaptor tap.

When supersaturation in the bulk solution was maintained at a level below 3 (at 20 °C) only the stable phase of LGA was produced. There is no evidence of primary nucleation of the metastable form based on XRPD (Figure 5.25). The appearance of a small fraction of fines in the product PSD (Figure 5.20) may be due to deagglomeration or secondary nucleation. Based on these results by controlling seed loading, starting concentration and temperature profile, fouling can be successfully avoided, particle size can be tailored (to give a variety of ranges) whilst maintaining control over the polymorphic form and avoiding formation of metastable forms.
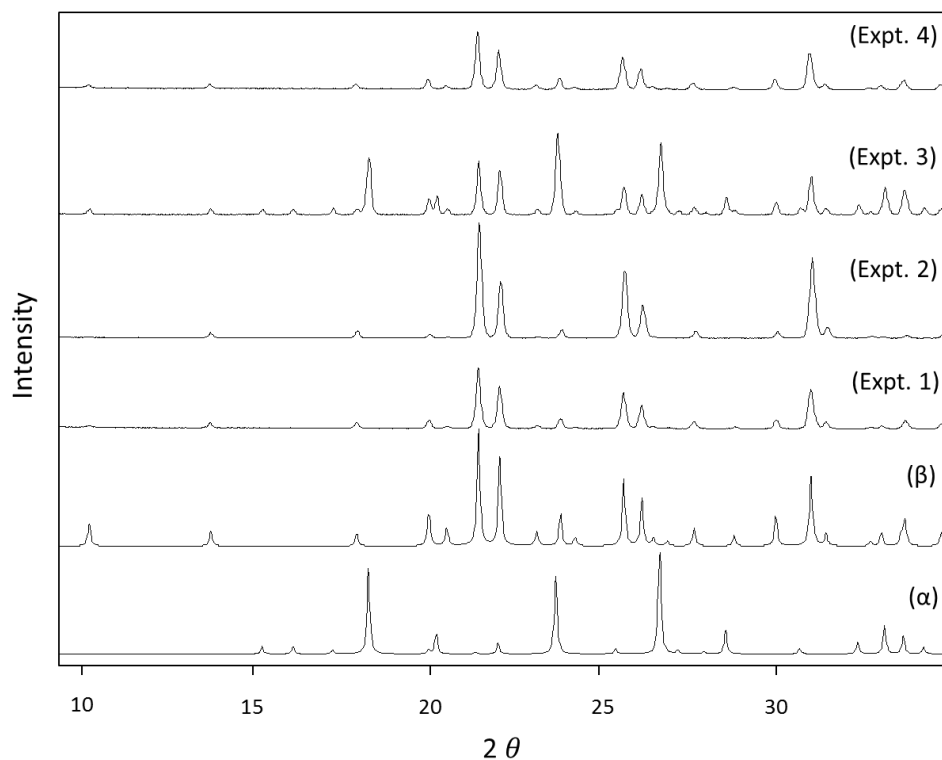
Figure 5.25:XRPD data from seeded continuous LGA crystallisations. Figure showing an overlay of product material from seeded experiments (Table 2), reference powder patterns of the pure alpha and beta (simulated from single crystal data)[198,199] are also shown.

5.3.4 Achieving steady state in the COBC

Steady state is a condition in which the variables of a system do not change as a function of time. These variables include process variables such as pressures, temperatures and flow rates as well as control system variables such as set-points. Whilst steady state is a useful idealisation used within many disciplines, any system never truly operates at steady state.[235] This non-steady state is due to natural disturbances such as fluctuations in pressure and temperature of the surroundings that lead to deviations in the rate of heat transfer. Electrical fluctuations in pumps, heater chillers, oscillators, overhead stirrers etc., can also result in changes to flow rates, temperatures and hydrodynamic environment. To meet the desired product attributes process variables may have to be altered to compensate for natural disturbances.

For a given process to fulfil its intended purpose, the critical quality attributes (CQA), e.g desired polymorphic form, purity or PSD, should remain within the specified critical limits. In some cases this may require operation with variation in processing values (e.g. changing flow rates or temperature), to compensate for any disturbances resulting in out of specification product.[235] Given true steady state will never be reached, it is advantageous to illustrate the sensitivity of processes to external fluctuations. The ability to predict and distinguish between processes rapidly reaching and maintaining steady state of CQAs i.e. processes relatively insensitive to natural disturbances, to those which are highly sensitive to natural disturbances, may start to allow recommendations to be made over operational procedures and platform of choice for a given specific solute/solvent system.

During continuous processing, there is a period where start up parameters change before the system stabilises. After this stabilisation period, steady state production of material meeting the desired CQA is sought after. To maximise process efficiency, the time period between start-up and consistent production of material within specifications should, ideally, be minimised.

Stabilisation time and process efficiency may be obtained from CQAs plotted against time. The robustness of the process can be assessed by variation in the response of these plots. Figure 5.26 shows an example of the evolution of the recovered yield using two unseeded and two seeded crystallisations of LGA in the COBC. The graphs are plotted with respect to crystalliser RT. Here, it is shown that a steady state output is achieved after the first RT in seeded crystallisations. However, two RTs are required to achieve steady state for unseeded crystallisations. A difference in response between unseeded and seeded processing was expected because unseeded experiments reply upon a nucleation event before product crystals will be produced and grow. During seeded experiments, supersaturation within the feed solution will start to deplete on seed injection and seeds will grow resulting in an initial product yield after the first RT without the reliance on a nucleation event.
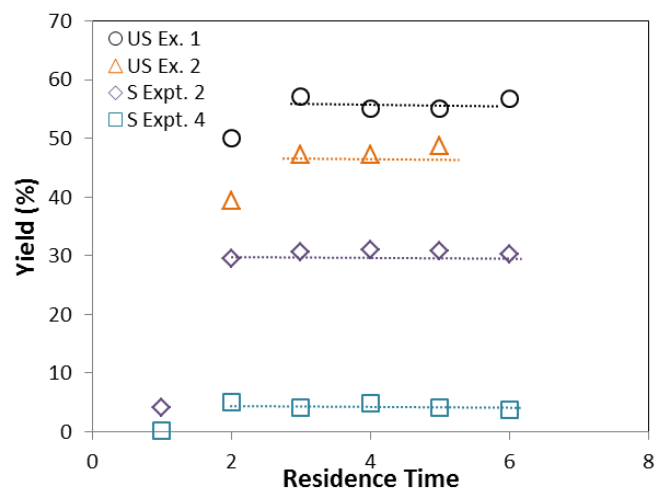
Figure 5.26: Evolution of LGA yield with crystalliser residence time. Graph showing product yield as a function of residence time. Plot shows that steady is reached by the third residence time for unseeded crystallisations (US Ex.1, US Ex. 2) whereas with seeded crystallisation (S Expt. 1, S Expt. 4) steady state appears to be reached by the second RT.

Whilst the yield indicates that the process reaches a steady state for both unseeded and seed crystallisations, an overlay of the product PSDs for each method of crystallisation show that steady state is not reached with respect to size at any stage during the unseeded crystallisations. Figure 5.27 shows the change in PSD for each product sample collected at different RT values. On comparison to the seeded crystallisation, Figure 5.28, a constant product PSD output is obtained after the second RT. This deviation from steady state can be explained as a consequence of fouling during unseeded operation. The product PSDs suggest secondary nucleation events and/or detachments of encrusted solids from the vessel walls during operation, create a shift from a unimodal distribution to a bimodal distribution with respect to time. Where seeded COBC crystallisations are carried out under a controlled supersaturation regime encrustation does not occur and PSDs suggest controlled growth of the seed particles resulting in a consistent product PSD output. This steady state illustration of PSD with seeded experiments also highlights the insensitivity of the process to fluctuations in equipment operation and external environment therefore indicating a robust process for PSD control of LGA is achievable.
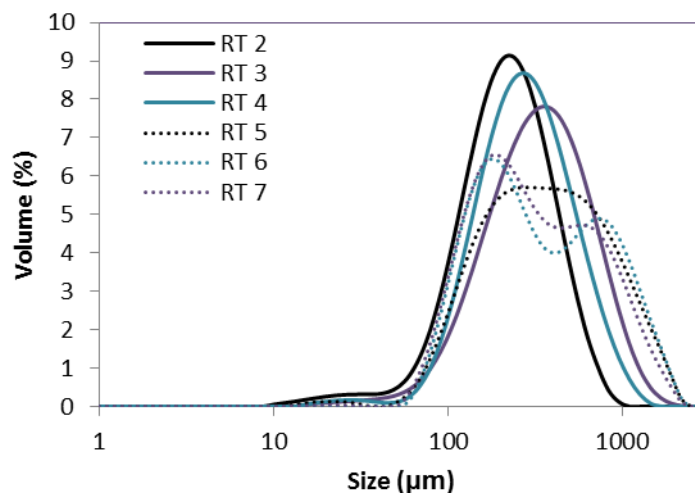
Figure 5.27: Evolution of PSDs for an unseeded COBC crystallisation. Overlay of 6 product sample PSDs collected from an unseeded LGA COBC

crystallisation. Plot shows PSD moves from a unimodal distribution to a bimodal distribution indicating non steady state.
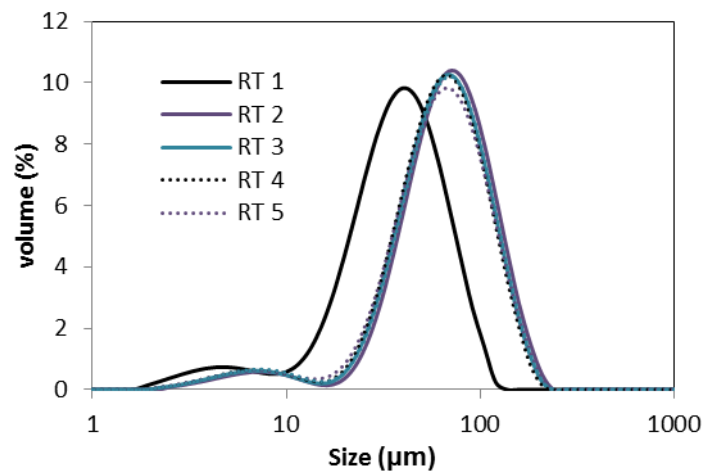
Figure 5.28: Evolution of PSDs for a seeded COBC crystallisation. Graph Overlay of 6 product sample PSDs collected from a seeded LGA COBC crystallisation. Plot shows that the process produces a product with a constant PSD after the second RT therefore indicating the process has reached steady state PSD.

5.3.5 Practical considerations for operation of COBC

Several operational issues occurred during the running of the COBC, this lead to the design and construction of several new items and procedures during this work to facilitate successful running which are described in detail in the following sections (5.3.5.1 – 5.3.5.6).

5.3.5.1   Use of jacketed feed lines

Jacketed feed lines (Figure 5.29) where designed and manufactured to be used for the seeding tube lines to prevent complications, for example blockages, associated with temperature fluctuations and associated variations in temperature and particle size, during addition from the seed tank to the COBC. Use of these to maintain constant slurry temperature during

transfer into the COBC prevented blockage of the feed pipes due to uncontrolled nucleation.
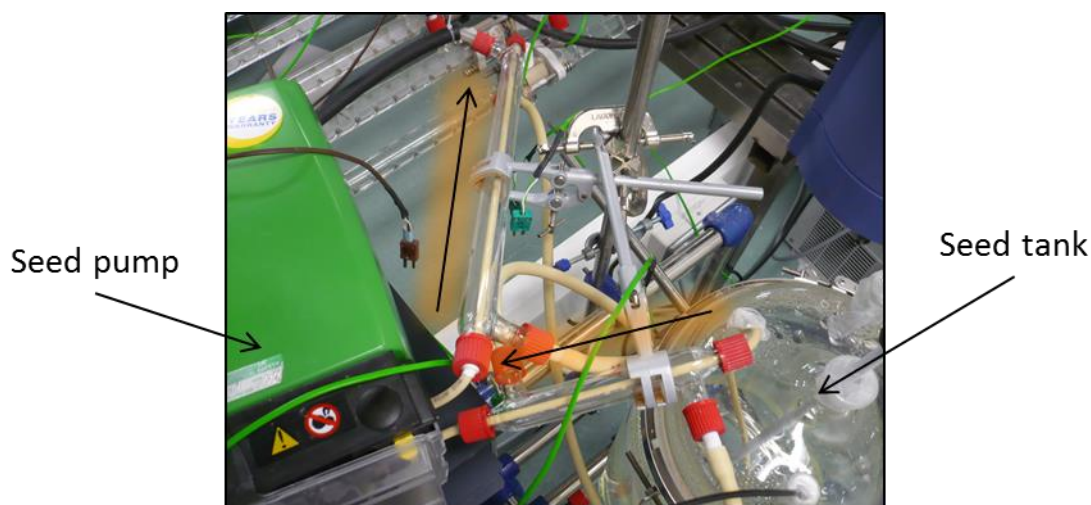
Figure 5.29: Jacketed lines for seed stream. Photograph showing the jacketed lines used around the tubing entering the seed pump from the seed suspension and tubing transferring from the pump into the COBC.

5.3.5.2 PAT insertion for online monitoring

The DN15 COBC as received did not provide an easy or accessible way to insert in-line PAT probes such as FBRM, UV, IR or PVM, restricting the ability to develop process understanding, carry out process monitoring or to implement real time process control in these or future studies. In order to gather real time information on continuous crystallisation processes, a new bend design incorporating PAT probe insertion and removal points during operation were developed (Figure 5.30). The application of these newly adapted bends provided a platform to map growth and supersaturation along the system for example. The successful application of these ports is demonstrated in Chapter 7.

Figure 5.30: Adapted bend for in-line PAT. Photograph showing a standard COBC bend modified with a minimised dead volume key tap adaptor and an ATR-FTIR probe inserted.

There are however a number of issues and challenges associated with inserting probes for in-line measurement of crystallisation processes.[152] These include the probe acting as a site for nucleation and fouling, introducing local changes in the hydrodynamic environment (i.e. acting as a baffle), ensuring adequate and representative sampling of the process stream e.g. ensuring an FBRM probe is inserted at close to 45° to the direction of suspension flow, and the introduction of dead zones where solids can accumulate around the probe shaft and lead to sedimentation and the formation of blockages. The design of appropriate probe ports is a challenging task and could be achieved from first principles using CFD simulations of the specific location.[236] Poor placement may well lead to detrimental effects to the process stream and so to support the increasing application of PAT it is essential that such requirements are routinely included in the design of novel reactor platforms. In-line PAT is routinely used due the advantages it offers including real-time information, and eliminating the need for manual sampling (which can introduce artefacts in the sample due to temperature variations or if pre-processing is required before analysis).

Alternatives to in-line PAT include non-invasive methods such as Raman and optical methods due to avoiding contact with the process stream. Non-invasive methods are the preferred choice if possible. However there are also challenges associated with these types of probes including measuring through jacketed vessel walls, contributions to the signal from reactor materials of constructions and optical effects arising from curvature of vessels for example.

5.3.5.3   Fluid filled bellow oscillation unit

The actuation of controlled oscillation is a basic requirement for delivering a well-defined process in a COBC owing to the dependence of mixing conditions and particle suspicion on the oscillatory environment. Various mechanisms for delivering oscillatory motion have been described (bellow,[124] piston,[237] diaphragm[238] and magnetic shaker[239]) however the platform used in this study utilised an unjacketed bellow system and this was shown to act as a cold spot during cooling crystallisation processes. As a consequence, solid accumulation was frequently observed in this region resulting in uncontrolled solids dosing into the process and, if left unaddressed, potential blockage of the system. The solution, implemented during this work, was to pump hot solution through the bellow rather than directly into the rig (Figure 5.31). Alternative means have also been demonstrated including the use of pistons, however given the extent of oscillation damping (section 4.3) observed with long COBC lengths, the volume displacement using the DN25 bellow unit was required to provide sufficient oscillations for operation. As a consequence the design implemented during this study has been adopted as the norm in other projects.
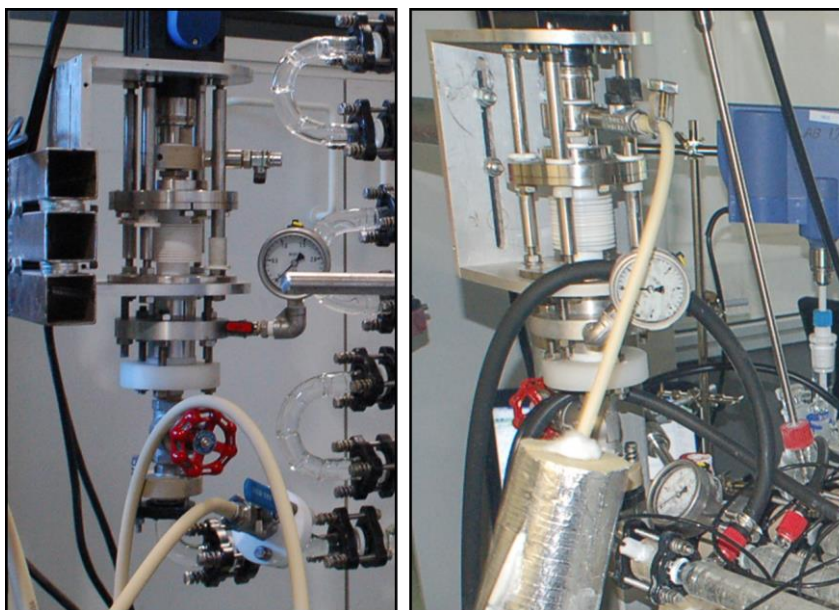
Figure 5.31: Main feed tubing line injection points. Photograph showing main feed tubing pumping directly into the rig (left) and through the bellow (right).

5.3.5.4   Rapid heat transfer within cooling zones

Observations made during the crystallisations suggested relying on the linear cooling profiles for calculation of cooling rates was insufficient and a need for more information about in-line temperatures and heat transfer of the COBC system was needed. The assumption of a linear profile within a temperature zone is shown in Figure 5.32 to be incorrect. Rapid heat transfer takes place during the operation and the bulk fluid temperature reaches the HC set-point temperature at about 1.4 m along the rig, i.e. after 2 COBC straights. As a consequence, batch and continuous OBC platforms have non-comparable temperature profiles. Cooling profiles have been shown to have a significant effect on crystallisation kinetics therefore, until control over temperature is achieved in the COBC, it is reasonable to assume there will be noticeable differences in crystallisation performance and product output from experiments carried out on each platform. This has further implications when assessing and comparing continuous test bed units to the COBC as developing workflows may illustrate inconsistences caused by these

variations in temperature control. Caution also needs to be made when developing COBC processes accounting for this rapid heat exchange and the supersaturation spikes generated, insuring the process does not move into regions beyond the metastable limit were spontaneous nucleation can occur leading to an uncontrolled process.
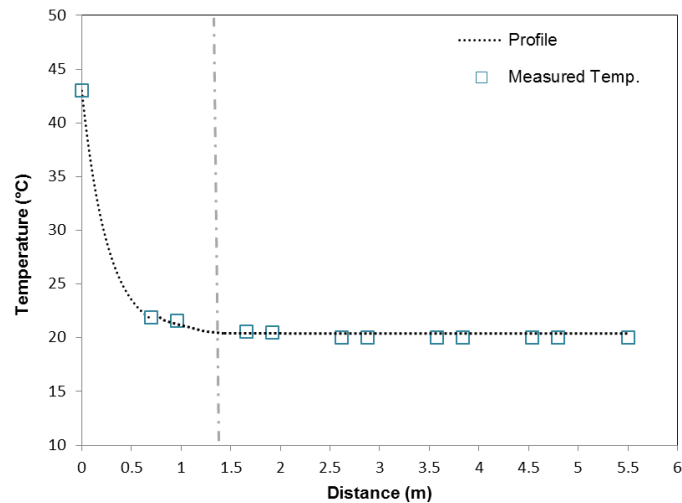
Figure 5.32: Heat transfer performance in a DN15 COBC. Plot showing the temperature response in COBC set-up with 6 straights and 6 bends. One heater/chiller was set counter current to flow and the internal net flow and oscillatory conditions of 50 g/min, and 1 Hz 30 mm were used respectfully. This set up mimics one typical temperature zone in a COBC crystallisation experiment. Adapted from Reference.[240]

5.3.5.5   Sedimentation.

Typically when designing continuous flow processes, settling velocity values are calculated to ensure there is sufficient turbulence to keep the desired particles suspended. A basic expression to describe the terminal velocity (V_t) of particles can be used as follows:[241]

$$V_t = \sqrt{\frac{4g\emptyset}{3C_d}\frac{(\emptyset_\rho - \rho)}{\rho}}$$

Eqn. 5.8

where g = gravitational acceleration (9.81 ms^{-2}), $\emptyset$ = crystal diameter (m), $\emptyset_\rho$= crystal density (kgm^{-3}), ρ = fluid density (kgm^{-3}), C_d = drag coefficient (0.5). When the net flow velocity is maintained at a value above V_t, particles should suspend without sedimentation. Using LGA in water as an example, where $\emptyset_\rho$= 1460, ρ = 1000 and flow rate = 50 gmin^{-1} (0.003993 ms^{-1}), Table 5.9 illustrates the settling velocity for a given size class of particles. This calculation suggests that for all sizes of LGA crystals (ranging from 50 – 500 µm), under the flow conditions described, sedimentation is likely to occur within the system.

Table 5.9: Settling velocity of LGA in water

Crystal size (µm)	V_t(ms^{-1})	Sedimentation
50	0.02451	Likely
100	0.03467	Likely
500	0.07753	Likely

However this calculation does not accurately describe settling velocities with oscillatory baffles systems and does not take into account the oscillatory motion or the increased turbulence from the periodically spaced baffles. Throughout the experiments conducted in this chapter sedimentation was not a dominant issues within the main platform, but sedimentation issues where

often observed at joins thought out the COBC, i.e. in-between straights and bends (Figure 5.33).
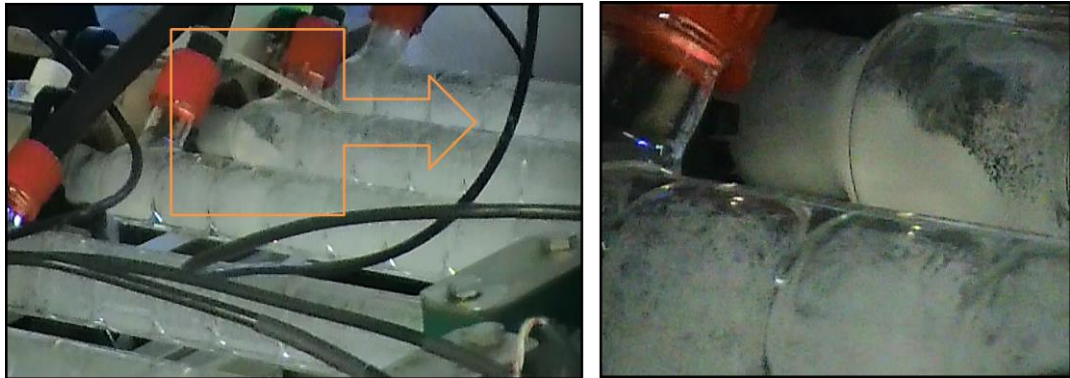
Figure 5.33: Example of sedimentation in a COBC. Photograph showing sedimentation of crystals in between two glass COBC straights (left) with a magnified image (right).

These sedimentation issues are caused by the suboptimal glassware design. The buttress extension on either side of the straights and bends did not include a baffle, leaving 2 interbaffle zones in each piece of glassware twice the desired length, thus significantly impacting on the hydrodynamic environment, reducing eddy generation and turbulence, thus the environment in these regions were closer to that of an unbaffled tube and as expected (according to the values presented in Table 5.9) sedimentation is likely. New adapted bends were designed and fabricated to minimise this issue, however all the glassware i.e. including all existing straights, ought to be adapted or replaced with the new design in order to optimise performance. Figure 5.34 shows an old and new bend, highlighting the difference between first baffle positions.
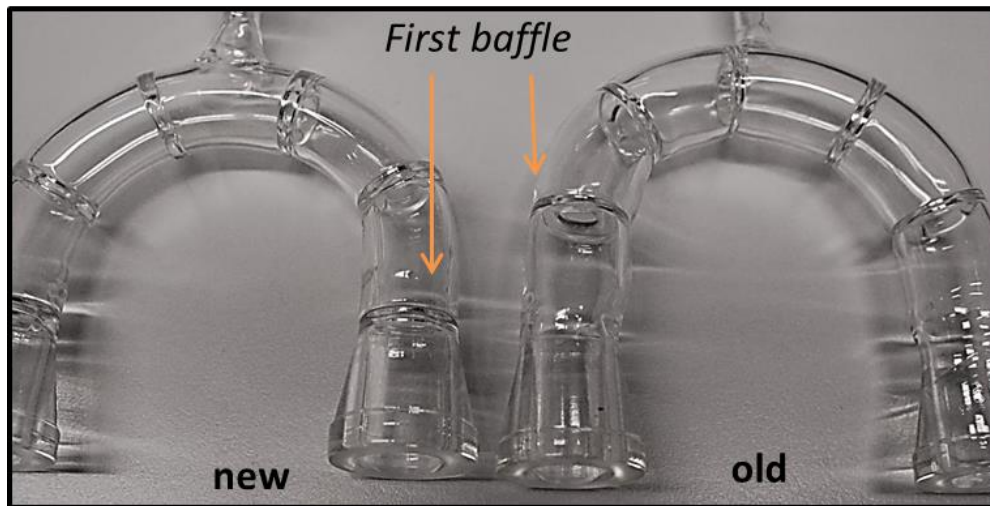
Figure 5.34: COBC bends. Photograph showing old (right) and new (left) COBC bends. Old bend has a baffle "missing" in the buttress therefore providing a hydrodynamic environment prone to sedimentation. The new bends include the "missing" baffle.

5.3.5.6   Temperature monitoring

The issue of heat transfer and the lack of access to comprehensive data showing actual temperature profiles across the length of the COBC system was highlighted in section 5.3.5.4. Following on from this, thermocouples were placed at all accessible locations within the COBC (Chapter 7) to accurately monitor the real bulk solution temperature and gain correct information of the temperature profile and how it varies. This increased the number of thermocouples from 6 (for unseeded LGA runs) to 24 (for seeded LGA runs). Building on this, 40 thermocouples have been implemented to provide comprehensive readings from the COBC during operation (chapter 7). To accommodate this and to facilitate automated readout of multiple data points, independent temperature loggers were utilised and combined with a bespoke automated temperature logging system. This allowed real time information from all thermocouples to be shown on a single display screen (Figure 5.35). This is enables ease of access to the temperature information and storage of all data in one place, laying the foundations for real time control over the temperature in the system.
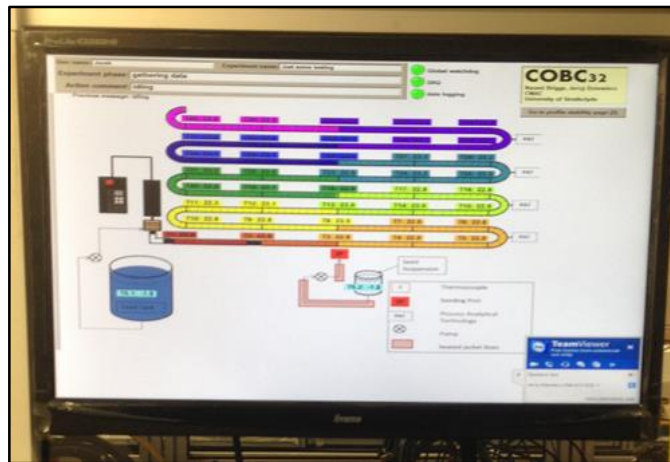
Figure 5.35: Display screen for live temperature profile readout. Photograph of a computer display screen showing the readout from a computer controlled temperature recording of 40 thermocouples. Interchangeable display screen provides live readings of temperature profile along the rig as well as fluctuation at any given fixed position.

5.4 Summary

Utilising the approach of a batch MBOBC to investigate process conditions before translating to the COBC is not sufficient for informing the development of a continuous crystallisation process for LGA. Nucleation kinetics were found not to be consistent between process conditions in different platforms leading to unexpected issues including encrustation and blockages that were not indicated during batch screening experiments. As a consequence the MBOBC has been shown to be of limited value in terms of the workflow towards COBC, contradicting previous practice. On further review of the MBOBC design and operation there are many fundamental differences between this and the COBC, details on this are discussed further in Chapter 6.

Throughout all unseeded continuous experiments, significant encrustation was observed and this could not be eliminated despite a multitude of changes to the operation and process conditions. For continuous LGA cooling crystallisation the overall recommendation would be to avoid primary nucleation in the system. Investigations on mitigating this encrustation phenomenon would provide experiments worthy of further investigation and the possibility of control, but until this is resolved and an understanding is gained on encrustation, relying on primary nucleation during cooling crystallisation in a COBC is not recommended. The stable beta polymorph could not be isolated in pure phase during unseeded continuous COBC experiments and in all cases the metastable alpha form was produced as the major phase, despite the batch system showing selectivity over polymorph control under similar conditions to that applied in the COBC.

There have however been reports over challenges around producing the stable beta form of LGA during operations with other continuous crystallisations platforms. Myerson *et al*,[142] describe a MSMPR process for the continuous crystallisation of LGA and illustrate (due to increased growth kinetics of the metastable alpha, when compared to the stable beta), a polymorphic phase switch occurs during production and prolonged

continuous operation will result in the production of the metastable phase. It should be feasible to obtain the stable beta polymorph of LGA from unseeded crystallisations if favourable hydrodynamic environment for nucleation is maintained at all times and prevention of nucleation of alpha that would lead to these competitive kinetic effects.

When a seeded approach was taken PSD steady state operation for 8 residence times was illustrated without fouling or blockage of the system. When the bulk solution supersaturation remained below a value of about 3, encrustation could be avoided routinely. Seeding with 10 µm crystals could be grown to sizes ranging from ca. 70 – 320 µm within a RT of about 1 hour allowing for the tailoring of crystal particle size. Seeded crystallisation has delivered control of form and size whilst avoiding fouling. Seeding raises questions over the best method for production of seeds, however this work has also demonstrated the utilisation of seeds produced from a separate continuous nucleation approach emphasising one of the benefits for continuous PFR in enabling the physical separation of distinct transformation steps. This means control over primary nucleation (i.e. preventing through a combination of concentration and seed loading) was achieved but more work is required to achieve control over secondary nucleation and/or agglomeration.

Adaptations and incorporation of specially designed glassware and implementation of new operating procedures removed some of the practical challenges of operation of the DN15 COBC, allowing for successfully running of continuous cooling crystallisations process. It also further enhanced capabilities to obtain real-time information of the process rather than relying on assessment of only the end product, hence moving away from the QbT approach and providing a means to adapt a QbD methodology. This also advanced the capabilities to move towards the utilisation of a feedback control approach for continuous crystallisation control.

Chapter 6. Developing a Test bed for Continuous Oscillatory Baffled Crystallisation

6.1 Introduction

Within the pharmaceutical industry, the inability to efficiently scale crystallisation systems is one of the largest barriers preventing the introduction of novel drugs to the market. Standard procedures for scaling crystallisation are sparse and few, particularly because of the non-linearity of mixing and heat transfer when increasing vessel size (Section 1.5). This work (Chapter 5) and previous approaches[220] have demonstrated that the experimental approach for scaling crystallisation processes from a batch oscillatory baffled crystalliser (OBC) to a continuous oscillatory baffled crystalliser (COBC), utilising moving baffle (MB) OBC platforms are ineffective considering the variations in process performance, dissimilarity in kinetic data and the dominance of encrustation during continuous operation.

As industrial development is limited by time and a pre-determined capital investment, the development of successful manufacturing processes and the chance of supporting clinical and commercial requirements are increasingly dependent on effective scaling workflows.[242] These workflows should provide a route to assess and predict crystallisation behaviour at a manufacturing scale, or at least provide enough information that the process development stage is not a lengthy and costly one. As a consequence of the general expense and limited available quantities of novel pharmaceuticals during early API development, process design approaches usually rely on small scale crystallisations.[243] Process conditions may then be carried to larger platforms where crystallisation conditions and process parameters may be altered to ensure desired product outcome, with sufficient yield. Hence, the design and development of robust platforms for improving hydrodynamic similarity between batch and continuous systems, in addition to methods for detecting encrustation during crystallisation, is essential for the development of successful workflows.

6.1.1 Scaling crystallisation within oscillatory flow systems

In terms of mixing performance, the scale-up of oscillatory flow systems have been well studied and is generally illustrated using Re_o as the scaling parameter.[178,244] If Re_o remains constant across scales, hydrodynamic consistency is ensured if geometric similarity is also retained, i.e constant baffle-spacing ratio and baffle-constriction ratio. These scaling rules have been shown to hold true for fluid flow patterns.[170,179] However, relying on geometric similarity and constant Re_o may not be sufficient when the systems are utilised for crystallisation and incorporate additional rate processes i.e. nucleation and growth of solids.

Given the sensitivity of crystallisation processes,[29] there are many considerations in addition to heat and mass transfer, which should be addressed for the purpose of crystallisation scale-up within oscillatory flow, and so far these have received little attention. For example, it has been demonstrated that construction materials impart effects on nucleation.[245] Thus, to mitigate any derogatory effects, materials should remain consistent when scaling processes.

A recent example of the role of surface properties on crystallisation performance is illustrated by the study of Heng *et al*.[246] The effects of chemical modification of glass surfaces on the crystallisation of four common proteins (Lysozyme, Thaumatine, Catalase and Ferritin) are presented. Variation in surface chemistry was shown to impact the size, morphology and number of crystals formed.[246] Another study investigated the effects of surface chemistry and morphology of various polymeric substrates, on nucleation behaviour,[247] and demonstrated a reduction in nucleation induction time for the crystallisation of aspirin. Control over polymorphic forms of carbamazepine has also been achieved through surface modification with various silane molecules.[248] With no surface modification of glass, forms II and III were shown to nucleate concomitantly. However, preferential nucleation of form II and form III was shown when treated glass surfaces with different polarities were used. Again, the induction time to

nucleation was shown to significantly decrease when surface modifications were made.

As crystallisation is readily influenced by many external factors, platforms utilised during small scale investigations, process development, and scale up should be as similar as possible to maximise the likelihood of obtaining reliable information on representative process performance. When batch MBOBC systems were designed and used for investigating oscillatory flow prior to scale-up, investigations typically focused on reactive chemistries and polymerisation.[249-251] As such, the platforms were not optimised for crystallisation. To date, batch oscillatory baffled crystallisation studies have almost exclusively focused on moving baffles (MB) arrangements. With the exception of two studies that utilised a moving fluid (MF) OBC arrangement,[218,219] all of the studies described in Table 5.2 use MB OBCs. Following on from reported methodology for successful crystallisation in a COBC,[35,124] a MB arrangement was utilised (Chapter 5). However given the differences in crystallisation performance observed in Chapter 5 and elsewhere,[220] the need for a more reliable batch OBC system, that enables process development and to deliver routine translation from batch to continuous, is clear.

6.1.2 Design approach and considerations

To address possible sources of variation in crystallisation performance, during the design and development process of a new batch platform, differences between the MB OBC and the COBC were considered i.e. system geometry, materials and operation. A summary of the identified differences are outlined in Table 6.1. When the dimensionless geometric numbers (the baffle free ratio and baffle spacing ratio) of each system are compared, dissimilarity in geometry is evident. The method of agitation is another source of dissimilarity between the systems. In the batch system the baffles are moving through the solution to generate mixing, whereas in the

continuous platform the fluid is agitated whilst the baffles remain fixed. The MB arrangement also has a small gap between the vessel wall and the baffle string to allow for movement within the column. This movement may be why encrustation was not observed when utilising this system for LGA investigations (Chapter 5), as the encrusted crystals may be sheared or scraped off the vessel wall during the displacement of the baffle along the column.

Table 6.1: Differences between batch and continuous OBCs. Table of comparison illustrating inconsistencies between platform parameters.

Parameter	MB OBC	MF OBC	COBC
Baffle free ratio	0.19	0.25	0.25
Baffle spacing ratio	1.3	1.6	1.6
Baffles set-up	Moving	Fixed	Fixed
Baffle shape	Sharp	Smooth	Smooth
Baffle material	PTFE	Glass	Glass
Net flow	No	No	Yes
Cooling	Smooth	Smooth	Step change
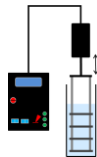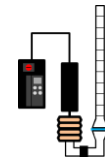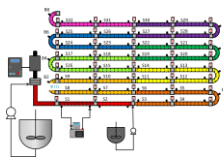
A recent CFD study compared the mixing performance between a MB and a MF arrangement of a DN25 system.[252] This study reported the shear rate dispersion of the MB arrangement was up to 17 % higher than the MF. Additionally, shear rates were significantly higher in the MB system, compared to the MF. Of interest to the present work, areas of lowest mixing

intensity are observed in MF systems at the position where the stationary baffles meet the vessel wall (Figure 6.1). These stagnant regions are not observed in MB systems due to oscillation of the baffle string along the vessel wall.[252]
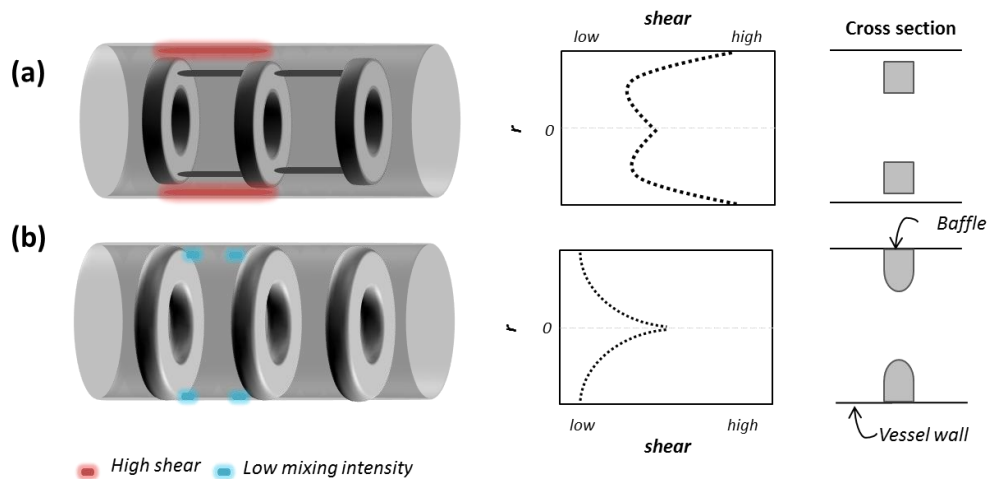
Figure 6.1: Baffle designs for batch and continuous platforms. Schematic illustrating baffle design for a batch (a) and continuous (b) platform. Regions of high shear and low mixing intensity are highlighted in the diagram and graph, left and centre respectively, the cross sections area (right) for both designs is also shown. The batch system contains baffles with sharp edges, whilst the COBC system has a smooth cross sectional area.

Another crystallisation study using a DN40 MBOBC[218] investigated the nucleation behaviour of the platform when the baffle string was fixed loose or tight around the wall of the vessel. Here, seeded aqueous crystallisations of sodium chlorate were carried out and during the crystallisation process the baffle string either scraped or did not scrape the column walls, respectively. When the system was not scraped, 100 % similarity to the seed crystal was obtained from the product, however when scraping occurred the product contained dissimilar seeds. Thus, this study[217] demonstrates that different nucleation mechanism may occur in MB systems, depending on the baffle arrangement.

A further study,[219] of aqueous sodium chlorate crystallisation investigated the use of a MFOBC arrangement and compared the crystallisation performance to the aforementioned scraping and non-scraping MB system.[218] This study demonstrated further deviation form product crystal similarity, i.e. product similarity to seed crystal, in descending order as follows; the non-scraped MB system, the scraped MB system, and the MF system. Such observations highlight the need for consistent baffle arrangements and agitations when scaling between systems during crystallisation process development. Considering the significant differences between the MBOBC (Figure 5.6) and the COBC (Figure 5.8) platforms, an improved design for a batch OBC system was developed to provide a test-bed for the assessment of continuous crystallisation behaviour (Figure 6.2). The development of such a system removes 5 of the 7 differences highlighted in Table 6.1, leaving differences in net flow (and subsequent effects on the cooling profile due to heat transfer) and in RTD profiles obtained under various operating conditions. The absence of net flow is expected to have a minimal impact on the effective conditions in the MFOBC system compared to the COBC. The concept is simple: utilising a COBC glass straight as a batch reactor to provide an exact match of the prevailing mixing conditions in both batch and continuous modes. In this chapter, the performance of the novel OBC platform is described in terms of temperature control, fouling and nucleation.
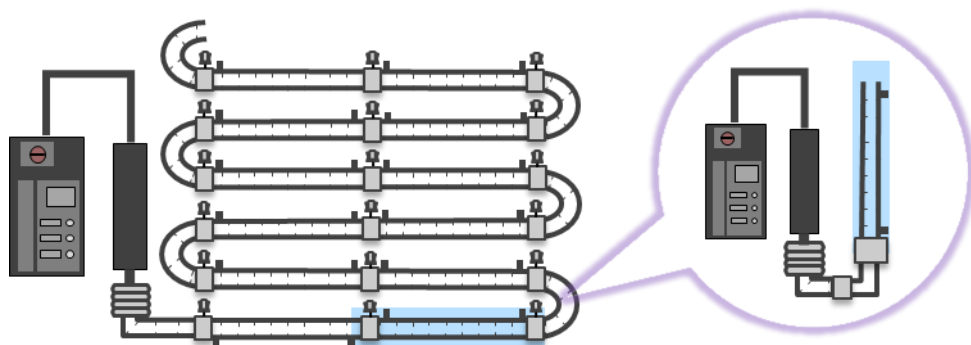
Figure 6.2: Concept for a continuous crystallisation test-bed. Schematic diagram illustrating the concept of turning a COBC glass straight (left) into a batch crystallisation unit (right).

6.1.3 Encrustation

In developing a small-scale platform for improvement on the prediction of continuous crystallisation behaviour, the assessment of when encrustation will be of detriment to the crystallisation process should be a priority. Encrustation is thought to be a result of three possible mechanisms[253] (Figure 6.3). The build-up of solid material on vessel walls may result in deviations in heat transfer, increases in pumping power requirements, as well as pressure build up and blockages. If material should detach from the walls, the product quality may be adversely affected, as detached solids will most likely not meet size specifications. Indeed, encrustation is generally unfavourable in all types of processing scenarios. For example, in industrial batch crystallisation, the formation of solid crusts can result in large detachments that block and damage pumps during slurry removal. Arguably, encrustation is easier to handle during batch processing than in continuous as during continuous operation encrustation can have a more immediate detrimental impact leading to process failure.[254]
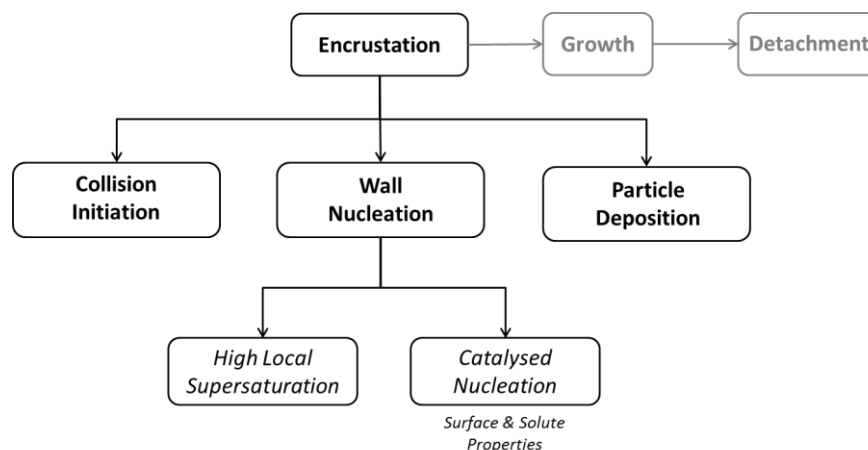
Figure 6.3: Mechanisms of encrustation formation. Flow diagram illustrating the various proposed routes that may induce encrustation. Adapted from Reference [253].

The most common cause of encrustation within crystallisers are regions of high supersaturation, such as cooling coils or jackets, where there is a temperature gradient between the bulk fluid and the cooling source. This temperature gradient is present in every cooling crystallisation for a certain period of time (the extent of which depends on the efficiency of heat extraction from the bulk solution), as a result of mixing performance around the cooling source. Where not driven by high supersaturation, encrustation can still occur due to the thermodynamic driving force and surface interactions between the solute, solvent and crystalliser surface, as well as solid collision with the vessel walls and particle deposition (adhesion and cohesion, Figure 6.3). Given that the specific surface areas of COBCs are much greater than that of STCs, the likelihood of surface induced nucleation, collision initiation and particle disposition is increased.[255]

A comparison of surface area in contact with crystallisation solution between STCs and the COBC can be made by modelling the vessels as cylinders. In this scenario, the surface area of a vessel (A_v) can be described by:

$$A_v = 2\pi r L + \pi r^2$$ Eqn. 6.1

As, in this model, the liquid is only in contact with the fluid at one end of the cylinder (as the other end is exposed to an air interface) this calculation only includes the surface area of the walls and the surface area at one end of the reactor. In reality the COBC surface area will be greater than that described by equation 6.1 (due to the baffles). The surface area of each baffle, A_B, can be described by:

$$A_B = 2((\pi D^2) - (\pi D_o^2))$$ Eqn. 6.2

Thus, the surface area of a baffled COBC (A_{COBC}) may be being described by:

$$A_{COBC} = 2\pi r (L - B_T B_N) + \pi r^2 + (A_B B_N)$$ Eqn. 6.3

where B_T is the baffle thickness and B_N is the total number of baffles in the system. Table 6.2 shows the surface area of the DN15 COBC (Figure 5.10) with a 5L STC (with a circumference of 0.69 m and height of 0.2 m). As the surface area of the COBC is an order of magnitude larger than that of a volume equivalent STC, the potential of solids nucleating or depositing on the walls of a COBC is significantly higher.

Table 6.2: Surface area of an STC and COBC. Table showing a comparison between the surface area of a 5L STC and a 4.6L COBC

	Surface area (m^2)	
STC	COBC (unbaffled)	COBC (baffled)
0.18	1.25	2.57

Monitoring and measurement of encrustation can be a challenging task. To gain an understanding of how process parameters and equipment design affect the progression of encrustation, methods for detection and quantification must be developed. Current methods include measurements of the reduction in heat transfer, the change in pressure drop, and the collection and weighing of the resulting deposited mass. Imaging techniques are beginning to emerge as a method of detecting surface fouling and can be used to indicate when cleaning procedures should be carried out.[256] Cho *et al*,[257] used a microscope imaging technique to study the surface fouling of calcium carbonate in a mini channel heat exchanger. Using this technique, the generation of nuclei and growth on the fouled surface were imaged. Fouling induction time was found to be dependent on inlet temperature and coolant flow rates.

Once encrustation occurs during continuous crystallisation, the crystallisation process can no longer be considered a steady state operation nor a robust or reliable operation. Crystals growing on the vessel wall will compete with crystals growing in the bulk solution and this may impact upon growth rates

and process performance. Mitigating such degradation is essential to achieve robust continuous operation and, as such, a method of monitoring encrustation should be deployed when carrying out experiments on platforms replicating desired continuous platforms for scale-up.

6.2 Experimental

6.2.1 Platform development

The concept of the batch MFOBC platform was a DN15 COBC glass straight as the crystallisation vessel (working volume ~120ml), whilst oscillation of the fluid through the stationary baffles (matching the COBC agitation mechanism). As the working volume of the non-jacketed, non-baffled bellow and connecting 90° glass bends totalled approximately 70 ml, ca. 40 % of the total system volume was uncontrolled (i.e. under separate hydrodynamic conditions and with no temperature control). A method of isolating this uncontrolled region, where potentially unwanted nucleation could occur, was required. The isolation method must permit the transfer of oscillations at sufficient amplitudes for crystallisation investigations, alongside preventing unwanted materials contaminating the bulk solution leading to contamination and/or false nucleation, thus, the use of a flexible membrane was deemed the most appropriate method.

During the development of this platform, a MF set-up incorporating a half straight (hot section) between the bellow unit and the full COBC straight was built. Here the hot section was attached to a HC and maintained at a temperature above the solubility, therefore acting as a dissolution chamber for any crystalline material that may be generated in the non-jacketed bellow unit and non-jacketed glass bends connecting to the straight, (Figure 6.4, set-up 1).

In preliminary experiments, a nitrile membrane was placed in-between a DN15 COBC glass straight and the bellow unit. Achievable oscillation amplitudes (ca. 5 mm) were not sufficient to provide good mixing or solid suspension. To increase the oscillation amplitude, the connected ends of the glass bend and the COBC straight were expanded to a diameter of 25 mm (Figure 6.4, set-up 2). The volume displacement permitted peak-to-trough amplitudes of ca. 40 mm to be achieved.
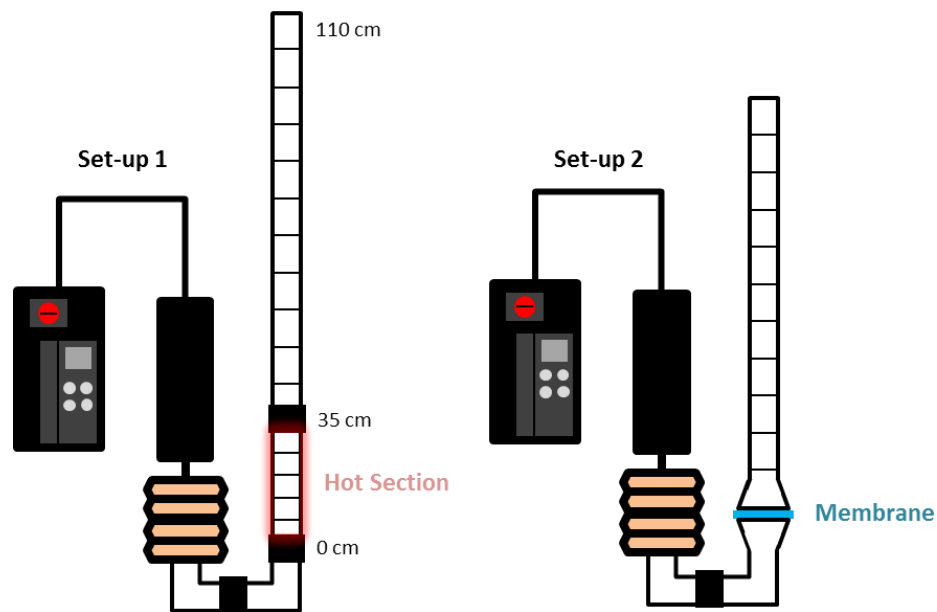
Figure 6.4: MFOBC designs. Schematic showing the MFOBC designs investigated. Set-up 1(left) utilises a hot section at the bottom to separate the crystallising solution from the fluid filled bellow unit, whereas set-up 2 (right) uses a membrane.

Temperature profiles within the MFOBC platform were assessed by positioning a series of thermocouples inside various interbaffle zones along the distance of the COBC glass straight. Temperature readings were taken every 30 seconds over the duration of the experiment. With set-up 1, the HC of the hot section was maintained at 75°C and the HC controlling the crystallisation section was programmed to cool at the desired rate. Where FBRM was used, nucleation time was determined when the total number of counts reached above 500.

6.2.2 Image analysis

CMOS cameras (*Microsoft* LifeCam VX-3000) were positioned alongside the MFOBC and focussed on one interbaffle zone (Figure 6.5). Images were acquired at a rate of 1 per minute using the freeware software, YAWCAM. Subsequently, images were converted to 8-bit greyscale and background subtracted, using the first recorded image under constant light intensity, in *ImageJ*. The mean intensity value of a region of interest (ROI) was calculated

and plotted with respect to time (Figure 6.5). To determine nucleation a signal to noise ratio (3:1), of the mean grey scale (mgs) value, was used.
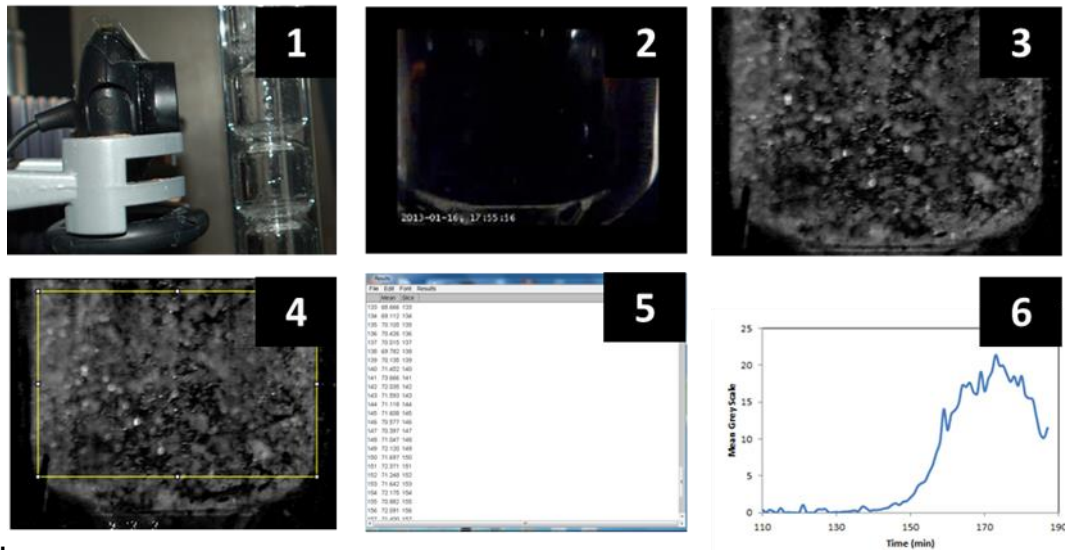
Figure 6.5: Image analysis process. Figure showing the main stages for collecting and processing images. Photograph of the web camera focused on one interbaffle zone (1), images recorded by webcam (2-4), first image recorded taken as background (2), background subtraction of all images (3), ROI selected (4), screen shot of mean grey scale level calculated using *Image J* (5), graph showing the intensity plotted against time (6).

6.2.3 Crystallisation experiments

Based on results from Chapter 5, experimental conditions were selected to cover the range of supersaturation levels under optimal oscillatory conditions investigated during spontaneous nucleation in the COBC. Solutions were heated to approximately 10 °C above solubility and held for 30 minutes to insure dissolution of all solids. Solutions were then cooled to the desired end temperature and held at this constant temperature for nucleation to occur. Where crash cooling was carried out, a HC was set to the desired target end temperature and, after the dissolution hold time, the jacket inlet to the straight was changed over. Due to rapid heat transfer, this crash cooling process took approximately 6 minutes. Examples of temperature profiles are shown in

Figure 6.6. Constant oscillation frequency (2 Hz) and amplitude (20 mm) where used throughout. When Set-up 1 was used, the dissolution chamber HC was maintained at 75°C.
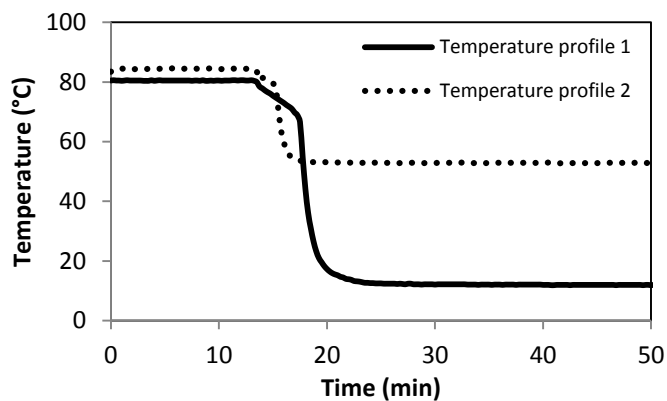
Figure 6.6: Example of crash cooling profiles. Plot showing two crash cooling profiles in a MFOBC with a start temperature of about 80 °C. Example 1 (solid black) was crash cooled to 10 °C whilst example 2 (dotted back) was crash cooled to 50 °C. These plots illustrate, from the HC changeover point, the system reaching an isothermal state within ~6 minutes.

6.3   Results & Discussion

6.3.1 Temperature characterisation

Temperature profiling, along the length of the glass straight in Set up 1, was performed to investigate effect of the hot straight on the bulk crystallisation solution. The temperature profile along the MFOBC, at 5 different time points during a cooling process is shown in Figure 6.7. It should be noted that the temperature along the straight is reasonably uniform, with a variation of about 2 °C, when the difference between the hot section and cooling straight is < 30 °C (0-15 min). This variation increases to around 5 °C when the temperature difference is > 30 °C (20 min).
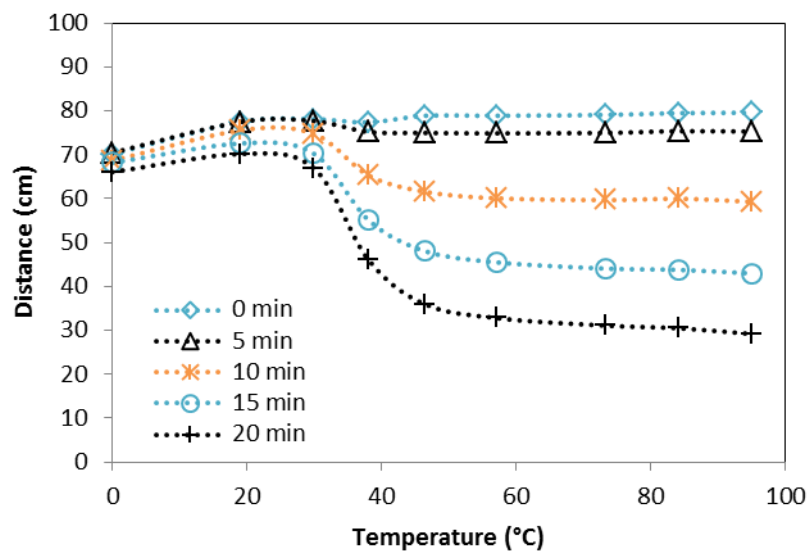
Figure 6.7: Temperature profiling along the MFOBC. Graph showing temperature uniformity profiling over 5 time points during a cooling process within the MFOBC set-up 1 (Figure 6.4).

To illustrate temperature fluctuations due to mixing between two temperature zones, temperature profiles at fixed positions are shown in Figure 6.8. The temperature profile at any given position was stable. During a hold time (20 - 30 minutes), the mixing temperature between the hot and cooling section

(solid black) is as expected (45 °C, measured at 38 cm, when the temperature of hot and cooling sections were 65 °C and 25 °C, respectively). This data demonstrates efficient mixing between sections and rapid heat transfer from the HC to the bulk solution. Thus, when a dissolution chamber is used, desired temperatures can be maintained and segregated along the COBC crystallisation straight in the MFOBC (set-up 1).
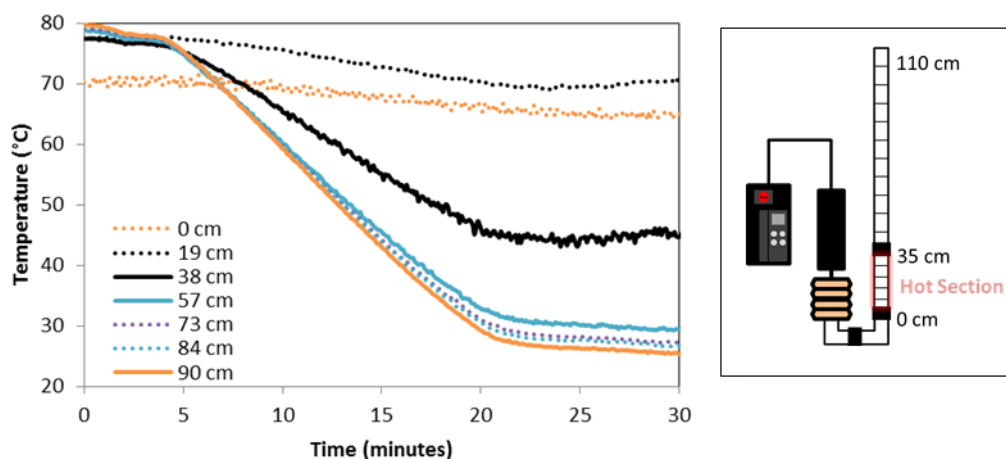
Figure 6.8: Temperature profiling at a fixed point. Graph (left) showing the temperature profile during a cooling process at 7 positions within the MFOBC, set-up 1 is shown for reference (right).

Similar temperature profiling studies were completed for the MFOBC system without a hot section (i.e. set-up 2). Temperatures were recorded at 3 positions: one inside the unjacketed DN25 expansion connection and two in the straight (positioned in cells 10 and 16, 30 and 50 cm up from the membrane at base of the COBC straight, respectively). The temperature difference between the average bulk temperature (taken from cells 10 and 16) and the unjacketed DN25 expansion, and the difference between temperature readings in cell 10 and 16 are shown in Figure 6.9. Three different heating and cooling cycles were used to assess the system under changing temperature profiles, representing those used for cooling crystallisations, before a 30 minute hold time; cycle 1 heating and then

cooling at 1 °C/min, cycle 2 heating and then cooling at 2 °C/min, and cycle 3 heating at 2 °C/min before cooling at 0.5 °C/min.
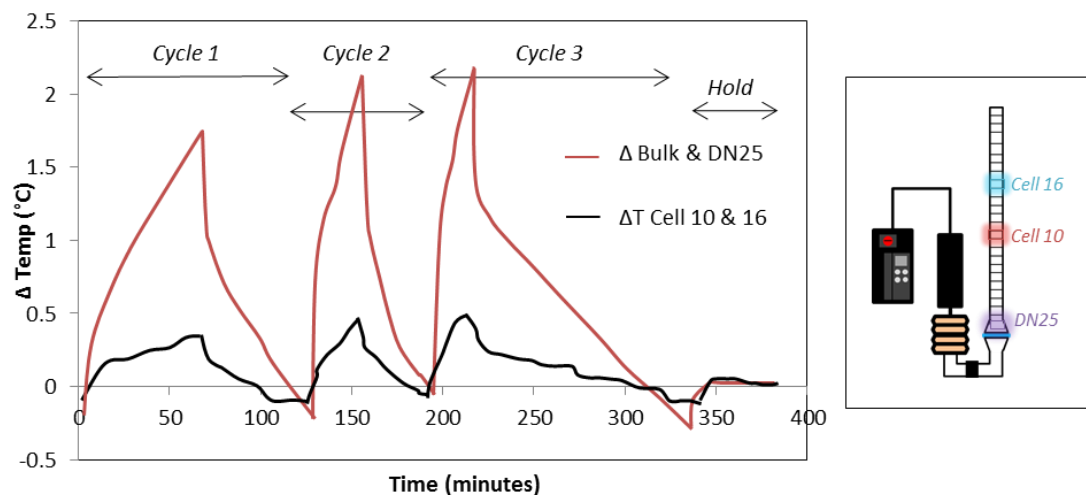
Figure 6.9: Temperature profiling in MFOBC set-up 2. Graph (left) showing the ΔT between the bulk temperature measured in cell 10 and 16 (red) and ΔT the average bulk temperature with the non-jacketed DN25 expansion (black). Three successive heating and cooling cycles were implemented before a 30 minute hold time; cycle 1 heating and then cooling at 1 °C/min, cycle 2 heating and then cooling at 2 °C/min, and cycle 3 heating at 2 °C/min before cooling at 0.5 °C/min. Schematic (right) of set-up is shown for reference to illustrate thermocouple positions.

The data shown in Figure 6.9 demonstrates that bulk temperature does not vary by more than 0.5 °C, illustrating uniform bulk temperature, a desired attribute of a crystallisation vessel. The maximal ΔT between the bulk solution and the unjacketed DN25 expansion at the base of the COBC straight was ca. 2 °C. As this temperature is colder than the bulk temperature, this may adversely affect crystallisation experiments. However, the DN25 expansion volume (ca. 15 ml) only equates to approximately 10 % of the total platform volume and as such (given mixing time within the system can be assumed to be sufficiently rapid), this temperature difference can be assumed to be insignificant. All of the above ΔTs observed are only occurred during heating

and cooling cycles, when the system was held at a constant temperature all values of ΔT remained below 0.3°C within 5 minutes of holding, demonstrating rapid stabilisation of temperature within the system. This temperature characterisation illustrates better control is achieved in set-up 2 where maximum ΔT is 2 °C whereas in set-up 1 ΔT can be up to 5 °C

6.3.2 Imaging

The response of the mean intensity was calculated and plotted with respect to time. Figure 6.10 shows an example of the imaging response when encrustation is heavily observed in the MF system. Here the raw data response of temperature and intensity are plotted with respect to time, and corresponding time stamped images are also shown. The image intensity begins to increase after ca. 40 mintues (after the temperature has stabilised thus generation the fixed supersaturation level). Images show crystal growth on the surfaces of the glass walls. This is in contrast to Figure 6.11 where predominantly nucleation in the bulk occurs without encrustation on the vessel walls. Again a plot of intensity and temperature are shown in addition to and FBRM response collected in-line through the use of an adapted straight including a probe port. The time stamped images show no significant crystal growth on the wall surface. Table 6.3 shows the results from 5 experiments where both FBRM and imaging techniques where used, the average difference in time response between techniques was determined to be ca. 3 minutes illustrating that imaging was reliable for monitoring a crystallisation event within the MFOBC set-up.
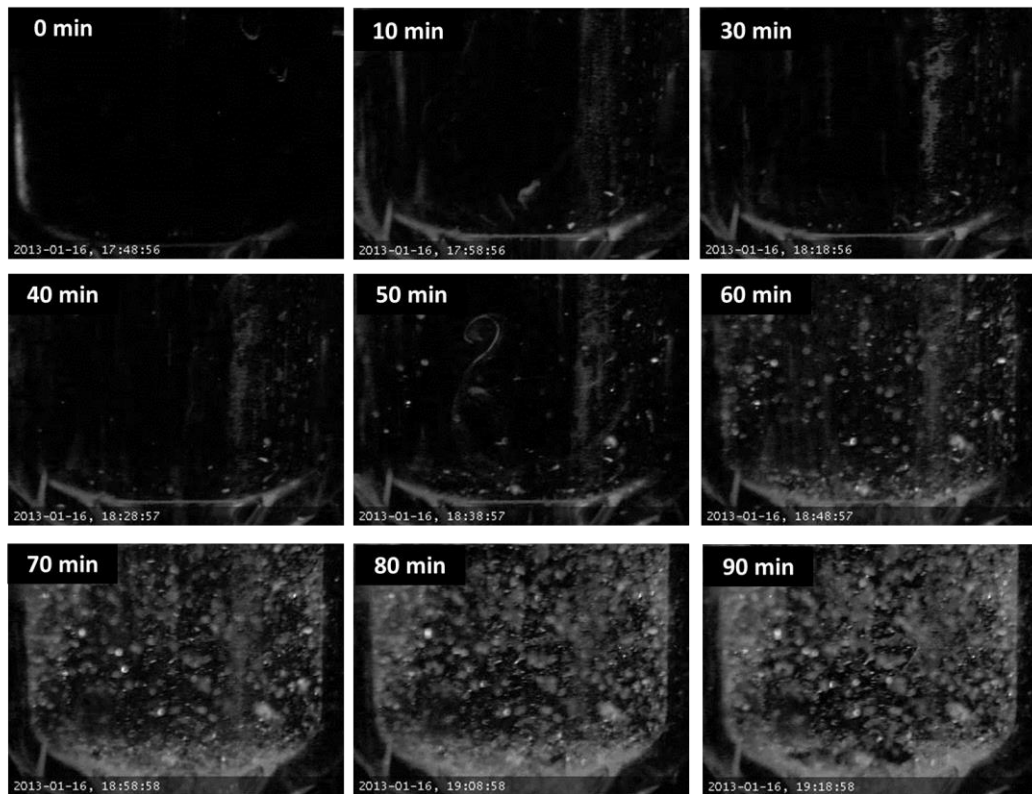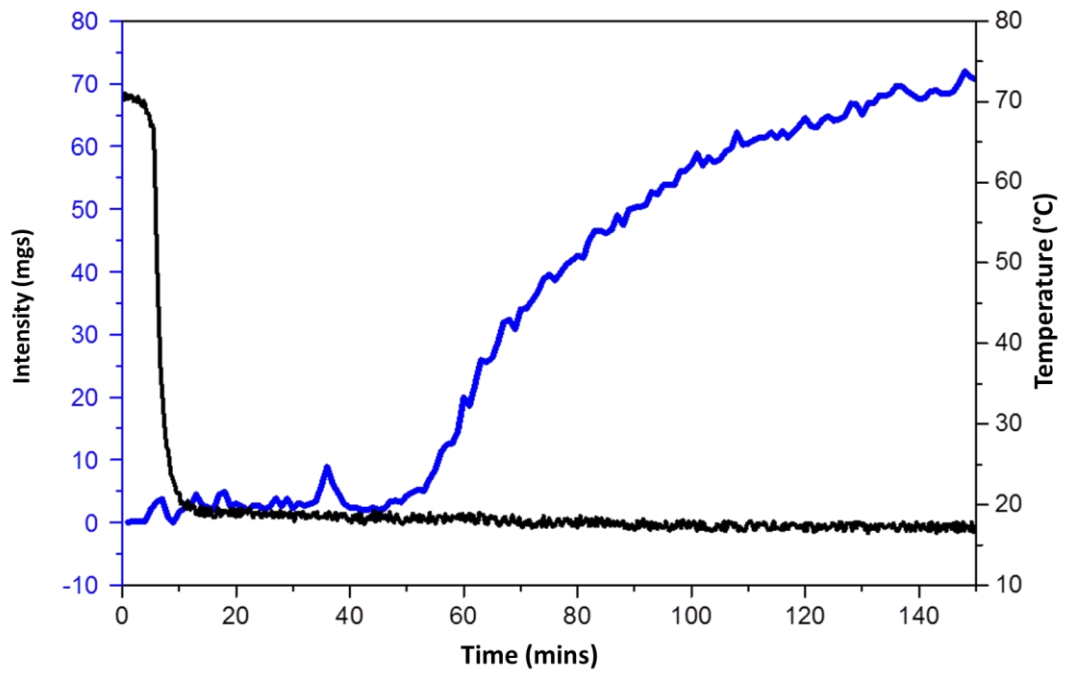
Figure 6.10: Monitoring of encrustation in a MFOBC. Plot (top) showing the response of imaging and webcam (bottom) time stamped background subtracted raw data images during the nucleation of alpha LGA in a MFOBC.
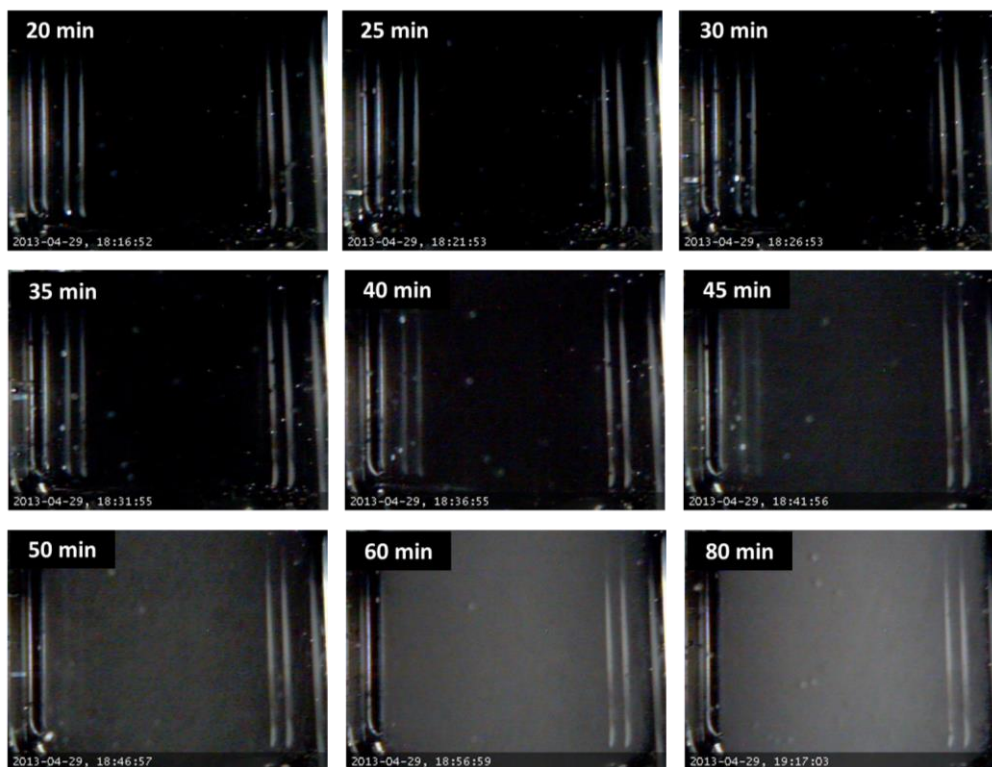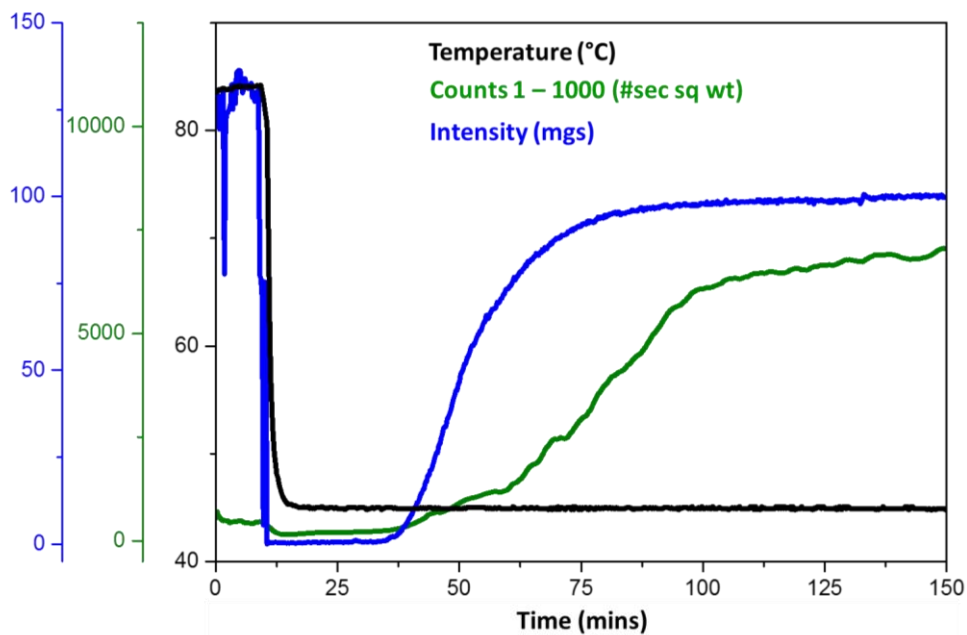
Figure 6.11: Monitoring of nucleation in a MFOBC. Plot (top) showing the response of imaging with FBRM and webcam (bottom) time stamped raw data images during the nucleation of beta LGA in a MFOBC.

Table 6.3: Nucleation detection with FBRM and imaging. Table showing a comparison of FBRM and imaging for the time taken to nucleate during induction time experiments in the MFOBC.

Experiment	Nucleation time (min)	
	FBRM (counts)	Image Intensity (mgs)
1	17	15
2	36	32
3	11	8
4	24	19
5	30	30

One of the advantages of using an imaging technique was that images could be used to observe the process at a given point in time. This helped in determining when encrustation took place and when crystals began to detach from the wall surface moving into the bulk solution (Figure 6.12). Observations in previous experiments (Figure 6.13) showed that encrustation appeared to be dominant at the centre of the inter-baffle regions and around the baffle, almost forming alternating "rings" of LGA deposits. It was originally postulated that the glass surface was smoother at positions where it was not manipulated during the manufacturing process and encrustation was not favoured here. When imaging was used it was concluded this hypothesis was incorrect, encrustation appeared to occur over the entire surface of the glass but as the process continued detachment from the surface occurred creating this ring pattern. This is most likely due to the increased fluid velocity around the baffle constriction where eddy formation begins, these regions of higher shear provide sufficient force to dislodge adhering solids once a given deposition level is reached.
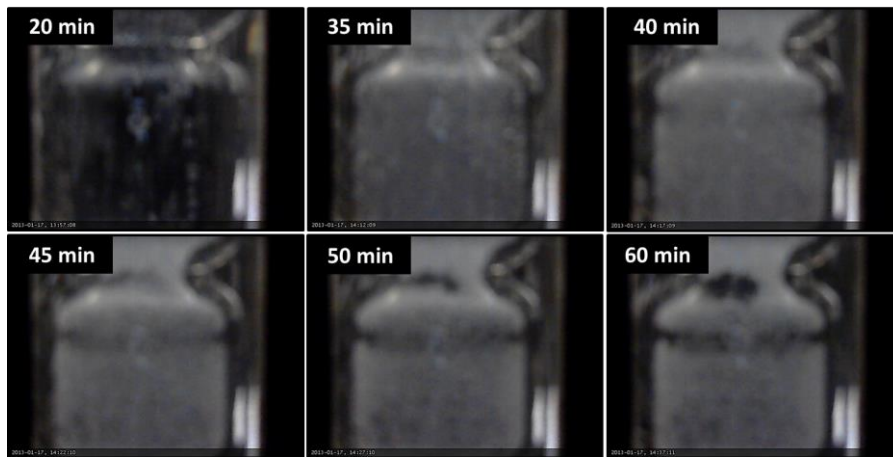
Figure 6.12: Encrustation detachment over time. Webcam raw data images collected during encrustation in a MFOBC. Time stamped images show the formation of encrustation and successive detachment of crystals during process creating a ring like pattern.

Figure 6.13: Encrustation patterns on a DN15 COBC glass straight. Photographs illustrating an alternating ring pattern of encrusted LGA during MFOBC crystallisations.

The output files from the web camera are JPEG images with a resolution of 320 x 240 pixels. The colour intensity of these pixels allows an intensity value to be captured in the range of 0 to 255. Crystals moving through the camera view result in a variation in pixel intensity compared to the background, as do crystals that are stuck on the vessel walls. Crystals moving in the bulk will reflect light providing pixel intensity but this will not remain constantly high due to 3D movement at various velocities throughout the reactor. However fouling crystals are stationary, closer to the camera and reflect more light leading to higher constant pixel intensity at a given position.

Given the intensity of a pixel is much higher when the crystals are fouled on the vessel wall when compared to crystals in the bulk, by identifying pixels with the highest intensity for a consecutive number of frames (to avoid false positive of larger and/or brighter crystals in the bulk) statistical analysis can distinguish between fouling and bulk crystallisation.[258]

6.3.3 Crystallisation experiments

Experiments were designed around experimental conditions used for spontaneous COBC crystallisations during Chapter 5, details of experimental conditions and results from MFOBC investigations with LGA can be found in Table 6.4. Here the time taken for the system to nucleate under isothermal conditions, with respect to supersaturation, can be found alongside MSZW (kinetic) information from controlled cooling experiments. Whilst not a quantitative study, there is a clear trend that an increase in supersaturation results in a decrease in induction time. This is illustrated in a plot of supersaturation against induction time found in Figure 6.14. Similar times are observed for both concentrations illustrating that temperature is probably not a dominant factor on the nucleation kinetics of LGA under isothermal conditions. This decrease in induction time with increasing supersaturation is to be expected as higher supersaturations create a higher driving force for nucleation.

Table 6.4: Crystallisation experiments in MFOBCs. Table of experimental results obtained from crystallisation in MFOBC set-ups (Figure 6.4).

Set-up	Conc.	End T	$S^{\#}$	S^*	CR	Form	t_{ind}	Nuc. T
		15	5.0	3.9	CC	α	135	(15)
	30	15			0.5	α	(120)	15
		15			0.2	α	(320)	15
1		27	5.0	3.8	CC	α	10	(27)
	45	27			0.5	α	(45)	52
		27			0.2	α	>480	-
		53	2.1	1.5		β	53	(53)
	45	45	2.7	2		Mix	13	(45)
		33	4.1	3		Mix	11	(33)
2		26	5.2	4		Mix	17	(26)
		30	2	1.5		Mix	45	(30)
	20	22	2.6	2		Mix	35	(22)
		11	3.9	3		Mix	25	(11)
		3	5.1	4		Mix	13	(3)
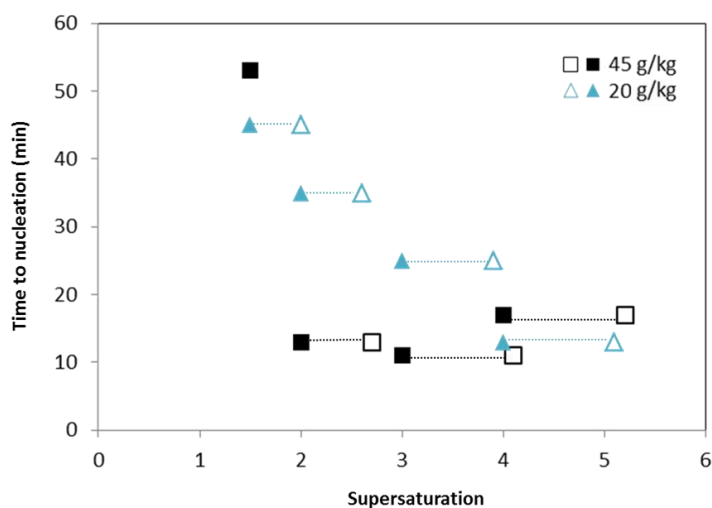
Figure 6.14: LGA induction time. Plot showing a decrease of induction time with an increase in supersaturation, during the crystallisation of LGA in a MFOBC (set-up 2, Figure 6.4) under isothermal conditions at two concentrations, 45 g/kg (■,□) and 30 g/kg (▲,△). Closed and open symbols relate to supersaturation values for the nucleation of alpha and beta polymorphs respectfully.

Interestingly, on comparison of the induction time and resulting polymorphic form, under similar supersaturations in both set-ups, a clear difference is observed (Table 6.4). Nucleation takes a significantly longer time to occur in set-up 1 and alpha was solely produced, whereas in setup 2, the induction times are shorter and the stable beta form was always present in the resulting product. These unexpected results are possibly due to temperature and solution history effecting nucleation properties. For example, a recent study on solution history effect during the crystallisation of fenoxycarb shows the induction time is significantly influenced by pre-treatment time and temperature, with longer pre-treatment times and higher temperatures resulting in a longer time for a nucleation event to occur.[259] The crystallisation of *m*-hydroxybenzoic is another example where solution history effects are observed.[260] The report illustrates impact of solution history on resulting polymorphic form where the metastable form II is isolated readily when the solution has experienced a more rigorous heating and for longer times whereas under a reduced time a lowered thermal environment there is an

increased favourability to produce the stable form I. The observations made within this study (Chapter 6) are therefore in agreement with previous reports,[259,260] i.e. the nucleation mechanisms are different in both set-ups. This may be explained by, in set-up 1, the solution experiencing a temperature cycling process during the over the course of platform operation i.e. a longer time at higher temperatures, whereas in set-up 2 (where no hot section is present), the solution only experiences isothermal conditions before nucleation.

Encrustation was also always observed with set-up 1, however this was not observed to any significant extent in set-up 2. Given the resulting product polymorph was different in both set-ups these results illustrate the potential encrustation tendencies of different polymorphic forms, where alpha LGA appears to favour encrustation on surfaces whereas beta appears to prefer nucleation in the bulk solution. This possibly relates to variations in the surface chemistry of LGA polymorphs. For example, nucleation of isonicotinamide (INA) polymorphs was studied with and without the presence of heterogeneous templates.[261] Four templates were investigated, including titanium dioxide (TiO_2) rutile and TiO_2 anatase, to explore the influence of templates on induction time. Form III INA was isolated with and without any template present, with the exception of TiO_2 anatase. Crystallisations in the presence of TiO_2 anatase resulted in the production of form I and III.[261] Another study investigated the crystallisation of 1,3-bis(m-nitrophenyl)urea (MNPU), in 3 solvents, on 11 different modified siloxane templates.[262] Here, the modified surfaces were shown to have a tendency to promote nucleation of the metastable phases, isolating 4 of 5 polymorphic forms of MNPU. Both studies[261,262] present the possibility of surface directed nucleation and growth of different polymorphic forms, however further work is needed to better understand the underlying mechanisms.

In light of the extended effort to develop and assess both set up 1 and 2, fouling was not systematically assessed in this chapter, exploiting the image analysis approach in section 6.2.2. However it has clearly been established

that the platform offers a useful approach for investigating this important and potentially problematic process. Commercially availability laboratory batch crystallisation platforms generally do not include different temperature zones. The usual requirement is for platforms with rapid heat transfer capabilities. This is to ensure uniform temperature control is maintained at all times within the bulk (as variations can lead to supersaturation gradients and hence loss of control). Considering the observed results and intended application it was decided to concentrate platform development of set-up 2 as this best satisfied the system requirements.

6.3.4 MFOBC automated platform

The MFOBC (set-up 2) system was automated by *Perceptive Engineering* providing a control interface for automated experimental operations. *PharmaMV* software was used for experimental control and data storage alongside temperature and supersaturation control utilising feedback responses from in-line apparatus including thermocouples, FBRM and IR probes.
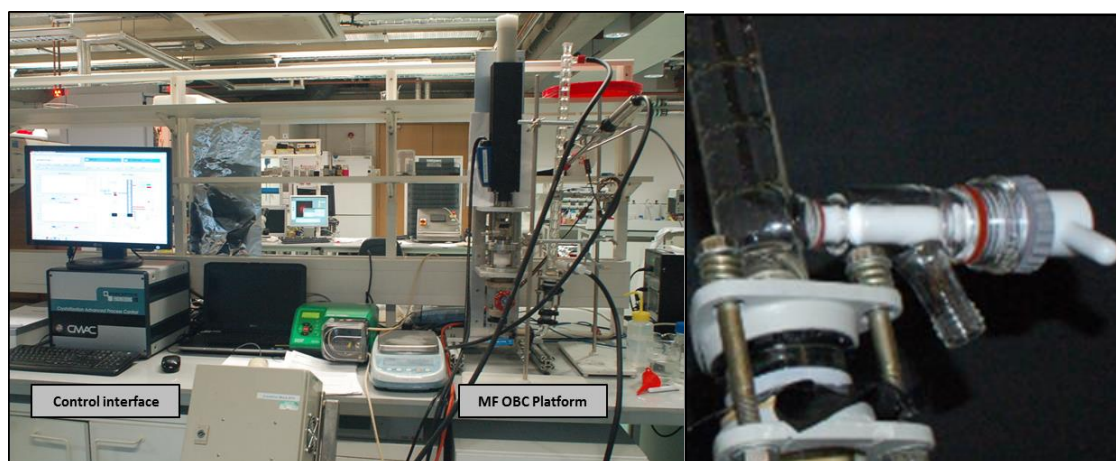
Figure 6.15: Automated MFOBC platform. Photographs showing the automated MFOBC platform with the *Perceptive Engineering* control interface

(left) and the tap design incorporated at the base of the COBC straight (right) to allow for manual extraction of material from the process.

6.3.5 Challenges

6.3.5.1 Camera positioning

During experiments positioning of the stainless steel thermocouple appeared to play a role on the encrustation process, Figure 6.16. It appears that encrustation has a higher preference to stainless steel surface opposed to the glass. In areas where the thermocouple was not present solids would grow on the glass surface however, in areas where it was present, encrustation appeared to predominantly favour the stainless steel hence for encrustation monitoring care needed to be taken to ensure the camera was positioned correctly to monitor the surface where sacrificial materials were not present. This observation further highlights the need for understanding over how materials of construction can impact on the crystallisation process.

Figure 6.16: Sacrificial encrustation. Photograph showing encrustation along the COBC straight of a MFOBC. Image shows preferential encrustation on the stainless steel thermocouple (left) and in area where the thermocouple is not present (right) dominant encrustation on the vessel walls.

As surface roughness is known to promote nucleation events, alongside various metals showing different fouling properties,[263] an attempt to prevent fouling of the stainless steel thermocouple was to replace it with a Teflon®

coated thermocouple, however this proved unsuccessful and encrustation with LGA still occurred (Figure 6.17). There are reports illustrating how modifying the surface through the use of coatings, the induction time to fouling during crystallisation can be extended.[264,265]
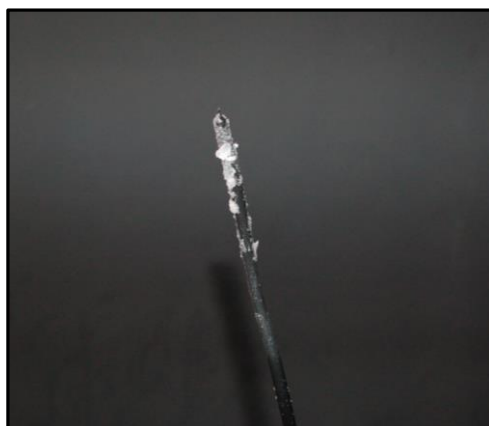
Figure 6.17: LGA encrustation on a Teflon coated thermocouple. Photograph showing encrustation on a Teflon® coated thermocouple after crystallisation in a MFOBC.

6.3.5.2   Surface renewal

The possibility of the surface renewal was evident in several experiments, an example is shown in Figure 6.18. Due to oscillations in the batch vessel the liquid level is moving up and down along the glass walls within the MF set-ups. Here a thin film of solution is constantly being generated on the down stroke and washed back into the bulk solution on the upstroke (at a frequency dictated by the input settings). Due to the air liquid interface along this film and possible evaporation effects, local regions of high supersaturation could be generated. These highly supersaturated areas could create an environment generating nuclei which will be washed into the bulk solution on the oscillatory upstroke. This surface renewal process could therefore impact the crystallisation and the resulting product form if it is not controlled and/or eliminated. Surface renewal would not be a dominant

process during continuous operation because the COBC does not display any air-water interfaces during normal operation.
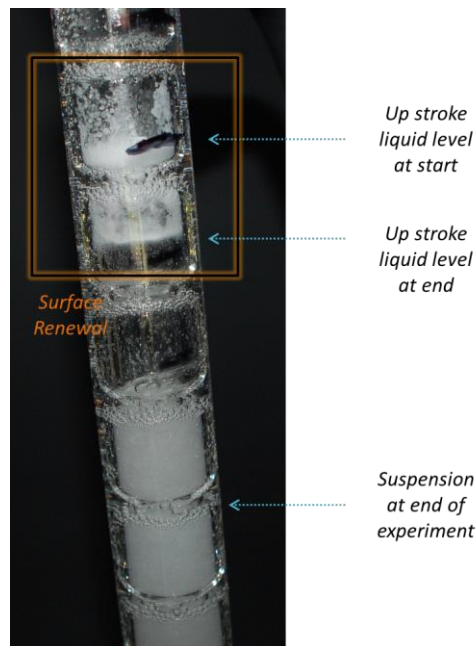
Figure 6.18: Evidence of surface renewal. Photograph showing the possibility of surface renewal at the top of the MFOBC after a crystallisation. Solid deposits are observed above the liquid level at the end of a crystallisation experiment. The volume level on the upstroke of the oscillation, at the beginning and end of the experiment, are indicated illustrating a change in bulk solution volume over a temperature range of about 50 °C.

Figure 6.18 also highlights the impact of evaporation and/or temperature dependant volume constriction over the course of an experiment. As can be observed in Figure 6.18 there is a loss of about 1 cell volume from the start to end of the experiment. This possible evaporation could also be creating a sublimation effect where solids crystallise above the liquid level. To minimise evaporation effects a balloon was placed on the top of the apparatus to create a saturated gaseous environment and prevent solvent evaporation from the vessel to the surrounding environment.

6.4 Summary

The successful design and development of a novel operational batch MFOBC system, designed to minimise differences between the batch and COBC platforms, has been described. The MFOBC is a significant improvement on the previous design (Chapter 5, Figure 5.6) as it delivers a more consistent hydrodynamic environment in addition to using consistent materials of construction between the batch and continuous platforms. This should minimise differences in the observed crystallisation processes to ease the transfer from batch to continuous. Whilst better than the moving baffle system, some inconsistencies were still observed due to surface renewal and from differences in the temperature control between the two systems leading to different polymorphic outcome.

The application of a bespoke imaging system using a low cost commercially available CMOS camera has provided information on the conditions under which encrustation occurs during oscillatory flow crystallisation. This imaging technique combined with the mean grey scale intensity analysis was shown to provide comparable sensitivity with high cost systems for detecting the onset of primary nucleation and of fouling (FBRM, Turbidity). The combination of these techniques was used to identify that the mechanism of encrustation was most likely due to surface nucleation rather than particle deposition, collision or adhesion. In addition to providing process information on the acceptable operating conditions to avoid encrustation, this work demonstrates a novel and inexpensive method for gathering reliable process data at a fraction of the cost of commercial imaging probes e.g. PVM. Experimental results were used to develop an improved imaging technique where fouling on the glass surface could be distinguished from nucleation in the bulk.[258]

Induction time experiments were used to investigate the influence of supersaturation on primary nucleation kinetics of LGA from aqueous solution. As supersaturation was varied from 1.5 – 4, the induction time displayed a decrease of 1 hour to ca. 10 minutes. This was used as the basis to attempt

controlled isothermal primary nucleation of beta LGA in a COBC. However under supersaturations of up to 6 in the COBC, although primary nucleation was observed within comparable timescales, only alpha LGA was produced. The results from the two MFOBC setups developed in this work also confirm the sensitivity of the unseeded LGA crystallisation to subtle differences in process conditions. These batch platforms show significant differences in terms of both polymorphic outcome and encrustation characteristics during crystallisation. When LGA experienced a temperature cycling type process (MFOBC setup 1) the metastable form was produced exclusively and significant encrustation on the vessel walls was observed. Where no temperature cycling was effected (MFOBC setup 2) the stable beta form of LGA could be isolated without significant encrustation. Whilst the specific reasons for these differences are unclear, as surface renewal effects would impact both systems similarly, solution history and differences in the temperature cycling experienced by the solutions appears to be the major factor influencing the outcome of nucleation.

The results of the fouling experiments in both systems highlight differing encrustation propensities during the crystallisation of the different polymorphic forms. alpha LGA appears to show a preference to nucleate on surfaces whereas beta LGA will nucleate in the bulk without fouling on the surface. This may well relate to differences in the surface chemistry expressed in the two crystalline forms. Further work is needed to capture the underlying mechanisms.

This platform was also adapted with a control system to incorporate PAT enabling solubility curve determination and assessment of nucleation and growth kinetics systematically mimicking commercial laboratory STR development platforms. This will significantly reduce the time required for extensive manual experimentation therefore accelerating the development of continuous crystallisations for the COBC.

Chapter 7. Workflow for Continuous Seeded Cooling Crystallisation: A Study on Polymorph Control of Carbamazepine

7.1 Introduction

A range of considerations are required for the design and control of optimised crystallisation process.[266] These include the characterisation of the solute in terms of solubility, stability, impurity profile, nucleation and growth kinetics. Additionally, the target objectives, including purity, yield, form, size, PSD, shape and cycle time, should be defined. These factors will inform the selection of a suitable mode of crystallisation (for example, anti-solvent, cooling or melt crystallisations). Control of crystallisation has been demonstrated using several methodologies including direct control or model based design approaches.[63,267] Thus, identifying the relationships between critical process parameters (supersaturation, flow, mixing, shear rates, temperature) and the quality attributes (Figure 1.26) should allow a suitable control strategy for crystallisation processes to be defined.

Using a direct control approach, the successful development and control of an anti-solvent crystallisation process for the production of a pharmaceutical compound, eliminating secondary nucleation, was achieved.[268] Here concentration control was utilised using feedback from inline FBRM and ATR IR to maintain relative supersaturation. This automated approach enabled optimal addition rates of the anti-solvent, *n*-heptane, to the API toluene system, to be identified quickly for the control over desired product attributes. A further example utilises direct control of supersaturation during the cooling crystallisation of a multicomponent salt system from aqueous solution in an STC.[269] Inline FBRM and ATR IR were used to control supersaturation profiles during the cooling process and implementation resulted in larger crystals when compared to a linear cooling profile.

A model based strategy has been used for controlling the PSD of paracetamol during crystallising from ethanol in a batch STC.[270] This included model validation and parameter estimation through on-line monitoring of supersaturation and PSD with PAT. A population balance model accounting for solution thermodynamics, crystal growth, and nucleation, models considering the mixing characteristics of the vessel where

also included. Here, the experimental product PSD was shown to be close to the desired unimodal distribution, therefore it is a suitable methodology to design crystallisations for targeted output CQAs. Another similar strategy using modelling, within a PFR, describes the control and optimisation of flufenamic acid crystals during anti-solvent crystallisation.[271] Here multiple anti-solvent addition points within the PFR are modelled and optimal anti-solvent addition rates calculated. It was found that predicted anti-solvent profiles simulated better product crystals, larger size with narrower PSD, compared to the cases with equal additions of anti-solvent. However this work[271] does not report an experimental validation.

7.1.1 Carbamazepine

Carbamazepine (CBZ), Figure 7.1, is the active pharmaceutical ingredient in Tegretol® administered for the therapeutic treatment of epilepsy, bipolar disorder, and trigeminal neuralgia. Due to pharmaceutical relevance, and highly polymorphic nature, the crystallisation behaviour and solid state aspects of this compound have received much attention. Studies include solid form screening, physical characterisation, discovery and prediction of new polymorphs, solvates and co-crystals in addition to solution mediated polymorphic transformations (SMPTs).[272-278] The majority of these investigations are at small scale, within vials and batch vessels (<500 ml), and there are no reported studies on continuous crystallisation of CBZ from solution. Recently, a continuous co-crystallisation study was reported for this API, where hot melt extrusion was utilised, in place of crystallisation from solution, to deliver a continuous process for the production of CBZ trans cinnamic acid co-crystals.[279]
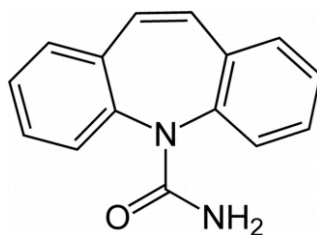
Figure 7.1: Molecular structure of CBZ. Figure showing the molecular structure of CBZ, chemical name 5H-dibenzo[b,f]azepine-5-carboxamide.

CBZ is known to have 5 polymorphic forms[272] (Figure 7.2) alongside a range of solvates and co-crystals. 10,11-dihydrocarbazmazpine is a minor impurity in CBZ raw material and that also been investigated as a template for the initiated growth of a new predicted polymorph, form V.[280] Computational methods were used to predict the structure and direct the experimental discovery of form V CBZ using templating on an isostructural form, dihydrocarbamazepine.[280,281] No studies on the effects of this impurity on CBZ crystallisation have been reported.
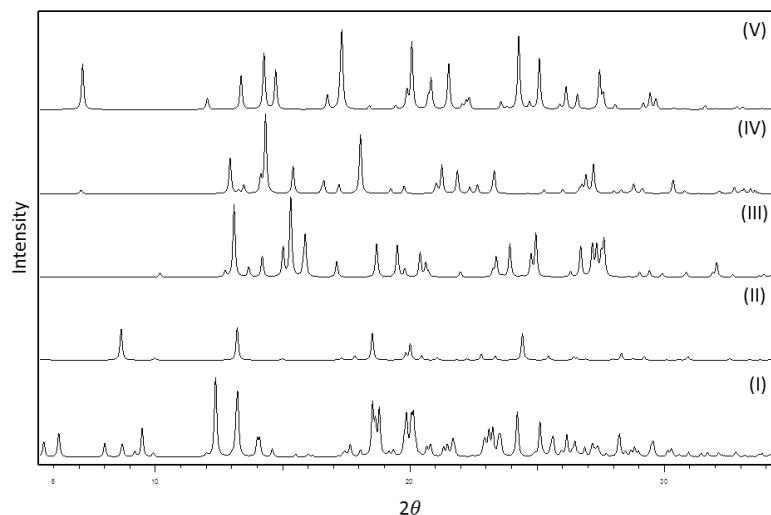
Figure 7.2: XRPD patterns of CBZ polymorphs. Diagram showing a stacked plot of XRPD powder patters for the 5 polymorphs of CBZ. Patterns are ordered I - V from bottom to top respectfully. Powder patterns are simulated from single crystal data.[280,282-285]

The most commonly observed forms of CBZ during solution crystallisation are forms I, II and III, and the monoclinic form III is the thermodynamically stable form at room temperature.[282] A dihydrate is also readily formed upon exposure to aqueous solution or high humidity. SMPT of non-solvated forms to the dihydrate in aqueous media can therefore complicate dissolution measurements.[286] Form IV has not been reported from traditional solution crystallisation techniques, it has however been produced through other methods including spray drying[287] and crystallisation in the presence of additives.[285] Form V CBZ has also still to be produced, at a larger scale, since the first experimental observation in 2011.

Given the range of CBZ polymorphs, care is required to prevent the formation of undesired polymorphs as well as to avoid transformation from metastable to stable forms during crystallisation and storage. Sefcik *et al,*[288] investigated the effect of agitation on the crystallisation of CBZ during cooling crystallisation in ethanol. Under quiescent conditions, the metastable form II was produced, irrespective of the cooling profile applied. Form II subsequently converted to the more stable form III over time. Effects of impurities on nucleation kinetics were also demonstrated; when commercial CBZ was purified, a significant reduction in induction time, up to 6-fold, was observed.[288] Rohani *et al,*[275,289] investigated the phase transformation between form II and form III, during cooling crystallisation in propan-1-ol, using in-line ATR-IR, FBRM and Raman. This confirmed an enantiotropic relationship between forms II and III, with a transition temperature of 34 °C. This is comparable to the transition temperature of 40 °C reported in the same solvent system by Sun *et al.*[274] The SMPT of triclinic form I, to monoclinic form III, has been shown to occur in the temperature range of 79 - 82 °C in isopropyl benzene,[276] and 77 °C in methanol.[273] These transition temperature are summarised in Figure 7.3. Whilst the transition temperature is independent of solvent,[290] the rate of transformation can be accelerated or retarded by solvent choice. For example, the SMPT of form I to form II sulfamerazine was studied in 10 solvents and 6 co-solvent systems.[291] The transformation process was shown to range from 0.25 – 54 hours, the longer

transformation times corresponding to solvents with stronger hydrogen bonding propensity. Another example, using *D*-mannitol with an ethanol-water co-solvent system, demonstrates an accelerated rate of transformation of the metastable alpha to the thermodynamically beta when ethanol content is increases.[292]
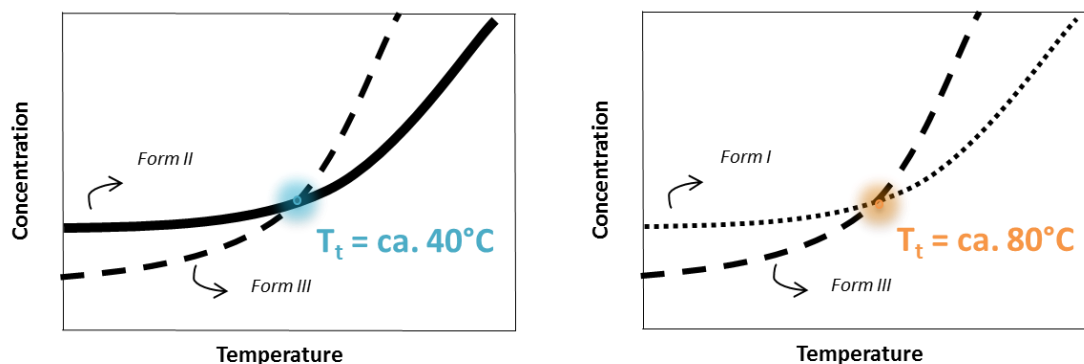
Figure 7.3: CBZ transition temperatures. Solution mediated polymorphic phase transition temperatures of CBZ forms I, II and III. T_t between forms II and III is shown to be ca. 40°C,[274,275,289] whereas the T_t between forms I and III is higher ca. 80°C.[273,276]

Given the accessibility of forms I, II and III from solution crystallisation (found in Table 7.1) and the rapid formation of dihydrate in the presence of water,[286] the production of physically pure CBZ represents a challenge for polymorph control in continuous crystallisation. The importance of polymorph control in CBZ is highlighted by the clinical failure in 1988, which occurred due to uncontrolled conversion to the dihydrate.[11] Several recent studies have demonstrated crystallisation resulting in mixed phase products.[293-296] Additionally, the variability in polymorphic phase purity of commercially available CBZ from four independent commercial suppliers has been reported.[297]

Table 7.1: Conditions for CBZ polymorph production. Table showing conditions reported to isolate forms I, II and III of CBZ from solution.

Form	Crystallisation conditions	Ref.
Triclinic	Laser induced nucleation from acetonitrile.	296
I	Completive slurry experiments in isopropylbenzene.	276
	Cooling crystallisation in isoproplybenzene and dichloromethane.	276,298
Trigonal	Cooling crystallisation from Ethanol, 1-propanol, isopropylbenzene, dichlormethane.	274,276,282,288
II	Anti-solvent addition (ethyl ether) to a chloroform solution.	299
	Cooling crystallisation from ethanol in silanised glass.	248
	Quiescent conditions from ethanol.	288
Monoclinic	Evaporation from ethanol.	282
III	Cooling crystallisation from ethanol in silanised glass.	248
	Laser induced nucleation from methanol and acetonitrile.	296
	SMPT of form I in ethanol and methanol, SMPT of form II in 1-propanol and ethanol.	273-275,288
	Aqueous solutions at different pH values.	295,300
	Cooling crystallisation form isopropylbenzene.	276

Due to the challenges associated in controlling physically phase pure products of the highly polymorphic API CBZ, reliable kinetic information and control strategies are needed to isolate pure forms without cross contamination of other polymorphs. In addition to control strategies, the requirement of successful workflows and scaling platforms (for the prediction of crystallisation behaviour at manufacturing scale) is a necessity given the general expense and limited quantities of novel APIs. Considering the COBC offers uniform flow environments (Chapter 4), with the ability to control polymorphism and PSD for prolonged periods of time (Chapter 5), it is possible that the continuous crystallisation of CBZ, in the COBC, may allow greater control over the process dynamics when compared to previous studies.

In an effort to improve the translation of batch to continuous processing, a MFOBC was developed, characterised and automated (Chapter 6). This system is a significant improvement in matching the hydrodynamic conditions experienced within continuous oscillatory flow. Utilisation of this continuous test-bed unit should provide more reliable data of control parameters to inform decisions for operation when moving from batch to continuous OBCs. Thus, allowing the rapid development of an effective continuous crystallisation process. As such, the focus of the work described in this chapter is the design and application of a standard workflow for polymorph control of CBZ during continuous crystallisation.

7.2   Experimental

7.2.1 A systematic workflow for continuous crystallisation process development

In light of the potential complexity associated with a range of variables and interactions influencing multiphase rate processes (Figure 1.26), it is desirable to deploy a systematic approach for crystallisation process development. The goal of a work flow for crystallisation, is to establish the key control parameters, inform platform selection and select appropriate measurement and control strategies as quickly as possible. This is based on information gained from a minimum number of experiments. Figure 7.4 shows a basic workflow for crystallisation development that aims to provide a systematic approach to the acquisition of process understanding. The application of this knowledge is to deliver a reliable continuous process in a COBC. The highlighted orange arrows, indicate the methodology used throughout this chapter to develop a continuous cooling crystallisation of CBZ.
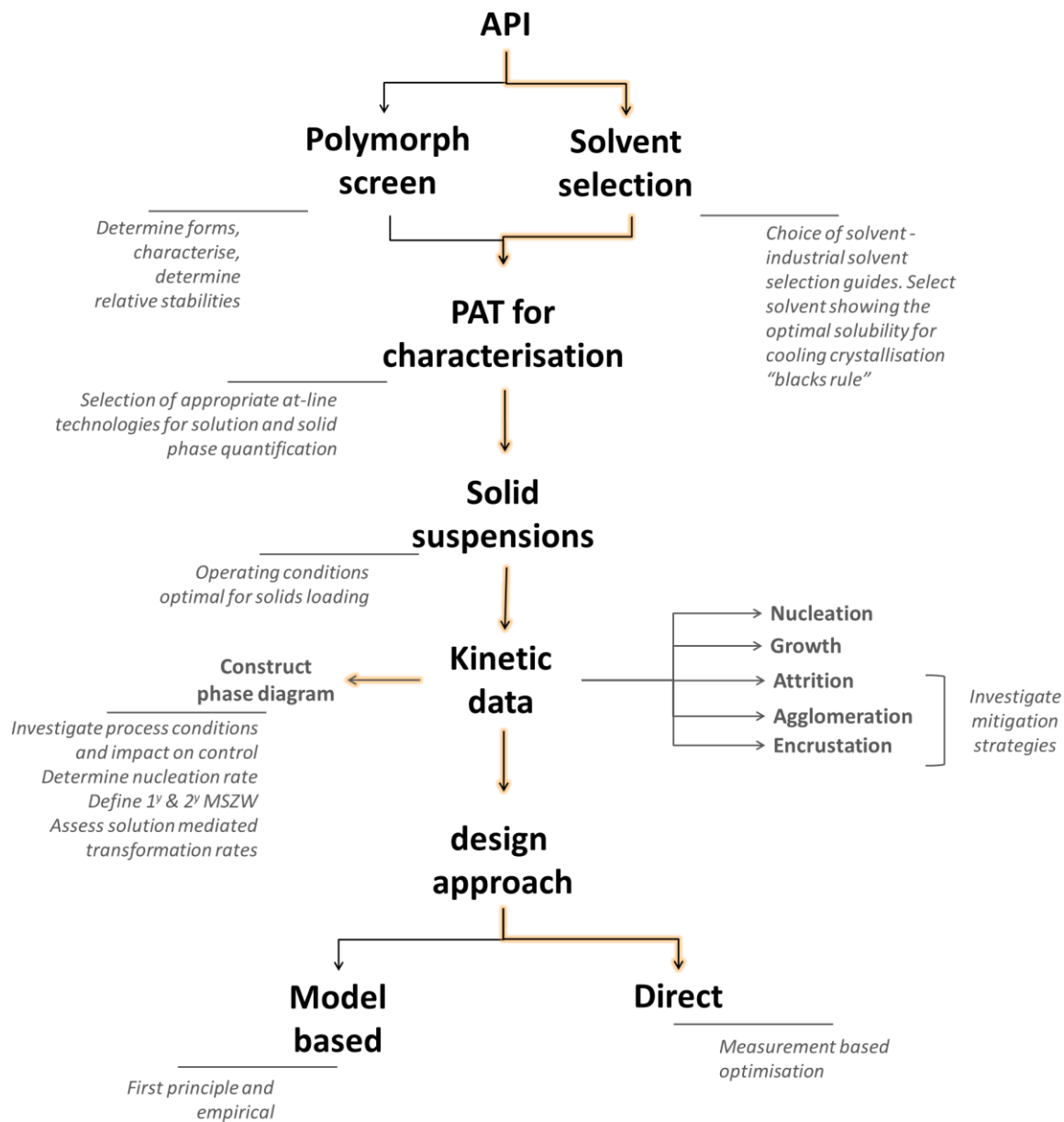
Figure 7.4: Workflow towards CBZ crystallisation in a COBC. Flow diagram illustrating a workflow for COBC crystallisation. The arrows highlighted in orange illustrate the pathway taken during the development of a continuous crystallisation process for CBZ within this chapter.

7.2.2 Solvent selection and solubility

Measurement of the phase diagram in selected solvents and screening of kinetic information were applied to determine the acceptable operating conditions for a controlled cooling crystallisation of form III CBZ. Solubility data and nucleation kinetics, in the form of MSZW measurements, were performed in small scale batch crystallisers (*Avantium Technologies Crystalline*). The system is a small volume parallel crystalliser consisting of eight independently controlled reactor positions fitted for 8ml glass vials. Each position was equipped with turbidity sensing, overhead stirring and cameras for imaging (experimental conditions can be found in Table 7.2).

After an initial solubility screen was carried out, a more accurate measure of the temperature dependence of the solubility were carried out in a larger vessel 1 L STC workstation equipped with PAT (*Mettler Toldeo Optimax*). The workstation was configured with a Pt(100) thermocouple, flat baffle, FBRM (for particle size) and a mid IR ATR probe (for concentration measurement). An excess of CBZ in ethanol was added to the STC (100 g CBZ, 600g of ethanol) and the experimental procedure was followed, as per Figure 7.5.

Table 7.2: Operation conditions for small volume parallel crystallisations. Table showing the various input parameters used for solubility screening of CBZ with ethanol and methanol.

Parameter	Value
Heating rate	0.3 °C/min
Cooling rate	0.5 °C/min
Impeller	Hook
Stirring rate	600 rpm
Scale	3 ml
Hold time at T_{max}	20 min
Hold time at T_{min}	30 min
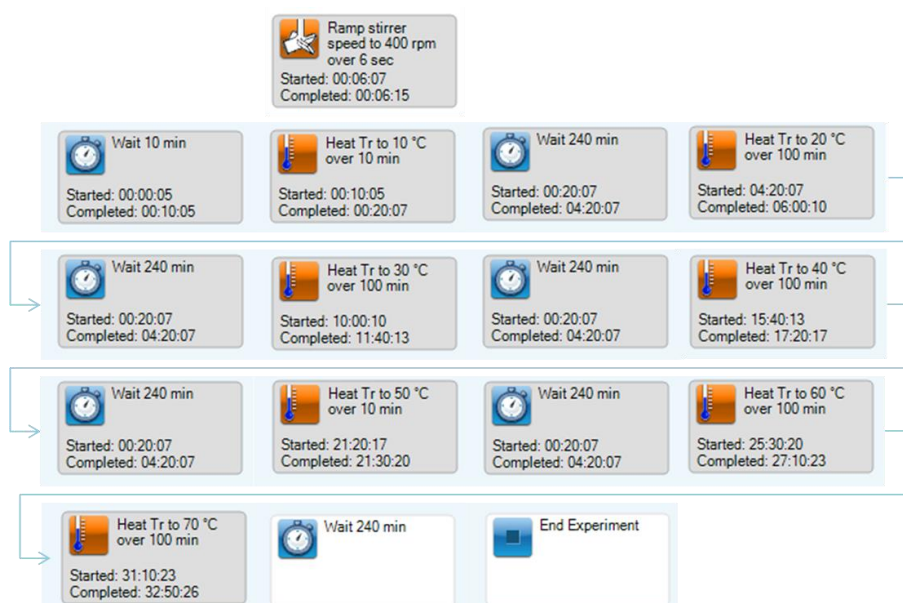
Figure 7.5: Experimental procedure in the 1 L STC. Flow diagram showing the experimental procedure for solubility determination of CBZ in ethanol. Flow diagram adapted from the *iContol* software interface.

7.2.3 PAT for process characterisation

The built-in turbidity system used within the *Crystalline* platform is based on the light obscuration principle. This provides a tool to detect clear points (solubility) and cloud points (nucleation) of solute molecules. Figure 7.6 shows an example of the clear and cloud points obtained during a solubility and MSZW experiment. This method reliably distinguishes when particles dissolve or precipitate upon heating and cooling, providing initial information on the metastable zone width: an operating domain in which growth can be effectively controlled without unwanted primary nucleation.
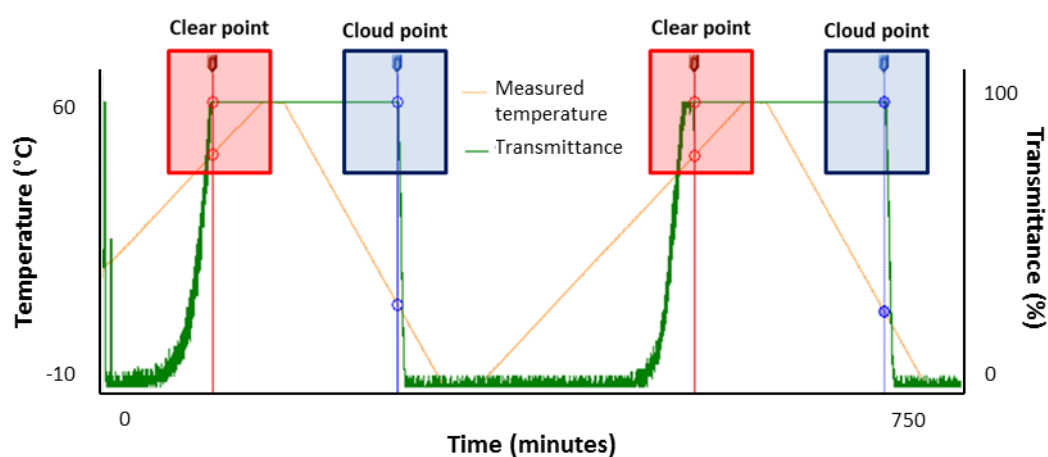
Figure 7.6: Clear and cloud points from turbidity measurements. Screen shot of experimental data, with clear point (■) and cloud point (■) indicated, as viewed with *Crystal Clear* software during solubility and MSZW measurements in a small scale parallel crystalliser.

Monitoring solution concentration provides a more direct measure of supersaturation: the driving force for nucleation and growth (Section 1.3). ATR IR allows solution concentration to be monitored, provided the material has detectable characteristic peaks. This technique has been used in many crystallisation studies to monitor and control solution concentration.[301-303] ATR allows the acquisition of liquid phase IR spectra in the presence of solids due to the small effective path lengths, which are ca. 1 µm.[304] Within

this chapter, ATR FTIR was used in-line for solubility determination during process design in addition to monitoring concentration during continuous process operation.

A series of standard concentrations, between 20 - 100 g/kg, were prepared, providing a calibration series to convert the absorbance values from the relative solubility curve to concentrations. To assess possible effects on the absorbance due to thermal changes, the temperature dependence of the IR response was also investigated (by applying temperature cycles to known solution concentrations). To determine the temperature dependent solubility curve using ATR IR, an excess of CBZ was added to the 1 L STC and slowly heated by 0.1 °C/min over a 10 degree range, the temperature was then held for a 4 hour hold period, and this was repeated over the temperature range of 10 – 70 °C (Figure 7.5). Absorbance values were then converted to concentration using the IR calibration.

Raman spectroscopy can be used to monitor both the solid and liquid phase of a suspension.[152] It has been used extensively to monitor polymorphs and SMPTs occurring during crystallisation process.[305] In this chapter Raman is used only as a qualitative technique for in line assessment of solid phase purity. Reference spectra from CBZ forms II, III and IV, as well as the dihydrate, were recorded and a diagnostic peak selected to monitor the presence of the stable form III.

FBRM allows in-situ measurements of particle size yielding a CLD that relates to the particle size and shape.[306-308] Limitations of FBRM and the CLD, compared with other techniques, have been described elsewhere.[309] The feedback response from FBRM, used during the MSZW determination in the MFOBC, was set to a value of 500 counts, i.e. when the FBRM signal detected more than 500 particles in solution the software would trigger a response to the HC to start the next heat cycle. FBRM was also used inline of the COBC to monitor CLD at fixed positions and the changes in CLD with respect to distance associated with crystal growth, breakage, nucleation and or agglomeration.

7.2.4 Oscillatory conditions for solids suspension

To assess the suspension of solids within the system, a 10 % w/w suspension of CBZ was agitated within the MFOBC platform under various oscillatory conditions, mapping those conditions achievable in the 25m DN15 COBC. Given the solubility profile of CBZ in ethanol and the temperature range used for cooling crystallisation, 10 % is an over estimate for the maximum solids loading that could be obtained from the continuous crystallisation process. The suspension was oscillated over a range of conditions (1 - 3 Hz and 20 - 30 mm) and conditions that provided optimal solids suspension were selected for the subsequent COBC studies. Where optimum amplitude is between 20 and 30 mm, considering the OBC geometry (Section 4.1.2), the minimum frequency (providing consistent suspension of all particles in the sample with no evidence of particle sedimentation) was determined as 1.5 Hz.

7.2.5 Seed preparation

Seeds were prepared via wet milling in a jacketed 1 L STC using recirculation. The set-up used was similar to processes previously reported for wet milling seed generation.[310] An *IKA Magic Lab* rotor-stator was used and Figure 7.7 shows the set-up for the milling process.
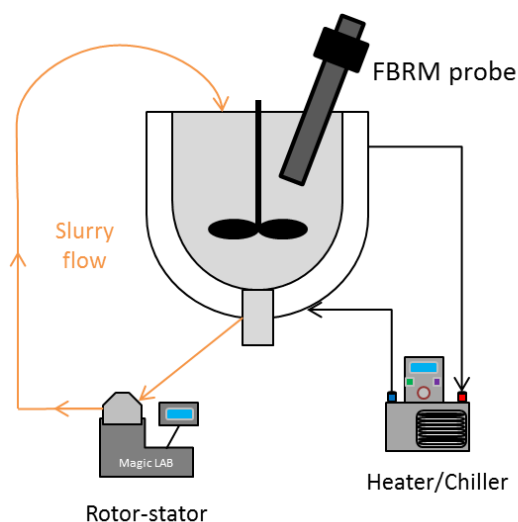
Figure 7.7: Wet milling set-up. Schematic illustrating the wet milling process for the preparation of CBZ seeds.

The STC was connected to a water bath set at 50 °C and an agitation of 250 rpm applied to the overhead 4 blade turbine impeller. Three rotor stator pairs were used in the set-up, the coarse, medium and fine generators with a setting of 22000 rpm. Seeds were prepared in 1 L batches by wet milling 140 g of CBZ with 800 g of ethanol.

7.2.6 Automated MSZW

Many methods have been reported for the determination of MSZW as part of crystallisation development.[311-314] MSZW measurements were conducted using the automated MFOBC system (Chapter 6, Figure 6.15). Where dilutions were needed for measurements at different concentrations, manual extractions of solvent were made through a tap at the base of the MFOBC the weighted. The system responded by automatically dosing an equal mass of solvent, to the weight of solution removed, into the MFOBC. Oscillatory frequency and amplitude were 2 Hz and 20 mm respectfully, and a cooling and heating profile of 0.5 °C/min was used for MSZW determination.

7.2.7 Continuous crystallisation of CBZ

The step-up was similar to that described in Chapter 5, with a range of modifications designed to improve process monitoring and analysis during crystallisation runs. The modified COBC platform is illustrated in Figure 7.8. This upgraded system incorporated sample and probe port bends at every position in the COBC to allow for in-line information to be gathered from the PAT array. In addition, a Teflon® coated thermocouple was placed in every collar joining each straight and bend to obtain a higher resolution view of the temperature profile along the reactor. A surrounding ventilated enclosure was constructed for sample and solvent containment, enabling use of non-aqueous solvent systems and ensuring safe operation of the system. Manual sampling was carried out using the same methods as described previously (Section 5.3.3). Operating conditions used for experimental work can be found in Table 7.3.
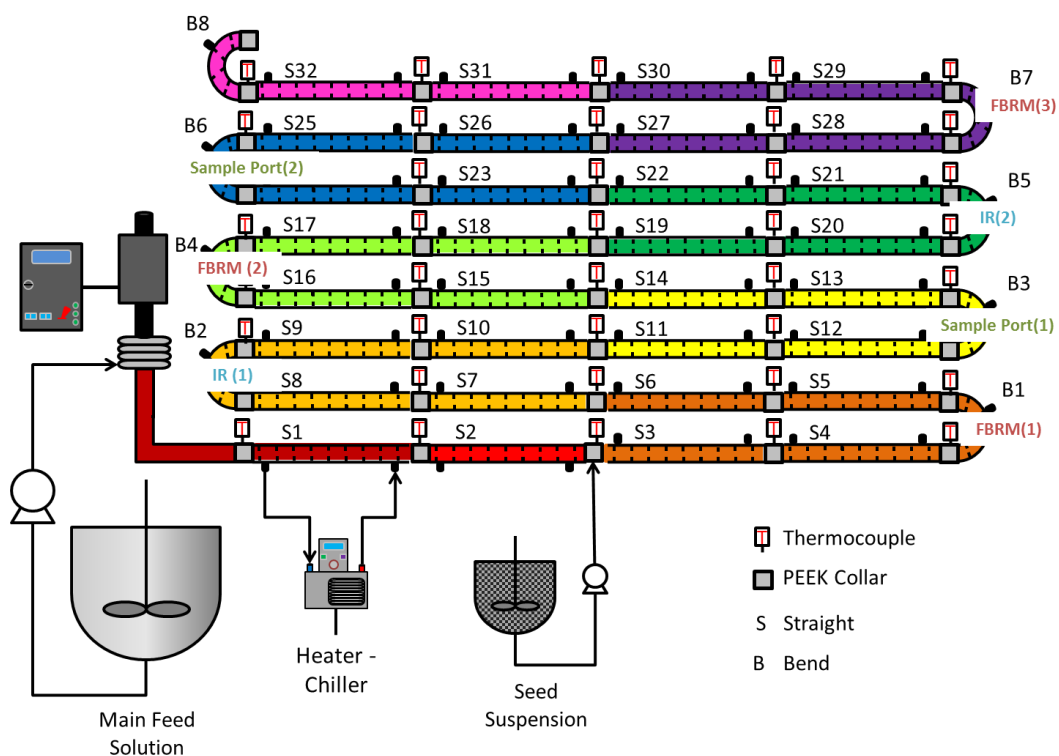
Figure 7.8: COBC set-up for CBZ crystallisation. Photograph (top) and schematic (bottom) of the COBC set-up for continuous CBZ crystallisations. 10 temperature zones where utilised illustrated by colours, zone 1 S1, zone 2 S2, zone 3 S3–S6, zone 4 S7-S10, zone 5 S11-S14, zone 6 S15–S18, zone 7 S19–S22, zone 8 S23–S26, zone 9 S27–S30 and zone 10 S31–S32.

Table 7.3: Constant operating conditions for COBC with CBZ. Table showing the oscillatory conditions and dimensionless numbers governing the hydrodynamic environment with the COBC during CBZ crystallisation.

Frq. (Hz)	Amp. (mm)	Re_n	Re_o	Ψ	St
2	20	85	1880	22	0.12

Table 7.4: Experimental concentrations for CBZ COBC investigations. Table showing concentration and flow conditions used for experiments.

	Main feed		Seed flow	
Expt.	FR (g/min)	Conc. (g/kg)	FR (g/min)	Conc. (g/g)
1	45	79	15	0.015
2	50	79	10	0.011

7.3 Results & discussion

7.3.1 Solvent selection and solubility

The solubility and MSZWs of CBZ in methanol and ethanol measured in a small scale parallel crystallisation STC platform (section 7.2.2) are shown in Figure 7.9. The solubility of CBZ in methanol is significantly higher than in ethanol, however the MSZW in both solvents was determined to be ca. 40 °C. The crystals obtained from recrystallization in ethanol solution exhibited a more regular morphology compared to those from methanol. However XRPD confirmed solid phases of CBZ were the thermodynamically stable form III.
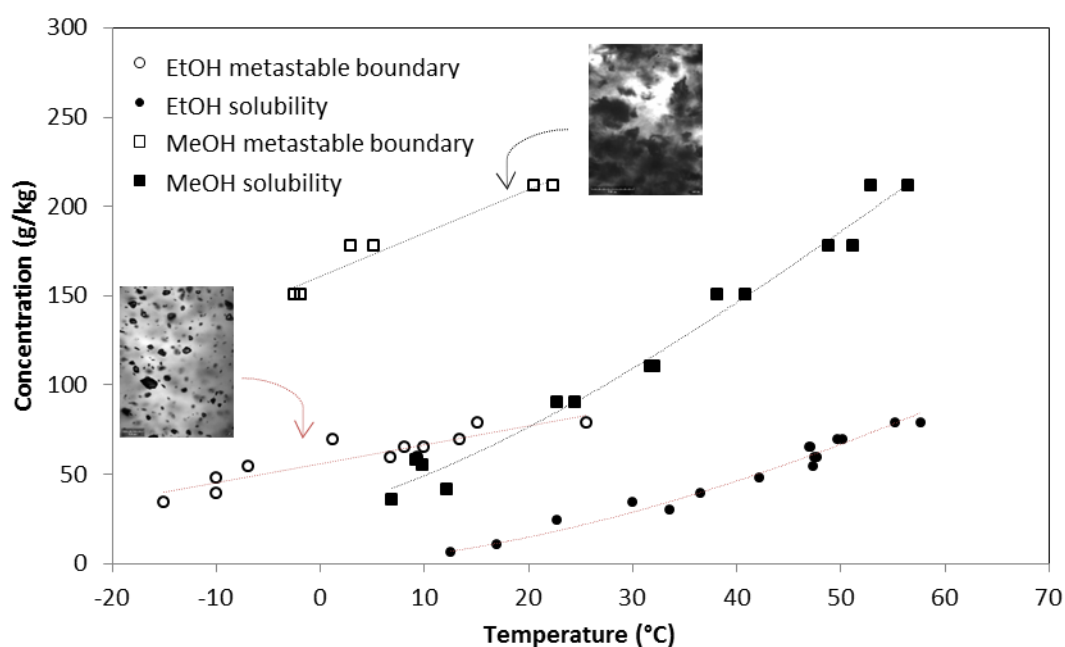
Figure 7.9: CBZ phase diagram. Graph showing the solubility of CBZ in ethanol and methanol collected in an automated small scale parallel crystallisation platform. Graph shows the solubility of CBZ is significantly higher in methanol, however the MSZW is about 40 °C in both solvents. Images collected (using the in-line cameras) show that product crystals collected in ethanol (a) appear to be more regular in shape than those produced during the crystallisation in methanol (b).

As previously discussed in Chapter 1 (and illustrated in Figure 1.13), choice of solvent can effect solid attributes, such as polymorphic form and

morphology. Images, collected from the inline cameras, suggest a solvent effect on the crystal habit of CBZ form III. A larger number, of smaller less well formed crystals, were produced with methanol in contrast to crystals obtained from ethanol. Effects of solvents on crystal morphology are documented,[71,315,316] proposed mechanisms include the favourable interaction between solute and solvent on specific crystal faces, leading to reduced interfacial tensions and fast growth of that face.

Guidelines for solvent selection, based on temperature dependence of the solubility, have been proposed.[317] This includes a number of criteria: ideally the solubility should double every 20 °C to provide adequate yield in a reasonable range; the maximum temperature (T_{max}) should be around 60 °C to minimise solvent loss from evaporation; the solute solubility should be in the range of 50 – 150 g/L at T_{max}; minimum temperature (T_{min}) + 60 < T_{max} and the solubility > 5g/L at $T_{min.}$ Considering these selection criteria, and based on the initial solubility data collected from the small scale experiments, ethanol was selected as the best suited solvent for crystallisation of CBZ.

Having selected ethanol, accurate solubility data were then collected in a 1 L crystallisation workstation (section 7.2.2) using inline ATR FTIR. The temperature dependence of form III CBZ solubility in ethanol is shown in Figure 7.10. The data were fitted to a third order polynomial (R^2 = 0.9996) showing agreement with solubility values from the literature.[318] The data collected using turbidity deviates slightly when compared to the ATR IR and literature, illustrating the small scale system is a good platform for screening experiments but once the desired solvent, or solvent systems, have been selected, it is recommended that a precise solubility phase diagram be assessed.
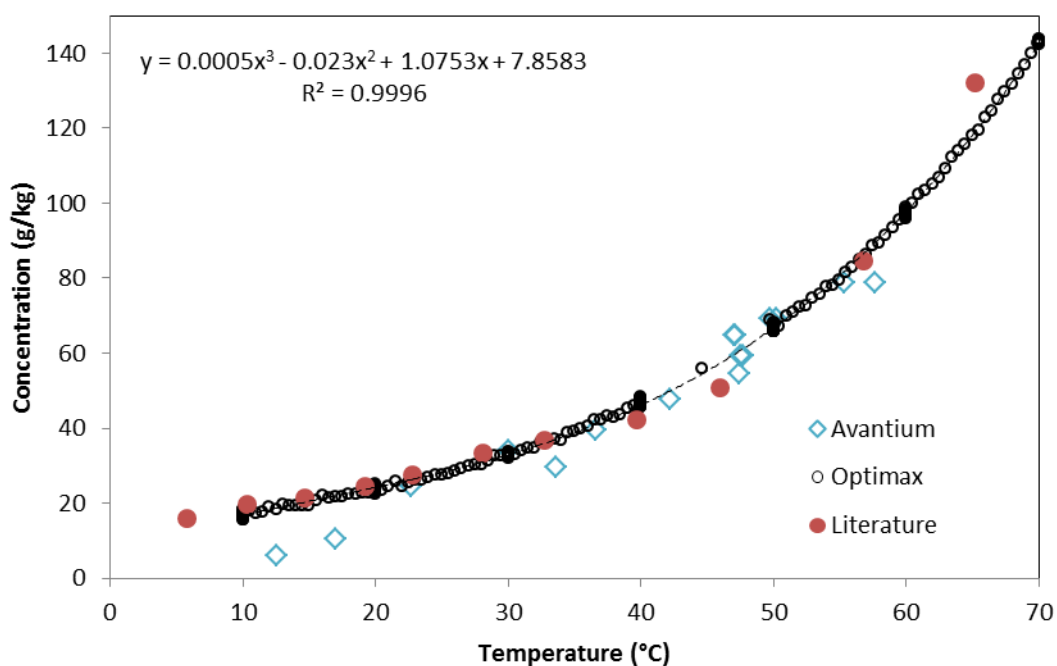
Figure 7.10: Solubility of CBZ. Graph showing the temperature solubility of CBZ in ethanol collected in a 1 L STC (O) with ATR-FTIR. The data has been overlaid with the turbidity data collected on the 8 ml parallel crystallisation system (◊) and reported solubility data using the synthetic method (●).[318] It can be noted that the data agrees with one another.

7.3.2 PAT Calibration

In order to generate a concentration response from the IR spectral data collected during crystallisation, the strongest peak of interest was determined to be at 1680cm^{-1} corresponding to the C=O stretching of the amide group[319] (Figure 7.11). Spectral analysis was carried out as illustrated in Figure 7.11. Raw spectra are normalised through application of the 2nd derivative to remove baseline effects, before background subtraction of ethanol and section of peak of interest. To minimise any temperature, or peak broadening effects, influencing the measured peak height, the area under the curve in the range of 1697 – 1667 cm^{-1} was used. Standard solutions collected over variable temperature ranges are illustrated in Figure 7.12. The flat absorbance responses confirm no temperature deviation over the range of 20 – 70 °C.
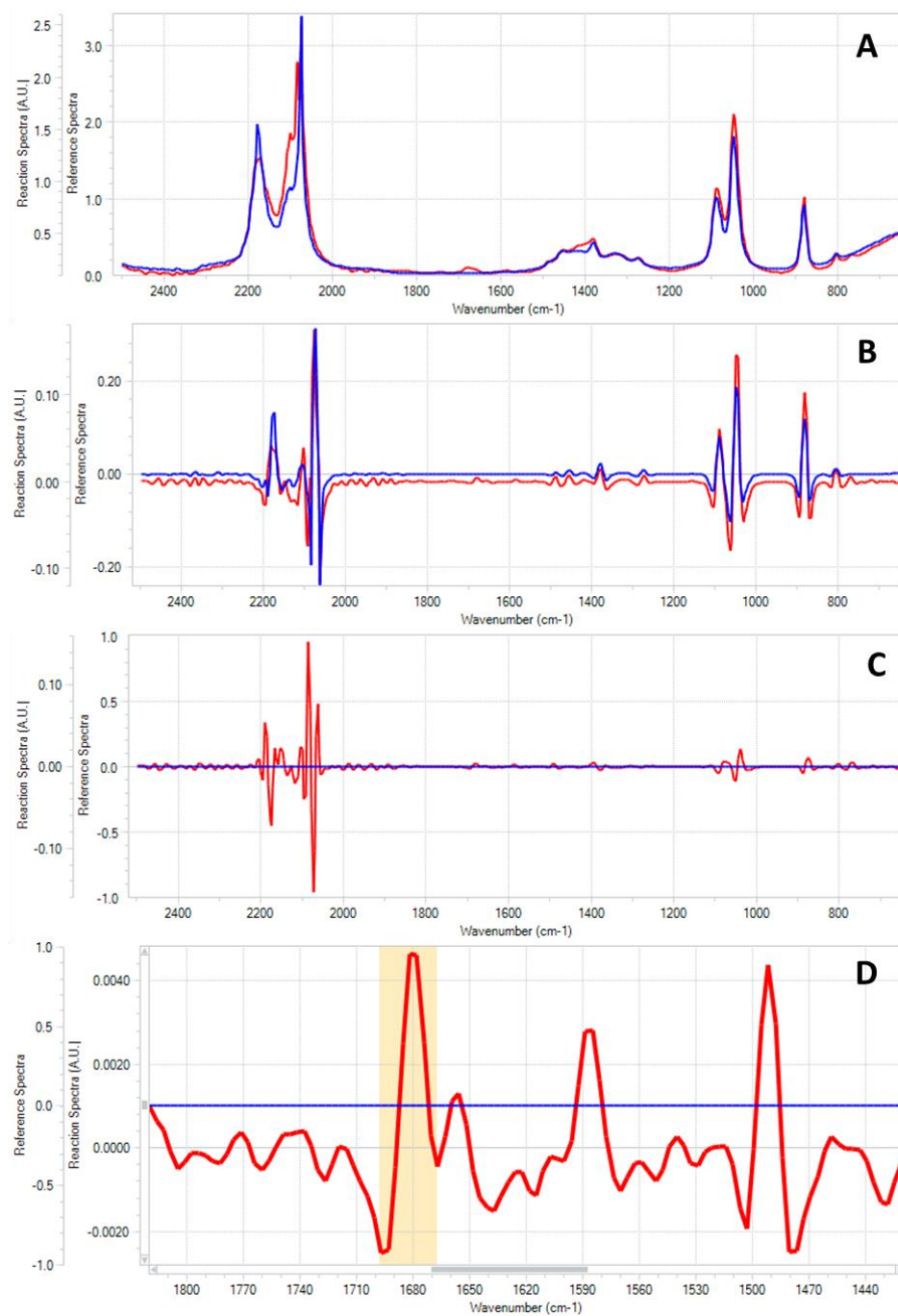
Figure 7.11: Figure illustrating spectra analysis of IR CBZ data. Raw spectra (A) showing IR spectra from ethanol (blue) and a CBZ ethanol solution (red) are normalised through application of the 2nd derivative (B) to remove baseline effects before background subtraction of ethanol (C) and selection of peak of interest (D) at 1680cm^{-1}. To minimise any temperature or peak broadening effects the area under the curve in the range of 1697 – 1667 cm^{-1} was used.
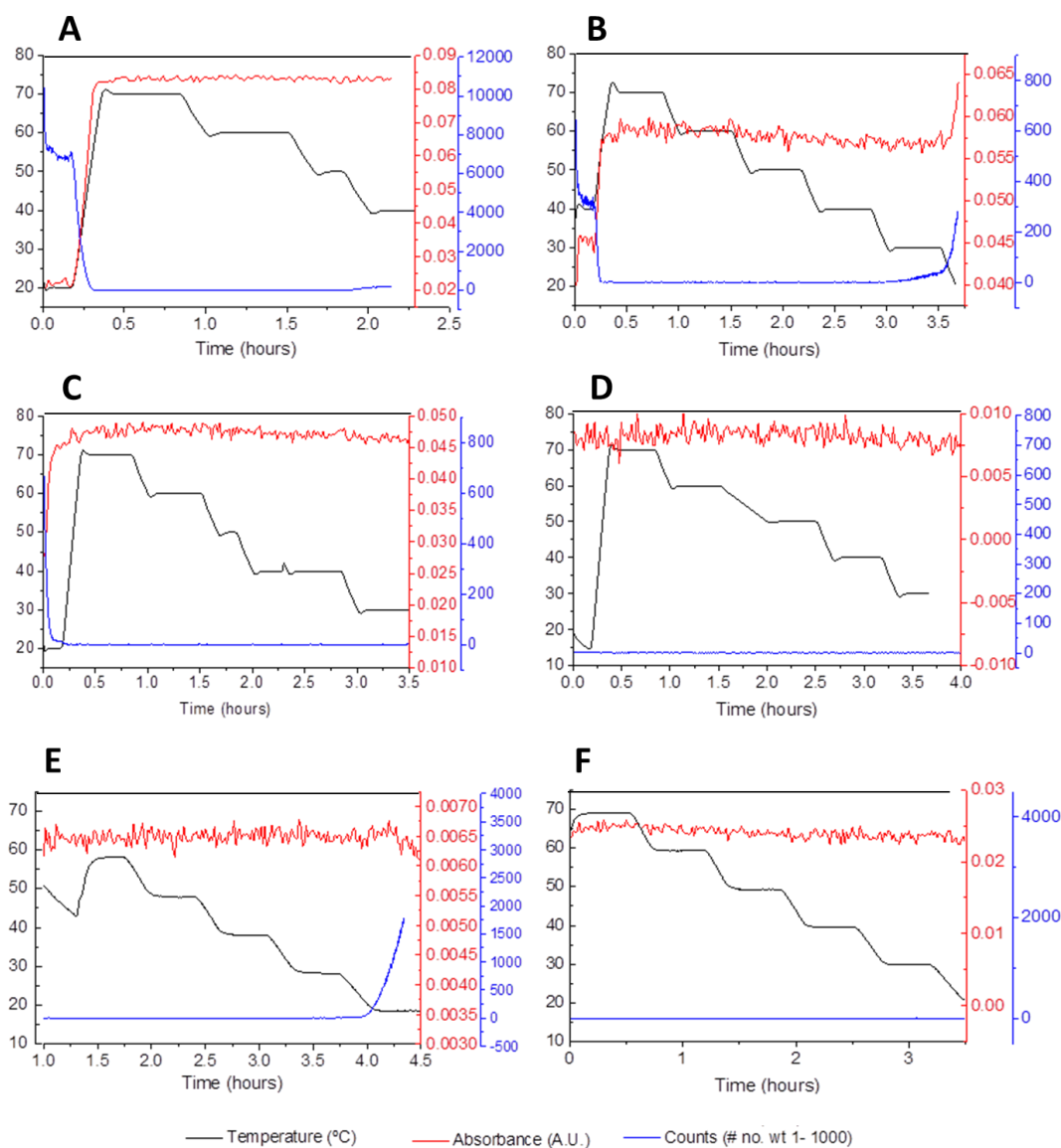
Figure 7.12: Figure illustrating effect of temperature on IR signals. Examples of absorbance response (red) to step changes in temperature (black). FBRM (blue) is used in line to assess when a crystallisation event occurs therefore marking the absorbance response after this point invalid for calibration. Examples illustrate data collected for the following concentrations 100 g/kg (A), 70 g/kg (B), 55 g/kg (C), 13 g/kg (D), 105 g/kg (E) and 30 g/kg (F).

The IR calibration with CBZ in ethanol returned a linear response (R^2 = 0.9795), Figure 7.13. This calibration was used to calculate the solubility curve shown in Figure 7.10. Data collected are a combination of IR results from 2 independent IR probes of the same make and model. Raman spectra

of CBZ were collected with the Raman PhAT probe (Section 3.2.2.1) to assess a diagnostic peak, for identification of form III CBZ on-line. Figure 7.14 shows a stacked plot of Raman spectra for forms II, III, IV and the dihydrate. Applying the first derivative, the region of interest selected, as unique to form III CBZ, was identified as 1314 cm^{-1} (Figure 7.15).
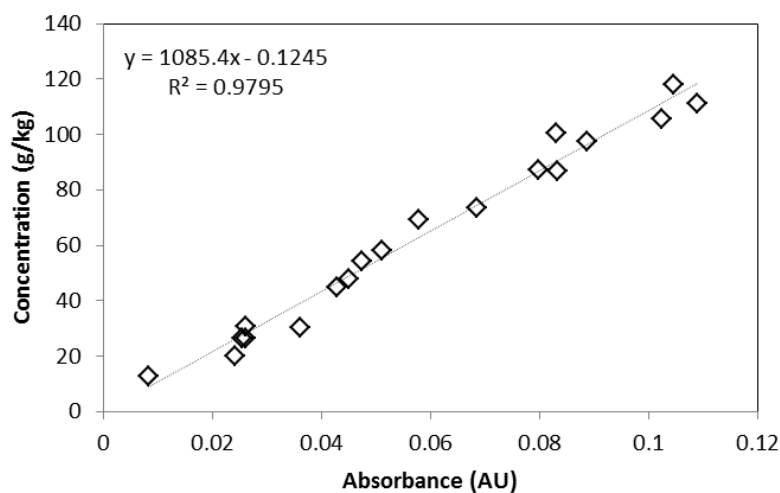
Figure 7.13: Calibration for CBZ in ethanol. Plot showing the linear response of absorbance as a function of concentration (absorbance measurement taken as area under the curve in the range of 1697 – 1667 cm^{-1}). Data acquired using 2 independent ATR IR probes (same make and model).
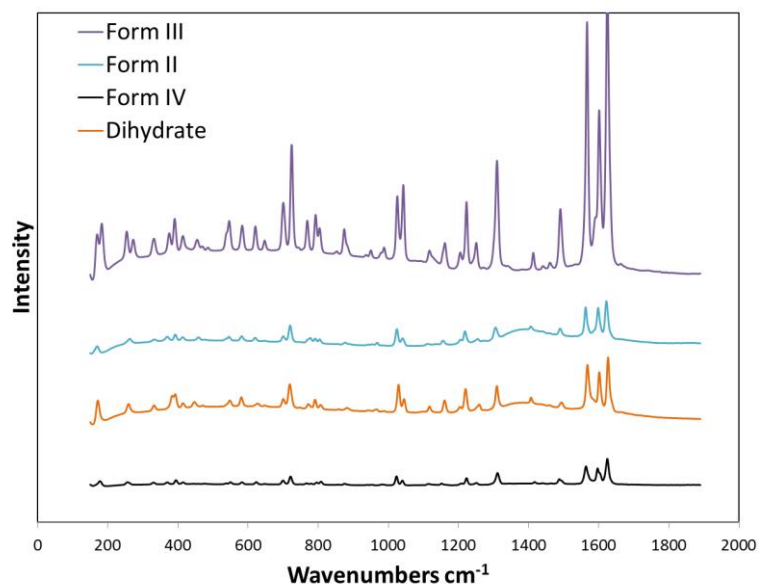
Figure 7.14: Raman spectra of CBZ solid forms. Stacked plot showing the raw Raman spectra for forms II, III and IV CBZ along with the dihydrate.
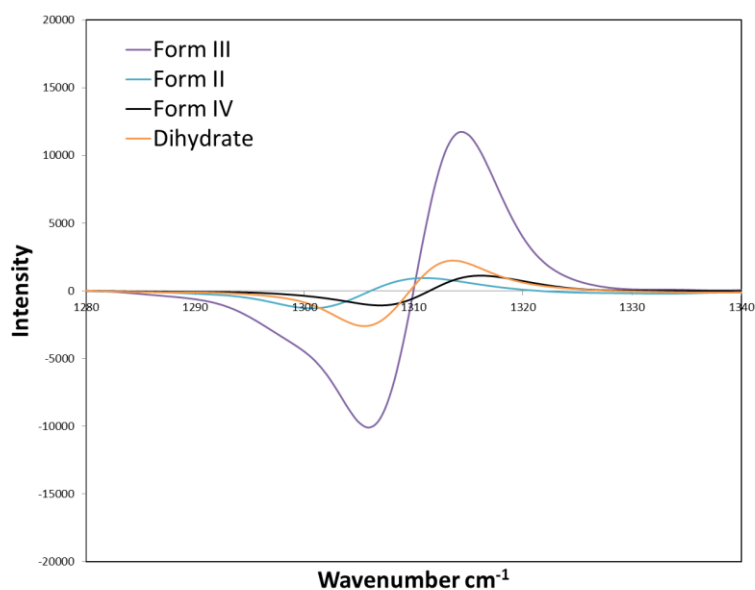
Figure 7.15: CBZ form III peak of interest using Raman. Plot showing the 1st derivative of CBZ forms II, III and IV with the dihydrate. Peak of interest to detect the presence of form III is positioned at 1314 cm^{-1}

7.3.3 CBZ seeds produced from wet milling

Figure 7.16 (A) shows the CLD obtained from in-line FBRM after the milling process. Here it can be seen that the CLD is unimodal with a mean seed size around 15 μm. The resulting PSD can be found in Figure 7.16 (B) and shows a mean crystal size of approximately 20 μm. However, a second larger population of particles is also evident, with a size of about 600 μm. Given the data collected by laser diffraction was taken from a pre-processed sample (i.e. extracted, filtered and dried) it can be postulated that this extraction process results in a partial agglomeration of the dried seed crop. When this material is then suspended for PSD analysis i.e. agitation within a dispersion unit, this resuspension causes some deagglomeration of the dried sample.

Inline PVM showed that wet milled CBZ seeds undergo agglomeration. In order to maintain better control over input PSD, insonation using an ultrasonic probe was tested as a method to control agglomeration. The setup used is similar to that shown in Figure 7.7, with the addition of an ultrasonic probe (*Qsonica* Q55, setting 90). Figure 7.16 (C) shows an FBRM trace collected with intermittent sonication of the seed slurry at 50 °C. When sonication is applied, a change in counts, for both fine and large particle sizes, is observed. After sonication was stopped, a gradual shift in particle counts to larger size ranges is observed over a 6 hour period, consistent with a slow agglomeration process of fine particles. PVM images (Figure 7.16) show CBZ seeds with, and without, applied sonication, clearly illustrating the separation of agglomerated particles resulting from the input of ultrasound energy.
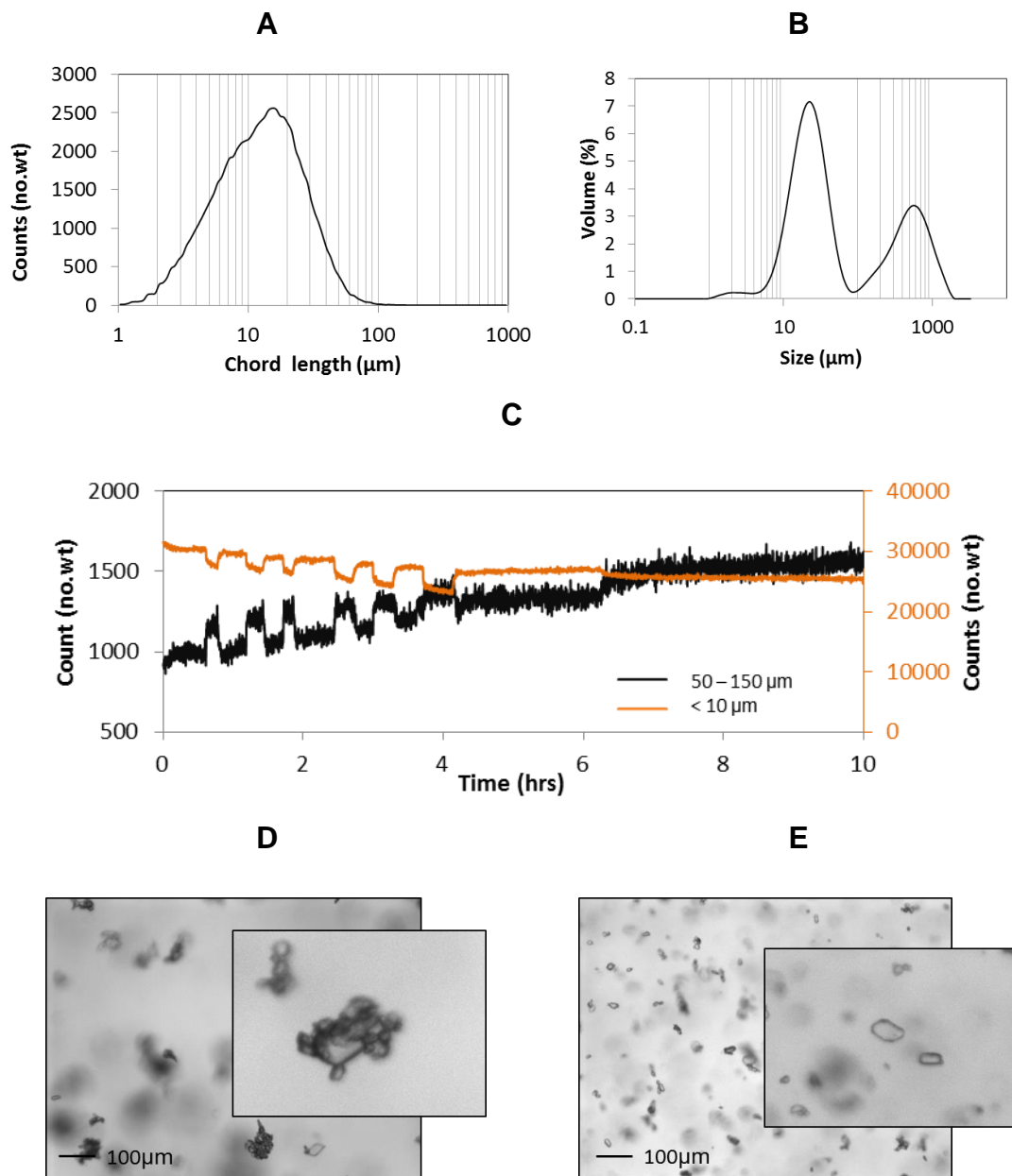
Figure 7.16: CBZ seed crop from wet milling process. Figure illustrating seed size and stability and agglomeration of wet milled CBZ. CLD (A) and PSD (B) data show mean crystal sizes of about 15 and 20 μm respectfully. Plot showing the influence of intermittent sonication on CLD. A series of pulses followed by a 6 hour rest period (C) illustrates the gradual shift to larger sizes in the populations of particles (i.e. an unstable and agglomerating seed suspension). PVM images of seed suspension when gently agitated (D) and agitated with sonication (E) (insets are a magnified agglomerate and de-agglomerate respectfully), illustrating a method for de-agglomerating clusters of seed crystals.

7.3.4 Automated MSZW measurements

The results from the automated solubility and MSZW experiments conducted in the automated MFOBC (Chapter 6) are shown in Figure 7.17. As expected, there is good agreement with the solubility data collected in the STR 1 L system. The MSZW is shown to be approximately 13 °C for CBZ in ethanol. This MSZW is 3 times smaller than the MSZW data collected in the small scale 8 mL STC platform. This emphasises the sensitivity of primary nucleation kinetics to the reactor geometry, process conditions used (e.g. agitation rate; shear rates; heat transfer), and volume. These results are in line with other reported oscillatory flow crystallisation studies where, on comparison to kinetics within an STC, oscillatory flow tends to produce narrower MSZWs.[35,37] It is suggested that oscillatory flow is more effective in promoting nucleation because of improved environment uniformity (e.g. temperature and shear). The MSZW of CBZ in ethanol equates to a supersaturation of ca.1.6. This was set as the upper limit for the temperature curve, to control bulk supersaturation in the COBC, and thus achieve a controlled seeded crystallisation without uncontrolled primary nucleation.
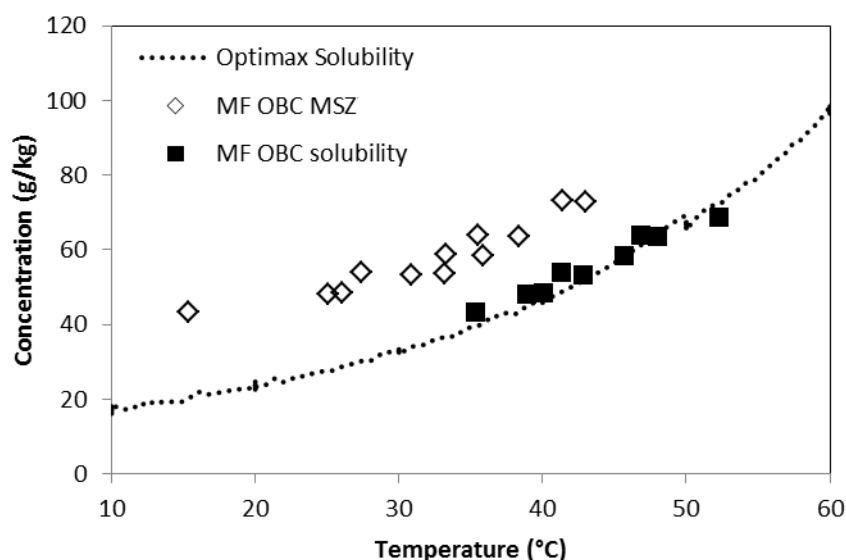
Figure 7.17: Automated solubility and MSZ. Graph showing the solubility and MSZ of CBZ in ethanol, collected on the automated MFOBC platform.

7.3.5 Continuous Crystallisation of Carbamazepine

Two continuous crystallization runs of CBZ were carried out. Based on the MFOBC data, cooling profiles were selected for both experiments and these are shown in Figure 7.18. The data points showing deviation can be explained by variation in the temperature profile over the non-jacketed bends, generally the temperature difference over a bend was recorded to be approximately 2°C. There were also some noted issues around positioning of the thermocouples where, on removal of collars, the tip was not completely in line with the flow.
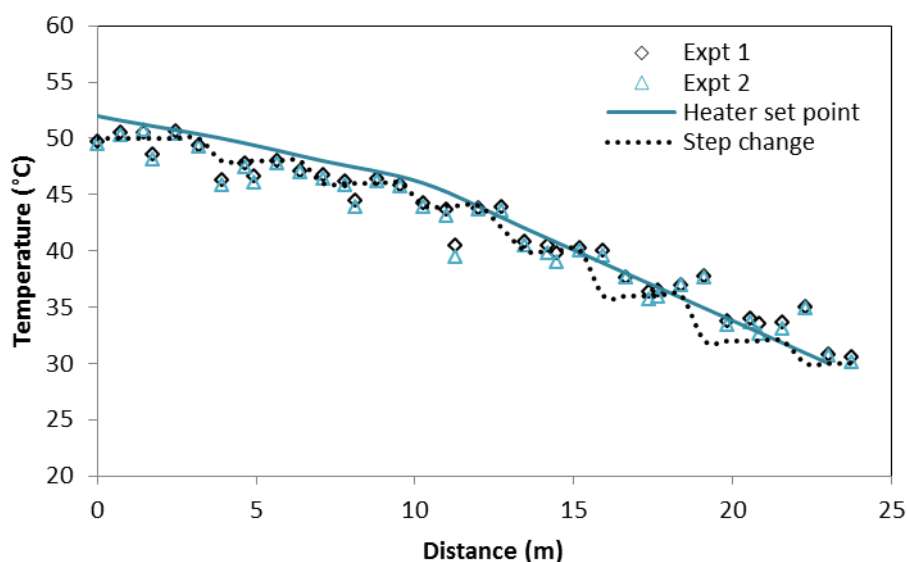
Figure 7.18: Cooling profiles for seeded CBZ COBC experiments. Plot showing the target temperature (heater set point), calculated profile (step change achieved in COBC) and measured cooling profiles used for the seeded CBZ experiments.

Through online IR measurements and manual sampling, supersaturation along the COBC length was determined. This is shown in Figure 7.19 and here it is demonstrated that supersaturation along the COBC length, for both experiments, is maintained at approximately 1.5.
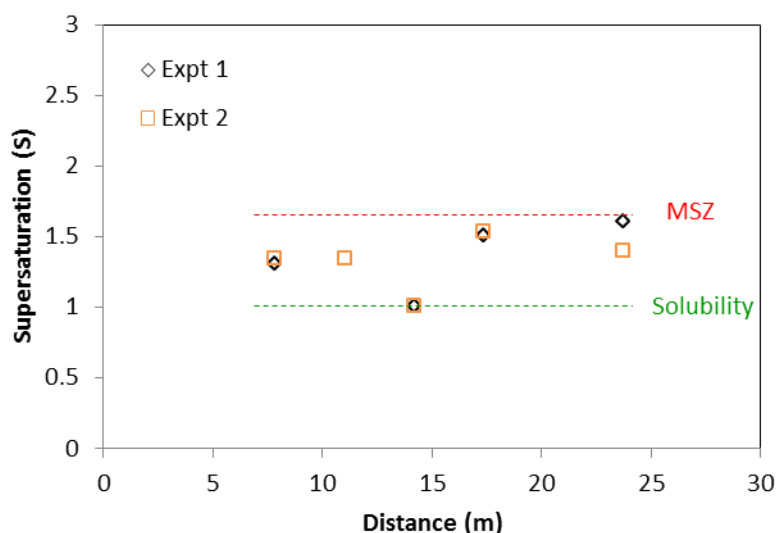
Figure 7.19: Supersaturation along the COBC. Plot showing the supersaturation level along the COBC system for experiment 1 (◊) and 2 (□). Plot shows the supersaturation along the system is ca. 1.5 (in between the solubility and metastable zone).

Data are further plotted on the CBZ phase diagram (Figure 7.20) illustrating bulk solution supersaturation levels do not cross the MSZW, therefore the system is operated within the stated supersaturation control limits. Given the system operates within the MSZW, as shown in Figure 7.20, it is expected that growth of seed particles will occur without any spontaneous primary nucleation of other CBZ polymorphs. The presence of form III (same polymorph as the seed crystals) is confirmed through online Raman monitoring as shown in Figure 7.21. The graph shows an inset of the spectrum around the peak of interest for form III and an overlay of signal response over several time points. This data illustrates no presence of CBZ from 0 – 30 minutes during process start-up, with CBZ form III present after 60 minutes (1 RT) as seed elutes through the platform. The Raman signal is shown to stabiles by 90 minutes, demonstrating a steady state response with respect to form III CBZ after 1.5 RTs. Phase pure product was further confirmed by offline XRPD (Figure 7.2), verifying the absence of any metastable phases of CBZ.
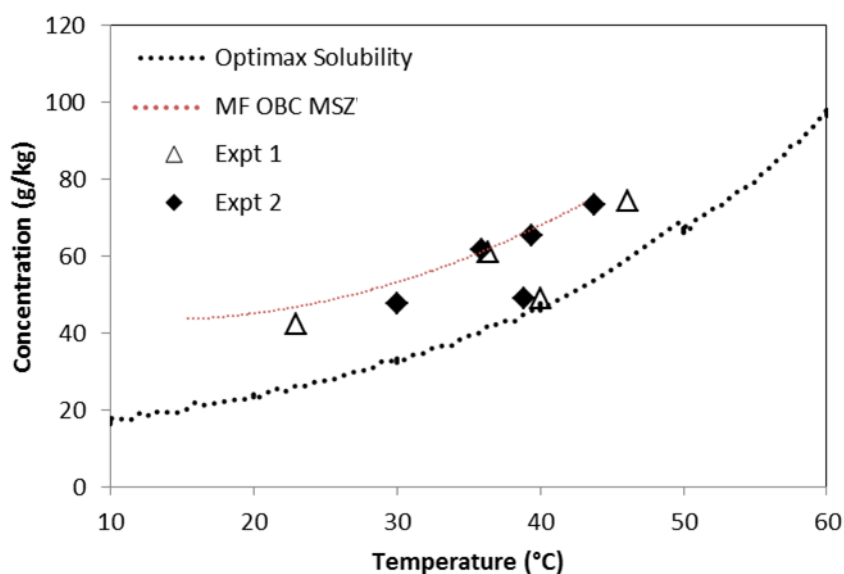
Figure 7.20: Phase diagram of CBZ. Plot showing the experimentally measures temperature dependant solubility of CBZ in ethanol (dotted black), with supersaturation profiles form both experiments (Δ,♦) and MSZW boundary (dotted red).
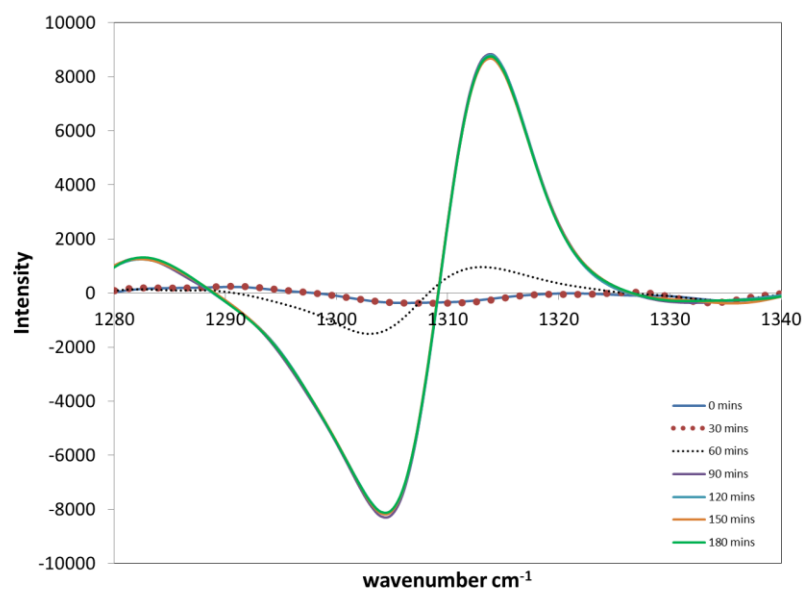
Figure 7.21: Online Raman monitoring. Graph showing the 1st derivative Raman signal of form III CBZ collected online during seeded COBC operation. Overlay illustrates no present of CBZ from 0 – 30 minutes, appearance after 60 minutes, before signal stabilisation after 90 minutes. Graph illustrates a steady state response of form III CBZ after 1.5 RTs.
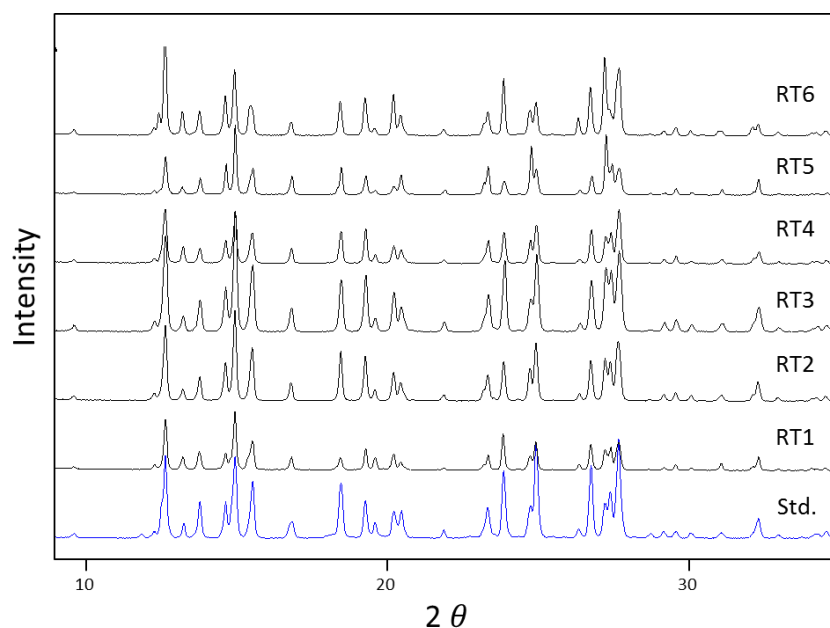
Figure 7.22: XRPD data from seeded continuous CBZ crystallisations.
Overlay of XRPD powder patterns of product crop (black) over 6 RTs with raw material (blue). Data illustrates product is phase pure form III CBZ.

Steady state operation with respect to CQAs was previously described (Section 5.3.4.) as a desired condition of a process. For the controlled cooling crystallisation of CBZ, the target criteria were to deliver a specific polymorphic form with a consistent PSD. Figure 7.23 and Figure 7.24 illustrate time to reach a steady state response of concentration, CLD and physical form during the experiments. Responses illustrate steady state condition of all monitored parameters after about 1 RT of operation, consistent with the start-up time to steady stale for continuous LGA seeded crystallisations (section 5.3.4). After about 3 RTs in experiment 2, Figure 7.24 shows a deviation from steady state before stabilisation reoccurs. This deviation is due to the manual changing of pump flow rate (to a maximum setting), flushing the system of solids, before returning input settings and allowing the system to return to a steady state.
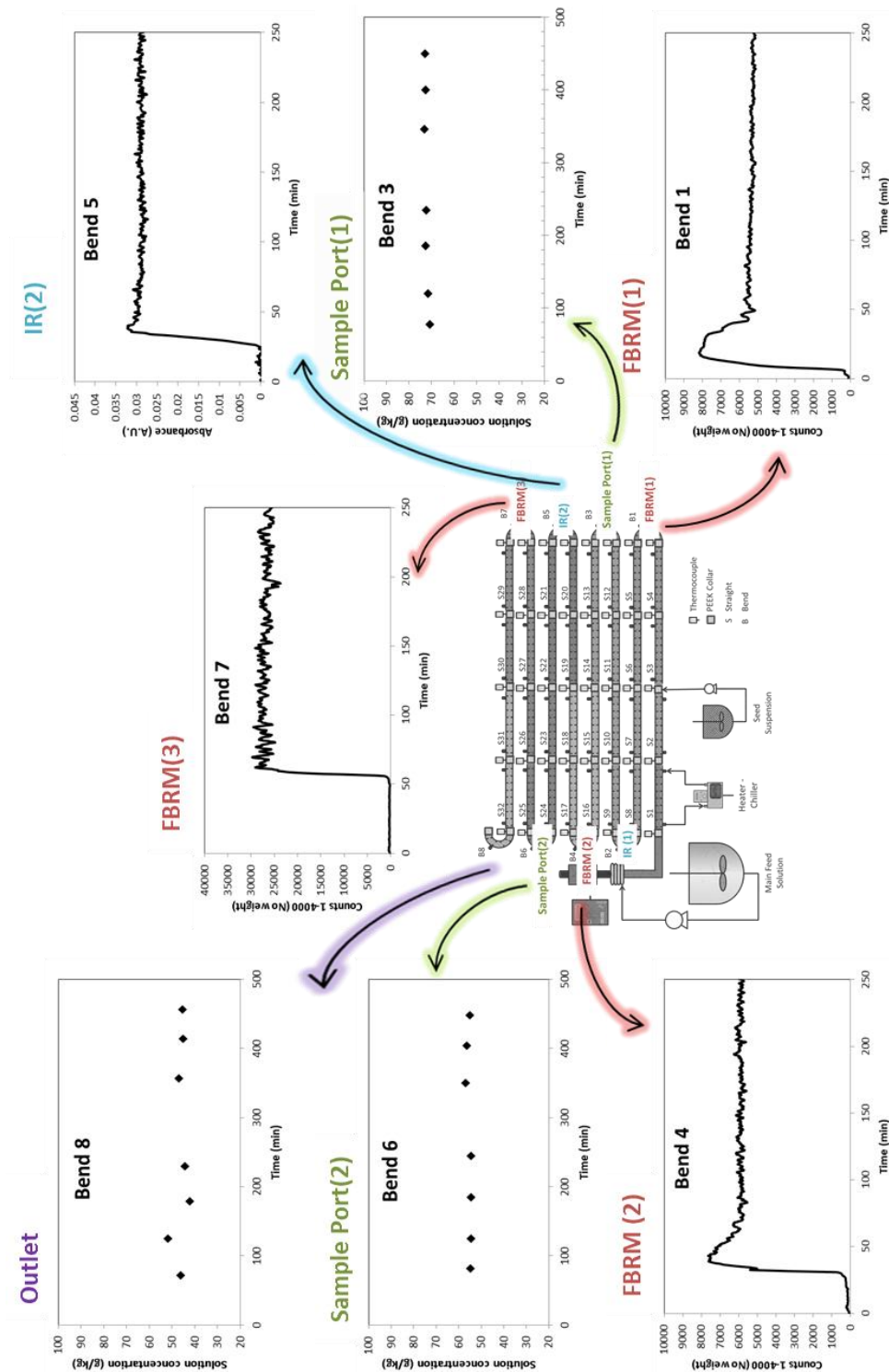
Figure 7.23: Expt. 1 steady state operation. Series of graphs corresponding to profile responses at bends within the COBC (Figure 7.8). Bend 1, 4 and 7 showing CLDs, bends 3, 6 and 8 showing solution concentrations profiles (calculated gravimetrically from manual sampling) and bend 5 showing the absorbance time response from inline IR. Graphs illustrate a steady state response of all parameters after about 1 RT (60 mins) of operation.
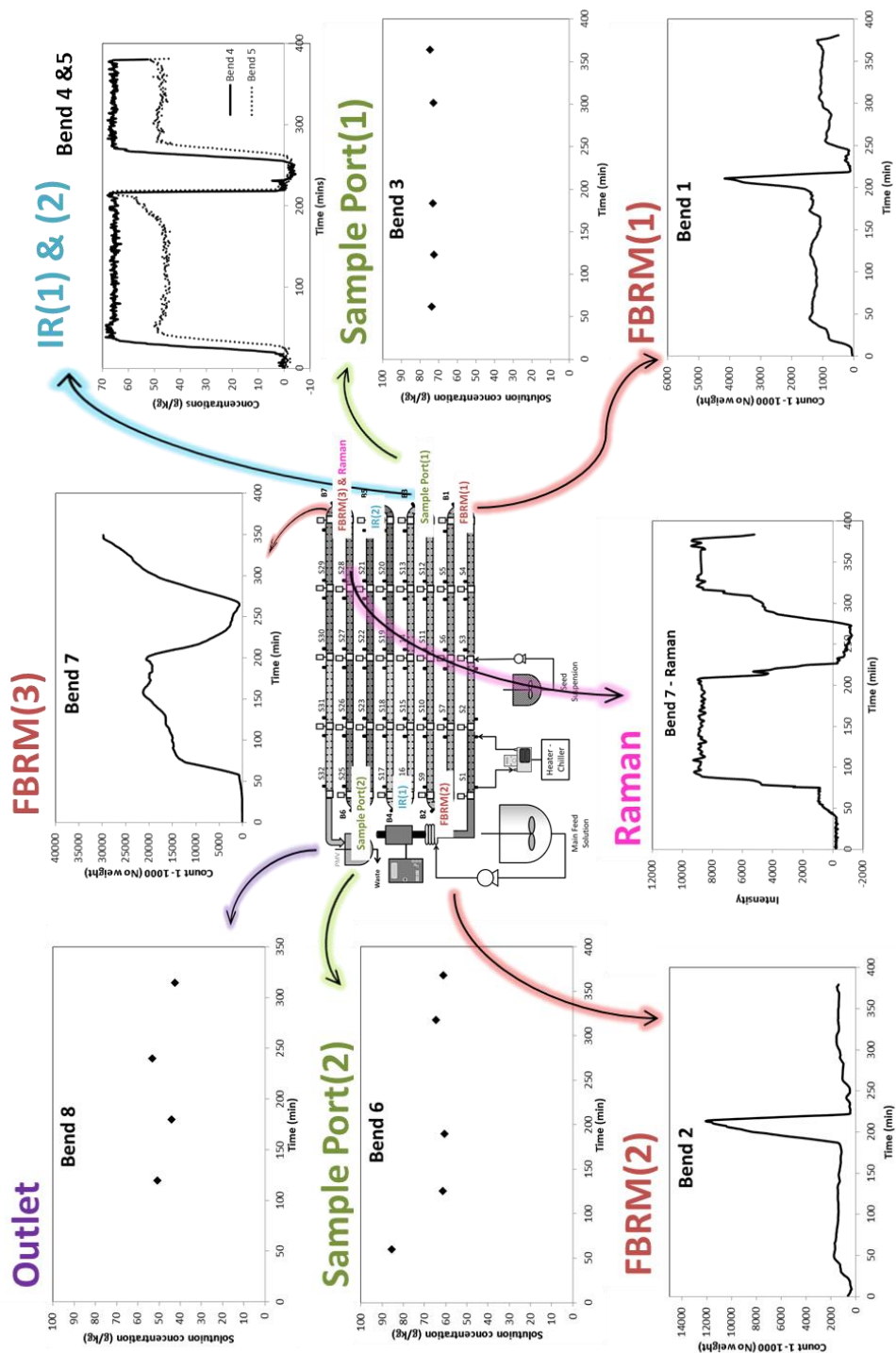
Figure 7.24: Expt. 2 steady state operation. Series of graphs showing process conditions at bends along the COBC (Figure 7.8). Bend 1, 2 and 7 show FBRM CLDs, bends 3, 6 and 8 show solution concentrations profiles (calculated gravimetrically from manual sampling) and bends 4 and 5 show the concentrations time response calculated from IR. Bend 8 shows Raman data corresponding to phase identity (form III CBZ). After ca. 3 RTs, pump flow rate was maximised to flush the system of solid before returning to operating conditions and allowing stabilisation.

Considering particle size as a CQA, it is important to confirm control over growth based on measurement of the resulting particle sizes. The ability to map growth over the course of an experiment allows detailed information about the growth process with respect to distance and the associated RTD. An overlay of CLDs obtained from inline monitoring using FBRM are shown in Figure 7.25. Here it can be observed that the particles have grown from ca. 15 to 200 µm (seed CLD to Bend 7 CLD respectfully). However, considering the positions of the probes (B1, B4, and B7) and the corresponding CLDs with respect to distance, it appears a breakage, de-agglomeration, or secondary nucleation event has occurred. As the seed crystals pass from B1 - B7, the particles first increase in size as expected however there is then an apparent decrease in counts for these larger 200 µm particles. An increase in smaller particles is also observed across the duration of the crystallisation that is consistent with breakage, de-agglomeration or secondary nucleation. The final size (200 µm) is reasonably consistent with images however no fines are evident in images from samples extracted from the process, highlighting an inconsistency between in-line and off-line measurements (Figure 7.26).
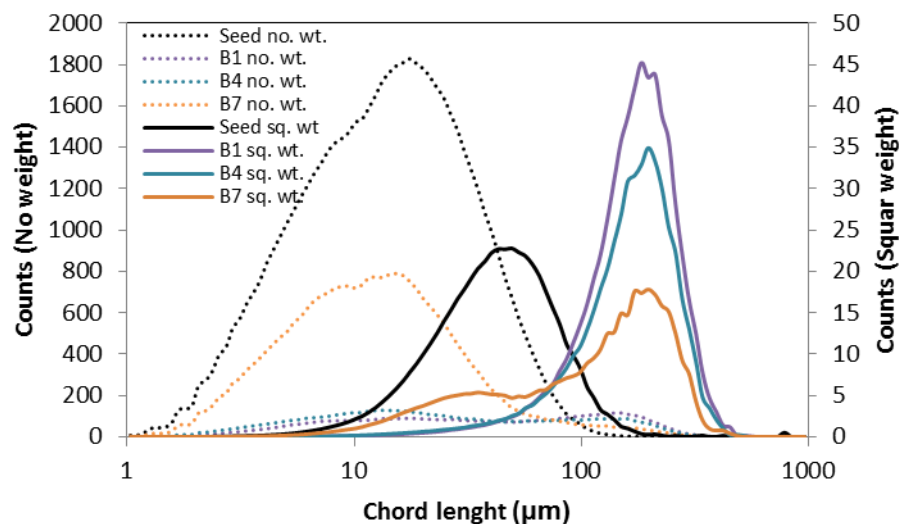
Figure 7.25: FBRM PSD overlay for Expt 1. Graph showing overlay of seed CLD FBRM responses at 3 positions in the COBC. The population of coarse particles first increases (—), then decreases (—), before a further reduction in large counts with an increase in fines (—).
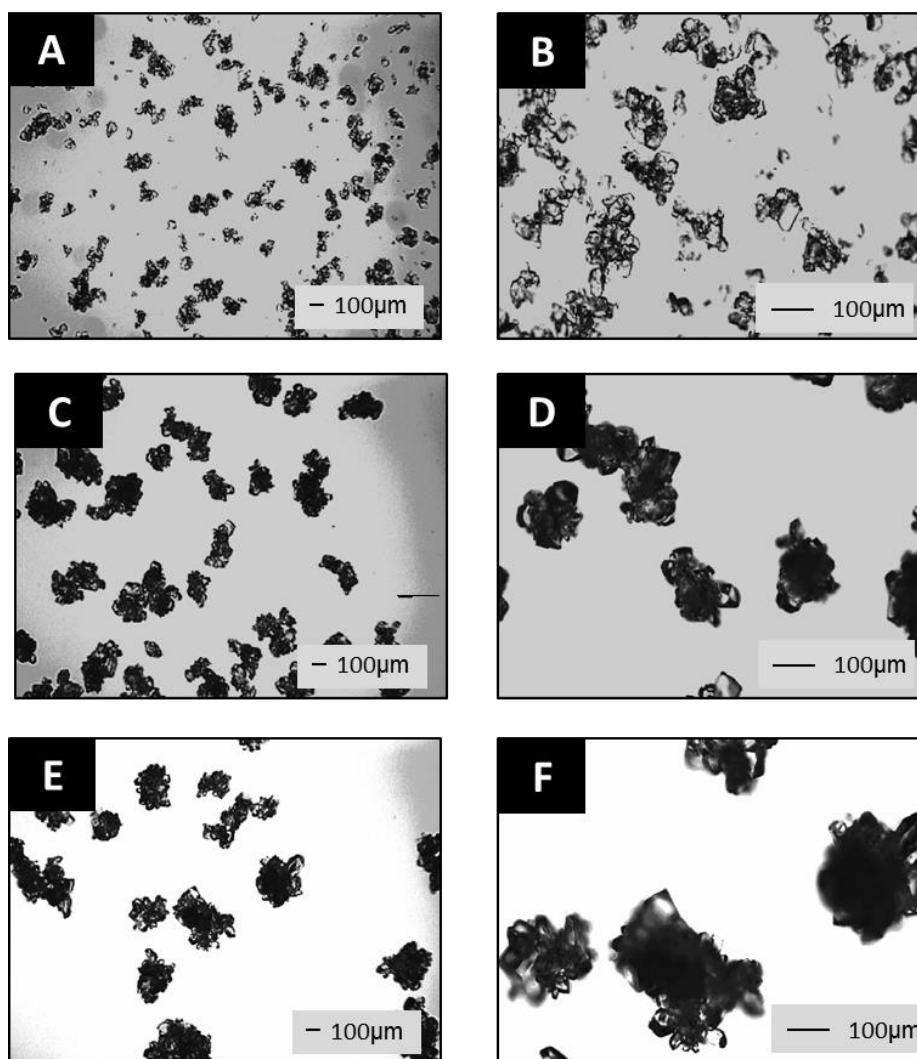
Figure 7.26: Optical images of CBZ crystals from the COBC. Figure showing microscope images of crystal products after 7 RTs in the COBC; bend 3 4x (A) and 10x (B) magnification; bend 6 4x (C) and 10x (D) magnification; bend 8 x4 (E) and 10x (F) magnification respectively. Images show continued growth of agglomerated particles with no evidence of fines.

Microscope images of product crystals, under two magnifications, after 7 RTs from seeded CBZ crystallisations are shown in Figure 7.26. Here continued growth of agglomerated particles, without evidence of fines, can be observed. Agglomeration of crystals was illustrated during the seed preparation (Section 7.3.3) and has been previously observed during cooling crystallisation of CBZ.[274] Due to sample processing (i.e. extraction and filtration) it could be postulated this may have induced further agglomeration

of fines produced within the COBC. However, inline PVM images (Figure 7.27), collected at the COBC outlet, show consistency with those collected from offline microscopy. Large CBZ agglomerates are observed without evidence of fine material suspended in the product slurry. Considering this, the FBRM data appears inconsistent with imaging methods. It is probable that the population of fines observed in the FBRM CLD at bend 7 (Figure 7.25) are generated through breakage of agglomerates or secondary nucleation. Given CBZ was shown to readily agglomerate in suspension (Figure 7.16), the latter conclusion is more reasonable.
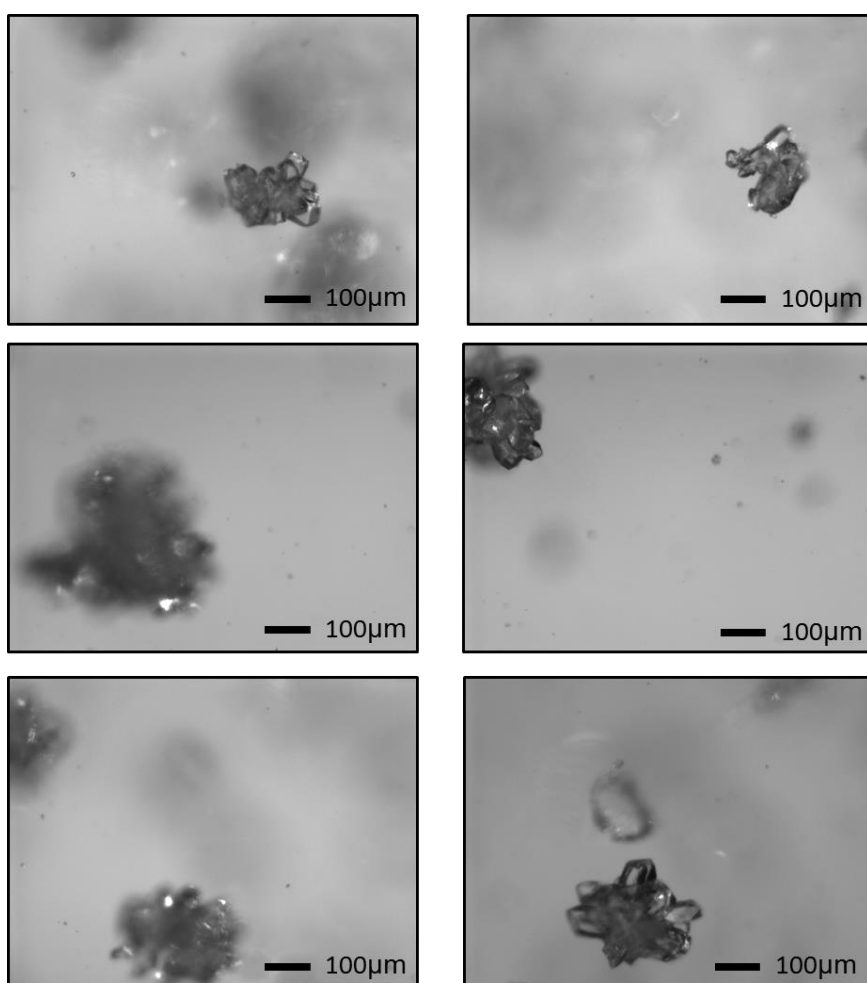
Figure 7.27: PVM images of CBZ agglomerates. Figure showing 6 examples of inline images of crystal product from seeded COBC cooling crystallisation.

Considering the system is operating very close to the primary MSZW (Figure 7.20), and no determination of the MSZW for secondary nucleation was conducted (Section 1.3), it is again reasonable to assume secondary nucleation is taking place resulting in the population of fines observed by the FBRM.[78,79] These fines may then be rapidly agglomerating, incorporating themselves onto the pre-existing larger agglomerates. Magnification of a CBZ agglomerate, collected in line with PVM, supports this theory (Figure 7.28). Further work with inline imaging is needed to confirm this hypothesis.
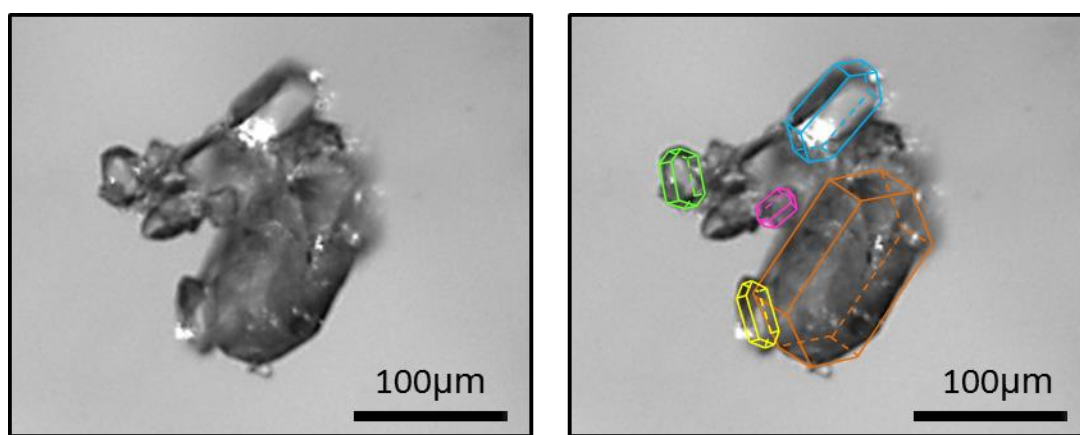
Figure 7.28 Magnified PVM image of a CBZ agglomerate. Original image (left), size guides overlaid (right).

As previously discussed in Section 1.4, agglomeration is typically an unwanted state of product crystals as it can have detrimental effects including hindering growth. However, for some API systems, agglomeration can be advantageous, producing spherical agglomerates with improved attributes, such as flowability[320] or tableting performance.[321] Carbamazepine has been shown to agglomerate during cooling crystallisation[274] and manipulation of the agglomeration process, with the addition of binding liquids, have been utilised in several studies on spherical crystallisation.[322-324] However, as shown in Figure 7.16, sonication appears to de-agglomerate CBZ particles in suspension, therefore mitigation of agglomeration during continuous operation could include the use of inline ultrasonic devices along

the length of the COBC. Further investigation of secondary nucleation (Section 1.3.2 and 1.4.4) of CBZ under the conditions in the COBC would provide further insight into the control of fines in this system. Critically, secondary nucleation will not impact on control of physical purity. The continuous crystallisation process for CBZ in the COBC therefore requires measurement and control over the interdependent processes of growth, agglomeration and secondary nucleation. These can be modelled utilising population balance equations, however an increase in the number of parameters to be estimated, increases the complexity and expense of the calculations.

Whilst the majority of practical challenges around operation of the COBC were addressed previously (5.3.5), allowing the development of a successful continuous cooling crystallisation for CBZ, sedimention issues (similar to those shown in Figure 5.33) were still observed. Sedmimentation was dominant at joins between glass straights and can be explained using the same reasons as discribed in section 5.3.5.5. The newly adapted bends (Figure 5.34) removed sedimentation issues between joins connecting bends and straights, however all existing straights still require to be adapted or replaced with the new design in order to optimise performance. Uncontrolled agglomeration will also impact on particle suspension within the COBC. A recommendation for platform design, to optimise successful operation, can be found in Appendix 3.

7.4   Summary

This work has demonstrated a systematic approach to continuous process design and testing for polymorph control of CBZ, based on an experimental workflow.   Initial small scale batch experimentations, supplemented with PAT, were used to determine solubility and inform MSZW. A Larger scale batch STC enabled accurate solubility data and a novel automated MFOBC platform was used to determine nucleation kinetics under conditions that mimic those in the COBC.   A seeding strategy was determined, although during development of this, a tendency for form III CBZ to agglomerate was identified.

A combination of supersaturation control through the temperature profile, rapid heat transfer and near plug flow operation (Chapter 4), combined with effective continuous seeding, provided control of polymorphic form with phase pure thermodynamically stable form III CBZ produced. When supersaturation within the COBC was maintained below 1.5, seed particles were demonstrated to grow from approximately 15 to 200 μm. However, growth of agglomerated particles was clearly observed. Ultrasound enabled prevention of agglomeration within seed suspensions, although evidence of agglomeration, from inline PAT and offline measurement of manually extracted samples, was observed. Further work, in terms of sonication strategies within the COBC and inline imaging along the COBC length, should be considered to control and monitor growth of individual particles.

Fouling was not observed during continuous operations when the system was operated within the MSZW of the CBZ ethanol phase diagram. This is in agreement with conclusions during LGA seeded crystallisations (Chapter 5). Steady state was also illustrated, with respect to the CQAs of particle size and polymorphic purity, through inline FBRM and Raman. Steady state of solution concentration using inline ATR IR and gravimetric analysis from manual samples was also shown. Steady state was reached by the second RT, consistent with the findings shown during seeded operation of LGA (Chapter 5), illustrating that short term changes to the process due to

fluctuations in equipment operation and external environment are not having significant impact on CQAs. This clearly emphasises the need to identify the critical process parameters for a given process and ensure adequate control is maintained. Thus, a robust process for the continuous production of form III CBZ is achievable when using COBC technology.

This is a direct control type approach that does not utilise a quantitative model of transformation kinetics. However this methodology enables rapid development, of an effective continuous crystallisation process, for a highly polymorphic pharmaceutical API. The application of specially designed glassware for PAT insertion enhanced capabilities to obtain real-time information, providing a base for automated direct control using a feedback approach for continuous crystallisation control.

Chapter 8. Conclusions & Future Work

8.1   Conclusions

Continuous crystallisation offers the potential to deliver robust continuous processes for the purification and isolation of chemicals and pharmaceuticals with consistent attributes. The DN15 COBC is of particular interest for crystallisation as it allows longer residence times, without high net flow rates, can operate with low axial dispersion and provides excellent heat and mass transfer properties.

In the work presented here (Chapter 4), in situ UV has been utilised and validated as a viable method for RTD studies for the first time, illustrating an extended application of PAT for platform characterisation. The development work is the first reported case of oscillatory dampening along extended lengths of the COBC. The damping of oscillations results in inconsistent system performance along platform length, highlighting the need to accurately characterise and verify the operational performance of continuous crystallisation platforms. When unmonitored or controlled changes occur during a continuous process, these parameters can have significant effects during the course of a crystallisation. For example, oscillation frequency and amplitude critically regulate the flow environment, mixing efficiency and shear rates present in the system. Intentional or uncontrollable changes to control parameters may result in undesired product attributes. Thus, the impact on the process environment needs to be characterised. The work presented in Chapter 4 demonstrates that variations in operating conditions (Re_o and Re_n) result in changes to RTD profiles. However, under the range of conditions tested, the DN15 COBC operates in a near plug flow domain, demonstrating potential to support controlled crystallisation processes.

The innovative use of an ELN system delivered significant efficiencies to the RTD measurements, this enabled automated input of raw data files, automatic calculation of parameters and modelling of variables. This work therefore presents an innovative application of an information control enabled technology infrastructure within the academic research laboratory environment. The benefits are manifold and include simplification of the

characterisation process through automation, reduced man power and reducing the likelihood of experimental error during transfer and manipulation of data.

For batch to continuous transfer of LGA crystallisation, the approach of a batch MBOBC to investigate process conditions was shown to be inadequate (Chapter 5). This is due to the significant difference in localised shear, under equivalent oscillatory conditions, as a consequence of the different mixing mechanism (moving baffle rather than moving liquid).[252] This lead to unexpected nucleation processes when conditions were replicated in the COBC.

Throughout all unseeded continuous LGA experiments (Chapter 5) significant encrustation was observed. In light of the high specific surface area operation (2.57 m^2), at elevated supersaturation to achieve nucleation (S = 2 - 6), this may increase the probability of uncontrolled growth on the vessel walls. Until the impact of these processes are understood (high surfaces area, rapid heat transfer, preferential nucleation and/or fouling propensity of polymorphs on surfaces) primary nucleation in the COBC should be avoided. Instead, crystallisation processes should be initiated by seed suspensions. In effect, the unavoidable encrustation during primary nucleation in the COBC, leads to the conclusion that the optimal application of the platform is to separate high supersaturation operations for nucleation into other units, such as the impinging jet mixer used for seed production[233] in Chapter 5, whilst leaving the COBC to act as a growth unit. This methodology allows COBC operation at lower levels of supersaturation, with controlled growth of seeds, and no observed encrustation (Chapter 5 and Chapter 7). The separation of unit operations is illustrated in Figure 8.1, where continuous processes should be completed within the metastable boundary of the phase diagram, operating in regions of low supersaturation as opposed to driving the system to high supersaturation to initiate nucleation.
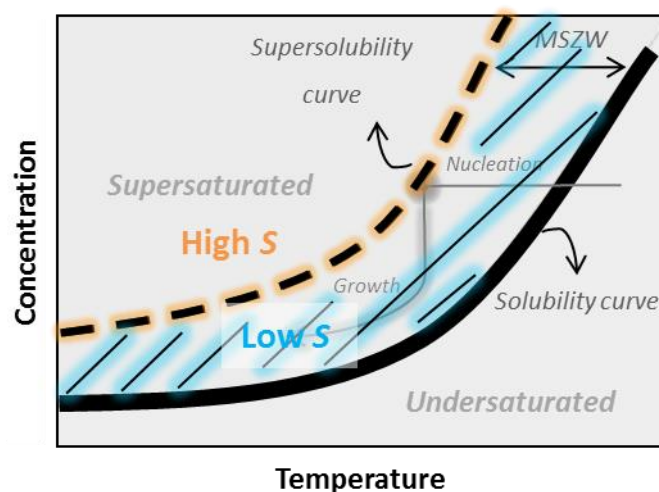
Figure 8.1: Cooling crystallisation phase diagram. Schematic illustrating the 2 main stages of crystallisation. High levels of supersaturation are required to initiate nuclei (orange) whereas growth of seed crystals can occur at lower supersaturations (blue).

As an alternative to primary nucleation through oscillatory mixing in the COBC, external fields such as ultrasound[325,326] or lasers[296,327] can be used to deliver controlled nucleation at a specific location early in the COBC process, thus reducing the risk of fouling occurring. Different materials of construction may also be of value in minimising fouling risks. Once a suitable seeding strategy was identified, steady state operation for 8 residence times without fouling or blockage of the system was demonstrated (Chapter 5). For LGA, this was achieved by maintaining the bulk solution supersaturation below 3 at all stages. Seed crystals of 10 μm could be grown to sizes ranging from 70 – 320 μm within 1 hour, illustrating control over particle size. The yields from these experiments were relatively poor (maximum 30%) due to parameters selected to understand and control supersaturation and growth within the system. If yield is considered a CQA of the process, this could certainly be tailored to maximise output by, for example, increasing RT and decreasing temperature along the reactor to provide longer times and sufficient supersaturation for growth whilst maintaining the system under the critical supersaturation level for controlled operation.

A novel batch MFOBC system was successfully designed and implemented to minimise differences between crystallisation performance in the batch and COBC platforms (Chapter 6). This MFOBC provided a closer similarity, in hydrodynamic environments and materials of construction, to the COBC than achieved by the MBOBC (Table 6.2). In principle, the MFOBC platform can support small scale development studies with far less material than required for the COBC, whilst still providing reliable kinetic data. The system was automated for operation and feedback control utilising on-line PAT. The application of a cheap CMOS camera for on-line monitoring was shown to be a reliable method to gather information on encrustation phenomena. Furthermore, the data collected using this camera for MSZW determination, was shown to be comparable to commercial high value FBRM probes. Results from this work were taken forward and an improved imaging technique was developed where encrustation could be distinguished from nucleation in the bulk.[258] Induction time experiments, with LGA under isothermal conditions in a MFOBC, show a reduction in induction time with an increase in supersaturation, providing information on design criteria for isothermal nucleation in a COBC. Experiments completed on different MFOBCs, during development, provided information on the favourability of polymorphic form to foul on surfaces, with alpha LGA preferentially nucleating on the surface whereas beta LGA preferentially nucleating within the bulk solution.

A developing work flow toward continuous COBC operation was presented (Chapter 7). This development work resulted in the first report of successful continuous crystallisation of polymorphic pure form III CBZ. This included a methodology commonly adopted in industry, using a small scale parallel crystallisation platform to scope initial thermodynamic and kinetic studies. Accurate solubility and MSZW data were then collected in the newly developed and automated MFOBC, and a seeding strategy adopted, thus utilising the COBC as a growth unit. Operating within the MSZW resulted in a polymorphic phase pure CBZ product, growing seeds from about 15 - 200

μm. However significant agglomeration of CBZ was observed after growth of seeds in the COBC.

Fouling was not observed during continuous operation when processes were operated within the MSZW of the aqueous LGA and ethanolic CBZ systems (Chapter 5 and Chapter 7). In-line PAT provided real time information on the process dynamics and confirmed the process reached rapid steady state operation, with respect to particle size, solution concentration and physical form, for both pharmaceutical materials studied. The prompt steady state condition of CQAs demonstrates repeatability and highly efficient process start-up, and minimum impact from natural fluctuations. Hence robust processing using the COBC can be achieved with a range of pharmaceutical materials.

A number of practical challenges were encountered during COBC operation (due to magnitude, see Appendix 3 for design recommendations). The challenges were minimised by the implementation of new operating procedures and the design of bespoke glassware permitted the successful continuous crystallisation of a polymorphic molecular solid, LGA and a polymorphic API, CBZ demonstrated in Chapter 5 and Chapter 7. The design of bespoke glassware enhanced the ability to obtain real-time information and provide a base to adapt a QbD approach, alongside the capabilities of feedback control for continuous crystallisation. Thus, the combination of supersaturation control and near plug flow operation is an effective route for continuous crystallisation of polymorphic materials.

8.2 Further work

8.2.1 COBC characterisation

The axial dispersion model was demonstrated to be applicable to the COBC (Chapter 4), however no predictive models simulating RTD curves for continuous oscillatory flow have been reported. Reports only provide recommendations of Re_o and Re_{on} where minimum axial dispersion can be achieved. Extension of the RTD study completed here (Chapter 4) would allow the completion of experiments covering the operating design space of the DN15 COBC and enable an accurate model for RTD prediction within oscillatory flow systems to be built. Once such a model is produced and validated, prediction of RTDs, without the need for systematic experimental investigation, may greatly improve the ability to design and control processes in the COBC.

A further extension of the work (Chapter 4) is the incorporation of RTD profiles with other predictive tools, (e.g. population balance models), to enrich modelling capabilities of resulting product attributes as a function of different mixing environments. For example, ice crystallisation during the production of sorbet in a heat exchanger has been successfully modelled with and without consideration of the RTD.[328] A comparison was made between the modelled data, when assuming plug flow and when incorporating an experimentally measured RTD profile, to the experimentally measure PSDs. In this case, both models were in good agreement with one another and provide a prediction within a 10% of the experimentally measured PSD.

The RTD experiments described in Chapter 4 were completed using a tracer dissolved in solution, with the assumption the liquid tracer dispersion is comparable to how suspended solids may behave within the COBC. Utilising a tracer of solids would provide a better model for the RTD behaviour of crystallising materials within a COBC. Modelling of various solvents and solid materials, where differences in properties including density, viscosity, number, size and size distributions, would provide an improved model of

crystallisation behaviour. Considering solute and solvents use for crystallisation will have various properties, it is important to understand and capture how system properties may affect the transfer of growing particles, within a changing slurry, throughout a crystalliser. For example, a study using a continuous tubular platform investigated the RTD behaviour of single particles, 1 % v/v suspensions, and particles with varying diameters (6-52 mm) and densities (1.065 -1.185).[329] This study demonstrated a decrease in mean residence time when particles with different properties are mixed, alongside effects of particle-particle on dispersion. This variability in mean residence times suggests the liquid tracer experiments completed in Chapter 4 did not capture the changes in RTD due to physical process (such as particle-particle interactions) occurring during a crystallisation.

Furthermore the RTD experiments (Chapter 4) were carried out at a fixed length of COBC system. Axial dispersion is a function of mean flow rate and length of system (i.e. RT) as describe in equation 2.10. Through investigation of RTD under various flow and oscillatory conditions, but at fixed residence time (various length of set-up), this would begin to provide a base of knowledge on the real impact of dispersion under various operating conditions. Hence, this would support understanding and control over crystallisations under the desired flow conditions.

Heat transfer was assessed at a basic level during this work for straight forward measurement of reactor temperature (section 5.3.5.4) but it is an important reactor parameter to characterise, to enable the development continuous crystallisation processes with predictive control. Rapid heat transfer has been illustrated within COBC temperature zones, heat transfer coefficients over straights and bends are shown to be in the range of 250-400 and 10-40 W/m^2K respectfully.[240] However, more complete modelling is needed to enable a better prediction and control of internal temperatures within the temperature zones of the COBC. This would also allow the utilisation of control valves and/or temperature manifolds to minimise the number of HCs required per COBC set-up. Furthermore, improved control

over heating/cooling would allow more flexible control of the cooling profile, moving the system away from one which induces step change cooling profile (Figure 5.19 and Figure 7.18) to one in which control over the cooling profile can be maintained along the reactor length, e.g. linear or parabolic, thus delivering desired supersaturation environments for required particle attributes. For example, the Cambridge Reactor Design *Rattlesnake* multiorifice COBC has 4 zones with a double shell heat exchanger, enabling smoother temperature profiles to be delivered across the reactor length rather than multiple fixed temperature zones as currently used in the DN15 COBC.

8.2.2 Crystallisation of LGA in oscillatory flow

Given the clear differences observed in crystallisation behaviour between the MBOBC, two MFOBC set-ups and the COBC (Chapter 5 and Chapter 6) further work is required to understand the effect of process conditions on the cooling crystallisation of LGA from aqueous solution. There appears to be several parameters effecting product outcome including temperature profile and sheer. A study in the MFOBC (set-up 2, Figure 6.4) where a step change temperature profile (Figure 5.9) is utilised, rather than an isothermal or controlled cool, should produce a comparable set of experiments to the actual cooling conditions in the COBC. Furthermore merging both MF designs but separating the hot section from the bellow via a membrane and applying a step change profile to both sections with and temperature offset (comparable to successive temperature zones within a continuous COBC), may provide an improved model considering the current temperature control within a COBC.

Given the alpha form of LGA was exclusively produced within the COBC during unseeded experiments (chapter 5), even under conditions suggested by the literature to produce beta,[38] a study on the polymorphic transformation of alpha to beta under oscillatory flow may provide a basis of understanding

how oscillatory flow may control and manipulate this transformation process. This would confirm how different process conditions influence the relative dissolution, nucleation and growth rates controlling the transformation. If conditions could be isolated to rapidly induce a SMPT this could be manipulated within the COBC, however given previous experience (Chapter 5 and Chapter 6) when alpha nucleates, simultaneous fouling also occurs and therefore mitigation of encrustation much first be addressed.

A study using the same seeding strategy for COBC crystallisation (Chapter 5 and Chapter 7), but using alpha LGA seed crystals, would provide a basis to inform and understand if fouling occurred due to surface nucleation or collision and/or particle deposition (Figure 6.3). A working hypothesis, based on the results presented in Chapter 5, is that alpha seeds can be grown to desired crystal sizes without transforming to beta, provided the supersaturation within the COBC remains below a value where spontaneous nucleation is favoured. If fouling occurs in conditions where spontaneous nucleation is unfavourable, fouling is most likely due to collision initiation of seed crystals with the vessel wall and/or deposition and adhesion of alpha seeds.

8.2.3 MFOBC workstation

Automation of the MFOBC (Chapter 6) progressed the platform, from manual operation and experimentally labour intensive, to one with control characteristics comparable to advanced control commercially available crystallisation platforms, such as the *Mettler Toledo Optimax*. Unfortunately extensive studies utilising this system were outwith the timescale of this project. However, an array of further work for understanding oscillatory crystallisations is merited on LGA including detailed phase diagram investigations, including the impact of oscillatory intensity and cooling profiles on nucleation rate, with attention to determination of primary and secondary MSZW boundaries. Also, measurement of growth rates, phase

transformation kinetics and utilising feedback control through PAT for supersaturation controlled cooling crystallisations, would extend the workflow approach to provide kinetic parameters to further aid crystallisation process design.

8.2.4 Crystallisation of CBZ

Fouling properties of CBZ where not investigated in this study, however throughout experimentation fouling was not observed when crystallising CBZ from ethanol under cooling. A study investigating kinetic parameters within the MFOBC would provide a base of knowledge to assess and model crystallisation performance within the COBC system. This would extend the workflow to deliver model based control, parameter estimation and support population balance to be implemented, thus enabling prediction of PSD from different process conditions.

Given the recommendation to operate within the MSZW and utilise the COBC as a growth unit, avoiding spontaneous nucleation (Chapter 5), unseeded experiments were not completed. It is reasonable to assume if the COBC operates under a favorable region in the phase diagram for the production of the common CBZ forms observed form solution crystallisations (Table 7.1), polymorphic phase pure CBZ can be produced. However due to the highly polymorphic nature of CBZ,[272] reported enantiotropism,[273] propensity to undergo SMPTs[274,288] and lack of kinetic information, there may be extreme difficulties in producing physically phase pure products.

Due to time scales around experimental work a comprehensive seeding study was not completed. However results observed (Chapter 7) illustrate a clear agglomeration process. Implementation of ultrasound at multiple positions within the COBC may help to insure crystals are singly suspended to counteract this agglomeration. Alternatively, manipulation of this agglomeration through the use of binding agents has been reported to product spherical agglomerates of CBZ form I and III with enhanced

performance,[300] including improved flowability and compaction properties. Utilising previously reported knowledge[322-324] and implementation with continuous oscillatory flow, this may provide a route to tailor and control agglomeration resulting in CBZ product with desired attributes.

8.2.5 Model based design approach

Building on the workflow (described in Figure 7.4), with a focus on the design approach, the key areas are highlighted in Figure 8.2. Control strategies (Section 7.1) allow the identification and optimisation of physical processes and relationships between critical process parameters (e.g. supersaturation, flow, mixing, shear rates and temperature) and the quality attributes (e.g. purity, particle size, shape, PSD, polymorph, filterability, surface characteristics, and yield). Building upon the work described in Chapter 7, incorporation of first principle and empirical modelling will provide a route to fundamental understanding of continuous processing.
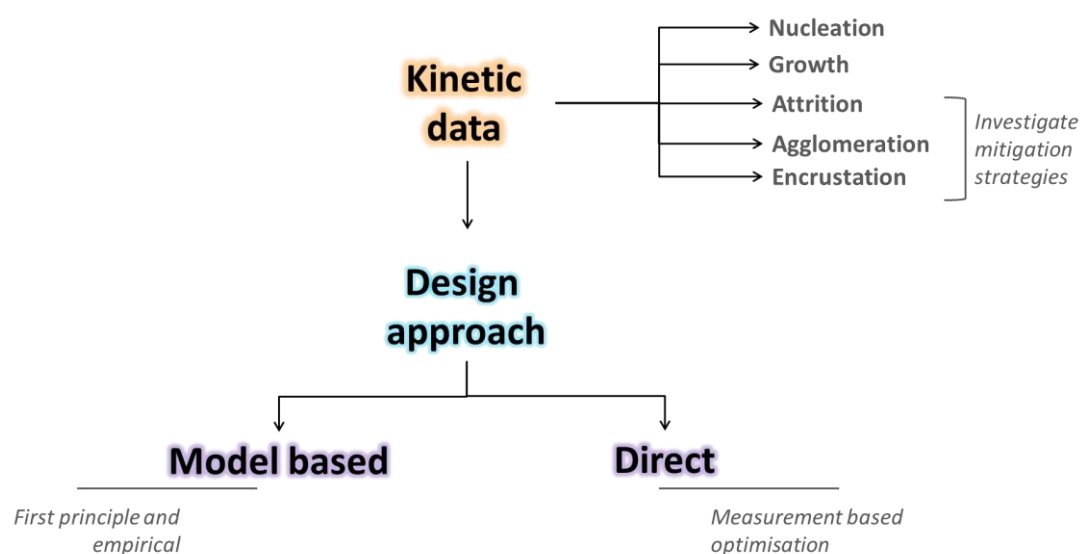
Figure 8.2: Design approach for controlled crystallisation.

Process parameters and resulting attributes can be modeled using first principles, empirical approaches, and using information acquired from PAT

with direct control methods. First principles, including population balance models accounting for solution thermodynamics, nucleation, crystal growth, and mixing characteristics of the platform etc., can provide a basis for developing controlled crystallisations, however given the array of mechanisms, increasing numbers of parameters to be estimated, increases the complexity and computation time for the calculations. This can lead to difficulties and expense of the calculations. Empirical approaches allow the development of models accounting for real process challenges (e.g. agglomeration, attrition and effect of impurities) that may not be easy to model from first principles. As direct control allows feedback from inline PAT, this can help to reach target attributes rapidly without the knowledge of the underlying mechanisms and process kinetics.

Desirably, a comprehensive work flow would devise and develop a process based purely on first principles. However, incorporation of all process dynamics, results in very complicated models with too many assumptions. It is also difficult, if not impossible, to account for every possible interaction and processes occurring during crystallisation. Direct control may be more appealing to industry, as this approach does not require the need for modelling expertise, however there is a regulatory challenge around direct control approaches for crystallisation manufacture. Semi-empirical modelling (simple models with general assumptions), tailored to the process, is somewhere in between first principle and direct control. Moving forward, the proposal for continuous process development and control is to use direct control (to give an estimate of critical parameters and responses), then parameter estimation, to have a semi-empirical modelling approach. However, understanding of fundamental crystallisation mechanisms, to better inform processes development, should also be investigated to improve upon assumptions made.

8.2.6 General

For the adoption of continuous manufacturing within the pharmaceutical industry there is a need for end-to-end continuous process,[12,17] i.e. all processes from work up and synthesis, through to secondary processes such as tableting and packaging, to be performed in a continuous and integrated manner. This work has illustrated the application of combining two continuous process streams (using a product from a continuous nucleator[233] and connecting to the COBC acting as a continuous growth unit, Chapter 5). To further illustrate the possibility of end-to-end continuous manufacturing, processes like the continuous crystallisation of LGA or CBZ could be further connected a continuous filtration/drier for example. Overall given the complexity of crystallisation (a complex multiphase dynamic process), real time control is required if processes are to be maintained under a steady controlled state, for extended periods, resulting in products with desired CQAs. Whilst PAT based direct control methods are now being implemented, rigorous understanding and validation using population balance modelling can provide a basis to verify the assumptions, made in direct control approaches, on the underlying transformation processes, as well as providing opportunities for first principles based model control.

References

(1)   Hilfiker, R. *Polymorphism: In the Pharmaceutical Industry*; John Wiley & Sons, 2006.

(2)   Yu, L. *Adv Drug Deliver Rev* **2001**, *48*, 27.

(3)   Shekunov, B. Y.; York, P. *J Cryst Growth* **2000**, *211*, 122.

(4)   Yadav, A. V.; Shete, A. S.; Dabke, A. P.; Kulkarni, P. V.; Sakhare, S. S. *Indian J Pharm Sci* **2009**, *71*, 359.

(5)   Miroshnyk, I.; Mirza, S.; Sandlert, N. *Expert Opin Drug Del* **2009**, *6*, 333.

(6)   Serajuddin, A. T. M. *Adv Drug Deliver Rev* **2007**, *59*, 603.

(7)   Aitipamula, S.; Banerjee, R.; Bansal, A. K.; Biradha, K.; Cheney, M. L.; Choudhury, A. R.; Desiraju, G. R.; Dikundwar, A. G.; Dubey, R.; Duggirala, N.; Ghogale, P. P.; Ghosh, S.; Goswami, P. K.; Goud, N. R.; Jetti, R. R. K. R.; Karpinski, P.; Kaushik, P.; Kumar, D.; Kumar, V.; Moulton, B.; Mukherjee, A.; Mukherjee, G.; Myerson, A. S.; Puri, V.; Ramanan, A.; Rajamannar, T.; Reddy, C. M.; Rodriguez-Hornedo, N.; Rogers, R. D.; Row, T. N. G.; Sanphui, P.; Shan, N.; Shete, G.; Singh, A.; Sun, C. Q. C.; Swift, J. A.; Thaimattam, R.; Thakur, T. S.; Thaper, R. K.; Thomas, S. P.; Tothadi, S.; Vangala, V. R.; Variankaval, N.; Vishweshwar, P.; Weyna, D. R.; Zaworotko, M. J. *Cryst Growth Des* **2012**, *12*, 2147.

(8)   Bugay, D. E. *Adv Drug Deliver Rev* **2001**, *48*, 43.

(9)   Richard A. Storey, I. Y. *Soild State Characterization of Pharmaceuticals* Wiley-Blackwell, 2011.

(10)   Bauer, J.; Spanton, S.; Henry, R.; Quick, J.; Dziki, W.; Porter, W.; Morris, J. *Pharm Res* **2001**, *18*, 859.

(11)   Lee, A. Y.; Erdemir, D.; Myerson, A. S. *Annu Rev Chem Biomol* **2011**, *2*, 259.

(12)   Byrn, S.; Futran, M.; Thomas, H.; Jayjock, E.; Maron, N.; Meyer, R. F.; Myerson, A. S.; Thien, M. P.; Trout, B. L. *J Pharm Sci* **2015**, *104*, 792.

(13)   Plumb, K. *Chem Eng Res Des* **2005**, *83*, 730.

(14)   Roberge, D. M.; Zimmermann, B.; Rainone, F.; Gottsponer, M.; Eyholzer, M.; Kockmann, N. *Org Process Res Dev* **2008**, *12*, 905.

(15)   Vervaet, C.; Remon, J. P. *Chem Eng Sci* **2005**, *60*, 3949.

(16)   Singh, R.; Ierapetritou, M.; Ramachandran, R. *Int J Pharmaceut* **2012**, *438*, 307.

(17)   Mascia, S.; Heider, P. L.; Zhang, H. T.; Lakerveld, R.; Benyahia, B.; Barton, P. I.; Braatz, R. D.; Cooney, C. L.; Evans, J. M. B.; Jamison, T. F.; Jensen, K. F.; Myerson, A. S.; Trout, B. L. *Angew Chem Int Edit* **2013**, *52*, 12359.

(18)   Poechlauer, P.; Manley, J.; Broxterman, R.; Gregertsen, B.; Ridemark, M. *Org Process Res Dev* **2012**, *16*, 1586.

(19)   Houson, I. *Process Understanding - For Scale-up and Manufacture of Active Ingredients*; Wiley, 2011.

(20)   Tung, H. H. *Org Process Res Dev* **2013**, *17*, 445.

(21)   Calabrese, G. S.; Pissavini, S. *Aiche J* **2011**, *57*, 828.

(22)   Poliakoff, M.; Licence, P. *Nature* **2007**, *450*, 810.

(23)   Anderson, N. G. *Org Process Res Dev* **2001**, *5*, 613.

(24)   Aksu, B.; De Beer, T.; Folestad, S.; Ketolainen, J.; Linden, H.; Lopes, J. A.; de Matas, M.; Oostra, W.; Rantanen, J.; Weimer, M. *Eur J Pharm Sci* **2012**, *47*, 402.

(25)   Allison, G.; Cain, Y. T.; Cooney, C.; Garcia, T.; Bizjak, T. G.; Holte, O.; Jagota, N.; Komas, B.; Korakianiti, E.; Kourti, D.; Madurawe, R.; Morefield, E.; Montgomery, F.; Nasr, M.; Randolph, W.; Robert, J.-L.; Rudd, D.; Zezza, D. *J Pharm Sci-Us* **2015**, *104*, 803.

(26)   Knox, M.; Trifkovic, M.; Rohani, S. *Chem Eng Sci* **2009**, *64*, 3555.

(27)   Nagy, Z. K.; Fujiwara, M.; Braatz, R. D. *J Process Contr* **2008**, *18*, 856.

(28)   Lindenberg, C.; Krattli, M.; Cornel, J.; Mazzotti, M.; Brozio, J. *Cryst Growth Des* **2009**, *9*, 1124.

(29)   Mullin, J. W. *Crystallisation*; 4th Ed. ed. Oxford, 2001.

(30)   Alatalo, H. M.; Hatakka, H.; Louhi-Kultanen, M.; Kohonen, J.; Reinikainen, S. P. *Chem Eng Technol* **2010**, *33*, 743.

(31)   Liotta, V.; Sabesan, V. *Org Process Res Dev* **2004**, *8*, 488.

(32)   Chew, J. W.; Chow, P. S.; Tan, R. B. H. *Cryst Growth Des* **2007**, *7*, 1416.

(33)   Barrett, P.; Glennon, B. *Chem Eng Res Des* **2002**, *80*, 799.

(34)   Kim, S. J.; Wei, C. K.; Kiang, S. *Org Process Res Dev* **2003**, *7*, 997.

(35)   Lawton, S.; Steele, G.; Shering, P.; Zhao, L. H.; Laird, I.; Ni, X. W. *Org Process Res Dev* **2009**, *13*, 1357.

(36)   Nagy, Z. K.; Fujiwara, M.; Woo, X. Y.; Braatz, R. D. *Ind Eng Chem Res* **2008**, *47*, 1245.

(37)   Ni, X. W.; Liao, A. T. *Cryst Growth Des* **2008**, *8*, 2875.

(38)   Ni, X. W.; Liao, A. T. *Chem Eng J* **2010**, *156*, 226.

(39)   O'Grady, D.; Barrett, M.; Casey, E.; Glennon, B. *Chem Eng Res Des* **2007**, *85*, 945.

(40)   Kadam, S. S.; Kulkarni, S. A.; Ribera, R. C.; Stankiewicz, A. I.; ter Horst, J. H.; Kramer, H. J. M. *Chem Eng Sci* **2012**, *72*, 10.

(41)   Gebauer, D.; Kellermeier, M.; Gale, J. D.; Bergstrom, L.; Colfen, H. *Chem Soc Rev* **2014**, *43*, 2348.

(42)   Davey, R. J.; Schroeder, S. L. M.; ter Horst, J. H. *Angew Chem Int Edit* **2013**, *52*, 2166.

(43)   Gebauer, D.; Colfen, H. *Nano Today* **2011**, *6*, 564.

(44)   Beckmann, W. *Crystallisation - Basic Concepts and Industrial Applications*; Wiley-VCH, 2013.

(45)   Aamir, E., Loughborough University, 2010.

(46)   Mullin, J. W.; Nyvlt, J. *Chem Eng Sci* **1971**, *26*, 369.

(47)   Otakar Söhnel, J. G. *Precipitation: Basic Principles and Industrial Applications*; Butterworth-Heinemann, 1992.

(48)   Garside, J.; Davey, R. J. *Chem Eng Commun* **1980**, *4*, 393.

(49)   Dunham, S. T.; Clejan, I.; Gencer, A. H. *Mat Sci Eng a-Struct* **1997**, *238*, 152.

(50)   Larson, J. E. H. a. M. A. *AIChE* **1977**, *23*, 822.

(51)   Chianese, A.; Diberardino, F.; Jones, A. G. *Chem Eng Sci* **1993**, *48*, 551.

(52)   Matthews, H. B.; Miller, S. M.; Rawlings, J. B. *Powder Technol* **1996**, *88*, 227.

(53)   Patience, D. B., University of Wisconsin, 2002.

(54)   Erdemir, D.; Lee, A. Y.; Myerson, A. S. *Accounts Chem Res* **2009**, *42*, 621.

(55)   Ulrich, J.; Strege, C. *J Cryst Growth* **2002**, *237*, 2130.

(56)   Rawlings, J. B.; Miller, S. M.; Witkowski, W. R. *Ind Eng Chem Res* **1993**, *32*, 1275.

(57)   Beckman, J. R.; Randolph, A. D. *Aiche J* **1977**, *23*, 510.

(58)   Choong, K. L.; Smith, R. *Chem Eng Sci* **2004**, *59*, 329.

(59)   Garside, J.; Jancic, S. J. *Chem Eng Sci* **1978**, *33*, 1623.

(60)   Garside, J. *Chem Eng Sci* **1985**, *40*, 3.

(61)   Larsen, P. A.; Patience, D. B.; Rawlings, J. B. *Ieee Contr Syst Mag* **2006**, *26*, 70.

(62)   Patel, D. D.; Anderson, B. D. *J Pharm Sci-Us* **2013**, *102*, 1544.

(63)   Fujiwara, M.; Nagy, Z. K.; Chew, J. W.; Braatz, R. D. *J Process Contr* **2005**, *15*, 493.

(64)   Fujiwara, M.; Chow, P. S.; Ma, D. L.; Braatz, R. D. *Cryst Growth Des* **2002**, *2*, 363.

(65)   Heng, J. Y. Y.; Thielmann, F.; Williams, D. R. *Pharm Res* **2006**, *23*, 1918.

(66)   Chikhalia, V.; Forbes, R. T.; Storey, R. A.; Ticehurst, M. *Eur J Pharm Sci* **2006**, *27*, 19.

(67)   Descamps, M.; Willart, J. F.; Dudognon, E.; Caron, V. *J Pharm Sci-Us* **2007**, *96*, 1398.

(68)   Variankaval, N.; Cote, A. S.; Doherty, M. F. *Aiche J* **2008**, *54*, 1682.

(69)   Butler, J. M.; Dressman, J. B. *J Pharm Sci-Us* **2010**, *99*, 4940.

(70)   Use, T. I. C. o. H. o. T. R. f. R. o. P. f. H., Ed.

(71)   Stoica, C.; Verwer, P.; Meekes, H.; van Hoof, P. J. C. M.; Kaspersen, F. M.; Vlieg, E. *Cryst Growth Des* **2004**, *4*, 765.

(72)   Berkovitchyellin, Z.; Vanmil, J.; Addadi, L.; Idelson, M.; Lahav, M.; Leiserowitz, L. *J Am Chem Soc* **1985**, *107*, 3111.

(73)   Davies, M. J.; Kerry, T. D.; Seton, L.; Murphy, M. F.; Gibbons, P.; Khoo, J.; Naderi, M. *Int J Pharmaceut* **2013**, *446*, 34.

(74)   Guo, X. H.; Yu, S. H.; Cai, G. B. *Angew Chem Int Edit* **2006**, *45*, 3977.

(75)   Joseph K. H. Ma, B. H. *Basic Physical Pharmacy*; Jones and Bartlett Learning, 2013.

(76)   Vasconcelos, T.; Sarmento, B.; Costa, P. *Drug Discov Today* **2007**, *12*, 1068.

(77)   Morales, J. O.; Watts, A. B.; McConville, J. T. *Aaps Adv Pharm Sci* **2012**, *3*, 133.

(78)   Nagy, Z. K.; Aamir, E.; Rielly, C. D. *Cryst Growth Des* **2011**, *11*, 2205.

(79)   Saleemi, A.; Rielly, C.; Nagy, Z. K. *Crystengcomm* **2012**, *14*, 2196.

(80)   Saleemi, A. N.; Steele, G.; Pedge, N. I.; Freeman, A.; Nagy, Z. K. *Int J Pharmaceut* **2012**, *430*, 56.

(81)   Doherty, M. F. *Comput-Aided Chem En* **2007**, *24*, 9.

(82)   Kim, S.; Lotz, B.; Lindrud, M.; Girard, K.; Moore, T.; Nagarajan, K.; Alvarez, M.; Lee, T.; Nikfar, F.; Davidovich, M.; Srivastava, S.; Kiang, S. *Org Process Res Dev* **2005**, *9*, 894.

(83)   Kovacic, B.; Vrecer, F.; Planinsek, O. *Acta Pharmaceut* **2012**, *62*, 1.

(84)   Bosquillon, C.; Lombry, C.; Preat, V.; Vanbever, R. *J Pharm Sci-Us* **2001**, *90*, 2032.

(85)   Sarma, B.; Chen, J.; Hsi, H. Y.; Myerson, A. S. *Korean J Chem Eng* **2011**, *28*, 315.

(86)   Yu, L. *Acc Chem Res* **2010**, *43*, 1257.

(87)   S. L. Morissettea, S. L. A., M. L. Petersona, J. F. Remenara, M. J. Reada, A. V. Lemmoa, S. Ellisa, M. J. Cimab, C. R. Gardnera *Advanced Drug Delivery Reviews* **2004**, *56*, 275.

(88)   Day, G. M.; Cooper, T. G.; Cruz-Cabeza, A. J.; Hejczyk, K. E.; Ammon, H. L.; Boerrigter, S. X. M.; Tan, J. S.; Della Valle, R. G.; Venuti, E.; Jose, J.; Gadre, S. R.; Desiraju, G. R.; Thakur, T. S.; van Eijck, B. P.; Facelli, J. C.; Bazterra, V. E.; Ferraro, M. B.; Hofmann, D. W. M.; Neumann, M. A.; Leusen, F. J. J.; Kendrick, J.; Price, S. L.; Misquitta, A. J.; Karamertzanis, P. G.; Welch, G. W. A.; Scheraga, H. A.; Arnautova, Y. A.; Schmidt, M. U.; van de Streek, J.; Wolf, A. K.; Schweizer, B. *Acta Crystallogr B* **2009**, *65*, 107.

(89)   Bardwell, D. A.; Adjiman, C. S.; Arnautova, Y. A.; Bartashevich, E.; Boerrigter, S. X. M.; Braun, D. E.; Cruz-Cabeza, A. J.; Day, G. M.; Della Valle, R. G.; Desiraju, G. R.; van Eijck, B. P.; Facelli, J. C.; Ferraro, M. B.; Grillo, D.; Habgood, M.; Hofmann, D. W. M.; Hofmann, F.; Jose, K. V. J.; Karamertzanis, P. G.; Kazantsev, A. V.; Kendrick, J.; Kuleshova, L. N.; Leusen, F. J. J.; Maleev, A. V.; Misquitta, A. J.; Mohamed, S.; Needs, R. J.; Neumann, M. A.; Nikylov, D.; Orendt, A. M.; Pal, R.; Pantelides, C. C.; Pickard, C. J.; Price, L. S.; Price, S. L.; Scheraga, H. A.; van de Streek, J.; Thakur, T. S.; Tiwari, S.; Venuti, E.; Zhitkov, I. K. *Acta Crystallogr B* **2011**, *67*, 535.

(90)   Singhal, D.; Curatolo, W. *Adv Drug Deliver Rev* **2004**, *56*, 335.

(91)   Munroe, A.; Croker, D. M.; Rasmuson, A. C.; Hodnett, B. K. *Cryst Growth Des* **2014**, *14*, 3466.

(92)   Maher, A.; Croker, D. M.; Seaton, C. C.; Rasmuson, A. C.; Hodnett, B. K. *Cryst Growth Des* **2014**, *14*, 3967.

(93)   Yashina, A.; Meldrum, F.; deMello, A. *Biomicrofluidics* **2012**, *6*.

(94)   Mo, Y. X.; Dang, L. P.; Wei, H. Y. *Ind Eng Chem Res* **2011**, *50*, 10385.

(95)   Srinivasan, K.; Dhanasekaran, P. *Amino Acids* **2011**, *40*, 1257.

(96)   Jiang, S. F.; Jansens, P. J.; ter Horst, J. H. *Cryst Growth Des* **2010**, *10*, 2541.

(97)   Mangin, D.; Puel, F.; Veesler, S. *Organic Process Research & Development* **2009**, *13*, 1241.

(98) Hermanto, M. W.; Chiu, M. S.; Woo, X. Y.; Braatz, R. D. *Aiche Journal* **2007**, *53*, 2643.

(99) Llinas, A.; Goodman, J. M. *Drug Discov Today* **2008**, *13*, 198.

(100) Kordikowski, A.; Shekunov, T.; York, P. *Pharmaceut Res* **2001**, *18*, 682.

(101) Saleemi, A. N.; Rielly, C. D.; Nagy, Z. K. *Chem Eng Sci* **2012**, *77*, 122.

(102) Pomerantsev, A. L.; Rodionova, O. Y. *Journal of Chemometrics* **2012**, *26*, 299.

(103) Yu, Z. Q.; Chew, J. W.; Chow, P. S.; Tan, R. B. H. *Chem Eng Res Des* **2007**, *85*, 893.

(104) Barrett, P.; Smith, B.; Worlitschek, J.; Bracken, V.; O'Sullivan, B.; O'Grady, D. *Org Process Res Dev* **2005**, *9*, 348.

(105) Kadam, S. S.; Vissers, J. A. W.; Forgione, M.; Geertman, R. M.; Daudey, P. J.; Stankiewicz, A. I.; Kramer, H. J. M. *Org Process Res Dev* **2012**, *16*, 769.

(106) Thirunahari, S.; Chow, P. S.; Tan, R. B. H. *Cryst Growth Des* **2011**, *11*, 3027.

(107) Castagnoli, C.; Yahyah, M.; Cimarosti, Z.; Peterson, J. J. *Org Process Res Dev* **2010**, *14*, 1415.

(108) Koh, P. T. L. X., F. In *Second international conference on CFD in the minerals and process industries* Melbourne, Australia 1999, p 369.

(109) Chew, C. M.; Ristic, R. I.; Reynolds, G. K.; Ooi, R. C. *Chem Eng Sci* **2004**, *59*, 1557.

(110) Ni, X. W.; Pereira, N. E. *Aiche J* **2000**, *46*, 37.

(111) Harvey, A. P.; Mackley, M. R.; Stonestreet, P. *Ind Eng Chem Res* **2001**, *40*, 5371.

(112) Carpenter, N. G.; Roberts, E. P. L. *Chem Eng Res Des* **1999**, *77*, 212.

(113) Trachsel, F.; Gunther, A.; Khan, S.; Jensen, K. F. *Chem Eng Sci* **2005**, *60*, 5729.

(114) Khan, M. J. H.; Hussain, M. A.; Mansourpour, Z.; Mostoufi, N.; Ghasem, N. M.; Abdullah, E. C. *J Ind Eng Chem* **2014**, *20*, 3919.

(115) Defraeye, T. *Appl Energ* **2014**, *131*, 323.

(116) Carlomagno, G. M.; Ianiro, A. *Exp Therm Fluid Sci* **2014**, *58*, 15.

(117) Westerweel, J.; Elsinga, G. E.; Adrian, R. J. *Annu Rev Fluid Mech* **2013**, *45*, 409.

(118) Mohammadi, M.; Sharp, K. V. *J Fluid Eng-T Asme* **2013**, *135*.

(119) Wiederseiner, S.; Andreini, N.; Epely-Chauvin, G.; Ancey, C. *Exp Fluids* **2011**, *50*, 1183.

(120) Kunn Hadino, Y. Y. *Int J Pharmaceut* **2014**, *473*, 644.

(121) Jiang, M.; Wong, M. H.; Zhu, Z. L.; Zhang, J. Q.; Zhou, L. F.; Wang, K.; Versypt, A. N. F.; Si, T.; Hasenberg, L. M.; Li, Y. E.; Braatz, R. D. *Chem Eng Sci* **2012**, *77*, 2.

(122) Cichy, B.; Kuzdzal, E. *Ind Eng Chem Res* **2014**, *53*, 6593.

(123) Quon, J. L.; Zhang, H.; Alvarez, A.; Evans, J.; Myerson, A. S.; Trout, B. L. *Cryst Growth Des* **2012**, *12*, 3036.

(124) Zhao, L. H.; Raval, V.; Briggs, N. E. B.; Bhardwaj, R. M.; McGlone, T.; Oswald, I. D. H.; Florence, A. J. *Crystengcomm* **2014**, *16*, 5769.

(125) Hou, G. Y.; Power, G.; Barrett, M.; Glennon, B.; Morris, G.; Zhao, Y. *Cryst Growth Des* **2014**, *14*, 1782.

(126) Alvarez, A. J.; Singh, A.; Myerson, A. S. *Cryst Growth Des* **2011**, *11*, 4392.

(127) Kozik, A.; Hutnik, N.; Piotrowski, K.; Matynia, A. *Chem Eng Res Des* **2014**, *92*, 481.

(128) Zhang, H. T.; Quon, J.; Alvarez, A. J.; Evans, J.; Myerson, A. S.; Trout, B. *Org Process Res Dev* **2012**, *16*, 915.

(129) Alvarez, A. J.; Myerson, A. S. *Cryst Growth Des* **2010**, *10*, 2219.

(130) Gerard, A.; Muhr, H.; Plasari, E.; Jacob, D.; Lefaucheur, C. E. *Powder Technol* **2014**, *255*, 134.

(131) Vacassy, R.; Lemaitre, J.; Hofmann, H.; Gerlings, J. H. *Aiche J* **2000**, *46*, 1241.

(132) Ferguson, S.; Ortner, F.; Quon, J.; Peeva, L.; Livingston, A.; Trout, B. L.; Myersont, A. S. *Cryst Growth Des* **2014**, *14*, 617.

(133) Ferguson, S.; Morris, G.; Hao, H. X.; Barrett, M.; Glennon, B. *Chem Eng Sci* **2013**, *104*, 44.

(134) Narducci, O.; Jones, A. G.; Kougoulos, E. *Chem Eng Sci* **2011**, *66*, 1069.

(135) Eder, R. J. P.; Schrank, S.; Besenhard, M. O.; Roblegg, E.; Gruber-Woelfler, H.; Khinast, J. G. *Cryst Growth Des* **2012**, *12*, 4733.

(136) Eder, R. J. P.; Schmitt, E. K.; Grill, J.; Radl, S.; Gruber-Woelfler, H.; Khinast, J. G. *Cryst Res Technol* **2011**, *46*, 227.

(137) Wong, S. Y.; Tatusko, A. P.; Trout, B. L.; Myerson, A. S. *Cryst Growth Des* **2012**, *12*, 5701.

(138) Wierzbowska, B.; Piotrowski, K.; Koralewska, J.; Matynia, A.; Hutnik, N.; Wawrzyniecki, K. *Cryst Res Technol* **2008**, *43*, 381.

(139) Wong, S. Y.; Bund, R. K.; Connelly, R. K.; Hartel, R. W. *Cryst Growth Des* **2010**, *10*, 2620.

(140) de Paz, G. D. *Int Sugar J* **2002**, *104*, 14.

(141) Wojcik, J. A.; Jones, A. G. *Chem Eng Res Des* **1997**, *75*, 113.

(142) Tsai-Ta C. Lai, S. F., Laura Palmer, Bernhardt L. Trout, and Allan S. Myerson *Organic Process Research and Develpoment* **2014**.

(143) Tai, C. Y.; Shei, W. L. *Chem Eng Commun* **1993**, *120*, 139.

(144) Abbott, M. S. R.; Harvey, A. P.; Perez, G. V.; Theodorou, M. K. *Interface Focus* **2013**, *3*.

(145) Kougoulos, E.; Jones, A. G.; Wood-Kaczmar, M. W. *Org Process Res Dev* **2006**, *10*, 739.

(146) Rielly, C. D.; Marquis, A. J. *Chem Eng Sci* **2001**, *56*, 2475.

(147) Anderson, N. G. *Practical Process Research & Development*; Academic Press, 2000.

(148) Chung, F. H. S., D. k. *Industrial applications of x-ray diffraction* Marcel Dekker AG: New York, 2000.

(149) Brittain, H. G. *J Pharm Sci-Us* **2008**, *97*, 3611.

(150) Bezzon, V. D. N.; Antonio, S. G.; Paiva-Santos, C. O. *J Pharm Sci-Us* **2014**, *103*, 3567.

(151) Watson, D. G. *Pharmaceutical analysis*; Churchill Livingston Elsevier, 2012.

(152) Chianese, A.; Kramer, H. J. M. *Industrial crystallization process monitoring and control*; Wiley-VCH ;

John Wiley distributor: Weinheim

Chichester, 2012.

(153) Bakeev, K. A. *Process Analytical Technology*; Second Edition ed.; John Wiley and Sons Ltd, 2010.

(154) Hsien-Hsin Tung, E. L. P., Michael Midler, James A. McCauley *Crystallization of Organic Compounds - An Industrial Perspective*; Wiley, 2009.

(155) Mackley, M. R.; Smith, K. B.; Wise, N. P. *Chem Eng Res Des* **1993**, *71*, 649.

(156) Sobey, I. J. *Journal of Fluid Mechanics* **1980**, *96*, 1.

(157) Stonestreet, P.; Van der Veeken, P. M. J. *Chem Eng Res Des* **1999**, *77*, 671.

(158) Zheng, M. Z.; Mackley, M. *Chem Eng Sci* **2008**, *63*, 1788.

(159) Reis, N.; Vincente, A. A.; Teixeira, J. A.; Mackley, M. R. *Chem Eng Sci* **2004**, *59*, 4967.

(160) Ni, X. W. In *Chemical Engineer* 2006; Vol. 779, p 26.

(161) Ni, X. W. *J Chem Technol Biot* **1995**, *64*, 165.

(162) Nauman, E. B. *Ind Eng Chem Res* **2008**, *47*, 3752.

(163) Gao, Y. J.; Muzzio, F. J.; Ierapetritou, M. G. *Powder Technol* **2012**, *228*, 416.

(164) Levenspiel, O. *Chemical Reaction Engineering* 3rd ed.; Wiley: New York, USA, 1999.

(165) Phan, A. N.; Harvey, A. P. *Chem Eng J* **2012**, *180*, 229.

(166) Phan, A. N.; Harvey, A.; Lavender, J. *Chem Eng Process* **2011**, *50*, 254.

(167) Phan, A. N.; Harvey, A. P. *Chem Eng J* **2011**, *169*, 339.

(168) Phan, A. N.; Harvey, A. *Chem Eng J* **2010**, *159*, 212.

(169) Mackley, M. R.; Ni, X. *Chem Eng Sci* **1991**, *46*, 3139.

(170) Smith, K. B., University of Cambridge, 1999.

(171) Aris, R. *Chem Eng Sci* **1959**, *9*, 266.

(172) Dickens, A. W.; Mackley, M. R.; Williams, H. R. *Chem Eng Sci* **1989**, *44*, 1471.

(173) Howes, T.; Mackley, M. R. *Chem Eng Sci* **1990**, *45*, 1349.

(174) Mackley, M. R.; Ni, X. *Chem Eng Sci* **1993**, *48*, 3293.

(175) Ni, X. W. *J Chem Technol Biot* **1994**, *59*, 213.

(176) Mackley, M. R.; Stonestreet, P.; Roberts, E. P. L.; Ni, X. *Chem Eng Res Des* **1996**, *74*, 541.

(177) Fitch, A. W.; Ni, X. *Chem Eng J* **2003**, *92*, 243.

(178) Ni, X.; Brogan, G.; Struthers, A.; Bennett, D. C.; Wilson, S. F. *Chem Eng Res Des* **1998**, *76*, 635.

(179) Smith, K. B.; Mackley, M. R. *Chem Eng Res Des* **2006**, *84*, 1001.

(180) Nadeau, P.; Berk, D.; Munz, R. J. *Chem Eng Sci* **1996**, *51*, 2607.

(181) Antony, J. *Design of Experiments for engineers and Scientists*; Butterworth-Heinemann, 2003.

(182) Weissman, S. A.; Anderson, N. G. *Org Process Res Dev* **2014**.

(183) Howes, T.; Mackley, M. R.; Roberts, E. P. L. *Chem Eng Sci* **1991**, *46*, 1669.

(184) Liu, J.; Svard, M.; Rasmuson, A. C. *Cryst Growth Des* **2014**, *14*, 5521.

(185) Wong, S. Y.; Bund, R. K.; Connelly, R. K.; Hartel, R. W. *J Food Eng* **2012**, *111*, 642.

(186) Baell, J.; Congreve, M.; Leeson, P.; Abad-Zapatero, C. *Future Med Chem* **2013**, *5*, 745.

(187) Dutta, S.; Ray, S.; Nagarajan, K. *Saudi Pharm J* **2013**, *21*, 337.

(188) Gubellini, P.; Pisani, A.; Centonze, D.; Bernardi, G.; Calabresi, P. *Progress in neurobiology* **2004**, *74*, 271.

(189) McEntee, W. J.; Crook, T. H. *Psychopharmacology* **1993**, *111*, 391.

(190) Cashell, C.; Corcoran, D.; Hodnett, B. K. *J Cryst Growth* **2004**, *273*, 258.

(191) Ferrari, E. S.; Davey, R. J. *Cryst Growth Des* **2004**, *4*, 1061.

(192) Kitamura, M.; Ishizu, T. *J Cryst Growth* **1998**, *192*, 225.

(193) Ono, T.; Kramer, H. J. M.; ter Horst, J. H.; Jansens, P. J. *Cryst Growth Des* **2004**, *4*, 1161.

(194) Ono, T.; ter Horst, J. H.; Jansens, P. J. *Cryst Growth Des* **2004**, *4*, 465.

(195) Khan, S.; Ma, C. Y.; Mahmud, T.; Penchev, R. L. Y.; Roberts, K. J.; Morris, J.; Ozkan, L.; White, G.; Grieve, B.; Hall, A.; Buser, P.; Gibson, N.; Keller, P.; Shuttleworth, P.; Price, C. J. *Org Process Res Dev* **2011**, *15*, 540.

(196) Grier, J. S. In *United States Patent Office* 1964; Vol. 442,684.

(197) Ni, X. W.; Valentine, A.; Liao, A. T.; Sermage, S. B. C.; Thomson, G. B.; Roberts, K. J. *Cryst Growth Des* **2004**, *4*, 1129.

(198) Hirokawa, S. *Acta Crystallogr* **1955**, *8*, 637.

(199) Hirayama, N.; Shirahata, K.; Ohashi, Y.; Sasada, Y. *B Chem Soc Jpn* **1980**, *53*, 30.

(200) Kee, N. C. S.; Tan, R. B. H.; Braatz, R. D. *Cryst Growth Des* **2009**, *9*, 3044.

(201) Gron, H.; Borissova, A.; Roberts, K. J. *Ind Eng Chem Res* **2003**, *42*, 198.

(202) Qu, H. Y.; Alatalo, H.; Hatakka, H.; Kohonen, J.; Louhi-Kultanen, M.; Reinikainen, S. P.; Kallas, J. *J Cryst Growth* **2009**, *311*, 3466.

(203) Scholl, J.; Bonalumi, D.; Vicum, L.; Mazzotti, M.; Muller, M. *Cryst Growth Des* **2006**, *6*, 881.

(204) Ma, C. Y.; Wang, X. Z.; Roberts, K. J. *Adv Powder Technol* **2007**, *18*, 707.

(205) Cornel, J.; Lindenberg, C.; Mazzotti, M. *Cryst Growth Des* **2009**, *9*, 243.

(206) Ma, C. Y.; Wang, X. Z. *Chem Eng Sci* **2012**, *70*, 22.

(207) Kitamura, M.; Funahara, H. *J Chem Eng Jpn* **1994**, *27*, 124.

(208) Shan, G.; Igarashi, K.; Noda, H.; Ooshima, H. *Chem Eng J* **2002**, *85*, 169.

(209) Black, S. N.; Davey, R. J.; Halcrow, M. *J Cryst Growth* **1986**, *79*, 765.

(210) Ricardo, C.; Ni, X. W. *Org Process Res Dev* **2009**, *13*, 1080.

(211) Chew, C. M.; Ristic, R. I.; Dennehy, R. D.; De Yoreo, J. J. *Cryst Growth Des* **2004**, *4*, 1045.

(212) Chew, C. M.; Ristic, R. I. *Aiche J* **2005**, *51*, 1576.

(213) Ristic, R. I. *Chem Eng Res Des* **2007**, *85*, 937.

(214) Brown, C. J.; Ni, X. W. *Cryst Growth Des* **2011**, *11*, 3994.

(215) Brown, C. J.; Ni, X. W. *Cryst Growth Des* **2011**, *11*, 719.

(216) Brown, C. J.; Ni, X. W. *Crystengcomm* **2012**, *14*, 2944.

(217) Callahan, C. J.; Ni, X. W. *Cryst Growth Des* **2012**, *12*, 2525.

(218) Callahan, C. J.; Ni, X. W. *Crystengcomm* **2014**, *16*, 690.

(219) Callahan, C. J.; Ni, X. W. *Can J Chem Eng* **2014**, *92*, 1920.

(220) Palmer, L., University of Strathclyde, 2013.

(221) Brown, C. J.; Lee, Y. C.; Nagy, Z. K.; Ni, X. *Crystengcomm* **2014**, *16*, 8008.

(222) Ni, X.; Mackley, M. R.; Harvey, A. P.; Stonestreet, P.; Baird, M. H. I.; Rao, N. V. R. *Chem Eng Res Des* **2003**, *81*, 373.

(223) Ni, X. W.; de Gelicourt, Y. S.; Baird, M. H. I.; Rao, N. V. R. *Can J Chem Eng* **2001**, *79*, 444.

(224) Jian, H.; Ni, X. *Chem Eng Res Des* **2005**, *83*, 1163.

(225) Sinnott, R. K. *Coulson and Richardson's Chemical Engineering*; Butterworth-Heinemann: Oxford, 1999; Vol. 6.

(226) Baird, M. H. I.; Stonestreet, P. *Chem Eng Res Des* **1995**, *73*, 503.

(227) Nienow, A. W.; Miles, D. *Ind Eng Chem Proc Dd* **1971**, *10*, 41.

(228) Zhao, X.; Chen, X. D. *Heat Transfer Eng* **2013**, *34*, 719.

(229) Wong, S. Y.; Cui, Y. Q.; Myerson, A. S. *Cryst Growth Des* **2013**, *13*, 2514.

(230) Evans, T. W.; Margolis, G.; Sarofim, A. F. *Aiche J* **1974**, *20*, 950.

(231) Yu, Z. Q.; Chow, P. S.; Tan, R. B. H. *Org Process Res Dev* **2006**, *10*, 717.

(232) Aamir, E.; Nagy, Z. K.; Rielly, C. D. *Cryst Growth Des* **2010**, *10*, 4728.

(233) Schacht, U., University of Strathclyde, 2014.

(234) Wohlgemuth, K.; Schembecker, G. *Comput Chem Eng* **2013**, *52*, 216.

(235) Myerson, A. S.; Krumme, M.; Nasr, M.; Thomas, H.; Braatz, R. D. *J Pharm Sci* **2015**, *104*, 832.

(236) Jaworski, Z.; Dudczak, J. *Comput Chem Eng* **1998**, *22*, S293.

(237) Lobry, E.; Lasuye, T.; Gourdon, C.; Xuereb, C. *Chem Eng J* **2015**, *259*, 505.

(238) Ni, X.; Mackley, M. R. *Chemical Engineering Journal and the Biochemical Engineering Journal* **1993**, *52*, 107.

(239) Reis, N.; Harvey, A. P.; Mackley, M. R.; Vicente, A. A.; Teixeira, J. A. *Chem Eng Res Des* **2005**, *83*, 357.

(240) McGinty, J., University of Strathclyde, 2013.

(241) Perry, R. H. *Perry's Chemical Engineers' Handbook*; Eight Edition ed.; McGraw Hill Professional: USA, 2007.

(242) Jolliffe, H. G.; Gerogiorgis, D. I. *Chemical Engineering Research and Design*.

(243) Desikan, S.; Anderson, S. R.; Meenan, P. A.; Toma, P. H. *Current opinion in drug discovery & development* **2000**, *3*, 723.

(244) Stonestreet, P.; Harvey, A. P. *Chem Eng Res Des* **2002**, *80*, 31.

(245) Liang, K. P.; White, G.; Wilkinson, D.; Ford, L. J.; Roberts, K. J.; Wood, W. M. L. *Cryst Growth Des* **2004**, *4*, 1039.

(246) Tsekova, D. S.; Williams, D. R.; Heng, J. Y. Y. *Chem Eng Sci* **2012**, *77*, 201.

(247) Diao, Y.; Myerson, A. S.; Hatton, T. A.; Trout, B. L. *Langmuir* **2011**, *27*, 5324.

(248) Parambil, J. V.; Poornachary, S. K.; Tan, R. B. H.; Heng, J. Y. Y. *Crystengcomm* **2014**, *16*, 4927.

(249) Ni, X.; Zhang, Y.; Mustafa, I. *Chem Eng Sci* **1999**, *54*, 841.

(250) Gao, P.; Ching, W. H.; Herrmann, M.; Chan, C. K.; Yue, P. L. *Chem Eng Sci* **2003**, *58*, 1013.

(251) Stonestreet, P.; Djemai, A.; Mackley, M. R. *Bhr Gr Conf Ser Publ* **1999**, 45.

(252) Manninen, M.; Gorshkova, E.; Immonen, K.; Ni, X. W. *J Chem Technol Biot* **2013**, *88*, 553.

(253) Vendel, M.; Rasmuson, A. C. *Chem Eng Res Des* **2000**, *78*, 749.

(254) Rein, P.

(255) Amjad, Z. *J Colloid Interf Sci* **1988**, *123*, 523.

(256) Marroquin, M.; Vu, A.; Bruce, T.; Wickramasinghe, S. R.; Zhao, L. X.; Husson, S. M. *J Membrane Sci* **2014**, *465*, 1.

(257) Kim, W. T.; Bai, C.; Cho, Y. I. *Int J Heat Mass Tran* **2002**, *45*, 597.

(258) Tachtatzis, C.; Sheridan, R.; Michie, C.; Atkinson, R. C.; Cleary, A.; Dziewierz, J.; Andonovic, I.; Briggs, N.; Florence, A. J.; Sefcik, J. *Chem Eng Sci* **2015**.

(259) Kuhs, M.; Zeglinski, J.; Rasmuson, A. C. *Cryst Growth Des* **2014**, *14*, 905.

(260) Nordstrom, F. L.; Svard, M.; Malmberg, B.; Rasmuson, A. C. *Cryst Growth Des* **2012**, *12*, 4340.

(261) Caridi, A.; Kulkarni, S. A.; Di Profio, G.; Curcio, E.; ter Horst, J. H. *Cryst Growth Des* **2014**, *14*, 1135.

(262) Capacci-Daniel, C.; Gaskell, K. J.; Swift, J. A. *Cryst Growth Des* **2010**, *10*, 952.

(263) Kazi, S. N.; Duffy, G. G.; Chen, X. D. *Appl Therm Eng* **2010**, *30*, 2236.

(264) Geddert, T.; Bialuch, I.; Augustin, W.; Scholl, S. *Heat Transfer Eng* **2009**, *30*, 868.

(265) Al-Janabi, A.; Malayeri, M. R. *Chem Eng Technol* **2015**, *38*, 147.

(266) Myerson, A. S. *Handbook of industrial crystallization*; Butterworth-Heinemann, 2001.

(267) Nagy, Z. K.; Braatz, R. D. *Annual Review of Chemical and Biomolecular Engineering, Vol 3* **2012**, *3*, 55.

(268) Zhou, G. X.; Fujiwara, M.; Woo, X. Y.; Rusli, E.; Tung, H. H.; Starbuck, C.; Davidson, O.; Ge, Z. H.; Braatz, R. D. *Cryst Growth Des* **2006**, *6*, 892.

(269) Griffin, D. J.; Kawajiri, Y.; Grover, M. A.; Rousseau, R. W. *Cryst Growth Des* **2015**, *15*, 305.

(270) Worlitschek, J.; Mazzotti, M. *Cryst Growth Des* **2004**, *4*, 891.

(271) Ridder, B. J.; Majumder, A.; Nagy, Z. K. *Ind Eng Chem Res* **2014**, *53*, 4387.

(272) Childs, S. L.; Wood, P. A.; Rodriguez-Hornedo, N.; Reddy, L. S.; Hardcastle, K. I. *Cryst Growth Des* **2009**, *9*, 1869.

(273) O'Mahony, M. A.; Croker, D. M.; Rasmuson, A. C.; Veesler, S.; Hodnett, B. K. *Org Process Res Dev* **2013**, *17*, 512.

(274) Liu, W. J.; Wei, H. Y.; Zhao, J. T.; Black, S.; Sun, C. *Org Process Res Dev* **2013**, *17*, 1406.

(275) Zhao, Y.; Bao, Y.; Wang, J.; Rohani, S. *Pharmaceutics* **2012**, *4*, 164.

(276) Getsoian, A.; Lodaya, R. M.; Blackburn, A. C. *Int J Pharmaceut* **2008**, *348*, 3.

(277) Johnston, A.; Johnston, B. F.; Kennedy, A. R.; Florence, A. J. *Crystengcomm* **2008**, *10*, 23.

(278) Porter, W. W.; Elie, S. C.; Matzger, A. J. *Cryst Growth Des* **2008**, *8*, 14.

(279) Moradiya, H. G.; Islam, M. T.; Halsey, S.; Maniruzzaman, M.; Chowdhry, B. Z.; Snowden, M. J.; Douroumis, D. *Crystengcomm* **2014**, *16*, 3573.

(280) Arlin, J. B.; Price, L. S.; Price, S. L.; Florence, A. J. *Chem Commun* **2011**, *47*, 7074.

(281) Price, S. L. *Phys Chem Chem Phys* **2008**, *10*, 1996.

(282) Grzesiak, A. L.; Lang, M. D.; Kim, K.; Matzger, A. J. *J Pharm Sci-Us* **2003**, *92*, 2260.

(283) Lisgarten, J. N.; Palmer, R. A.; Saldanha, J. W. *J Cryst Spectrosc* **1989**, *19*, 641.

(284) Lowes, M. M. J.; Caira, M. R.; Lotter, A. P.; Vanderwatt, J. G. *J Pharm Sci-Us* **1987**, *76*, 744.

(285) Lang, M. D.; Kampf, J. W.; Matzger, A. J. *J Pharm Sci-Us* **2002**, *91*, 1186.

(286) Young, W. W. L.; Suryanarayanan, R. *J Pharm Sci-Us* **1991**, *80*, 496.

(287) Kipouros, K.; Kachrimanis, K.; Nikolakakis, I.; Malamataris, S. *Anal Chim Acta* **2005**, *550*, 191.

(288) Sypek, K.; Burns, I. S.; Florence, A. J.; Sefcik, J. *Cryst Growth Des* **2012**, *12*, 4821.

(289) Zhao, Y. Y.; Yuan, J. S.; Ji, Z. Y.; Wang, J. K.; Rohani, S. *Ind Eng Chem Res* **2012**, *51*, 12530.

(290) Svard, M.; Nordstrom, F. L.; Hoffmann, E. M.; Aziz, B.; Rasmuson, A. C. *Crystengcomm* **2013**, *15*, 5020.

(291) Gu, C. H.; Young, V.; Grant, D. J. W. *J Pharm Sci-Us* **2001**, *90*, 1878.

(292) Su, W. Y.; Hao, H. X.; Barrett, M.; Glennon, B. *Org Process Res Dev* **2010**, *14*, 1440.

(293) Wang, M.; Rutledge, G. C.; Myerson, A. S.; Trout, B. L. *J Pharm Sci-Us* **2012**, *101*, 1178.

(294) Diao, Y.; Whaley, K. E.; Helgeson, M. E.; Woldeyes, M. A.; Doyle, P. S.; Myerson, A. S.; Hatton, T. A.; Trout, B. L. *J Am Chem Soc* **2012**, *134*, 673.

(295) Javadzadeh, Y.; Mohammadi, A.; Khoei, N. S.; Nokhodchi, A. *Acta Pharmaceut* **2009**, *59*, 187.

(296) Ikni, A.; Clair, B.; Scouflaire, P.; Veesler, S.; Gillet, J. M.; El Hassan, N.; Dumas, F.; Spasojevic-de Bire, A. *Cryst Growth Des* **2014**, *14*, 3286.

(297) Flicker, F.; Eberle, V. A.; Betz, G. *Int J Pharmaceut* **2011**, *410*, 99.

(298) Edwards, A. D.; Shekunov, B. Y.; Kordikowski, A.; Forbes, R. T.; York, P. *J Pharm Sci-Us* **2001**, *90*, 1115.

(299) Otsuka, M.; Hasegawa, H.; Matsuda, Y. *Chem Pharm Bull* **1999**, *47*, 852.

(300) Nokhodchi, A.; Maghsoodi, M.; Hassanzadeh, D. *Iran J Pharm Res* **2007**, *6*, 83.

(301) Chanda, A.; Daly, A. M.; Foley, D. A.; LaPack, M. A.; Mukherjee, S.; Orr, J. D.; Reid, G. L.; Thompson, D. R.; Ward, H. W. *Org Process Res Dev* **2015**, *19*, 63.

(302) Yu, Z. Q.; Chow, P. S.; Tan, R. B. H.; Ang, W. H. *Org Process Res Dev* **2013**, *17*, 549.

(303) Schaefer, C.; Lecomte, C.; Clicq, D.; Merschaert, A.; Norrant, E.; Fotiadu, F. *J Pharmaceut Biomed* **2013**, *83*, 194.

(304) Mirabella, F. M. *Internal Reflection Spectroscopy*; Marcel Dekker: New York, 1993.

(305) Fevotte, G. *Chem Eng Res Des* **2007**, *85*, 906.

(306) Kempkes, M.; Eggers, J.; Mazzotti, M. *Chem Eng Sci* **2008**, *63*, 4656.

(307) Leyssens, T.; Baudry, C.; Hernandez, M. L. E. *Org Process Res Dev* **2011**, *15*, 413.

(308) Ma, Y.; Zhu, J. W.; Chen, K.; Wu, Y. Y.; Chen, A. M. *J Cryst Growth* **2009**, *312*, 109.

(309) Braatz, R. D.; Hasebe, S. In *AIChE Symposium Series*; New York; American Institute of Chemical Engineers; 1998: 2002, p 307.

(310) Engstrom, J.; Wang, C. C.; Lai, C. J.; Sweeney, J. *Int J Pharmaceut* **2013**, *456*, 261.

(311) Chaitanya, K. K.; Sarkar, D. *Chem Eng Technol* **2014**, *37*, 1037.

(312) Liu, Y.; Pietzsch, M.; Ulrich, J. *Cryst Res Technol* **2014**, *49*, 262.

(313) Gherras, N.; Fevotte, G. *J Cryst Growth* **2012**, *342*, 88.

(314) He, G. W.; Hermanto, M. W.; Tjahjono, M.; Chow, P. S.; Tan, R. B. H.; Garland, M. *Chem Eng Res Des* **2012**, *90*, 259.

(315) Keraliya, R. A.; Soni, T. G.; Thakkar, V. T.; Gandhi, T. R. *Dissolut Technol* **2010**, *17*, 16.

(316) Cano, H.; Gabas, N.; Canselier, J. P. *J Cryst Growth* **2001**, *224*, 335.

(317) Muller, F. L.; Fielding, M.; Black, S. *Org Process Res Dev* **2009**, *13*, 1315.

(318) Liu, W. J.; Dang, L. P.; Black, S.; Wei, H. Y. *J Chem Eng Data* **2008**, *53*, 2204.

(319) Fleming, D. H. W. I. *Spectroscopic methods in organic chemistry*; fifth ed.; McGraw-Hill International (UK) Limited, 1995.

(320) Kawashima, Y.; Imai, A.; Takeuchi, H.; Yamamoto, H.; Kamiya, K.; Hino, T. *Powder Technol* **2003**, *130*, 283.

(321) Nokhodchi, A.; Maghsoodi, M. *Aaps Pharmscitech* **2008**, *9*, 54.

(322) Tayel, S.; Soliman, I. I.; Nassif, D. L. *Egyptian Journal of Pharmaceutical Sciences* **2003**, *44*, 101.

(323) Maghsoodi, M.; Derakhshandeh, K.; Yari, Z. *Advanced pharmaceutical bulletin* **2012**, *2*, 25.

(324) Maghsoodi, M.; Hajipour, A. *Drug Dev Ind Pharm* **2014**, *40*, 1468.

(325) Jordens, J.; Gielen, B.; Braeken, L.; Van Gerven, T. *Chem Eng Process* **2014**, *84*, 38.

(326) Zamanipoor, M. H.; Mancera, R. L. *Trends Food Sci Tech* **2014**, *38*, 47.

(327) Clair, B.; Ikni, A.; Li, W. J.; Scouflaire, P.; Quemener, V.; Spasojevic-de Bire, A. *J Appl Crystallogr* **2014**, *47*, 1252.

(328) Arellano, M.; Benkhelifa, H.; Alvarez, G.; Flick, D. *Chem Eng Sci* **2013**, *102*, 502.

(329) Baptista, P. N.; Oliveira, F. A. R.; Sannervik, J.; Oliveira, J. C. *J Food Eng* **1996**, *29*, 361.

(330) Wilson, B.; Sherrington, D. C.; Ni, X. *Ind Eng Chem Res* **2005**, *44*, 8663.

(331) Fabiyi, M. E.; Skelton, R. L. *Journal of Photochemistry and Photobiology a-Chemistry* **1999**, *129*, 17.

(332) Ni, X.; Zhang, Y.; Mustafa, I. *Chem Eng Sci* **1998**, *53*, 2903.

Appendices

Appendix 1 Supporting information related to chapter 4

Appendix 1 Table 1: Experimental data for perfect pulse modelling

Amp (mm)	Frq. (Hz)	Re_n	Re_o	ψ	St_r	Pe	E	D
33	3	283	4642	16	0.073	48	0.0015845	0.021
14	3	283	1957	7	0.172	1000	0.0002943	0.001
33	3	283	4642	16	0.073	23	0.0032444	0.043
14	3	283	1957	7	0.172	1000	0.0002943	0.001
33	3	71	4642	66	0.073	30	0.0006214	0.033
14	3	71	1957	28	0.172	295	0.0002498	0.003
33	3	71	4642	66	0.073	23	0.0008065	0.043
14	3	71	1957	28	0.172	227	0.0003239	0.004
141	1	283	7069	25	0.016	30	0.0024899	0.033
66	1	283	3104	11	0.036	167	0.0017656	0.006
141	1	283	6663	24	0.017	33	0.0022635	0.030
66	1	283	3105	11	0.036	200	0.0014713	0.005
141	1	71	6663	94	0.017	16	0.0012066	0.064
66	1	71	3105	44	0.036	61	0.0012102	0.016
141	1	71	6663	94	0.017	9	0.0019911	0.106
66	1	71	3105	44	0.036	86	0.0008575	0.012
18	3	283	2531	9	0.133	143	0.0005282	0.007
9	3	283	1343	5	0.251	1000	0.0002943	0.001
18	3	283	2531	9	0.133	167	0.0004527	0.006
9	3	283	1343	5	0.251	1000	0.0002943	0.001
18	3	71	2531	36	0.133	49	0.000382	0.020
9	3	71	1343	19	0.251	693	0.0001061	0.001
18	3	71	2531	36	0.133	35	0.0005317	0.028
9	3	71	1343	19	0.251	663	0.0001109	0.002
55	1	283	2597	9	0.043	63	0.0012072	0.016
38	1	283	1773	6	0.063	50	0.0058852	0.020
55	1	283	2597	9	0.043	67	0.0011318	0.015
38	1	283	1773	6	0.063	50	0.0058852	0.020
55	1	71	2597	37	0.043	50	0.0003783	0.020
38	1	71	1773	25	0.063	122	0.0006037	0.008
55	1	71	2597	37	0.043	18	0.0010741	0.057
38	1	71	1773	25	0.063	173	0.0004252	0.006
25	2	141	2336	17	0.096	114	0.0007262	0.009
36	2	141	3378	24	0.067	91	0.0009095	0.011
36	2	141	3378	24	0.067	101	0.0008181	0.010
36	2	141	3378	24	0.067	103	0.0007992	0.010
33	3	283	4642	16	0.073	48	0.0015845	0.021

Appendix 1 Table 2: Experimental validation for RTD experiments

Expt.	Flow rate (g/min)	COBC length(m)	τ experimental (min)	τ measured (min)	Calculated tracer conc. (g)
1	50	4	14.3	14.2	0.0106
2	50	4	15	14.2	0.0099
3	50	4	14.4	14.2	0.0105
4	50	4	14.3	14.2	0.0107
5	50	4	16.1	14.2	0.0106
6	50	4	16.8	14.2	0.0113
7	50	4	14.1	14.2	0.0105
8	50	4	14.5	14.2	0.011
9	200	4	3.7	3.5	0.0106
10	200	4	3.7	3.5	0.0108
11	200	4	3.7	3.5	0.0101
12	200	4	3.7	3.5	0.0099
13	200	4	3.9	3.5	0.0113
14	200	4	3.8	3.5	0.0109
15	200	4	3.7	3.5	0.0108
16	200	4	2.2	3.5	0.0832
17	50	15.6	56.1	55.3	0.0127
18	50	15.6	55.8	55.3	0.0109
19	50	15.6	55.8	55.3	0.0105
20	50	15.6	55.6	55.3	0.0107
21	50	15.6	55.9	55.3	0.0106
22	50	15.6	55.5	55.3	0.0108
23	50	15.6	55.7	55.3	0.0115
24	50	15.6	55.4	55.3	0.0108
25	200	15.6	14.1	13.8	0.0114
26	200	15.6	14.1	13.8	0.0107
27	200	15.6	13.8	13.8	0.0104
28	200	15.6	14.1	13.8	0.0106
29	200	15.6	14.2	13.8	0.0115
30	200	15.6	14	13.8	0.011
31	200	15.6	14	13.8	0.0108
32	200	15.6	14	13.8	0.0122

Appendix 1 Table 3: Experimental data for imperfect pulse modelling

Amp	Freq	Re_n	Re_o	ψ	St_r	Pe	E	D
14	3	260	1997	8	0.2	2600	0.00012	0.0004
14	3	260	1997	8	0.2			
14	3	65	1997	31	0.2	500	0.00015	0.002
14	3	65	1997	31	0.2			
66	1	260	3329	13	0.04	250	0.00124	0.004
66	1	260	3329	13	0.04			
66	1	65	3329	51	0.04	180	0.00048	0.0062
66	1	65	3329	51	0.04			
9	3	260	1383	5	0.29	1700	0.0006	0.0019
9	3	260	1383	5	0.29			
9	3	65	1383	21	0.29	4750	0.00022	0.0028
9	3	65	1383	21	0.29			
38	1	260	1946	7	0.07	875	0.00123	0.004
38	1	260	1946	7	0.07			
38	1	65	1946	30	0.07	350	0.00425	0.0548
38	1	65	1946	30	0.07			
30	1	260	1536	6	0.09	500	0.00062	0.002
30	1	260	1536	6	0.09			
30	1	65	1536	24	0.09	145	0.00054	0.0069
30	1	65	1536	24	0.09			
30	1	130	1536	12	0.09	475	0.00034	0.0022
30	1	130	1536	12	0.09			

Appendix 2 Supporting information relating to chapter 5

Appendix 2 Table 1: Unseeded COBC operating conditions

Expt.ID	Frq (Hz)	Amp (mm)	FR	Conc.	T_s	CC_t	T_f	CR	RT	Re_n	Re_o	Ψ	St
NB_02_03	2	20	70	35	70	10			20				
NB_02_007	1	20	73	35	80	40	10	2.5	20	103	942	9	0.119
NB_02_019	1	20	117	20	80	55	10	3	20	166	942	6	0.119
	1	20	117	35	80	55	10	3	20	166	942	6	0.119
NB_02_023	1	20	59	30	80	40	10	1	30	83	942	11	0.119
NB_02_027	1	20	31	20	80	48	20	0.5	56	44	942	21	0.119
	1	20	31	30	80	40	10	0.5	60	44	942	21	0.119
NB_02_031	1	30	23	30	80	48	20	0.5	56	33	1414	43	0.080
NB_02_041	2	20	29	30	80	55	20	0.5	80	41	1885	45	0.119
NB_02_066	2	20	39	30	80	60	30	0.5	60	55	1885	34	0.119
NB_02_069	2	20	56	30	80	56	31.6	0.5	40	79	1885	24	0.119
NB_02_072	1	30	74	30	80	45	31	0.5	30	105	1414	13	0.080
	1	30	59	30	80	39	30	0.3	30	83	1414	17	0.080
NB_02_075	1	30	111	30	80	38.9	20.4	1	20	157	1414	9	0.080
NB_02_077	1	30	111	30	70	38.9	20.4	1	20	157	1414	9	0.080
NB_02_081	1	30	74	30	70	39.2	24.5	0.5	30	105	1414	13	0.080

Expt. ID	Fq	Amp	FR	Conc	t_s	CC_t	t_f	CR	RT	Re_n	Re_o	Ψ	St
NB_01_002	1	30	52	45	70	48.3	19.9	0.5	60	73	1414	19	0.080
NB_01_005	1	30	51	45	70	47	29.7	0.3	60	72	1414	20	0.080
NB_01_012	1	30	51	45	70	47	37.6	0.3	60	72	1414	20	0.080
NB_01_015	1	30	53	45	70	45	40	0.1	50	75	1414	19	0.080
NB_01_019	1	30	78	45	80	58.9	40	0.5	40	110	1414	13	0.080
NB_01_022	1	30	78	45	80	59.5	50	0.25	40	110	1414	13	0.080
NB_01_043	1	30	111	35	80	66	59	0.25	28	157	1414	9	0.080
NB_01_046	1	30	111	35	80	65	56	1	28	157	1414	9	0.080
NB_01_048	1	30	111	35	80	56	42	0.5	28	157	1414	9	0.080
NB_01_050	1	30	111	35	80	50	36	0.5	28	157	1414	9	0.080
NB_01_053	1	30	111	45	80	56	43	0.5	28	157	1414	9	0.080
NB_01_026	1	30	99	40	80	44.2	30	0.5	30	140	1414	10	0.080
NB_01_029	1	30	111	30	70	45.5	20.3	1	28	157	1414	9	0.080
NB_01_032	1	30	78	45	80	62.9	45	0.5	38	110	1414	13	0.080
NB_01_035	1	30	51	45	80	46.7	30.2	0.3	60	72	1414	20	0.080
NB_01_040	1	30	78	30	70	36	30	1	40	110	1414	13	0.080

Appendix 2 Table 2: Unseeded COBC experimental results

Expt. ID	Nuc. T	S*	S#	Form	yield	PSD d(0.5)	PSD span	Notes
NB_02_03		5.5	7.0	α				
NB_02_007	25.7	3.2	4.2	α	73	247	2.0	Encrust.
NB_02_019		3.1	4	α				No nuc. after 4 RTs
	21.8	3.5	4.6	α	38	294	2.0	Encrust.
NB_02_023	40	1.8	2.5	α & β		284	1.7	Encrust.
NB_02_027		2.2	2.8					No nucleation after 2 hours
		4.7	6					No nucleation after 2 hours
NB_02_031	32.7	2	2.7	α		215	1.8	Encrust. & sedimentation
NB_02_041	32.9	2	2.7			134	1.1	
NB_02_066	45.0	1.1	1.6	α		411	1.5	Encrust. Sedimentation
NB_02_069	38.8	1.6	2.2	α		248	2.1	Encrust. Oscillation Intensity investigated, 1Hz 30 visually showed best mixing
NB_02_072	38.2	1.7	2.3	α		227	1.7	Encrust.
	33.9	2	2.7	α		332	1.9	Encrust.
NB_02_075	23.1	2.9	3.8	α				Encrust. & Sedimentation
NB_02_077	28.3	2.4	3.2	α		240	1.9	Encrust. & Sedimentation
NB_02_081	30.4	2.3	3	α		271	1.8	Encrust. & Sedimentation

Expt. ID	Nuc. T	S*	S#	Form	yield	PSD d(0.5)	PSD span	Notes
NB_01_002	36.9	2.6	3.6	α		280	1.8	Encrust. & Sedimentation.
NB_01_005	39.3	2.4	3.3	α		500	1.8	Encrust. & Sedimentation.
NB_01_012	42.8	2.1	2.9	α				Encrust. Temperature cycling expt.
NB_01_015	43.9	2	2.8	α				
NB_01_019	53.2	1.5	2.1	α & β				
NB_01_022	51.9	1.5	2.1	α				
NB_01_043		0.9	1.3	α				No nuc. after 4 RTs
NB_01_046		1	1.4	α				No nuc after 4 RTs
NB_01_048		1.2	1.7	α				No nuc. after 4 RT
NB_01_050	41.3	1.8	2.4	α	22	232	2.6	
NB_01_053	51.7	1.6	2.2	α	30	273	3.0	
NB_01_026	40.6	2.1	2.8	Trace β				Mixed baffle rig
NB_01_029	25.6	2.6	3.5					Mixed baffle rig
NB_01_032	54.4	1.4	2	Trace β				Mixed baffle rig
NB_01_035	41.5	2.3	3.1	α				Mixed baffle rig
NB_01_040	35.9	1.8	2.5	α				Encrust. Temperature cycling expt.

Appendix 2 Table 2: Heater/chiller set-points for seeding experiments

	Distance (m)	Thermocouple	Heater/Chiller set Temp			
			Expt. 1	Expt. 2	Expt. 3	Expt. 4
S1	-0.725	T1	70	70	70	70
S2	0	T2	63	43	68	42
S3	0.725	T3	60.6	40.2	57.5	39.4
S4	1.45					
B1	1.735					
S5	2.46	T4				
S6	3.185	T5				
S7	3.91	T6	60.6	38.6	56.7	39
S8	4.635					
B2	4.92					
S9	5.645	T7				
S10	6.37	T8				
S11	7.095	T9	55	37.4	55.8	37.8
S12	7.82					
B3	8.105					
S13	8.83	T10				
S14	9.555	T11		34.7	51.9	36.2
S15	10.28	T12				
S16	11.005		49.6			
B4	11.29					
S17	12.015	T13		32.6	50.4	34.2
S18	12.74	T14				
S19	13.465	T15	43.4	30.6	47.1	32.6
S20	14.19					
B5	14.475					
S21	15.2	T16	36.9	28.1	40.5	30.3
S22	15.925	T17				
S23	16.65	T18	31.4	25.5	37	27.7
S24	17.375					
B6	17.66					
S25	18.385	T19				
S26	19.11	T20				
S27	19.835	T21	26.2	22.5	28.5	23.9
S28	20.56					
B7	20.845					
S29	21.57	T22	20.4	20	20.6	20
S30	22.295	T23				
S31	23.02	T24	14	17.1	17.1	17
S32	23.745					

Appendix 3 Recommendations for system design

The COBC system was previously used for reactive chemistries[330,331] and polymerisations[249,332] therefore not specifically optimised with a focus on crystallisation processes. Given the number of practical issues and observation made within this research, the proposed changes should be made to ensure successful operation and maximum control when operating with this technology. These are as follows;

1) Redesign of the glass straights.

   The issue of sedimentation was highlighted in 5.3.5.5, here the missing baffle in between the joins for the bends was illustrated. The design and implementation of new bends significantly improved mixing and solid suspension in these dead zones. Given all of the glass straights have this missing baffle, at both ends, new straights should be made in a similar manner to ensure consistent solid suspension thought-out the rig.

2) Redesign of the jacked circulation.

   As previously outlined in sections 5.3.5.4 and 8.2.1, the COBC obsesses rapid heat transfer capabilities. Further investigation is required for understanding and controlling heat transfer due to the desired controlled cooling for temperature sensitive crystallisations. Solutions to improve heat transfer properties include mixing coils within the COBC jacked shell, oscillation of the coolant and a manifold and/or flow valves from the heater/chillers to the jacket. One such scenario for achieving the best temperature control would be to use 1 heater/chiller per COBC straight, but this would lead to 32 heaters and hence is economically unviable, a more suitable solution needs to be reached e.g. the *Cambridge Reactor Design* Rattlesnake uses a double shell jacket for heat exchange, over four DN70 straights, to improve control and reach desired smooth cooling profiles.

3) Implementation of jacked bends.

On average, the difference in temperature at the bends varied by approximately 2 °C. Depending on the nature of the crystallisation system investigated, a temperature difference of 2 °C could have significant detrimental effects on the crystallisation process, e.g. MSZWs for some materials can be in the order of a 2 °C super cooling therefore the lack of temperature control in these unjacketed bends could result in spontaneous nucleation and hence loss of crystallisation control. Implementation of temperature controlled bends will minimise these cold spots to move towards a more controlled and robust process.

4) Oscillation source.

Due to the oscillation damping effect there are considerations that should be made during continuous oscillation. This could be both problematic and advantageous, as highlighted in Section 4.4. However a detailed assessment of the damping of oscillation process needs to be made to improve understanding of the change in the mixing environment of the length of a COBC. Alternatively, other options could be implemented, for example implementation of a double acting piston to provide oscillation at both the start and the end of the COBC system. Another example would be a series of short length COBCs each with independent bellows or pistons driving the oscillation. These alternatives may reduce the observed effects and provide a base to achieve a higher performance in oscillation intensities.

5) Automated control system.

Implementation of computer control for all equipment units (pumps, heater/chillers, oscillator, thermocouple readers etc), will provide a base to move away from the labour intensive manual operating COBC platform to a fully automated system. Similar to the automation made on the MFOBC system, computer control and storage of data will allow

for a more QbD approach to be utilised where real-time display and feedback control can be used. This will move the system into a direct controlled workspace where rapid development of controlled crystallisations could be achieved.

Publications

1) **Image-based Monitoring for Early Detection of Fouling in Crystallisation Process**.

Christos Tachtatzisa, Rachel Sheridan, Craig Michie, Robert C. Atkinson, Alison Cleary, Jerzy Dziewierz, Ivan Andonovic, Naomi Briggs, Alastair J. Florence, Jan Sefcik, Chemical Engineering Science, 2015, doi:10.1016/j.ces.2015.01.038

2) **Seeded Crystallization of β-l-Glutamic Acid in a Continuous Oscillatory Baffled Crystallizer**

Naomi E. B. Briggs, Ulrich Schacht, Vishal Raval, Thomas McGlone, Jan Sefcik, and Alastair J. Florence, Organic Process Research and Development, 2015, *(submitted)*

3) **Oscillatory Flow Reactors (OFRs) for Continuous Manufacturing and Crystallization**

Thomas McGlone, Naomi E. B. Briggs, Catriona A. Clark, Cameron J. Brown, Jan Sefcik, and Alastair J. Florence, Organic Process Research and Development, 2015, *(submitted)*

4) **Residence time distribution and heat transfer performance in continuous oscillatory baffled flow with application to continuous crystallisation control** *(drafting)*

5) **Automated feedback control in a moving fluid oscillatory baffled crystalliser for pharmaceutical crystallisation control** *(drafting)*